Lecture Notes in Networks and Systems 940

Manuel N. Cardona · José Baca ·
Cecilia Garcia · Isela G. Carrera ·
Carol Martinez *Editors*

Advances in Automation and Robotics Research

Proceedings of the 4th Latin American Congress on Automation and Robotics, San Salvador, El Salvador 2023

Springer

Lecture Notes in Networks and Systems 940

The series "Lecture Notes in Networks and Systems" publishes the latest developments in Networks and Systems—quickly, informally and with high quality. Original research reported in proceedings and post-proceedings represents the core of LNNS.

Volumes published in LNNS embrace all aspects and subfields of, as well as new challenges in, Networks and Systems.

The series contains proceedings and edited volumes in systems and networks, spanning the areas of Cyber-Physical Systems, Autonomous Systems, Sensor Networks, Control Systems, Energy Systems, Automotive Systems, Biological Systems, Vehicular Networking and Connected Vehicles, Aerospace Systems, Automation, Manufacturing, Smart Grids, Nonlinear Systems, Power Systems, Robotics, Social Systems, Economic Systems and other. Of particular value to both the contributors and the readership are the short publication timeframe and the worldwide distribution and exposure which enable both a wide and rapid dissemination of research output.

The series covers the theory, applications, and perspectives on the state of the art and future developments relevant to systems and networks, decision making, control, complex processes and related areas, as embedded in the fields of interdisciplinary and applied sciences, engineering, computer science, physics, economics, social, and life sciences, as well as the paradigms and methodologies behind them.

Indexed by SCOPUS, INSPEC, WTI Frankfurt eG, zbMATH, SCImago.

All books published in the series are submitted for consideration in Web of Science.

For proposals from Asia please contact Aninda Bose (aninda.bose@springer.com).

Manuel N. Cardona · José Baca · Cecilia Garcia ·
Isela G. Carrera · Carol Martinez
Editors

Advances in Automation and Robotics Research

Proceedings of the 4th Latin American Congress on Automation and Robotics, San Salvador, El Salvador 2023

Springer

Editors
Manuel N. Cardona
Universidad Don Bosco
Soyapango, El Salvador

José Baca
Texas A&M University – Corpus Christi
Texas, TX, USA

Cecilia Garcia
Universidad Politécnica de Madrid
Madrid, Spain

Isela G. Carrera
Universidad Autónoma de Coahuila
Monclova, Coahuila, Mexico

Carol Martinez
University of Luxembourg
Kirchberg, Luxembourg

ISSN 2367-3370 ISSN 2367-3389 (electronic)
Lecture Notes in Networks and Systems
ISBN 978-3-031-54762-1 ISBN 978-3-031-54763-8 (eBook)
https://doi.org/10.1007/978-3-031-54763-8

This Springer imprint is published by the registered company Springer Nature Switzerland AG
The registered company address is: Gewerbestrasse 11, 6330 Cham, Switzerland

Paper in this product is recyclable.

Preface

LACAR 2023 was the 4th Latin American Congress on Automation and Robotics that promotes an open forum with research, scientists, and engineers from academia and private industries come together to present current and exciting research application and also discuss future challenges in this fascinating field. It aims to generate activities in research development and application on automation and robotics by exchanging knowledge experience and the synergy of research groups from different places from Latin America.

This year the acongress was held at Universidad Don Bosco, El Salvador. The Congress highlights different research areas such autonomous robots, rehabilitation robotics, control techniques, digital twins, parallel robots, kinematics and dynamics analysis, ROS, eye tracking, robotics modeling and simulation, and robotics and mechanism design. Main workshop and forum was centered in advanced control techniques and the discussion of challenges of robotics in Latin America.

We would like to extend our sincere gratitude to our esteemed keynote speakers, Dra. Cecilia García with the keynote: Advances in bioinspired underwater robotics; Dr. Sunil Agrawal with the keynote: Rehabilitation Robotics: Improving Everyday Human Functions; Dr. José Baca with the keynote: Modularity in Autonomous Systems across Ground, Maritime, Air, and Space Domains.

We would like also to extend our sincere gratitude and appreciation for all the hard work and dedication provided by the members of the organizing committee, program committee, and volunteers; moreover, we would like to thank all the authors and reviewers who have contributed to this event by preparing papers of high quality. We would like to express our grateful thanks to the publisher and editorial staff of Springer for accepting and supporting the publication of this proceeding volume. We believe the LACAR 2023 proceedings are a value source of reference for the future research and development that considers the sustainable economic and social development in Latin American countries.

November 2023

Manuel N. Cardona
José Baca
Cecilia Garcia
Isela G. Carrera
Carol Martinez

Contents

Technology in Higher Education: A Collaborative Innovation Ecosystem Model

Ignacio Chang[1], Elvira Durán-Rojas[2], Héctor Montes[1], Olga Jape Collins[3], Pablo Cárdenas[4], Leslie Cieza[1], and Víctor López Cabrera[1(✉)]

[1] Universidad Tecnológica de Panamá, Panama City, Panama
{hector.montes1,victor.lopez}@utp.ac.pa, ycieza@pucp.edu.pe
[2] Grupo Investigación Gestión en Salud Global, Universidad de Córdoba, Colombia, Montería, Colombia
edrojas@correo.unicordoba.edu.co
[3] Universidad Autónoma de Santo Domingo, Santo Domingo, Dominican Republic
ojape92@uasd.edu.do
[4] Pontificia Universidad Católica del Perú, San Miguel, Peru
p.cardenasc@pucp.pe

Abstract. The current reality places technology at the forefront of the educational communication process, especially considering the health emergency brought on by COVID-19. Creating mechanisms to facilitate the continuity of teaching represented one of the greatest challenges during the pandemic. A collaborative, innovative ecosystem model targeted towards the teaching-learning process is developed. An exploratory, descriptive study with a mixed-methods approach is conducted; cases from universities in Colombia, Panama, Peru, and the Dominican Republic are examined, surveys are implemented, and classroom and university experiences are recounted. Each study experience generates a space for teachers to discuss and reflect on the students' progress and the methodologies applied for flexibility and adaptability to available information technologies. In this way, the foundation for a collaborative innovation ecosystem is proposed to organically strengthen student knowledge through articulated structures, functional relationships, and supportive methods and procedures. An active control system is also proposed to ensure meaningful learning. This experience leaves alternative options for all universities and the education system for health emergencies that prevent face-to-face interaction, taking advantage of new information technologies and the era of artificial intelligence.

Keywords: Innovation ecosystem · control system · educational methodology · educational innovation · technological innovation

1 Introduction

Technology in the educational communication process opens a horizon of applications, from the field of robotics, embedded systems, 3D printing, applied electronics, Industry 4.0, to disruptive technology [1], among others. Innovating in education brings about

M. N. Cardona et al. (Eds.): LACAR 2023, LNNS 940, pp. 1–19, 2024.
https://doi.org/10.1007/978-3-031-54763-8_1

significant changes to encourage permanent improvements [2], where disruptive innovation has fostered online courses that make education more inclusive [3]. Additionally, the development of modular robotics also makes its way into technology [4–6], with Colombia pioneering in Latin America with developments for secondary education [7]; its applicability knows no limits and is a powerful learning tool.

There are experiences of innovation applied to teaching and learning processes, whose indicators make them attractive for incorporation into methodologies. For example, technological innovation parks [8] that link the university, businesses, and the State, or virtual learning environments aimed at collaborative knowledge generation for a culture of transformation and continuous improvement [9].

The sanitary conditions caused by COVID-19 changed the dynamics of traditional education, which had to cope with operational limitations of not being able to bring teachers and students together in one place. Virtuality was the best option: the Internet and its technological tools were used to meet this need [10].

During the years 2020, 2021, and the first semester of 2022, creating mechanisms to facilitate the continuity of teaching at all educational levels represented one of the greatest challenges. Also, variations in socio-economic conditions, the ability to embrace changes in educational systems, the implications of these changes in daily dynamics, and the possibilities for equitably accommodating government-proposed continuity measures were observed worldwide. However, the identification of successful educational strategies was conditioned by health recommendations, where physical distancing took precedence, followed by the mandatory use of masks.

Universities, as entities responsible for training the professionals a country needs, must commit to sustainable development and humanity [11, 12] by applying and disseminating flexible practices that develop greater social sensitivity in students and generate solutions to each country's needs with new educational approaches.

Therefore, administrative management must adapt to new educational models for optimal long-term operation, aligned with strategies and with effective, flexible communication and information systems. A review and update of traditional conceptualizations and established processes concerning teaching, research, and extension are required [13].

In the post-COVID-19 academic culture, actors in the teaching-learning process will require adjustments so that educational technologies facilitate learning where the teacher is the mentor, learning guide, and time manager for virtual and face-to-face periods; and where the student applies knowledge in seeking technological solutions to community or general societal problems. Therefore, the model that develops the teaching-learning process must incorporate new, effective, efficient learning experiences with learning challenges that encourage research and development, both in the classroom and society.

It is known that higher education worldwide faces significant challenges due to the contradictions generated by development or economic power [14]. Hence, an innovative model should include an ecosystem, understood as a set of organisms in a community and its environment, linked to the teaching-learning process that allows autonomous, collaborative, project-based, meaningful, innovative, emotional, and discovery learning.

This innovative model should create a space for teachers to discuss and reflect on young people's progress and the applied methodologies, aiming to enable their flexibility and adaptability. Therefore, the question arises: how to generate quality teaching-learning processes that, from an innovative university, respond assertively to the conditions imposed by COVID-19? To answer this question, university teachers from various specialties in Colombia, Panama, Peru, and the Dominican Republic joined with their experiences to design a model of an innovation ecosystem in higher education to strengthen learning environments.

2 Methodological Aspects

The foundations of a collaborative innovation ecosystem are proposed as an initiative to strengthen the knowledge acquired by students organically, with an articulated structure, functional relationships, and supportive methods and procedures.

Initially, an exploratory investigation was conducted to achieve a more concrete approach to the problem to be solved, followed by a descriptive study through case studies. The hypothetical-deductive method was employed, which is very useful because it provides a logical path for finding solutions to the challenges and issues faced by students [15]. Likewise, a quantitative approach focused on the outcome and a qualitative approach focused on the process were used, where the researcher is part of the study to describe their experience in the classroom.

The population of the study consisted of students and professors from universities in Colombia, Panama, and Peru where courses and/or subjects were taught in Health Administration and Engineering programs. Project-based learning and problem-based learning were employed, to which a collaborative component was added, as students dialogued among themselves, consulted the teacher for doubts, and acted either individually or collectively, actively participating in the entire solution process.

For the case of the Dominican Republic, a documentary review of the institution was conducted with respect to academic aspects, institutional policies, and implemented practices; communication was maintained with the authorities who were present during the time of interest for the study to address concerns that would arise while gathering information for its validity. Central tendency measures were used to analyze the collected data, and qualitative information was analyzed through narrative analysis.

3 Educational Experiences During the Pandemic

3.1 A Program from the University of Córdoba, Colombia

The Health Administration program of the University of Córdoba uses a distance learning methodology and consists of a learning structure with four moments: direct accompaniment, mediated accompaniment, guided accompaniment, and independent work. These aim to guarantee that students achieve learning outcomes, developing cognitive competencies specific to the discipline and profession, attitudinal competencies to assume an active role concerning available resources and their environment, and socio-affective

competencies promoting commitment, leadership, and engagement. Courses or subjects are hosted on the Moodle platform, uniformly structured around learning objectives. Teachers have training in Information Technology (IT) to encourage self-learning through teaching strategies, active communication, and using online library resources. Most courses involve a classroom project integrating all learning outcomes, which is completed and presented by the students at the end of the semester.

Given the preventive isolation protocols due to the COVID-19 pandemic, the public University of Córdoba, considering the challenges some students faced to continue their studies, facilitated internet access, computers, electronic tablets, and, in some cases, grocery kits. For the Health Administration program, teaching and communication with the students were initially conducted via WhatsApp groups and phone calls. For direct accompaniment (synchronous classes), video conferencing tools like Zoom and Google Meet were used. These classes were recorded and shared with the students through their emails and on the Moodle platform. On this platform, mediated accompaniment, guided accompaniment, and independent work were maintained. Given the situation, assessments were incorporated through the "quiz" activity.

An innovative experience in the Market Research course, which used Project-Based Learning as defined by the Buck Institute for Education, developed a classroom project focused on food waste and loss in households. Students carried out all aspects involved in conducting market research. They initially posed the problem, set the framework, designed objectives, hypotheses, types, methods, and research techniques, and types of sampling. They created a questionnaire aimed at heads of households. The teacher reviewed the questionnaire, grouped and consolidated the best questions into one, and shared it with students for review in Google Forms. The best questionnaire was chosen, adjusted, and shared for application. Upon closing the questionnaire, the Excel data sheet was downloaded and sent to the students, who conducted descriptive analysis and drafted the final research report. Students uploaded the report and a presentation video on Moodle for teacher evaluation according to the grading rubric.

Despite limitations imposed by the biosecurity protocols of the pandemic, and the use of internet and computing equipment, student motivation in the Health Administration program was evident. Students managed to secure resources, learned to use technological tools autonomously, implemented the knowledge imparted during the course based on the realities of the studied households, and thereby achieved the learning competencies.

3.2 Methodological Design. Technological University of Panama, Panama

Due to COVID-19 restrictions, Higher Education Institutions (HEIs) had to switch to remote learning, whether they were prepared for it or not. This posed a new challenge where the main premise was that the teacher should become, more than a source of knowledge, a facilitator to guide the student to achieve the competencies required for their professional training through their own research on the subject matter. Thus, to enhance their capabilities, it was necessary to qualitatively determine the impact of using learning methods that encouraged collaborative work, and how to help students learn, unlearn, and relearn was the challenge of this situation.

For this purpose, a survey was conducted among teachers at the Technological University of Panama (UTP) to identify methodologies and technological tools they

used to create learning spaces, as well as to understand current societal challenges in problem-solving (Fig. 1).

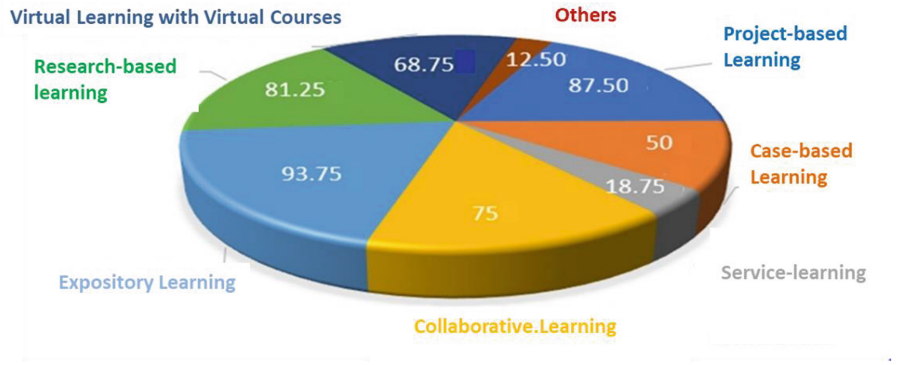

Fig. 1. Methodology and technological tools used by UTP teachers.

Although expository learning was the most widely used method (93.75%), as shown in Fig. 1, followed by project-based learning (87.5%), the latter was chosen for adapting better to the pandemic situation.

Initially, a participatory and collaborative component aimed at students was introduced in the Control Theory I course. Students consulted information from reliable web sources to complement their knowledge, incorporating technology to create an educational way to learn the subject. Different computer tools were used, and tangible results were shared with other students for learning by doing.

Teams of up to five students were then formed, and each was assigned a different problem to solve, related to real cases or case studies, where they had to apply the knowledge learned throughout the semester. In addition, they were encouraged to voluntarily participate in a new challenge: to develop an educational way of learning to solve problems using some technique or digital tool that encouraged a simple interactive educational activity. This would not earn them extra points but would contribute to the learning of future students, i.e., they would create self-learning units to facilitate learning for other groups.

In the second edition of the Control Theory I course; efforts were made to improve what had been designed to turn them into self-learning units. Several surveys were conducted on the students, both at the beginning and midway through the semester, to evaluate the consolidation of their knowledge. Another survey was applied to another group to assess motivation and learning. The results were encouraging because the methodology and tools used were not only appreciated but also proved to be effective for knowledge acquisition, as shown in Fig. 2.

As it can be seen in Fig. 2, there were various forms of motivation based on the responses given by the students. In this way, the method employed facilitated better mastery of problem-solving techniques, detailed the procedures used, and allowed other

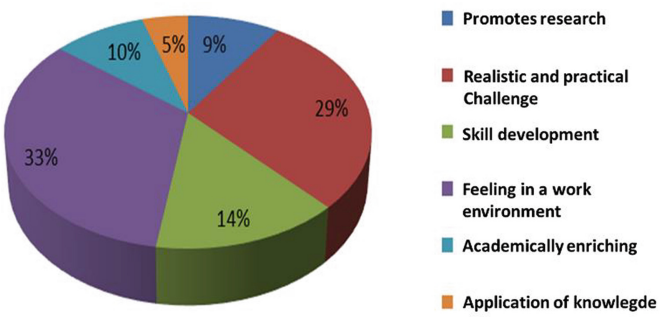

Fig. 2. Motivation and learning produced by incorporating self-learning units in students.

students to learn by following them. It also enabled the student to organize their time, coordinate with other group members, and be self-taught.

Given that the projects designed by the students only accounted for 15% of the final grade of the course, due to the commitment and dedication shown, it can be stated that the methods used—known as project-based learning and problem-based learning—stimulate students' interest in learning, encouraging them to participate more in classes, develop critical thinking, and become more self-intuitive. This was the case as the first time was voluntary participation and in the second version, extracurricular activities where all groups competed among themselves, thereby, the best works were chosen to be converted into self-instruction units for the course.

3.3 Technology and Educational Innovation. Pontifical Catholic University of Peru, Peru

In the Electronic Engineering program at the Pontifical Catholic University of Peru (PUCP), XSpace was developed: an innovative educational platform aimed at promoting self-learning among students in the Control Systems course, from the 2020-2 academic semester to the present time. The platform took as reference the stages of solving a control problem laid out by Chen & Naughton [17] and Silawatchananai & Ruangurai [18] for the identification and mathematical modeling of the physical system, controller design, and the simulation and implementation of the control system. Additionally, the competencies outlined in the exit profile for electronic engineers related to the course content were considered. These competencies highlight the constant need for an empirical approach to adequately complement control theory concepts. With the forced virtuality due to the pandemic, it became even more imperative to adequately implement this educational model with a sustainable methodology. The following stages were involved:

- **Full Availability of the XSpace Kit**: In the critical phase of virtuality, kits were developed with hardware oriented towards the implementation of control systems designed by the students. These consist of a development board (XSpace v2.0) and a geared motor (XSGMotor v1.0) with their respective sensors (incremental encoders with Hall-effect sensors). These kits were distributed on loan to students during each academic cycle (Fig. 3). Software components, like libraries to facilitate coding for

the XSpace v2.0 and dedicated Simulink blocks for interaction between the XSpace v2.0 and the users' computers (XSpace APS, XSpace Viewer, and XSpace HIL), were also developed. In this way, students had an innovative and friendly platform to practice what they had learned in class or even implement their own projects.

- **Teaching Environment**: In the completely virtual cycles, a home laboratory was set up for the course instructors, equipped with sufficient electronic devices for a demonstrative class (such as oscilloscopes, multimeters, and XSpace kits). The class content was shared via video conferencing with the students through the Zoom platform. Even from their homes, students had the opportunity to simultaneously perform the design and implementation along with the professor's explanation.

- **Constant Guidance**: The teachers and teaching assistants of the Control Systems course were available to answer questions and provide feedback during both synchronous (class and lab time) and asynchronous (outside class hours) sessions, whether in-person or virtual. For the latter, chat tools like Telegram were used (Fig. 4).

- **Evaluation System**: Practical laboratory assessments, exams, and the course project were considered, which had to be presented at the end of the academic semester. Every control solution had to include the stages previously described to characterize a control problem. For the laboratories, students were asked to present explanatory videos where each student developed their solution using their own kit, making it easier to demonstrate mastery over the topics. For the exams, students had to solve cases based on real-world industrial scenarios that required them to appropriately link theoretical concepts with a practical approach at various scales. For the project, students were expected to progressively design, model, and implement a control system using the XSpace kit to address a complex problem presented by the course instructors. Throughout the course, students would present milestones of their progress.

Greater detail on the correlation between competencies and the stage of the methodology is shown in Table 1.

The effectiveness of the methodology and the kit were evaluated through opinion surveys of the students in the course, to measure the influence of the methods implemented in the course and the effectiveness of the design and implementation of controllers. The results showed a positive effect of the platform and methodology on student performance, as well as high acceptance (91%) of the evaluation formats involved. Pearson's correlation method was used to evaluate the grades obtained by students in each cycle of the course between the years 2018 and 2022, according to the number of students enrolled per cycle. After applying the new methodologies, there was an increase in the number of enrolled students, in the average of their grades, and in the number of students who passed the course [19].

It is worth noting that the undergraduate course in Control Systems included elements of advanced conventional control, such as the use of cascade control structures and the implementation of real-time control systems, which also belong to the curriculum of the Master's in Control Engineering and Automation offered at PUCP. Likewise, the XSpace initiative has been recognized on several occasions: a group of students from the course

Fig. 3. Detail of the content of the XSpace kit (a), Students receiving the XSpace kit at home (b).

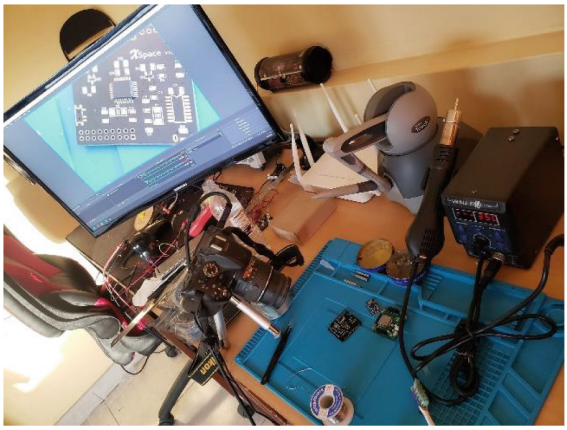

(a)

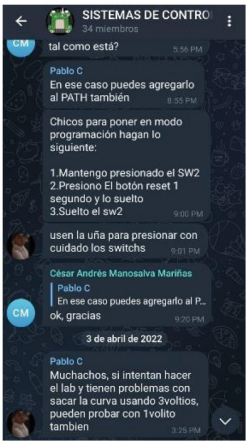

(b)

Fig. 4. Detail of the lab set up at a teacher's home for delivering the class (a), Guidance provided through the Telegram application in Spanish (b).

won first place in the National Industrial Automation Competition 2021 thanks to the application of some knowledge acquired in the course, and the XSpace platform itself received the Educational Innovation Award 2022 granted by PUCP.

3.4 Resilience and Adaptability. Autonomous University of Santo Domingo, Dominican Republic

The Autonomous University of Santo Domingo (UASD) faced an unprecedented challenge during the COVID-19 pandemic. Much like the rest of the world, the way courses were taught at all educational levels had to change. This necessitated a different approach to education, in light of the health crisis, to ensure academic continuity and safeguard the health of students, faculty, and administrative staff.

To address this, university authorities took one of the main steps of significantly expanding the number of virtual classrooms as part of the execution of a "Contingency and Academic Reprogramming Plan in the Face of the COVID-19 Pandemic." Given the impossibility of holding in-person classes, it was decided to convert the 29,599 planned sections of traditional classroom subjects into digital spaces to allow the teaching-learning process to continue remotely [20].

The transition process included migrating teacher assignments from the Barner System platform to the UASD Moodle virtual platform. This involved configuring and updating classrooms, designing and creating content, replicating classrooms, establishing a helpdesk system for students and faculty, initiating communication campaigns, and designing specific spaces for 45 monographic course rooms and 12 thesis course rooms, as well as 247 classrooms for diploma programs and 13 classrooms for doctoral programs.

UASD virtual records indicate that between the first semester of 2020 and the summer cycle of 2022, they had a population of 205,952 active students in higher technical and degree subjects distributed across 25,272 sections. Of these, 52% belonged to the Central

Table 1. Relationship between the competencies of the Electronic Engineering profile and stages of the methodology

Competencies	Stages			
	(1) Full Availability of the XSpace Kit	(2) Teaching Environment	(3) Constant Guidance	(4) Evaluation System
Ethical reflection on learning (C1)	x			
Effective communication of information (C2)				x
Application of engineering to analyze, design, and implement (C3)			x	
Application of engineering to develop projects that meet real needs (C4)		x	x	
Utilization of the latest technologies in various industries (C5)				x

Campus, and the rest were part of the university precincts, centers, and sub-centers, as the university has representation across the entire Dominican territory [21].

This transition was not without challenges, but the university community came together in a joint effort to ensure the success of this new contingency modality. Specific resources were allocated to successfully train 3,125 faculty members from the university's nine faculties through a faculty development program focused on the use and application of technological resources in virtual teaching. This involved 318 videoconferences in three stages between May and December of 2020 (Fig. 5). This program also included deans, school directors, and chair coordinators, thereby improving the digital and pedagogical skills of the teaching staff (Fig. 6), which ensured that they could offer a high-quality educational experience [21].

The expansion of virtual classrooms also involved a review and update of the curricula to adapt them to the online modality and ensure comprehensive education. This was especially important for creating special procedures for health science laboratories. In addition, efforts were made to provide access to electronic devices and internet connections for students who faced technological or financial difficulties. This process has been reinforced by the Ministry of Education of the Dominican Republic with a program

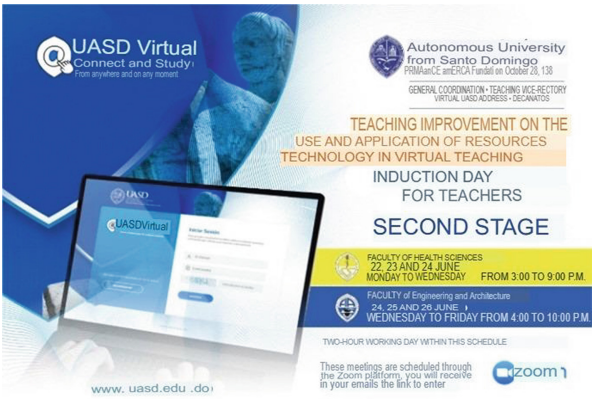

Fig. 5. Informational banners on stages of the teacher improvement program.

to supply electronic tablets to both students and faculty at the national level, as directed by the central government.

The implementation of these virtual classrooms went beyond the academic realm. UASD organized virtual spaces to foster interaction between students and teachers, promoting a sense of community and mutual support (Fig. 7). Moreover, extracurricular activities, conferences, and online events were held to enrich the student experience and maintain commitment to personal and professional development. The impetus provided by the pandemic served as a motivator for permanent expansion and prompted the much-needed upgrade of the Moodle platform, from version 1.9 to version 3.8, with virtual and hybrid offerings [21].

As a best practice, this Higher Education Institution (IES) kept virtual classrooms enabled as ongoing support for teaching even after returning to in-person activities. The management is directed towards maintaining a virtual environment for courses that, given their theoretical nature, can be conducted either virtually or in a hybrid format. This represents a significant advancement in the offerings of the state university of the Dominican Republic (Fig. 8 Figure X Screen Capture of semester. Information in Spanish).

The experience of expanding virtual classrooms at the Autonomous University of Santo Domingo during the COVID-19 pandemic became an example of resilience and adaptability. Despite the challenges, the university community demonstrated its ability to face adversity and continue providing quality education to its students, ensuring that the academic mission did not stop during times of crisis. This process marked a turning point in the way education is conceived, opening new opportunities for the integration of technology in teaching and preparing UASD to face future challenges.

4 Collaborative Active Control System

In accordance with the cases presented, methodological strategies for the quality of learning are proposed as shown in Fig. 9. These strategies address the learning environment from several points of view; first, to manage courses that allow a multidisciplinary

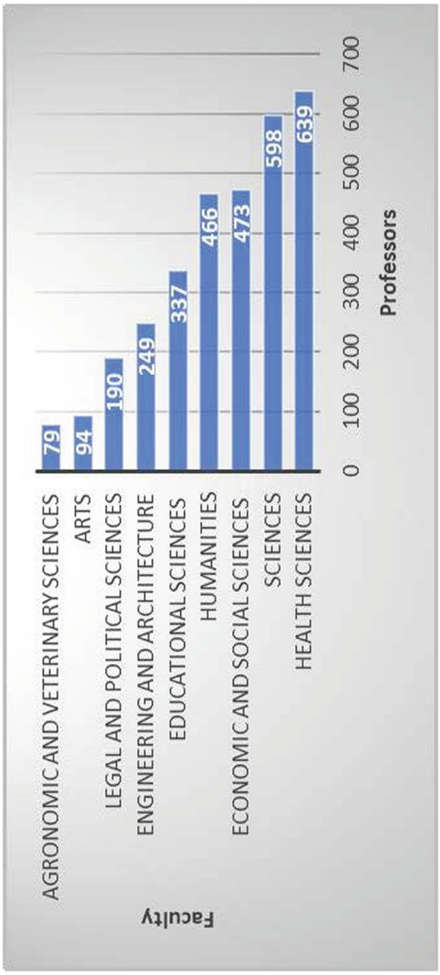

Fig. 6. Faculty by department trained in the teacher improvement program.

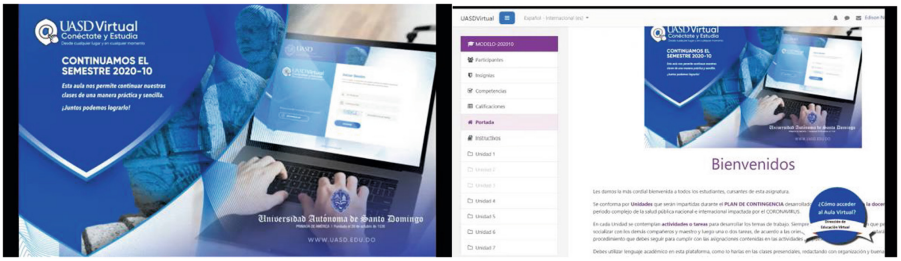

Fig. 7. Screenshot of replicated virtual environment during contingency plan.

Fig. 8. Official publication on the continued use of the virtual environment after the pandemic. Original in Spanish.

approach. Additionally, the focus should not only be on having physical spaces for labs within the university but also transforming the university itself into an experimental lab, for instance, through digital transformation. This way, the possible processes in which

students could get involved and propose technological solutions are increased. Lastly, the possibility of offering blended or hybrid courses should be evaluated.

This ecosystem provides adaptability and flexibility to the learning environment and, consequently, better performance and utilization by the students. Likewise, in its role as a reference or initial entry, it offers several definitions and specifications that are modifiable depending on time, environment, type of classes, etc., representing the desired objectives. Considering this, appropriate educational strategies (active, dynamic, and adaptive) must be designed and used to provide the required focus presented in Fig. 9. All of this will affect the active learning environment, the system to be controlled, where the protagonists are the students with the active guidance of the teacher. During this process, the mentioned strategies can be readjusted based on the actions and results achieved by the students. These results will enable innovative collaborative actions, which when observed, collected, and analyzed can be compared with the initial specifications of the collaborative innovation ecosystem.

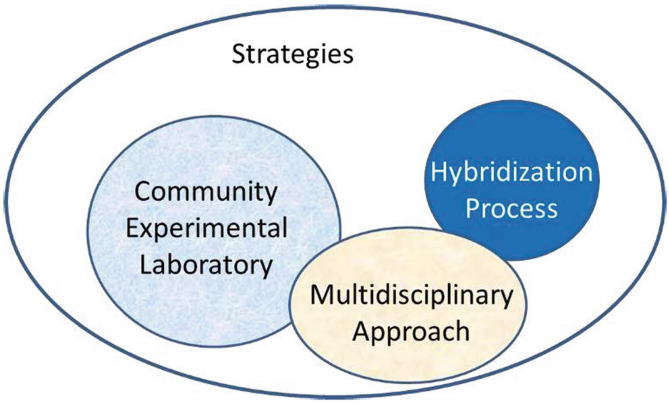

Fig. 9. Proposed Linked Strategies

Building on these strategies, a control system is proposed (Fig. 10), a concept used in robotics and industrial automation to represent a new method of active learning based on a collaborative innovation ecosystem that involves managing classes in a multidisciplinary manner.

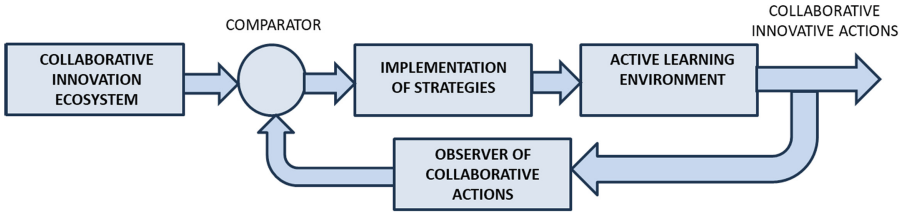

Fig. 10. Collaborative Active Control System

According to the above, three important actions are generated in the individual or group performance of students: firstly, modifying didactic strategies to achieve new innovative actions according to the initial specifications; secondly, positively validating the achievements obtained; and thirdly, ensuring that these results are relevant enough to shape the collaborative innovation ecosystem. Therefore, this control system approach allows the collaborative innovation ecosystem to also be modified through its own application on students.

5 Discussion

Several cases have been presented that address different scenarios for learning environments. Therefore, it is proposed to analyze as a team the capacity of each proposal, because determining what to do, how far to go, where to allocate resources, and setting priorities belongs to other instances of the ecosystem. This analysis does not emphasize the performance of the students who participated in the studies, but rather examined techniques, methods, and technological aspects to ensure the acquisition of meaningful learning. With all this information, the foundations of the active control system described above were established.

In the Colombian case, the resources and teaching methods used before the pandemic were continued to be employed, and during the pandemic, classes had to be adapted to the available resources. This demonstrated the resilience of teachers and students to fulfill learning outcomes by exploring new fields, such as increased use of ICT. According to Hernández [22], the use of technology makes education flexible and adaptable to changes over time, becoming increasingly dependent on it to acquire knowledge and create new understanding. In the presented case, the effectiveness of the project-based methodology and the use of available web tools to expand students' knowledge was demonstrated in a novel way, which continues to be used and expanded post-pandemic, with the new challenge of artificial intelligence.

Regarding the cases of Peru and Panama, innovations were made in both cases aimed at better utilization or reinforcement of theory for students related to control automation courses, focusing the learning action on the student. While both cases ensured the strengthening of knowledge with the techniques employed, in the Peruvian case, a comparative analysis was carried out on performance before and after the implementation of the new methodology. Although the learning environments were originally very theoretical and in a face-to-face format, the collaborative innovation ecosystem outlined included a perspective where students were active and empirical participants in the creation of their own knowledge, under the careful guidance of teachers and practical exercise coordinators in face-to-face and/or virtual sessions. The four-step methodology developed for the XSpace platform was one of the implemented strategies, and the evaluation system of the methodology was an observer of collaborative actions, in addition to the qualitative and quantitative analysis of the study conducted at PUCP.

In the case of the Dominican Republic, the UASD as a public university responded rapidly and flexibly in making well-informed decisions to ensure the continuity of education. The University demonstrated its technological capacity by providing the necessary infrastructure for administrative staff, teachers, and students to participate in the translation process effectively, as recommended by the Inter-American Development Bank

[23] with the need for "emergency remote teaching initiatives." The university adopted innovative and creative approaches to online teaching and learning, which included curating educational materials, developing new teaching materials, using virtual collaboration tools, and promoting effective interactions between non-face-to-face teachers and students.

This dynamic adaptation resolves the undeniable obligation to evolve that tends to guarantee the prolongation or survival in the face of expected or unexpected events. The mission functions of universities lead them to meet the requirements of society, and therefore, to transform and reinvent themselves by exploring new possibilities despite the complexities of their environments, taking advantage of emerging behaviors to maintain their symbolic status [24].

One aspect evident in all the presented cases is that higher education institutions (HEIs) must evaluate the education received by students during the pandemic and adjust their post-COVID-19 teaching model to a collaborative innovation ecosystem. The fact that all teachers have used some form of virtual environment tool to conduct their classes adds value to education that should not be lost [25]. HEIs must become true learning communities where students deploy their ability to learn, as the National Association of Universities and Higher Education Institutions of Mexico mentions [26], "This implies not only updating the content of curricula but incorporating substantial modifications that provide the necessary tools for continuous and independent learning, and that the forms of academic organization are more flexible to allow for more efficient and effective operation." In other words, as Serdyukov [27] indicates, the entire ecosystem that constitutes HEIs must innovate the teaching-learning process in both theory and practice because it is essential for creating a sustainable future.

Subsequently, an opportunity arises for a shift towards digital competencies and computational thinking, which currently allows for the achievement of a minimum of the objectives that guarantee the right to education. However, "the nightmare of the coronavirus wakes us from a certain educational lethargy and forces us to assume the change of the century and offers us the opportunity to greatly improve education through digital transformation" [28].

6 Conclusions and Recommendations

The presented cases demonstrate that a wealth of experiences has been gained that will allow for adjustments to the teaching-learning process so that in situations like the COVID-19 pandemic, a smooth transition to complete virtuality can be achieved. In this way, higher education institutions (IES) must be prepared with a variety of teaching methodologies, focused on both individual and group study models, and efficiently incorporate means and mechanisms of support.

Based on their own experiences and those presented, IES must tailor their collaborative innovative ecosystem model to ensure quality education in the face of any contingency that arises. This ecosystem can address multiple situations, whether simple or highly complex. Therefore, students at IES should be trained from the present to become agents of innovative and collaborative management to address unexpected and challenging situations, such as the case of COVID-19. Thus, the proposed control system

represents a significant step towards active student education, based on a collaborative and adaptive innovation ecosystem, to meet current and future needs.

This experience provides other options for all IES and the education system as a whole in the event of health emergencies that prevent physical presence, leveraging new information technologies and the era of artificial intelligence. However, fostering a humanized approach within the academic community is crucial to supporting solutions to problems that arise within the community through the knowledge imparted in the classrooms.

An interesting proposal described in this article, which could be considered for managing various local and global situations, is the implementation of an active control system with a collaborative innovation ecosystem. This ecosystem can address multiple situations, whether simple or highly complex. Therefore, students at IES should be trained from the present to become agents of innovative and collaborative management to address unexpected and challenging situations, such as the case of COVID-19. Thus, the proposed control system represents a significant step towards active student education, based on a collaborative and adaptive innovation ecosystem, to meet current and future needs.

References

1. Pérez, J.L.: Impacto de las tecnologías disruptivas en la percepción remota: Big data, internet de las cosas e inteligencia artificial. UD y la Geomática **14** (2019)
2. Ramos, B.: Análisis de la innovación en la educación superior y su impacto en la docencia. Observatorio de Innovación educativa. Tecnológico de Monterrey, México (2017)
3. Rose, E.: Disrupting «disruptive technology» in higher education. Educ. Technol. **54**(6), 56–57 (2014)
4. Piña, J.A.E.: Diseño y control de robots modulares autoconfigurables para entornos semiestructurados. Universidad Politécnica de Madrid. España, (2010)
5. Álvarez, R.: Este robot modular puede transformarse en lo que deseemos, el límite está en nuestra imaginación. Xataka. 17 de diciembre de 2016
6. Hernández, D.G.: EMERGE, pionero en robótica modular en Colombia. Un Periódico Digital 19 de agosto de 2019. Universidad Nacional de Colombia
7. Jiménez-Builes, J., Ramírez, J., González, J.: Sistema modular de robótica colaborativa aplicado en educación. Revista Facultad de Ingeniería, 58. Proyecto Robótica Educativa: Máquinas Inteligentes en Educación (2010)
8. Universidad Autónoma de Sinaloa Parque de Innovación Tecnológica. Sexto aniversario (2020). https://m.facebook.com/323574984515362/posts/1280516788821172/?notif_id=1589558405655284&notif_t=scheduled_post_published&ref=notif
9. Gros, S.B., Lara, N.P.: Estrategias de innovación en la educación superior: El caso de la Universitat oberta de Catalunya. Revista Iberoamericana de Educación **49**, 223–245. España (2009)
10. Gómez, N.P., Motta, D.V.: Subjetividad estudiantil: percepciones ante la pandemia COVID-19 y desafíos de la implementación de la metodología virtual. Cambios y Permanencias **11**(2), 465–495 (2020). https://revistas.uis.edu.co/index.php/revistacyp/article/view/11707
11. IESALC. Los retos de las universidades latinoamericanas para el siglo XXI/Mundo UNTREF. 2 octubre, 2019 Prácticas sustentables, Retos, Universidades (2019)

12. Chiroleu, A.: La educación superior en américa latina: ¿problemas insolubles o recetas inadecuadas?. Avaliação (Campinas) **16**(3), 631–653 (2011). ISSN 1414-4077. https://doi.org/10.1590/S1414-40772011000300008
13. Falcón, C.: Un Nuevo modelo de gerencia y gestión académico administrativo para la universidad venezolana. Palermo Business Review. Universidad de Palermo. MBA Graduate Scholl Business No. 13, pp. 111–129. Argentina (2016)
14. Paz, E., Hernández, E., Van de Water, H.: Los retos de la Educación Superior en el Siglo XXI. Revista Conrado **12**(55), 17–24 (2016). https://www.researchgate.net/publication/312043293_LOS_RETOS_DE_LA_EDUCACION_SUPERIOR_EN_EL_SIGLO_XXI
15. Cegarra, S.J.: Metodología de la investigación científica y tecnológica. Editorial Díaz de Santos, Madrid, España (2004)
16. Fondo de las Naciones Unidas para la Infancia (UNICEF). El Aprendizaje Basado en Proyectos En Planea: Enfoque general de la propuesta y orientaciones para el diseño colaborativo de proyectos. 1 ed., UNICEF, Buenos Aires (2020). https://www.unicef.org/argentina/media/10171/file/planea-ABP.pdf
17. Chen, Y., Naughton, J.: An undergraduate laboratory platform for control system design, simulation, and implementation. IEEE Control Syst. Mag. **20**(3), 12–20 (2000). https://doi.org/10.1109/37.845034
18. Silawatchananai, C., Ruangurai, P.: Designing a project-based plant to enhance mechatronics students for self-learning embedded control system. In: 29th International Conference on Computers in Education Conference, ICCE 2021 - Proceedings, vol. 2, pp. 631–636 (2021)
19. Cárdenas, P., Cieza, L., Horna, I., Pauyac, C., De-La-Cruz, C., Tafur, J.: XSpace: self-learning platform for implementation of digital control algorithms. In: 2023 IEEE Global Engineering Education Conference (EDUCON), Kuwait, Kuwait, pp. 1–5 (2023). https://doi.org/10.1109/EDUCON54358.2023.10125187
20. Universidad Autónoma de Santo Domingo [UASD]. Plan de contingencia y reprogramación académica ante la pandemia de COVID-19. Santo Domingo, Distrito Nacional. República Dominicana. (2020). https://hoy.com.do/wp-content/uploads/2020/05/Plan-de-Contingencia-y-Reprogramacion-Academica-UASD-2020.pdf
21. Universidad Autónoma de Santo Domingo [UASD]. Informe de gestión 2018–2022: Dirección de educación virtual. Santo Domingo, Distrito Nacional. República Dominicana (2022). https://www.calameo.com/read/0071203027c7a0fd6bd16
22. Hernández, R.M.: Impacto de las TIC en la educación: Retos y Perspectivas. Propósitos y representaciones **5**(1), 325–347 (2017). https://dialnet.unirioja.es/servlet/articulo?codigo=5904762
23. Banco Interamericano de Desarrollo. La educación en tiempos del coronavirus: Los sistemas educativos de América Latina y el Caribe ante COVID-19 (2020). https://doi.org/10.18235/0002337
24. Roncancio-Roncancio, P.: La adaptación y las instituciones de educación superior: conceptos y desafíos. Revista iberoamericana de educación superior **11**(32), 198–214 (2020). https://doi.org/10.22201/iisue.20072872e.2020.32.822
25. Segarra, P.: El escenario más probable en la Universidad es el que combine la docencia presencial con la virtual. 20 Minutos. (2020, 20 de mayo). https://www.madridmasd.org/notiweb/noticias/escenario-mas-probable-en-universidada-es-que-combine-docencia-presencial-virtual#utm_source=notiweb_newsletter&utm_medium=email&utm_campaign=noti1_20may20
26. Asociación Nacional de Universidades e Instituciones de Educación Superior de México (ANUIES). La Educación Superior en el Siglo XXI Líneas estratégicas de desarrollo. Una propuesta de la ANUIES (Asociación Nacional de Universidades e Instituciones de Educación Superior), ISBN 968-7798-59-9 Impreso y hecho en México (2000)

27. Serdyukov, P.: Innovation in education: what works, what doesn't, and what to do about it? J. Res. Innov. Teach. Learn. ISSN 2397-7604 Emerald insight, Serdyukov, P., Discover Journals, Books & Case Studies (2017). https://www.emerald.com/insight/content/doi/10.1108/JRIT-10-2016-0007/full/html
28. Cotino Hueso, L.: La enseñanza digital en serio y el derecho a la educación en tiempos del coronavirus. Revista de Educación y Derecho **21**, 1–29 (2020)

Swerve Drive Autonomous Robot for Tiles Thermographic Inspection

Humberto Rodríguez[1(✉)], Víctor Pérez[2], and Octavio Echeverría[2]

[1] LEADS Research Group, Universidad Tecnológica de Panamá, Panama city, Panama
humberto.rodriguez@utp.ac.pa

[2] Fab Lab-UTP, Universidad Tecnológica de Panamá, Panama city, Panama
fab.lab@utp.ac.pa

Abstract. Quality inspection of buildings is a task that can be tedious and prone to human errors, so the use of autonomous mobile robots is very attractive. In this work, a swerve drive mobile robot is proposed for tile hollowness inspection using an active thermographic approach. It integrates a hot air blower as heating source and an infrared thermal camera to observe the hollow region contour, which is the result of the characteristics of the thermal diffusion process in different media. In addition, image processing techniques were used to segment the hollow region contour. As a result, an automatic, fast and effective inspection strategy is proposed.

Keywords: swerve drive · inspection robot · thermographic inspection · hollowness inspection

1 Introduction

Applications of Robotics in the construction sector cover many areas such as, manufacturing of products, steel welding, finishing, tile placement, coating, material handling and inspection [1–3]. Specially, the use of robots for inspection has made significant progress in the last decade, with the application of drones for buildings and infrastructure inspection, ROVs for underwater inspection and mobile robots (wheeled and legged) for quality inspection [4]. In general, quality inspection is a task which can be tedious and prone to human errors, so robots can be more efficient and reliable in their execution than human workers. Moreover, when Non-destructive Testing (NDT) techniques need to be used, these can be easily integrated within the robot for a faster and more precise evaluation of the building condition. For instance, tile hollowness testing accuracy and reliability can be greatly improved by using mobile robots [5].

In this work a mobile robot is proposed for tile hollowness inspection using an active thermographic approach, instead of the more common percussion method, that can be found even in commercial robots [6]. The traditional way of testing tile hollowness is by knocking the tile and listening to the sound frequency, which is not an accurate method to distinguish the severity of the tile condition, even for a skilled worker. Thus, some inspection robots have integrated more

M. N. Cardona et al. (Eds.): LACAR 2023, LNNS 940, pp. 20–30, 2024.
https://doi.org/10.1007/978-3-031-54763-8_2

advanced signal processing techniques, such as the WICBOT, that uses wavelet packet decomposition, [7]. However, for a more accurate identification of the hollow area, thermographic inspection has proven to be a valuable diagnostic tool for facade and floors [8]. Both passive and active thermographic techniques have been investigated with good results in the detection no only of hollowness, but also cracks and general defects [9]. The ASTM C-1060-11a is the standard practice guideline for thermographic inspection of insulation installations in cavities of building structures [10]. It is worth to mentioned that, in general, the preferred heating method for inspection is infrared radiation which is much less efficient than convection heating. In this work, a new, more efficient heating method is proposed, which uses convective heat transfer instead of radiation heat transfer, and which was conveniently incorporated into an autonomous mobile robot for inspection.

2 Description of the Robotic System

In this section, the main components of the mechanical system, the electronic hardware and the sensory system of the robot are described.

2.1 Mechanical System Description

Figure 1 shows the mobile platform named OmniTrack, developed in our Lab (the Lab for Engineering Analysis, Design and Simulation, LEADS), which is based on a swerve steering mechanism (SSM), i.e., with independent driving and steering capabilities at each wheel. This type of drive model can provide a higher speed and maneuverability compared to the Ackermann steering, and Omni wheel drive models (with mechanum wheels). However, a higher number of motors is required for SSM and, also, a more complex control algorithm needs to be used to simultaneously control the speed and orientation of each wheel when moving along a trajectory.

In order to carry out nondestructive testing of tiles, OmniTrack has been equipped with a 1.8 KW hot air blower and a thermal micro-camera Lepton 3.5 (both shown in Fig. 1) to detect hollow regions under the tiles. On the other hand, for navigation and obstacle avoidance purposes, it also incorporates a RPLIDAR-A2 laser range scanner, a tracking camera T265 and depth camera D435, the latter two from Intel RealSense.

Every wheel has a brushless (BLDC) hub motor and a steering module, that includes a DC brushed dc motor, its driver and gears. Additionally, the BLDC motor driver is located inside this module.

A 4 wheel swerve drive platform is particularly well-suited for construction site inspection applications, as it can easily maneuver in tight spaces while maintaining orientation of the sensors. In addition, It has good traction and payload capacity. In general, a swerve drive exhibits the following advantages [11]:

- Mobility: Drive direction is independent from chassis orientation, thus swerve drive vehicles have a larger range of motion.

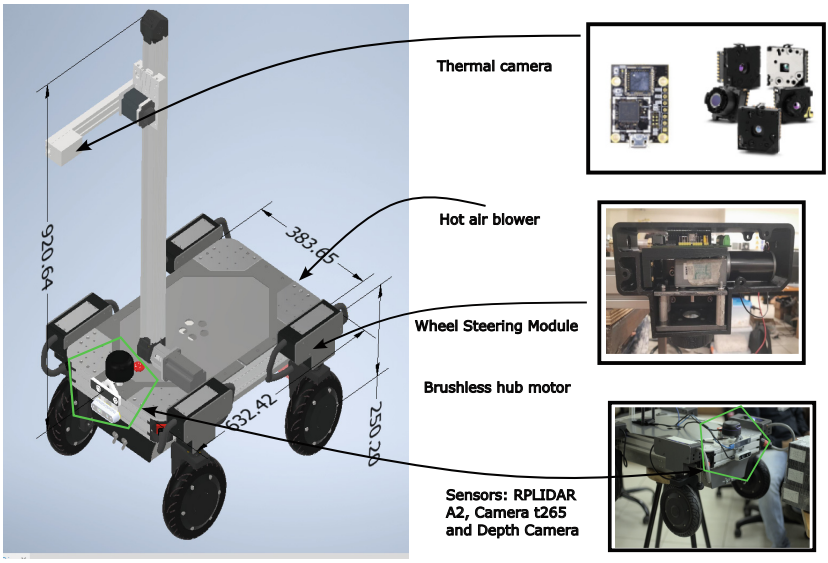

Fig. 1. OmniTrack main components

- Traction: The traction force can be aligned in any direction. In addition, high traction wheels can be used, unlike mecanum wheels which suffer from power loss.
- Irregular surface: Swerve-drives does not need an even ground and can be used outdoors.
- Flexibility: Ability to operate in different drive modes switchable through software. Serves as a single platform to test control and navigation algorithms for the different drive modes.
- Modularity: Each swerve module can be independently change if needed.

2.1.1 Inverse Kinematics of Swerve Drive Platforms

For a given angular and linear velocity of the platform, ω and v_R respectively, the inverse kinematics equations give the speed and orientation of each wheel. As shown in Fig. 2, the resultant linear velocity at each wheel, v_w, is given by the vector sum of the robot's linear velocity, v_R and the vector $R\omega$, [11].

$$v_w = v_R + R\omega \tag{1}$$

Decomposing the resultant linear velocity for the front right wheel, for instance, we obtain the x and y components as:

$$\begin{aligned} v_{1_x} &= v_{Rx} + R_x\omega \\ v_{1_y} &= v_{Ry} - R_y\omega \end{aligned} \tag{2}$$

Thus, writing the equations for the 4 wheels in matrix form gives:

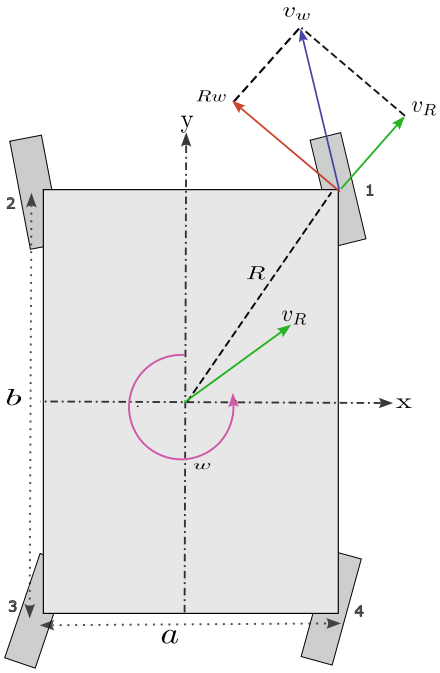

Fig. 2. Velocity vectors used for the inverse kinematics problem

$$\begin{bmatrix} v_{1_x} \\ v_{1_y} \\ v_{2_x} \\ v_{2_y} \\ v_{3_x} \\ v_{3_y} \\ v_{4_x} \\ v_{4_y} \end{bmatrix} = \begin{bmatrix} 1 & 0 & R_x \\ 0 & 1 & -R_y \\ 1 & 0 & R_x \\ 0 & 1 & R_y \\ 1 & 0 & -R_x \\ 0 & 1 & +R_y \\ 1 & 0 & -R_x \\ 0 & 1 & -R_y \end{bmatrix} \begin{bmatrix} v_{Rx} \\ v_{Ry} \\ \omega \end{bmatrix} \tag{3}$$

where, $R_x = b/2$ and $R_y = a/2$.

Finally, to determine the steering angle, Φ_i, and angular velocity, ω_i, for the ith wheel, the following equations are used.

$$\Phi_i(rad) = \tan^1\left(\frac{v_{i_y}}{v_{i_x}}\right) \tag{4}$$

$$\omega_i(rad/s) = \frac{\sqrt{v_{i_x}^2 + v_{i_y}^2}}{wheelradius} \tag{5}$$

2.2 Electronics and Communication

Figure 3 shows the main electronic components and the communication architecture of OmniTrack. The robot has a Jetson Xavier NX computer that is responsible for operating the systems navigation and high level motion control. It has four dc motors for steering of the wheels (BDC in the diagram) independently and four brushless motors located in the wheel's hubs that are responsible for spinning each wheel. Above each steering motor, a couple of electronic boards are located, which are responsible for carrying out the orientation and speed control of each wheel by means of a pair of ARM based microcontrollers, namely a Cortex-M0 for the BDC driver and a Cortex-M4 for the BLDC driver, therefore a good real time response is obtained.

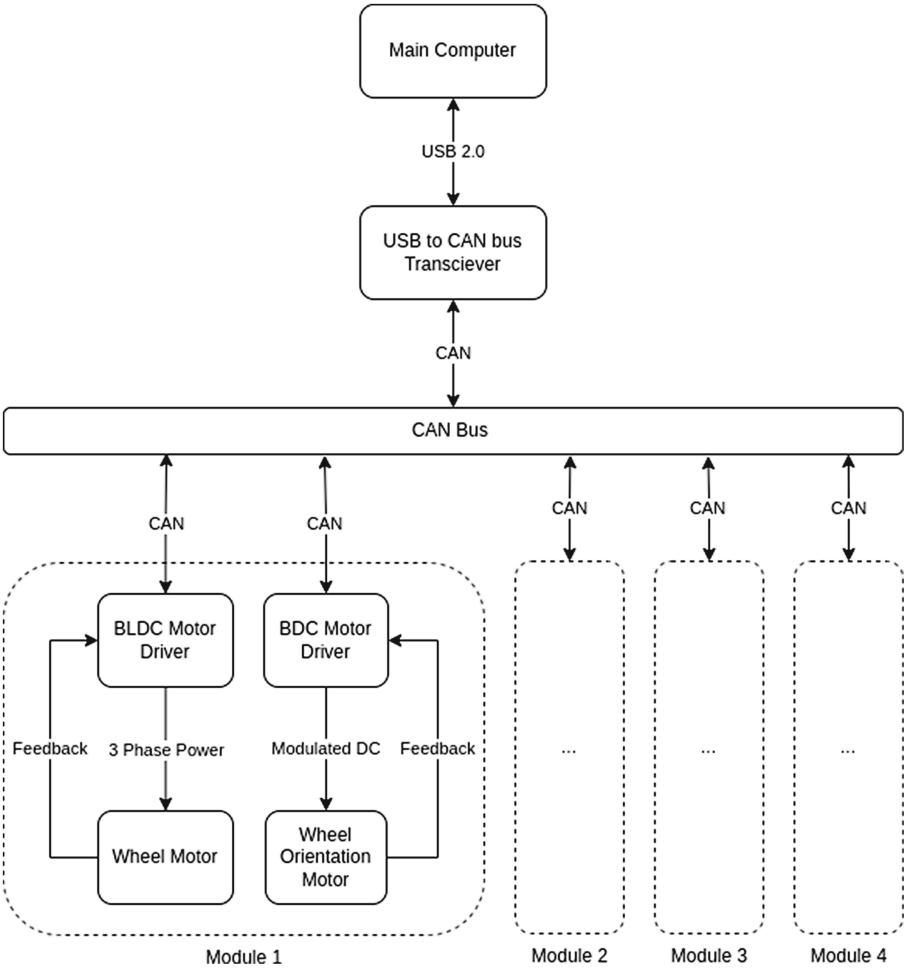

Fig. 3. OmniTrack communication diagram

All robot modules communicate via the CAN communication protocol and they are connected to a USB-CAN transceiver.

2.2.1 Thermal Vision Package

To obtain the thermal images, the Lepton 3.5 module was selected. This module can be used with OpenCV and its SDK is an open resource. It is a micro-thermal camera with an operating temperature range of +80 °C and a scene dynamic range of −10 °C to +400 °C in low gain mode, with 160 × 120 pixels of radiometric output. It is capable of capturing very accurate temperature data and easy to integrate with native mobile devices and other electronic equipment.

3 Control Architecture

In terms of the control system, a multi-level control is used, where the low-level control regulates the speed and orientation of each wheel drive relative to the robot's body. Meanwhile, high-level control is used to coordinate the movement of each wheel so that the results can make the robot to move according to the given trajectory. Figure 4 shows how the different components (CAN nodes, CAN devices, interfaces and applications) are organized in the ROS (Robot Operating System) environment.

3.1 Robot Description and Navigation Package

A robot description and navigation packages were developed for the swerve platform. The description package contains the visual URDF (Unified Robot Description Format) model and the interface elements for the robot. On the other hand,

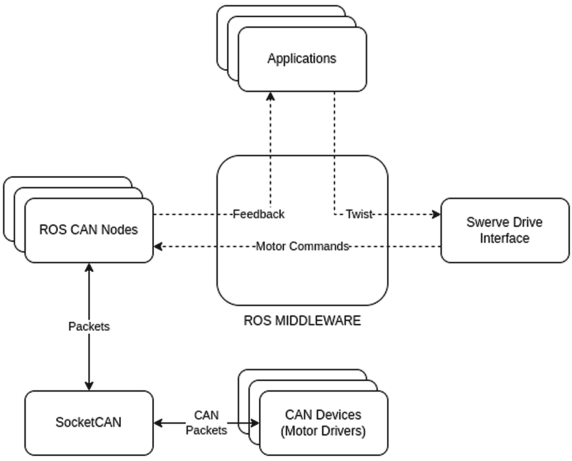

Fig. 4. OmniTrack ROS environment

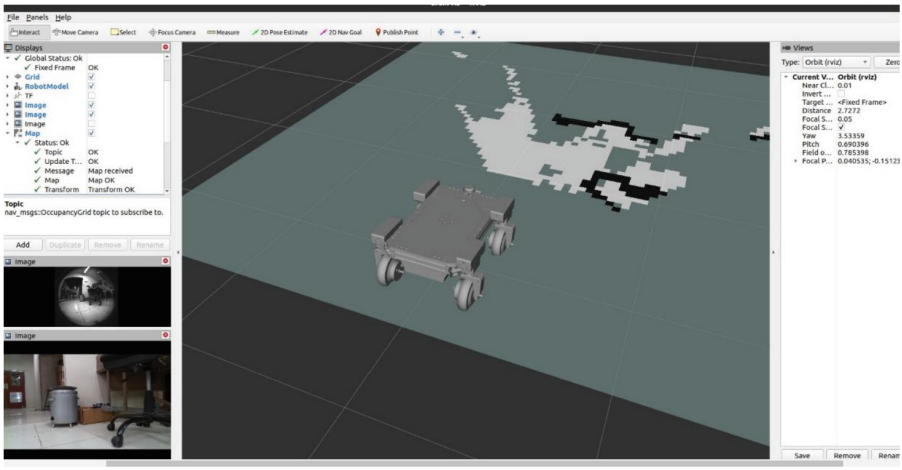

Fig. 5. Test of the OmniTrak navigation stack for SLAM

a ROS navigation stack was configured to process the sensors information and send the speed and orientation to the swerve drive interface as shown in 4.

In Fig. 5 the Omnirak is generating a map which was later used to command missions, so the robot could navigate autonomously avoiding obstacles. As mentioned above, this robot incorporates a lidar and an RGBD camera that were used to perform SLAM (Simultaneous Location and Mapping).

4 Inspection Test and Strategy

The hollowness inspection method proposed in this work focuses on using convection heating, on small areas, and automating the floor area coverage and data processing with a system installed on board of a swerve drive mobile platform. Hot air heating has the advantage of being more compact and cheaper than other heat sources, for instance IR lamps, that already have been used for active inspection [4].

Initially, as part of the feasibility evaluation of the proposed inspection method, multiple tests were carried out with different heating patterns, ambient temperatures and initial temperatures of the floor. The objectives of these tests were to verify what was the minimum heat input and its corresponding tile temperature increment, that would allow to see a clear image of the defect at some point during the thermal diffusion process; the accuracy of the contour obtained with respect to the real one and how the best time for observation of the defect was affected by the tile material and dimensions. The latter will no be addressed on this article, due to limited space to present the details.

The first step, before applying heat, was to use the percussion method to determine the contour of the hollow region of a defective tile. This initial contour was drawn on the tile surface for later comparison. Figure 6 shows a sequence

of images which represent the same experiment in which heat was applied for 25 to 30 s, follow by a pause of 10 to 15 s before taking the thermal images. Subsequently, thermal images were taken separated by 30 s. After this time we could perceive how the heat dissipates, producing a very clear contour in the thermal images (a) and (b). The hottest areas (in red) correspond to hollow areas, where the heat is stored for a longer time, due to larger thermal capacity of air than thermal capacity of ceramics. In images (c) and (d) we can still observe the presence of heat in the cavity of the tile, after several minutes.

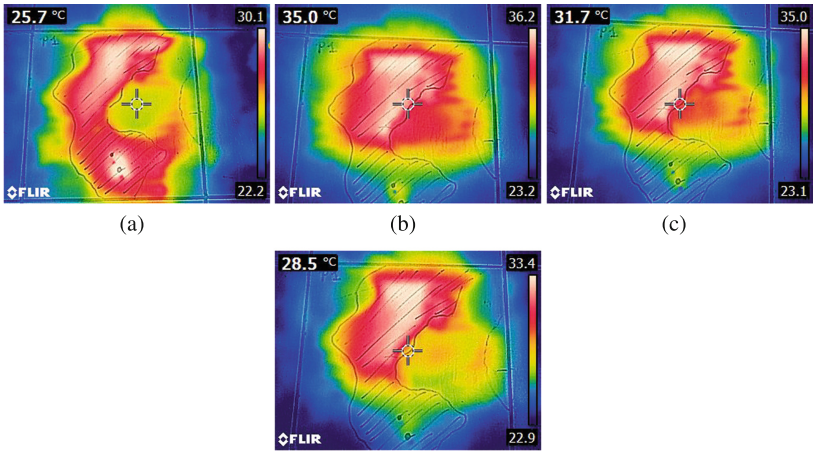

Fig. 6. Thermal images after applying heat, taken every 30 s. Image at 30 s (a), 130 s (b), 190 s (c) and 250 s (d)

This experiment was carried out with different heating times and it was possible to determine that, applying a heat flux of 20 kW/m^2, it is necessary to heat the surface of the tile for at least 30 s to obtain accurate results of the failure and consuming the least amount of energy possible. Moreover, it was observed that the closest contour to the actual hollow region contour happens before 40 secs have elapsed, after heat application, in general. This is an important outcome, since the inspection time directly depends on this time. The robot will need to wait this time to move to a new floor sector.

Based on the test results, the inspection strategy includes the following steps:

1. The robot move forward until it recognizes the edges of the tile.
2. Heat is applied with one or two diffusers (depending on the size of the tile) moving them transversely, while the robot advances.
3. After heating the tile for 30 s, the robot would move to the next tile.
4. While proceeding to heat the new tile, the thermal camera, located at the back of the robot, takes images of the previous tile. In other words, it would

have approximately 30 s (considering that some seconds has elapsed while the robot moved to the next region) to capture the moment in which the contour of the fault is better appreciated. According to the experiments, this would be enough time to have a good picture of the failure.
5. After capturing the images, segmentation techniques are used to extract the contour of the hollowness.
6. If the area of the contour is greater than a given threshold, the image of the hollow region is stored, together with the information of its coordinates, to download it at the end of the journey and include it in the inspection report.

4.1 Image Processing for Hollowness Identification

For the last step of the previous strategy, a processing method will be used that has already been tested with real images from hollowness inspections. The method consists of first converting the image to gray scale, and then applying local thresholding. Once the hollowness areas (with the lighter gray) are segmented, an algorithm that assets the severity of the defect is used to decide whether to reinstall the tile or not. In an intermediate step, the median filter is also applied to eliminate and impulsive noise or marks superimposed by the thermal camera, such as the cross-hair symbol that indicates the fixed coordinated where the camera is set to measure a temperature. For the tests of this segmentation method, a code was written in Python, making use of the OpenCV library. Figure 7 shows an example of the results obtained. The tile was later uninstalled and the actual hollowness area was verify, which turned out to be very close in shape and size of the image.

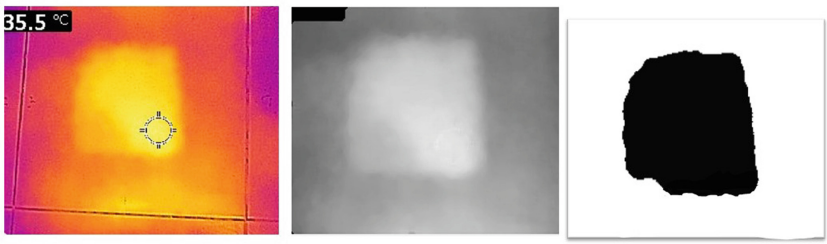

Fig. 7. a) original image b) trimmed gray scale image c)after applying median filter and local thresholding

5 Conclusions

In this work, the development of an autonomous robotic platform for non-destructive inspection of floor tiles has been presented. The inspection method is based on the difference in the heat diffusion process in the hollow region of

the tiles compared to the areas with good adhesion. The main contribution is in the form of a fast inspection strategy that uses a swerve drive autonomous platform, a new heating method and artificial intelligence (image processing) to automatically and accurately segment those areas poorly adhered to the floor. The new heating method uses hot air convection instead of the infrared radiation used by other authors. In addition, The integration of the hot air heating source in a mobile robot for active infrared thermographic inspection has shown to be a feasible and practical alternative. Heating the tiles with infrared radiation is less efficient than using convection heating, so the proposed heating method provides greater autonomy for autonomous robot inspection. In addition, a sequence of fast and effective image processing techniques for the segmentation of thermal images was successfully tested. The average root mean square error was of less than 4 mm of difference between the actual defect contour and the estimated with our autonomous robotic system. Furthermore, the resolution of our method is much better than lightly hammering the tile, for edge detection of the hollow area.

As for future work, machine learning will be used for the estimation of heat transfer parameters, so that the heat diffusion process can be simulated to obtain the optimal inspection time and robot speed. Those parameters depend on the composition of the tiles, the thickness of the tiles and also on the ambient temperature and humidity. Another line of research that has been considered is to use the robot for detecting other defects simultaneously, like cracks and misalignment. Furthermore, several robots could be used for large areas with the corresponding coverage path planning algorithm.

Acknowledgement. The authors thank the funding from the Secretaría Nacional de Ciencia, Tecnología e Innovación de Panama (SENACYT) under the project "Plataforma Robótica Móvil Multifuncional" with Grant No. INNOVATEC21-060, Contract No. 129-2022.

References

1. Halder, S., Afsari, K.: Robots en Inspección y Monitoreo de Edificios e Infraestructura: Una Revisiòn Sistemática. Ciencias Aplicadas **13**(4), 2304 (2023). https://doi.org/10.3390/app13042304
2. Asadi, B., Li, B., Chen, I.: A cooperative painting Pictobot: robot for interior finishing of industrial developments. IEEE Robot. Autom. Mag. **25**, 82–94 (2018)
3. Wang, S., Zhou, H., Zhang, Z., Zheng, X., Lv, Y.: Robot floor-tiling control method based on finite-state machine and visual measurement in limited FOV. In: Advances in Civil Engineering, vol. 2021, Article ID 8372815 (2021). 16 pages.https://doi.org/10.1155/2021/8372815
4. Yan, R.-J., Kayacan, E., Chen, I.-M., Tiong, L.K., Wu, J.: QuicaBot: quality inspection and assessment robot. IEEE Trans. Autom. Sci. Eng. **16**(2), 506–517 (2019). https://doi.org/10.1109/TASE.2018.2829927
5. Luk, B.L., Liu, K.P., Jiang, Z.D., Tong, F.: Robotic impact-acoustics system for tile-wall bonding integrity inspection. Mechatronics **19**(8), 1251–1260 (2009). https://doi.org/10.1016/j.mechatronics.2009.07.006

6. TRANSFORMA. https://www.transformarobotics.com/knockbot. Accessed 29 Apr 2023
7. Inoue, F., Doi, S., Okada, T., Ohta, Y.: Development of automated inspection robot and diagnosis method for tile wall separation by wavelet analysis. In: Caldas, C.H., O'Brien, W.J., Chi, S., Gong, J., Luo, X. (eds.) Proceedings of the 2009 International Symposium on Automation and Robotics in Construction (ISARC 2009), pp. 379–388 (2009). https://doi.org/10.22260/ISARC2009/0032
8. Garrido, I., Barreira, E., Almeida, M.S.F., R., Lagüela, S.: Introduction of active thermography and automatic defect segmentation in the thermographic inspection of specimens of ceramic tiling for building façades. Infrared Phys. Technol. **121**, 104012 (2022). https://doi.org/10.1016/j.infrared.2021.104012
9. Lourenço, L., Matias, L., Faria, P.: Anomalies detection in adhesive wall tiling systems by infrared thermography. Constr. Build. Mater. **148**, 419–428 (2017)
10. ASTM International: Standard practice for thermographic inspection of insulation installations in envelope cavities of frame buildings **C1060**, 11a (2015)
11. Tagliavini, L., Colucci, G., Botta, A., et al.: Wheeled mobile robots: state of the art overview and kinematic comparison among three omnidirectional locomotion strategies. J. Intell. Robot. Syst. **106**, 57 (2022). https://doi.org/10.1007/s10846-022-01745-7
12. Liu, L., Yan, R.-J., Maruvanchery, V., Kayacan, E., Chen, I.-M., Tiong, L.K.: Transfer learning on convolutional activation feature as applied to a building quality assessment robot. Int. J. Adv. Robot. Syst. **14**(3) (2017). https://doi.org/10.1177/1729881417712620

Crutch Load Monitoring System for an Adequate Rehabilitation

Alexandre Campos(✉), Wladymir Kulkamp, Jaqueline de Souza, Rafael Campos, and Deborah Kunzler

Universidade do Estado de Santa Catarina, Florianopolis, Santa Catarina, Brazil
{alexandre.campos,wladymir.kulkamp,jaqueline.souza,deborah.hizume}@udesc.br, rafael.campos2006@gmail.com

Abstract. A crutch accessory that provides real-time feedback, assisting lower limb injury patients in finding the predetermined force to be applied, is developed. Improper usage of forearm crutches, due to the user lack of sense regarding the correct forces to be applied, is a frequent misuse. Proper forces must be applied, both on the injured leg and the crutch, throughout the rehabilitation process. The mitigation of this misuse reduces the required time for complete recovery. Nowadays, this problem is alleviated by instructing the patient on the predetermined forces through verbal instruction and the use of scales, but only once at the beginning. Using this accessory and a motion capture suit, it is observed, that the predetermined force and proper ankle angles are reached easier and more consistently, whereas without the accessory, it was more difficult and without cadence, also being less comfortable. This device promotes the possibility for faster and proper rehabilitation, which will be researched in future works.

1 Introduction

The first study discusses patient compliance with weight-bearing protocols during lower extremity fracture recovery [3]. Patients often struggle to adhere to non-weight-bearing and partial weight-bearing protocols, with most compliance seen in weight bearing as tolerated. Furthermore, patients weight-bearing progressions varies, suggesting the ability to self-regulate without compromising healing outcomes. The second study explores the effects of early partial weight-bearing rehabilitative exercise on postoperative recovery after Sanders IV calcaneal fractures [4]. Patients who undergo early partial weight-bearing show notably superior foot function compared to the control group, indicating the effectiveness of this approach in promoting functional recovery without compromising internal fixation or calcaneus shape.

Despite providing instructions, both verbal and through use of scales, achieving patient compliance with partial load guidelines remains challenging, and quantifying the actual load applied is often subjective, although some authors

M. N. Cardona et al. (Eds.): LACAR 2023, LNNS 940, pp. 31–36, 2024.
https://doi.org/10.1007/978-3-031-54763-8_3

disagree [5]. This variability arises from factors such as cognitive comprehension, body awareness, and the inherent difficulty in accurately measuring the load exerted on the affected limb.

Forearm crutches play a significant role in lower limb injury rehabilitation, with correct weight-bearing being crucial for improved recovery rates [6,8]. Incorrect usage can lead to extended recovery periods and further damage to the limb. To address this, researchers developed an instrumented forearm crutch with wireless monitoring capabilities to track weight bearing throughout the patient's recovery, even in a home environment. The crutches are equipped with low-cost wireless sensor nodes, providing indicative measurements of weight, crutch tilt, and hand position. The initial results show the potential of this system to support physiotherapists and patients in monitoring usage effectively. Another study focuses on developing a prototype to monitor the axial force and tilt angles during gait cycles for patients using forearm crutches [7]. Promising experimental results indicate the possibility of identifying gait patterns and typical errors during crutch usage, offering individualized therapy for rehabilitation. Additionally, Smart Crutches, an instrumented crutch system, measures the weight placed on lower extremities and provide vibratory feedback [1]. Machine learning regression methods, particularly Gaussian kernel, shows improved accuracy in estimating ground reaction forces during crutch gait, offering an alternative to force plates for assessing patient progress. Such instrumented crutches could assist in ambulatory rehabilitation and aid in developing new assistive controllers for exoskeletons, making them a valuable tool in the rehabilitation process. Also a ROKOKO motion capture suit is used to accurately measure and monitor the rehabilitation progress of orthopedic patients [2]. The suit captures joint ranges and orientation during movement, allowing patients to self-monitor exercises within permitted ranges. The mocap suit connects to a computer visual feedback, and data representation to track progress.

2 Development

2.1 Materials and Method

The initial phase of the prototype construction involves developing a data acquisition system using components such as an Arduino Nano prototype board Fig. 1a, an analog-to-digital converter module with an amplifier Fig. 1b, and two balance-type load cells Fig. 1c. These load cells, which are half-bridge Wheatstone sensors, measure electrical resistance based on applied pressure. Incorporating two load cells forms a complete bridge. The system includes LEDs to offer immediate visual feedback to the physiotherapist or doctor regarding the load applied to the crutch Fig. 1d. A green LED indicates recommended load levels, while a red LED indicates overload. Additionally, the patient receives similar feedback through the crutch vibration, generated by a vibrating motor from LG used in Joysticks Fig. 1e.

The crutch used for the prototype construction was of the Canadian type, with an adjustable forearm handle and height adjustment. The load cells were

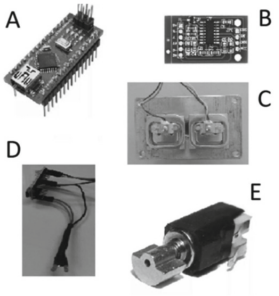

Fig. 1. Electronic components of the data acquisition system

mechanically incorporated into the central axis of the crutch, so that the load transfer was fully identified. Two load cells with a capacity of 50 kg each were used, allowing for overloads of up to 100 kg (as shown in Fig. 2).

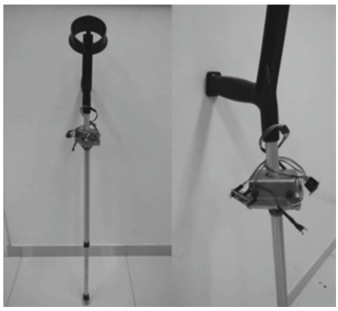

Fig. 2. Instrumented crutch prototype

The study procedures are comprised of two tests. The first test aims to assess the load cells linearity by using a progressive load approach. Known gym plates, ranging from 2 kg to 9.9 kg, were placed on the crutch and aligned with the load cells to serve as reference weights. The relationship between the known masses and the values recorded by the data acquisition system was analyzed using the coefficient of determination (R^2) as an indicator. An R^2 value greater than 0.99 ensured the validity and accuracy of the data acquisition system.

In the second test, the visual and vibratory feedback sensors incorporated into the crutch are examined. An overload threshold of approximately 300 N was programmed into the system's microcontroller. To evaluate the sensors activation capacity, a researcher conducts a load transfer while standing in an orthostatic position. The effectiveness of the feedback provided by the sensors during this test is thoroughly assessed.

2.2 Procedures

The testing protocol commences with the participant wearing a motion capture suit specifically calibrated to a neutral standing position. This step ensures accurate tracking of movements throughout the test. Next, the instrumented crutch is carefully calibrated using a known weight, guaranteeing precise and reliable measurements. During the setup, a qualified therapist provides a comprehensive verbal instruction, assisted by regular scales to check the user understanding. This preparatory phase ensures that the subsequent test results are as reliable as possible.

The test itself consists of a linear walk, during which the participant takes small, cadenced steps while relying on the instrumented crutch. The step is to be taken as the red LED turn off and the green LED turns on, serving as an indicator that the predetermined force for has been reached, therefore ensuring that the participant safely distributes their weight on the injured foot, reducing the risk of further discomfort or harm and rehabilitation time. To establish a basis for comparison, the entire procedure is then repeated using a regular crutch.

By doing so, the data, comprised of several joints angles and load cell values, obtained from both methods can be compared, enabling a thorough analysis of the effectiveness and potential benefits of the instrumented crutch for rehabilitation purposes.

3 Data Analysis

In this section, some statistical results are presented. Firstly, a correlation list for 103 columns, consisting of angles and translations, based on ankle angles is created. The result is that neck right-ward rotation is closely correlated with the injured ankle. Additionally, pelvis and ankle velocity increase as the applied

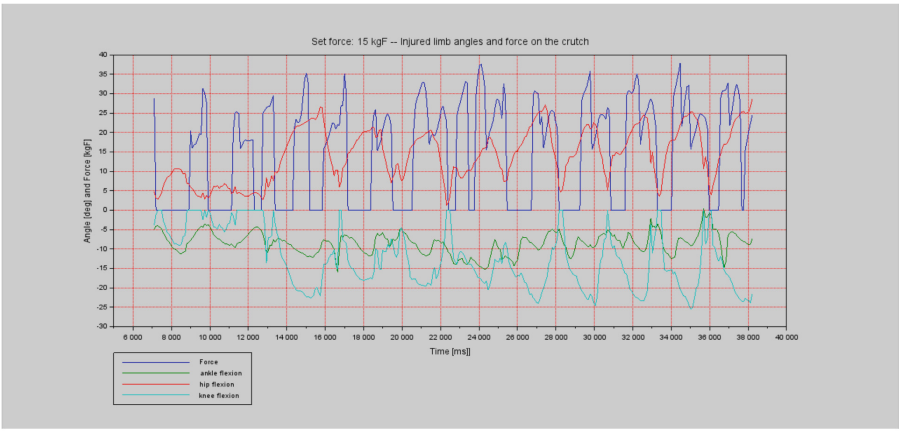

Fig. 3. Knee, Ankle and Hip Flexions alongside Force

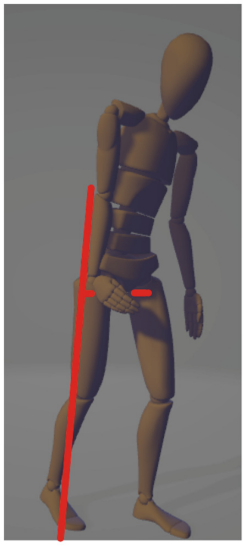

Fig. 4. 3D model with a crutch (as the red line)

force decreases. In the case of a 20-kilogram force applied with the instrumented crutch and a stock crutch, we identify a couple of significant relationships. The maximum angle of dorsiflexion is greater with the instrumented crutch, while the mean knee flexion is greater with the stock crutch. Moreover, in the test involving the stock crutch, we observe that the joints exhibit greater maximums, leading to increased effort for the user. A example graph for greater clarity is shown in Fig. 3. Also a in Fig. 4 a representation of the crutch and a 3D model of the individual using it.

4 Conclusions

The primary observation centers around the user ease in attaining the predetermined force level while maintaining a consistently low margin of error, which consistently fluctuates around the specified force threshold. Additionally, the cadence is characterized by a deliberate and controlled pace, accompanied by dorsiflexion angles that fall within the healthy range of motion. This deliberate movement encourages the ankle to exercise in an optimal manner while facilitating a swift recovery process. Moreover, this controlled approach to exercise appears to distribute less stress to other joints, leading to a thoroughly comfortable and effective workout experience. The user not only achieve their target force levels with precision but also do so in a manner that promotes overall joint health and comfort during the exercise regimen.

References

1. Chen, Y.F., Napoli, D., Agrawal, S.K., Zanotto, D.: Smart crutches: towards instrumented crutches for rehabilitation and exoskeletons-assisted walking. In: 2018 7th IEEE International Conference on Biomedical Robotics and Biomechatronics (Biorob), pp. 193–198 (2018)
2. Gupta, P.K., Verma, P., Gupta, R., Verma, B.: Movaid- a novel device for advanced rehabilitation monitoring. In: 2015 37th Annual International Conference of the IEEE Engineering in Medicine and Biology Society (EMBC), pp. 4655–4658 (2015)
3. Lajevardi-Khosh, A., et al.: Characterization of compliance to weight-bearing protocols and patient weight-bearing behavior during the recovery period in lower extremity fractures: a pilot study. Current Orthopaedic Practice **30**, 395–402 (2019)
4. Li, Y., Xie, L., Li, W.: Effect of early partial weight-bearing rehabilitative exercise on postoperative functional recovery of sanders iv calcaneal fractures. Am. J. Transl. Res. **13**(7), 8316–8322 (2021)
5. Malviya, A., Richards, J., Jones, R.K., Udwadia, A.D., Doyle, J.: Reproducibilty of partial weight bearing. Injury **36**(4), 556–9 (2005)
6. Merrett, G.V., Ettabib, M.A., Peters, C.M., Hallett, G., White, N.M.: Augmenting forearm crutches with wireless sensors for lower limb rehabilitation. Meas. Sci. Technol. **21**, 124008 (2010)
7. Narváez, M., Aranda, J.: Gait patterns monitoring using instrumented forearm crutches. Comput. Helping People Special Needs **12377**, 402–410 (2020)
8. Winstein, C.J., Pohl, P.S., Cardinale, C.L., Green, A., der Scholtz, L.V., Waters, C.: Learning a partial-weight-bearing skill: effectiveness of two forms of feedback. Phys. Ther. **76**(9), 985–93 (1996)

Robust Control of a Quadrotor UAV with Cable-Suspended Load for Safe Transport and Delivery Applications

J. Díaz-Téllez, J. R. Mendoza-Vázquez, I. D. Rojas-Cuevas(✉), S. J. Torres-Méndez, V. Ramírez-Palacios, and L. M. Meza-Martínez

Instituto Tecnológico de Puebla, Puebla, Mexico
juan.diaz@puebla.tecnm.mx , rojascid@yahoo.com.mx

Abstract. This work deals with the problem of controlling the transport of a load from one point to another through a cable connected to a quadrotor, and eliminating the oscillation generated by the suspended load. An ADRC controller is presented that asymptotically stabilises the desired position of the quadrotor while simultaneously limiting load oscillation and aligning it with the vertical position of the inertial reference frame. The proposed control scheme considers the dynamics generated by the suspended load to generate the control law. Unlike standard approaches in the scientific literature, feedback on the dynamics of the suspended load is not necessary since an extended state observer is designed to estimate it. The numerical simulation shows the effectiveness and stability of the proposed controller, thus contributing to the development of UAV-based sustainable mobility and safe transport applications such as purchased goods delivery, forest firefighting and aeromagnetic mapping.

1 Introduction

In recent years, unmanned aerial vehicles (UAVs) have become essential since we can classify them as mobile platforms capable of autonomously navigating various environments both indoors and outdoors. In a sustainable mobility sense, the challenge is to provide safe and accessible transport systems while minimising the environmental impact [10]. In particular, a UAV-based delivery system is taking a big boost since it is expected to revolutionise how customers receive purchased goods from urban or difficult access locations in a sustainable manner. Examples of suspended-load UAV-based transport applications include forest firefighting, aeromagnetic mapping, delivery of purchased goods and delivery of medical or first aid kits. Some advantages of using UAVs as delivery systems are the reduced shipping costs, less manual supervision and faster delivery times since they do not depend on the roadwork. Among other types of UAVs, the quadrotor has become the preferred aerial platform in aerial robotics due to its maneuverability, small size, hovering and landing/take-off ability. The technology involving

M. N. Cardona et al. (Eds.): LACAR 2023, LNNS 940, pp. 37–45, 2024.
https://doi.org/10.1007/978-3-031-54763-8_4

this kind of robot makes them very flexible according to the needs of each mission, which has generated multiple advances in implementing, designing, and building flight controllers and achieving improvements in their agility, mobility and safety [3]. Recently, the quadrotor has been used to transport cargo through some delivery and retrieval mechanism attached to it. In the case of suspended-load delivery, it is necessary to reduce the load swing as it may be fragile, vulnerable, or dangerous, and a large external disturbance can compromise flight stability. By utilising a quadrotor, the design of a reliable flight controller for safely transporting the load is imperative. Aerial manipulation is a complicated task and a challenge in the design of the control algorithm; a quadrotor with cable-suspended load is a multiple-input, multiple-output (MIMO) nonlinear system, underacted with eight degrees of freedom and four control inputs [1,2]. Suspended-load controllers can be divided into two categories: the first focuses on eliminating load swing, and the second is the generation of trajectories by considering the system dynamics. The present work focuses on the first category. For example, in [8] an adaptive controller and a trajectory generation for swing-free maneuvres of the suspended load based on dynamic programming are addressed; it recursively finds an optimal input to minimises an objective function depending on the current input and state. They show a suppression of 6% of load oscillation; however, the controller needs to know the position and speed of the suspended load. Differentially-flat hybrid property is introduced in [9]; that approach proposes trajectory generation and control for tracking the position of the suspended load, and experimental results demonstrate trajectory tracking for the suspended load for large oscillations and frequencies close to the natural frequency of the load. Most of the works cited above made the following assumptions: the load is modelled like a fixed and constant disturbance, and feedback of the suspended-load dynamics is needed, therefore, more instrumentation is required for the design of the control, and the system needs to be linearised at its equilibrium point to simplify the control design. The last condition limits the controller to operate in a small region of the state space while the minimal oscillation of the load is achieved only for slow maneuvers. In addition, in most of the aforementioned works, formal stability proof has not been addressed. This article presents the robust stabilisation of a quadrotor UAV with cable-suspended load, for safe transport and delivery applications based on the Active Disturbance Rejection Control (ADRC) approach, that was initially proposed by J. Han in [5]. The main objective is the online estimation of the oscillation generated by the suspended load that affects the behaviour of the quadrotoror, by means of an extended state observer (ESO). The rest of the document is structured as follows. Section 2 presents the mathematical model of the quadrotor with the suspended load. In Sect. 3, robust control is addressed. In Sect. 4, numerical simulations are presented. Finally, the conclusions in Sect. 5 are given.

2 Mathematical Model of UAV

In this paper, only the planar dynamics of the UAV is considered, as shown in Fig. 1. The authors consider that the 3-D control problem does not add value to the analysis since the remaining dynamics can be stabilized separately. Let us consider two orthogonal coordinate frames: the inertial frame, $E^i = [O, i, k]$, where vectors **i** and **k** point north and up respectively and the body frame, $E^b = [O, x, z]$, that is attached to the UAV's centre of mass. The angle θ is the rotation of the inertial frame to the body frame. An additional frame denoted as the load frame, $E^l = [O, x_l, z_l]$ is introduced; it is rotated with respect to the body frame by an angle α. L represents the cable length connecting to the suspended load and M is the mass of the UAV. The UAV is actuated by two motors generating forces $f_1 \in \mathbb{R}_{\geq}$ and $f_2 \in \mathbb{R}_{\geq}$, where $\mathbb{R}_{\geq} = \{\mathbb{R} \geq 0\}$.

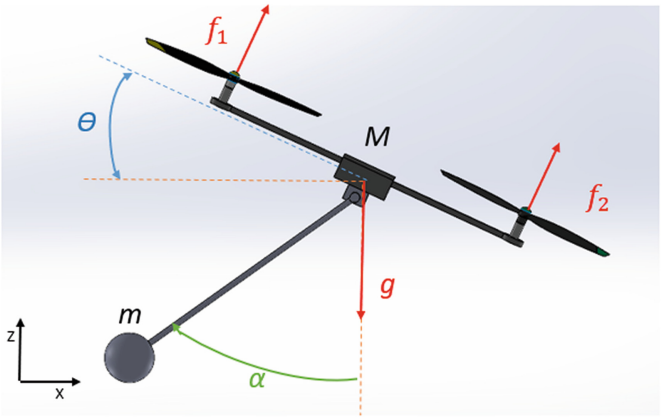

Fig. 1. Two-dimensional model of an UAV transporting a suspended load.

The system input are defined as $u_1 = f_1 + f_2$ and $u_2 = (f_1 - f_2)b$ where b is the distance between the motors and the center of the UAV. The modeling of the helicopter system with suspended load is inspired by the work carried out in [4,7]. Readers can refer to the cited references to better understanding of the model.

$$\Sigma_Q : \begin{cases} (M+m)\ddot{y} = u_1 \cos\theta - mL(\cos\alpha\ddot{\alpha}^2 + \sin\alpha\ddot{\alpha}) - (M+m)g \\ (M+m)\ddot{x} = u_1 \sin\theta - mL(\sin\alpha\dot{\alpha}^2 - \cos\alpha\ddot{\alpha}) \\ J\ddot{\theta} = u_2 \end{cases} \tag{1}$$

$$\Sigma_L : \left\{ mL^2\ddot{\alpha} = -mL\sin\alpha\ddot{z} + mL\cos\alpha\ddot{x} - mgL\sin\alpha \right. \tag{2}$$

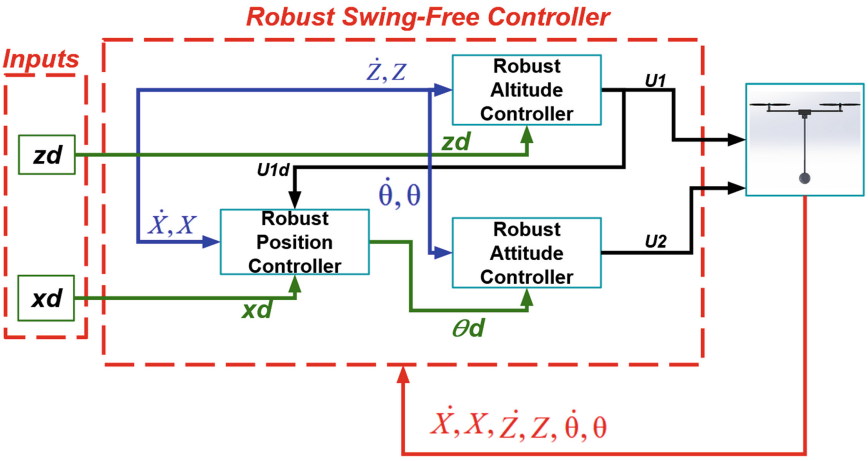

Fig. 2. Scheme of the proposed control algorithm (outer control loop and inner control loop).

Each rotor produces a force f_i and a torque M_i which are proportional to the square angular velocity of the rotor. The following equations approximate the dynamics of the rotors,

$$f_i = K_F \Omega_i^2, M_i = K_M \Omega_i^2 \tag{3}$$

where K_F, K_M are the parameters that depend on the air density, shape and yaw angle of the propeller.

3 Robust Swing-Free Cable-Suspended Load Control Using a Quadrotor

This work aims to stabilize the desired position of the UAV by minimizing the oscillation of the suspended load; that is, the position of the load is stabilized to the vertical axis of the inertial frame while the UAV moves to the desired position. The effect of the dynamics of the cable-load on the UAV has been considered. Unlike the aforementioned works, no sensor allows us to estimate the position and speed of the suspended load; instead, there is an extended state observer that allows estimating the dynamics of the suspended load. The control algorithm is structured by three components: altitude position control, horizontal position control and attitude control. Mathematically the above we can express it as (4) (Fig. 2).

$$q(t) \to q_d, \dot{q}(t) \to \mathbf{0}, \|\boldsymbol{\alpha}(t)\| \to \varepsilon, \text{according} \quad t \to \infty. \tag{4}$$

where $q = \left[z\ x\ \theta\right]^T \in \mathbb{R}^3$, ε is a number approximately equal to zero.

3.1 Robust Altitude Position Controller

The control algorithm for the UAV position is addressed. This has been divided into the control for the vertical dynamics and the control for the horizontal

dynamics. Consider the vertical dynamics of the UAV, then defining $\xi_z(\mathrm{t}) = -mL\left(\cos\alpha\ddot{\alpha}^2 + \sin\alpha\ddot{\alpha}\right) - (M+m)g$ as a disturbance with uniformly absolutely bounded first $\dot{\xi}_z(t)$ and second $\ddot{\xi}_z(t)$ derivatives. Therefore can be overwritten as,

$$\begin{aligned} \dot{z}_1 &= z_2 \\ \dot{z}_2 &= \frac{1}{\bar{m}}\left(u_1\cos\theta + \xi_z(t)\right) \end{aligned} \tag{5}$$

where $\bar{m}$ is defined as the sum of both masses, z_1 and z_2 are the vertical position and velocity respectively. The following observer is proposed to estimate $\xi_z(t)$, where l_2, l_1 and $l_0 \in \mathbb{R}_+$, the parameters are chosen such that the polynomial is Hurwitz.

$$\Sigma_{ESO_z} : \begin{cases} \dot{\hat{z}}_1 = z_2 + l_2\left(z_1 - \hat{z}_1\right) \\ \dot{\hat{z}}_2 = \dfrac{1}{\bar{m}}\left(u_1\cos\theta + \hat{z}_3\right) + l_1\left(z_1 - \hat{z}_1\right) \\ \dot{z}_3 = l_0\left(z_1 - \hat{z}_1\right) \end{cases} \tag{6}$$

A saturation function is used to limit the UAV to a desired operating region. The proposed controller generates a smooth response to the UAV's bounded permitted maximum angle θ_{max}. To facilitate the subsequent stability analysis, we introduce the following definition $f_{satN}(\varphi, \dot{\varphi}) : \mathbb{R} \to \mathbb{R}$ defined as:

$$f_{satN}(\varphi, \dot{\varphi}) = -\left(\bar{\lambda}\left(\tilde{\varphi} + \rho\dot{\varphi}\right), N\right) \tag{7}$$

where, given a positive constant a, a continuous non-decreasing function $(x_k, a) : \mathbb{R} \to \mathbb{R}$ is defined by

$$(x_k, a) = \begin{cases} x_k, & x_k \le a \\ a \cdot (x_k), & x_k > a \end{cases} \tag{8}$$

Theorem 1 *Consider the vertical dynamics described by* (6) *with the following control input:*

$$u_1 = \left(\frac{\bar{m} f_{sat}(z_1, z_2) - \hat{z}_3}{\cos\theta}, \Gamma_{max}\right) \tag{9}$$

Therefore (9) *stabilizes asymptotically to the desired position* $x(t) = x_d$, $\dot{x}(t) = \mathbf{0}$ *and* $\|\xi_x(t)\| \le \varepsilon$.

3.2 Robust Horizontal Controller

The control algorithm for the horizontal UAV position is addressed. Considering the horizontal dynamics of the UAV and defining $\xi_x(\mathrm{t}) = -mL\left(\sin\alpha\ddot{\alpha}^2 - \cos\alpha\ddot{\alpha}\right)$ as a disturbance with uniformly absolutely bounded first $\dot{\xi}_x(t)$ and second $\ddot{\xi}_x(t)$ derivatives,

$$\begin{aligned} \dot{x}_1 &= x_2 \\ \dot{x}_2 &= \frac{1}{\bar{m}}\left(u_1\sin\theta + \xi_x(t)\right) \end{aligned} \tag{10}$$

where x_1 and x_2 are the horizontal position and velocity respectively. The following observer is proposed to estimate $\xi_x(t)$,

$$\Sigma_{ESO_x} : \begin{cases} \dot{\hat{x}}_1 = x_2 + l_{x,2}\,(x_1 - \hat{x}_1) \\ \dot{\hat{x}}_2 = \dfrac{1}{\bar{m}}\,(u_1 \cos\theta + \hat{x}_3) + l_{x,1}\,(x_1 - \hat{x}_1) \\ \dot{x}_3 = l_{x,0}\,(x_1 - \hat{x}_1) \end{cases} \tag{11}$$

where $l_{x,2}$, $l_{x,1}$ and $l_{x,0} \in \mathbb{R}_+$, the parameters are chosen such that the polynomial is Hurwitz.

Theorem 2 *Consider the horizontal dynamics with the following control input:*

$$\theta_c(t) = \left(\arcsin \frac{\bar{m} f_{sat}(x_1, x_2) - \hat{x}_3}{u_1}, \theta_{max}\right) \tag{12}$$

Therefore (12) *stabilizes asymptotically to the desired position* $x(t) = x_d$, $\dot{x}(t) = 0$ *and* $\left\|\boldsymbol{\xi}_x(t)\right\| \leq \varepsilon$.

3.3 Robust Attitude Controller

Efficient control for orientation stabilization is crucial for the robot to reach the desired position.

$$\tau = K_p(\Lambda\tilde{\theta}) - K_v(\Upsilon\dot{\theta}), \tag{13}$$

where $\Delta U_a(K_p, \tilde{q}) = K_p(\Lambda\tilde{\theta}), f_v(K_v.\dot{q}) = K_v(\Upsilon\dot{\theta})$ They are positive gains and represent the function pending.

The closed-loop equation formed by the system model of rotation and the arc tangent control defined in is given as shown:

$$\frac{d}{dt}\begin{bmatrix}\tilde{\theta} \\ \dot{\theta}\end{bmatrix} = \begin{bmatrix}-\dot{\theta} \\ J^{-1}[K_p(\Lambda\tilde{\theta}) - K_v(\Upsilon\dot{\theta})]\end{bmatrix}. \tag{14}$$

The equilibrium point $[\,\tilde{q}^T\ \dot{q}^T\,]^T = [\,0^T\ 0^T\,]^T$ is unique.

4 Numerical Simulation

This section presents the results obtained in the simulation. Two scenarios have been established; the first scenario is the ability to stabilize the robot to the desired position (x_d, z_d) while limiting the oscillation of the load $(\alpha(t), \dot{\alpha})$. It is compared with the results obtained in [7] and [6]. The UAV tries to compensate for the vertical axis load. Conditions away from the equilibrium position are proposed for the cargo, while the UAV is hovering. Results are compared using the extended state observer and without the extended state observer.

The physical parameters used for the simulation are found in Table 1.

Table 1. Parameters

Symbol	Description	Value	Units
M	Quadrotor mass	2	Kg
m	Load mass	0.5	Kg
l	Cable length	0.1	m
J	Moment of inertia of the quadrotor	0.0043	kg m^2
g	Gravity	9.81	m/s^2

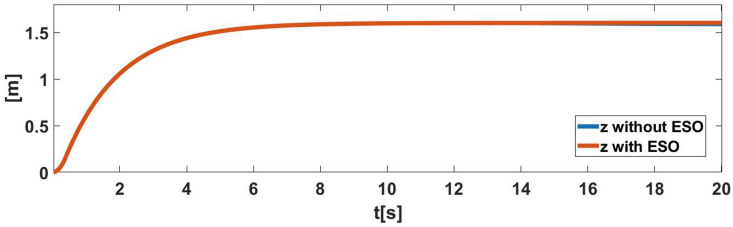

Fig. 3. Closed-loop behaviour of the UAV with cable-suspended load horizontal dynamics z(t).

The second scenario compares the control without the extended state observer. Figures 3,4,5 and 6 show the evolution of the state variables; the proposed robust control reduces the oscillation of the dynamics of the cable-load, simultaneously stabilise the UAV to the desired position (hover) with conditions far from the equilibrium point for the suspended load. Compared to non-observer control that fails to stabilise the load to equilibrium. Matching with other articles, you don't need to give feedback on the dynamics of the load coupled to the UAV, since the ESO estimates the dynamics. Comparing the results obtained in [7], for the first scenario, we observe that avoiding the need to have a sensor

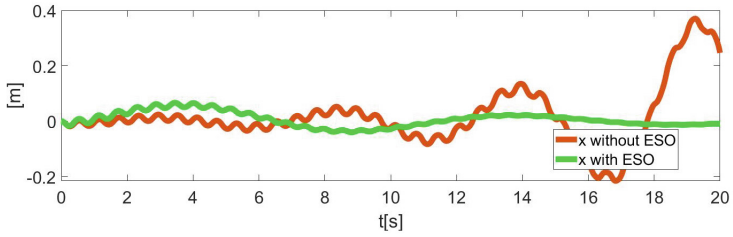

Fig. 4. Closed-loop behaviour of the UAV with cable-suspended load horizontal dynamics x(t).

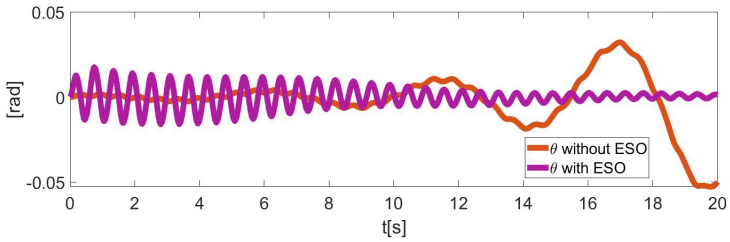

Fig. 5. Closed-loop behaviour of the UAV with cable-suspended load horizontal dynamics θ(t).

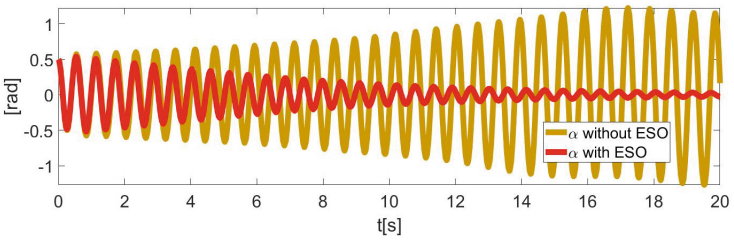

Fig. 6. Closed-loop behaviour of the UAV with cable-suspended load horizontal dynamics α(t).

which estimates the position of the load since it is only a disturbance taken as such by the robust control. Simulations are shown that demonstrate the effectiveness of the controller, as well as the dynamic load taken as a disturbance by the robust controller.

5 Conclusions

This article presented a new ADRC-based control strategy for robust stabilisation of a quadrotor UAV with cable-suspended load. Simulation results showed the stabilisation of the UAV to the desired position while simultaneously aligning the position of the load to the balance point (vertical axis). This approach does not need extra sensors to estimate the dynamics of the suspended load. Stabilisation was robust to disturbances and not modelled dynamics. The proposed controller behavior was compared with different control laws proposed in the literature showing a smoother response without over-elongation, a suitable settling time and no steady-state error. Effectiveness of the proposed controller showed its relevance to the development of UAV-based sustainable mobility and safe transport-delivery applications for wich the robust control law must be implemented on an onboard embedded system in a future work.

References

1. Díaz-Téllez, J., Guerrero-Castellanos, J.F., González-Guerrero, J.C., Estevez-Carreon, J., Silva-Juarez, A.: Robust angular velocity control of a VTOL-UAV for aggressive maneuvers flight. In: Moreno, H.A., Carrera, I.G., Ramírez-Mendoza, R.A., Baca, J., Banfield, I.A. (eds.) Advances in Automation and Robotics Research, pp. 26–33. Springer, Cham (2022). https://doi.org/10.1007/978-3-030-90033-5_4
2. G, J.K.G., Díaz-Téllez, J., Estevez-Carreon, J., Peréz-Peréz, J., Mendoza-Vazquez, R., Rosales-Carreón, M.: Bounded gradient attitude control of a quadcopter. In: 2022 International Symposium on Electromobility (ISEM), pp. 1–6 (2022). https://doi.org/10.1109/ISEM55847.2022.9976766
3. González-Guerrero, J.C., Díaz-Téllez, J., Estevez-Carreon, J., Mendoza-Vazquez, R., Meraz-Melo, M., Guerrero-Castellanos, J.F.: Low altitude control of the VTOL UAV tolerant to ground effect and actuator failures. In: 2022 International Conference on Unmanned Aircraft Systems (ICUAS), pp. 1504–1509 (2022). https://doi.org/10.1109/ICUAS54217.2022.9836161
4. Guerrero, M.E., Mercado, D.A., Lozano, R., García, C.D.: Passivity based control for a quadrotor uav transporting a cable-suspended payload with minimum swing. In: 2015 54th IEEE Conference on Decision and Control (CDC), pp. 6718–6723 (2015). https://doi.org/10.1109/CDC.2015.7403277
5. Han, J.: From PID to active disturbance rejection control. IEEE Trans. Ind. Electron. **56**(3), 900–906 (2009)
6. Martinez-Vasquez, A., Castro-Linares, R., Rodriguez-Mata, A.: Sliding mode control of a quadrotor with suspended payload: a differential flatness approach. In: 2020 17th International Conference on Electrical Engineering, Computing Science and Automatic Control (CCE), pp. 1–6 (2020). https://doi.org/10.1109/CCE50788.2020.9299140
7. Nicotra, M.M., Garone, E., Naldi, R., Marconi, L.: Nested saturation control of an UAV carrying a suspended load. In: 2014 American Control Conference, pp. 3585–3590 (2014). https://doi.org/10.1109/ACC.2014.6859222
8. Palunko, I., Cruz, P., Fierro, R.: Agile load transportation: safe and efficient load manipulation with aerial robots. IEEE Robot. Autom. Mag. **19**(3), 69–79 (2012). https://doi.org/10.1109/MRA.2012.2205617
9. Sreenath, K., Michael, N., Kumar, V.: Trajectory generation and control of a quadrotor with a cable-suspended load - a differentially-flat hybrid system. In: 2013 IEEE International Conference on Robotics and Automation, pp. 4888–4895 (2013). https://doi.org/10.1109/ICRA.2013.6631275
10. United Nations: Mobilizing Sustainable Transport for Development - Summary of the Report by the United Nations Secretary-General's High-Level Advisory Group on Sustainable Transport. Technical report (2016)

Kinematic Analysis of a Novel Leg-Wheel Transformable Mechanism

Héctor A. Moreno(✉)

Facultad de Ingeniería Mecánica y Eléctrica, Universidad Autónoma de Coahuila, Barranquilla S/N, 25720, Monclova, Coahuila, Mexico
h_moreno@uadec.edu.mx

Abstract. This paper presents the design of a leg-wheel transformable mechanism. This is a 7-link mechanism and has 2 degrees of freedom, which are controlled by actuators mounted on the vehicle chassis. The purpose of this mechanism is to combine the efficiency of the wheels with the ability of the legs to move in complex environments. The solutions of the direct and a simplified case of the inverse kinematics of the mechanism are presented. Finally the results of a simulation the mechanism performing one gait cycle are shown.

1 Introduction

In recent years, the design of hybrid locomotion systems has attracted the attention of several researchers. These locomotion systems consist of the integration of different elements, such as wheels, tracks and legs in the same vehicle in order to use the most appropriate method according to the terrain that is being traversed [1]. Hybrid systems that include wheels and legs provide the advantages of both locomotion systems. The efficiency of a locomotion system based on wheels is considerably superior to other methods when traveling across flat surfaces [24]. On the other hand, legged locomotion systems are known for their superior maneuverability in unstructured environments. The locomotion systems based on wheels and legs can be classified in:

- Platforms with legs and wheels [12,19].
- Wheeled legs [4,23].
- Legged wheels [5,13,20].
- Transformable legged wheels [2,15].
- Leg-wheel transformable mechanisms [10,26].

This paper presents the design of a new leg-wheel transformable mechanism. Some antecedents related to this research can be found in the design of transformable legged wheels. These designs allow transforming a circular wheel into a legged wheel. It has been experimentally demonstrated the ability of the legged wheels to overcome obstacles, to climb stairs, to traverse rough terrain [5], and they could be useful for improving the traction in sand, sludge, and snow. In the literature different designs of transformable legged wheels can be found. There are one [2], two [11,14,16,17,21,25,28], and three

M. N. Cardona et al. (Eds.): LACAR 2023, LNNS 940, pp. 46–55, 2024.
https://doi.org/10.1007/978-3-031-54763-8_5

[8] degrees of freedom transformable legged wheels. Most of the designs employ electric actuators, but there are some proposals that use pneumatic [27] and hydraulic actuation [7]. The designs of underactuated transformable legged wheels are described in [22] and [9].

In [26] Tadakuma et al. presented the design of a transformable wheel composed of a 3 degrees of freedom serial mechanism, at each joint there is one actuator, allowing the transformation between the wheel and leg. On the other hand, in [10] Lin and Shen introduced the design of a wheel that transforms into a C-shaped leg. The two halves of the wheel are rotated by an actuator in the rim of the wheel. In [3] Chen et al. presented the development of a 2 degrees of freedom module capable of transforming its shape between a wheel and a leg. The module consist of a 11-link mechanism, the rapid transition from a wheel to a leg endows the robot with wheel-to-leap behavior.

The next section introduces the design of the LW.Transmech, a leg-wheel transformable mechanism. After that, the solutions of the direct and inverse kinematics of the mechanism are presented. Then the results of a simulation of a simplified case of the inverse kinematics problem are shown. Finally the conclusions of this work are presented.

2 LW.Transmech

Figure 1 shows the design of the leg-wheel transformable mechanism LW.Transmech. This is a 7-link mechanism (6 mobile links and the base). The mechanism has 2 degrees of freedom, which are controlled by actuators mounted on the vehicle chassis. The power transmission must be coaxial, so Actuator 1 is connected to Link 1 by means of a shaft that passes through Link 2. Actuator 2 transmits power to Link 2 by means of a timing belt. Figure 2 shows the LW.Transmech mechanism in wheel and leg modes. In wheel mode, the actuators must move at the same speed to maintain that shape. In leg mode the actuators can generate any trajectory of the tip of the foot in the plane, such as a walking pattern. The 7-link mechanism provides a great extension in the leg mode, and also a lightweight structure since it does not include the weight of the actuators.

3 Direct Kinematics

The direct kinematics problem consist in determining the position of the tip of the leg $\mathbf{t} = \begin{bmatrix} t_x & t_y \end{bmatrix}^T$ given the value of the joint variables vector $\mathbf{q} = \begin{bmatrix} q_1 & q_2 \end{bmatrix}^T$. Joint variables q_1 and q_2 are the angles of the Link 1 and Link 2, respectively, and are controlled by the actuators. From Fig. 3, it is possible to write the following closed loop equation:

$$\mathbf{p}_1 + c_1\hat{\mathbf{d}}_1 = \mathbf{p}_2 + c_2\hat{\mathbf{d}}_2 \tag{1}$$

where $\mathbf{p}_i = p_i \begin{bmatrix} \cos q_i & \sin q_i \end{bmatrix}^T$, $\mathbf{d}_i = d_i \begin{bmatrix} \cos\theta_{di} & \sin\theta_{di} \end{bmatrix}^T$, $\hat{\mathbf{d}}_i = \mathbf{d}_i/d_i$ and $c_i = P_iC$ for $i \in [1,2]$. Equation (1) consist of a pair of transcendental equations, by summing the squares of the terms with θ_{d2} of those equations, the following expression can be obtained:

$$K_1 \cos\theta_{d1} + K_2 \sin\theta_{d1} = Q_1 \tag{2}$$

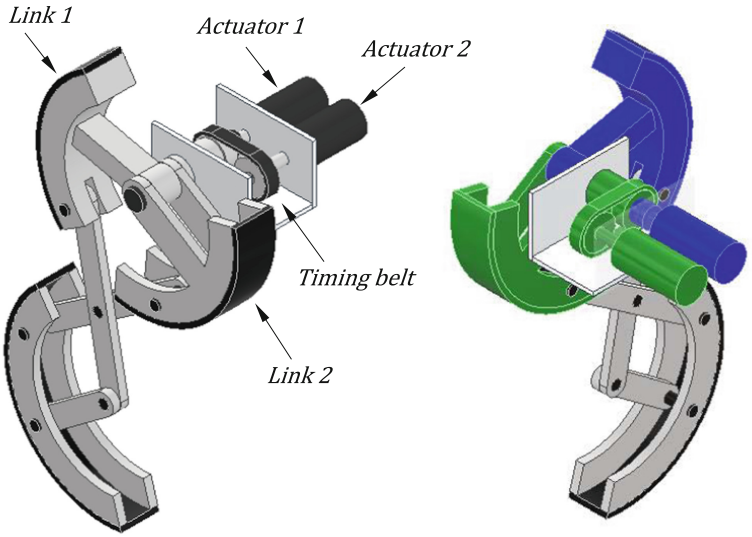

Fig. 1. Leg-Wheel transformable mechanism LW.Transmech

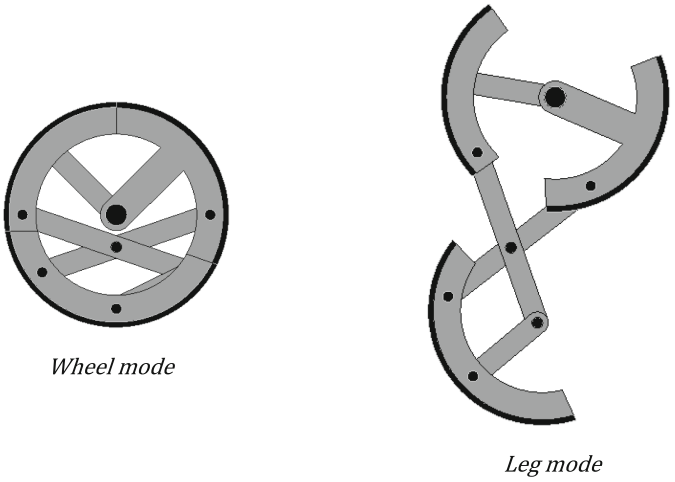

Fig. 2. Wheel and leg modes of the mechanism

where $K_1 = p_1 \cos q_1 - p_2 \cos q_2$, $K_2 = p_1 \sin q_1 - p_2 \sin q_2$ and $Q_1 = (c_2^2 - c_1^2 - K_1^2 - K_2^2)/2c_1$. Using the trigonometric identities $\cos\theta_{d1} = [1 - \tan^2(\theta_{d1}/2)]/[1 + \tan^2(\theta_{d1}/2)]$ and $\sin\theta_{d1} = 2\tan(\theta_{d1}/2)/[1 + \tan^2(\theta_{d1}/2)]$ a quadratic equation in terms

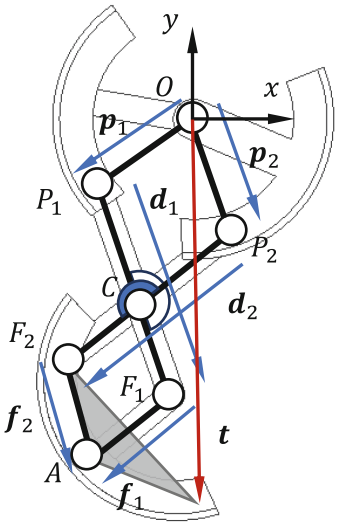

Fig. 3. Kinematic scheme of the LW.Transmech

of $\tan(\theta_{d1}/2)$ can be obtained, and its solution is:

$$\theta_{d1} = 2\tan^{-1}\left(\frac{K_2 \pm \sqrt{K_1^2+K_2^2-Q_1^2}}{K_1+Q_1}\right) \tag{3}$$

an analogous procedure can be followed to obtain θ_{d2}:

$$\theta_{d2} = 2\tan^{-1}\left(\frac{K_2 \pm \sqrt{K_1^2+K_2^2-Q_2^2}}{K_1+Q_2}\right) \tag{4}$$

where $Q_2 = (c_2^2 - c_1^2 + K_1^2 + K_2^2)/2c_2$. From Fig. 3, another closed loop equation can be obtained:

$$(d_1 - c_1)\hat{\mathbf{d}}_1 + \mathbf{f}_1 = (d_2 - c_2)\hat{\mathbf{d}}_2 + \mathbf{f}_2 \tag{5}$$

where $\mathbf{f}_i = f_i\left[\cos\theta_{fi}\ \sin\theta_{fi}\right]^T$ for $i \in [1,2]$. Given the values of θ_{d1} and θ_{d2}, the angle θ_{f2} can be obtained from Eq. (5) as follows:

$$\theta_{f2} = 2\tan^{-1}\left(\frac{R_2 \pm \sqrt{R_1^2+R_2^2-S^2}}{R_1+S}\right) \tag{6}$$

where $R_1 = (d_1 - c_1)\cos\theta_{d1} - (d_2 - c_2)\cos\theta_{d2}$, $R_2 = (d_1 - c_1)\sin\theta_{d1} - (d_2 - c_2)\sin\theta_{d2}$ and $S = (f_2^2 - f_1^2 + R_1^2 + R_2^2)/2f_2$.

Finally the solution of direct kinematics is:

$$\mathbf{t} = \mathbf{p}_2 + \mathbf{d}_2 + \left[(l_t/f_2)\mathbf{R}_\phi + \mathbf{I}_2\right]\mathbf{f}_2 \tag{7}$$

where l_t is the distance from point A to the tip of the leg, $\mathbf{R}_\phi$ is a rotation matrix around the z-axis for a given angle ϕ (see Fig. 4), and $\mathbf{I}_2$ is the identity matrix of size 2.

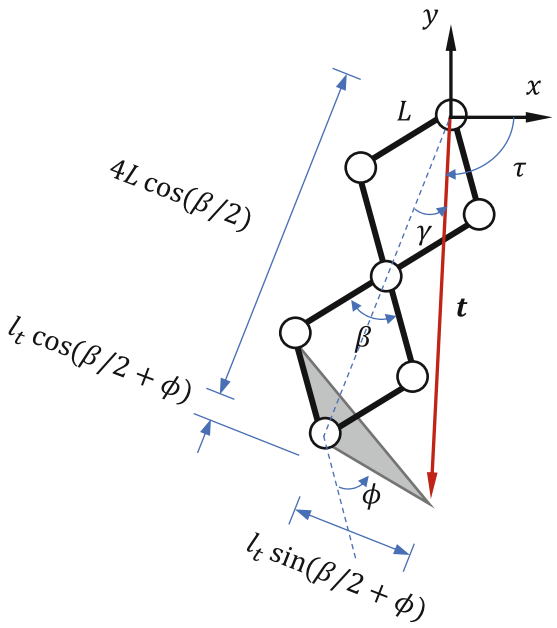

Fig. 4. Simplified symmetric case of the inverse kinematics

4 Inverse Kinematics

The inverse kinematics problem consist in determining of the joint variables vector $\mathbf{q}$ given a desired position of the tip of the leg $\mathbf{t}$. The solution of inverse kinematics is necessary to generate the gait patterns of the leg. This problem involves the solution of a system of six transcendental equations, given by eqs. (1), (5) and (7). The architecture of the mechanism has multiple assembly modes for a given value of $\mathbf{t}$, making it difficult to obtain a general analytical solution and requiring the use of numerical methods, such as Newton-Raphson [18] or Neural Networks [6].

Given the complexity of the general case, here we present the resolution of the inverse kinematics of a simplified symmetric case of the mechanism. In this case the lengths of the links are $p_i = c_i = f_i = L$ and $d_i = 2L$. Considering Fig. 4 the following expression can be written:

$$t_f^2 = [4L\cos(\beta/2) + l_t\cos(\beta/2+\phi)]^2 + l_t^2\sin^2(\beta/2+\phi) \tag{8}$$

where $t_f = \|\mathbf{t}\|$. Expanding the binomial and using the trigonometric identities $\cos^2(\beta/2) = (1+\cos\beta)/2$, $\cos(\beta/2)\cos(\beta/2+\phi) = [\cos(\beta+\phi)+\cos(\phi)]/2$ and

$\cos(\beta+\phi) = \cos\beta\cos\phi - \sin\beta\sin\phi$, the previous expression can be written as follows:

$$(2L + l_t\cos\phi)\cos\beta - l_t\sin\phi\sin\beta = \frac{t_f^2 - 8L^2 - 4Ll_t\cos\phi - l_t^2}{4L} \tag{9}$$

from the previous equation the angle β can be obtained:

$$\beta = 2\tan^{-1}\left(\frac{-l_t\sin\phi \pm \sqrt{4L(l_t\cos\phi + L) + l_t^2 - V^2}}{2L + l_t\cos\phi + V}\right) \tag{10}$$

where $V = (t^2 - 8L^2 - 4Ll_t\cos\phi - l_t^2)/4L$. The angle γ from Fig. 4 is computed with:

$$\gamma = \tan^{-1}\left(\frac{l_t\sin(\beta/2+\phi)}{4L\cos(\beta/2) + l_t\cos(\beta/2+\phi)}\right) \tag{11}$$

then, the solution of the inverse kinematics is given by:

$$q_1 = \tau - \gamma - \beta/2 \tag{12}$$

and

$$q_2 = \tau - \gamma + \beta/2 \tag{13}$$

where $\tau = \tan^{-1}(t_y/t_x)$ is the angle of $\mathbf{t}$.

5 Simulation

This section presents the results of a simulation of the inverse kinematics. The simulation consist in following the trajectory of one gait cycle, in this case the gait cycle has the form of a semi-ellipse. The parametric equations of this trajectory are the following:

$$t_x(t) = \begin{cases} C_{sx} + A_s\cos(\pi - 2\pi t/T) & \text{if } t < T/2 \\ C_{sx} + A_s - 4A_x(t - T/2)/T & \text{if } t \geq T/2 \end{cases} \tag{14}$$

and

$$t_y(t) = \begin{cases} C_{sy} + B_s\sin(\pi - 2\pi t/T) & \text{if } t < T/2 \\ C_{sy} & \text{if } t \geq T/2 \end{cases} \tag{15}$$

where C_{sx} and C_{sy} are the coordinates of the center of the semi-ellipse, and A_s and B_s are the lengths of the semi-axes. T is the period of time in which the trajectory is performed.

Figure 5 shows the values of $\mathbf{t}$ for a trajectory given by $C_{sx} = -10$ cm, $C_{sy} = -40$ cm, $A_=12$ cm, $B_s = 6$ cm and $T = 2$ s. In this simulation a mechanism with $L = 10$ cm is considered, and also $l_t = 10cm$ and $\phi = \pi/4$. Figure 6 presents the results of the inverse kinematics. Figures 7 and 8 show postures of the LW.Transmech in the first and second part of the step, respectively. These figures show a gray circle of diameter 30 cm, a mechanisms with the previously mentioned geometry could fit in a wheel of that diameter.

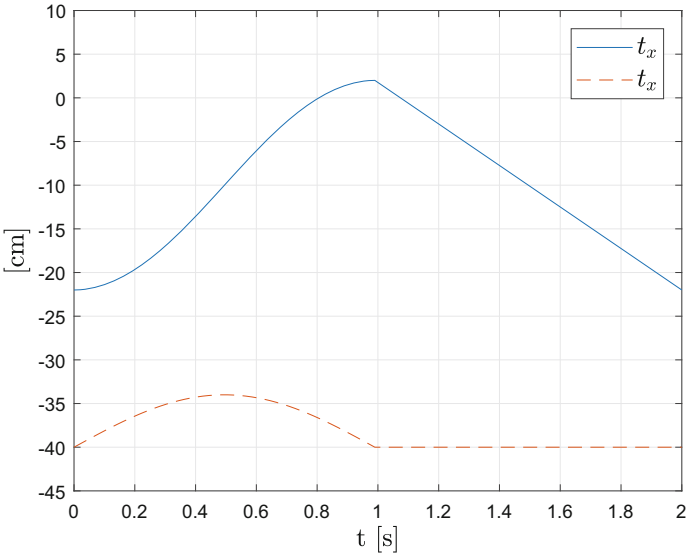

Fig. 5. Values of t_x and t_y for a semi-elliptic trajectory of one gait cycle

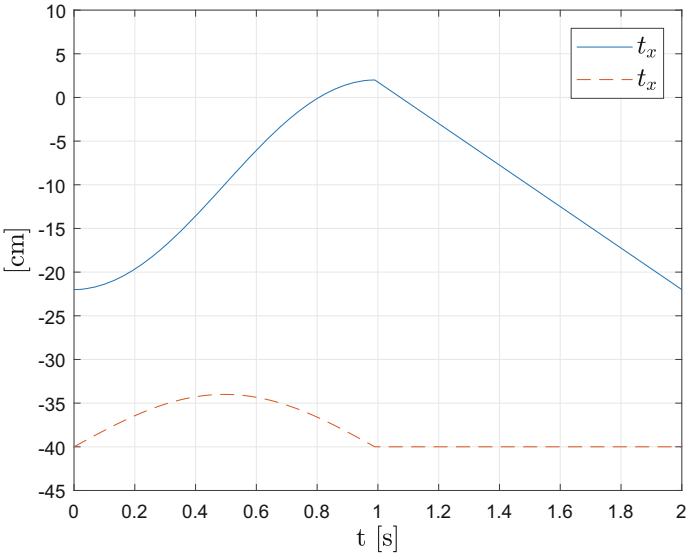

Fig. 6. Simulation of the inverse kinematics

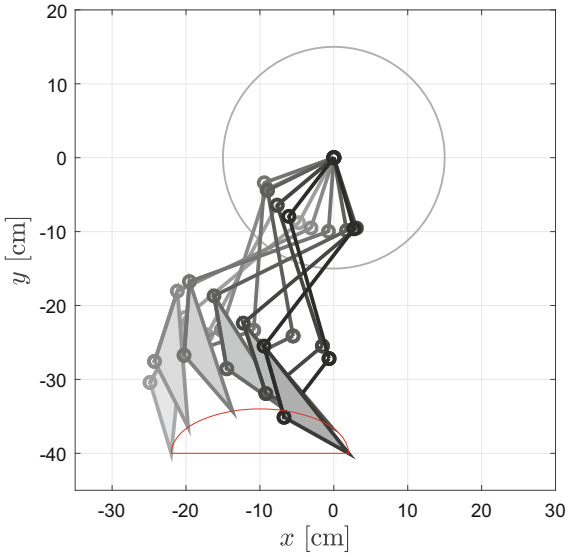

Fig. 7. Postures of the LW.Transmech in the first part of the gait cycle

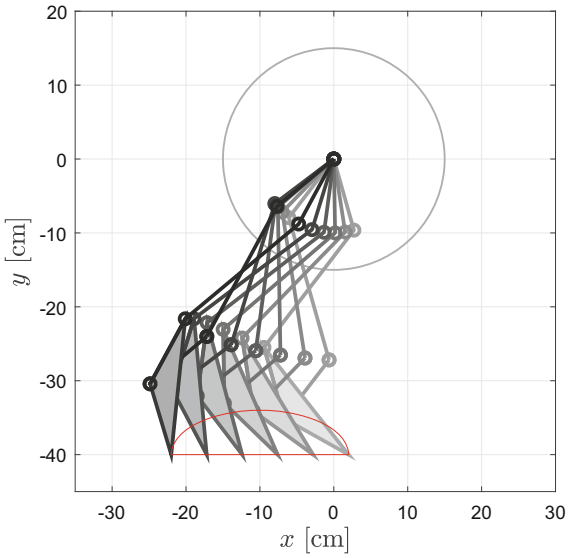

Fig. 8. Postures of the LW.Transmech in the second part of the gait cycle

6 Conclusions

This paper presented the design of a leg-wheel transformable mechanism. The aim of this mechanism is to combine the efficiency of the wheels with the ability of the legs to move in complex environments. The mechanism has 2 degrees of freedom, which are controlled by actuators mounted on the vehicle chassis. In wheel mode, the actuators must move at the same speed to maintain the circular shape. In leg mode the actuators can generate any trajectory of the tip of the foot in the plane, such as a walking pattern. The 7-link mechanism provides a great extension in the leg mode, and also a lightweight structure since it does not include the weight of the actuators.

The direct and inverse kinematics problems for this mechanism were analysed. In the case of the inverse kinematics, a simplified symmetric case of the mechanism was studied, since the general case involves the solution of a system of six transcendental equations making it difficult to obtain a general analytical solution. Future works are the dimensional synthesis of the mechanisms, the physical development of a prototype and the evaluation of mechanical performance of the mechanisms in different terrains.

Acknowledgements. The author would like to thank to Prof. R. Morin for his help during the resolution of the inverse kinematics problem.

References

1. Bruzzone, L., Quaglia, G.: Review article: locomotion systems for ground mobile robots in unstructured environments. Mech. Sci. **3**, 49–62 (2012)
2. Burt, I.T., Papanikolopoulos, N.P.: Adjustable diameter wheel assembly, and methods and vehicles using same, US 6860346 (2005)
3. Chen, H.-Y., Wang, T.-H., Ho, K.-C., Ko, C.-Y., Lin, P.-C., Lin, P.-C.: Development of a novel leg-wheel module with fast transformation and leaping capability. Mech. Mach. Theory **163**, 104348 (2021)
4. Cordes, F., Dettmann, A., Kirchner, F.: Locomotion modes for a hybrid wheeled-leg planetary rover. In: IEEE International Conference on Robotics and Biomimetics (ROBIO), pp. 2586–2592 (2011)
5. Eich, M., Grimminger, F., Kirchner, F.: A versatile stair-climbing robot for search and rescue applications. In: 2008 IEEE International Workshop on Safety, Security and Rescue Robotics, pp. 35–40 (2008)
6. Flores, J.F., Moreno, H.A., Carrera, I.G., Garcia, M.A., Adan, R.G.: Inverse kinematics of a RSRR heise wheel using neural networks. In: 2021 XXIII Robotics Mexican Congress (ComRob), pp. 19–24 (2021)
7. Hu, Y.: Automotive cat-claw-shaped telescopic antiskid wheel. CN 202716669 U (2013)
8. Kim, Y., Kim, H.S., Seo, T.: Type synthesis and kinematic analysis of a 2-DOF shape-morphing wheel mechanism for step-overcoming. IEEE Access **9**, 86500–86513 (2021)
9. Kim, Y.S., Jung, G.P., Kim, H., Cho, K.J., Chu, C.N.: Wheel transformer: a wheel-leg hybrid robot with passive transformable wheels. IEEE Trans. Rob. **30**, 1487–1498 (2014)
10. Lin, P., Shen, S.: Mobile platform, US 8307923 B2 (2012)
11. Lin, Y., Lin, H., Lin, P.: Slip-model-based dynamic Gait generation in a leg-wheel transformable robot with force control. IEEE Robot. Autom. Lett. **2**(2), 804–810 (2017)

12. Lu, D., Dong, E., Liu, C., Xu, M., Yang, J.: Design and development of a leg-wheel hybrid robot HyTRo-I. In: IEEE/RSJ International Conference on Intelligent Robots and Systems (IROS), pp. 6031–6036 (2013)
13. Moore, E., Buehler, M.: Stable stair climbing in a simple hexapod robot. In: 4th International Conference on Climbing and Walking Robots (CLAWAR) (2001)
14. Moreno, H., Carrera, I., García, J.P., Baca, J.: Heise wheels: a family of mechanisms for implementing variable geometry hybrid wheels. Revista Iberoamericana de Automática e Informática industrial **15**(4) (2018)
15. Moreno, H.A., Carrera, I.G., Alfonso Pamanes, J., Camporredondo, E.: 2 DOF mechanism for a variable geometry hybrid wheel. In: Chang, I., Baca, J., Moreno, H.A., Carrera, I.G., Cardona, M.N. (eds.) Advances in Automation and Robotics Research in Latin America. LNNS, vol. 13, pp. 30–35. Springer, Cham (2017). https://doi.org/10.1007/978-3-319-54377-2_3
16. Moreno-Avalos, H.A., Carrera, I.G., Saucedo, M., García-Murillo, M.A.: Kinematic analysis of the r subfamily of the Heise wheels. Proc. Inst. Mech. Eng. C J. Mech. Eng. Sci. **234**(15), 3004–3018 (2020)
17. Nagatani, K., Kuze, M., Yoshida, K.: Development of transformable mobile robot with mechanism of variable wheel diameter. J. Robot. Mechatron. **19**, 252–253 (2007)
18. Puglisi, L., Saltaren, R., Garcia, C., Cardenas, P., Moreno, H.: Implementation of a generic constraint function to solve the direct kinematics of parallel manipulators using Newton-Raphson approach. Control Eng. Appl. Inform. **19**(2), 71–79 (2017)
19. Qiao, G., Song, G., Zhang, Y., Zhang, J., Li, Z.: A wheel-legged robot with active waist joint: design, analysis, and experimental result. J. Intell. Rob. Syst. **83**, 485–502 (2016)
20. Quinn, R., Offi, J., Kingsley, D., Ritzmann, R.: Improved mobility through abstracted biological principles. vol. 3, pp. 2652–2657 (2002)
21. Rafique, R.: Reconfigurable mechanism for mobile robotic platform. In: Proceedings of the National Conference on Machines and Mechanisms (iNaCoMM2013), IIT Roorkee, India, pp. 714–721 (2013)
22. Sgherri, G., Spina, G.L.: Variable-diameter wheel, US 20120104834 A1 (2012)
23. Siegwart, R., Lamon, P., Estier, T., Lauria, L., Piguet, R.: Innovative design for wheeled locomotion in rough terrain. Robot. Auton. Syst. **0921–8890**(40), 151–162 (2002)
24. Siegwart, R., Nourbakhsh, I., Scaramuzza, D.: Introduction to Autonomous Mobile Robots, 2nd Edition. MIT Press (2011)
25. Sun, T., Xiang, X., Su, W., Wu, H., Song, Y.: A transformable wheel-legged mobile robot: design, analysis and experiment. Robot. Auton. Syst. **98**, 30–41 (2017)
26. Tadakuma, K., et al.: Mechanical design of the wheel-leg hybrid mobile robot to realize a large wheel diameter. In: 2010 IEEE/RSJ International Conference on Intelligent Robots and Systems, pp. 3358–3365 (2010)
27. Yun, S.S., Lee, J.Y., Jung, G.P., Cho, K.J.: Development of a transformable wheel actuated by soft pneumatic actuators. Int. J. Control Autom. Syst. **15**, 36–44 (2017)
28. Zhang, J., Zhang, P., Zhang, L., Hu, Y., Zheng, L.: Folding combined obstacle detouring wheel. CN 102350917 A (2011)

Robust H-Infinity Control of Delta Parallel Robot with Disturbances

Fernando E. Serrano[1,2,3(✉)] and Manuel Cardona[2]

[1] Instituto de Investigación en Energía IIE, Universidad Nacional Autónoma de Honduras UNAH, Tegucigalpa, Honduras
[2] Universidad Don Bosco, San Salvador, El Salvador
manuel.cardona@udb.edu.sv
[3] Instituto de Robótica (UPC-CSIC), Universidad Politécnica de Cataluña, Barcelona, Spain
fernando.serrano@upc.edu, serranofer@eclipso.eu, fernandoserr@gmail.com

Abstract. In this paper is presented the results of the research study regarding the robust H-Infinity control with disturbances. The first part of this study consists in the dynamic modeling of the delta parallel robot by the implementation of the Euler-Lagrange mathematical formulation. This dynamic model is obtained from the kinematic model of the delta robot in the task space in order to provide a feasible model for trajectory tracking purposes. The type of control strategy for this delta robot is the robust H-Infinity control in which by the implementation of an appropriate Lyapunov functional the control law is synthesized in order to minimize the error between the reference position and the measured position. In order to meet the H-infinity disturbance rejection properties of the proposed control strategy the necessary robust and disturbance rejection properties are considered. A numerical experiment is provided in order to validate the theoretical results obtained in this research study. Finally the discussion and conclusion of this research study are provided.

1 Introduction

Parallel robots are important in many industrial applications, so for this reason, it is important to synthesise new kinematic and dynamic modelling of this kind of robots for controller design purposes [5,6]. The delta robot is a well known parallel robot in which there are actuated and passive joints in order to drive the end effector to a specific position in the task space. It is important to remark that designing control strategies for parallel robots, in specific, Delta robots it is not an easy task, considering that unmodelled dynamics and disturbance are often found in this parallel robot. In this section are mentioned some kinds of kinematic, dynamic model and control of this parallel robot.

Referring to the kinematic modeling of Delta parallel robots it is important to mention some research studies found in the literature regarding this kind of mechanism. Interesting implementations of the kinematic of Delta parallel robots

M. N. Cardona et al. (Eds.): LACAR 2023, LNNS 940, pp. 56–67, 2024.
https://doi.org/10.1007/978-3-031-54763-8_6

are proposed for control and other purposes. For example in papers like [14] it is important to mention that the forward kinematic of a Delta robot is obtained by machine learning for safety analysis. Meanwhile in [11] a calibration method is implemented by measuring the robot kinematics error. In [21] the kinematic sensitivity and calibration of a non-fully symmetric delta robot is presented. Then in [3,22] are shown some important kinematic derivation methodology taking into consideration for robotic upper-limb rehabilitation system, something that is important for this research study, in the first case; and then an efficient calibration method for industrial robots with kinematic decomposition is proposed in the second case.

Dynamic modelling of Delta parallel robots are very important for this research study, so for this reason it is important to mention the following papers found in the literature. So for example in [27] it is proposed an important dynamic modelling technique for sensor based design of parallel robots. Meanwhile in [20] the parameter estimation of the dynamic model of a delta robot is evinced. In [17] important results for this research study are presented considering the dynamic model of a Delta robot considering uncertainties. Then in [8] the inverse dynamic model of a Delta parallel robot is proposed. In [13] the design of the inverse kinematic model is presented.

Robust control is important nowadays for the trajectory tracking of many serial and parallel robots. For this reason is important to mention the following robust control strategy for robots which are crucial for this research study. In [9] a robust neural decoding for an artificial hand is presented. Then in [16] an adaptive robust controller for a mobile robot manipulator is shown. Meanwhile in [24] the robust control of a space robot with two arms is shown. Moreover in [15,18] a robust control for a robotics biological system is provided, in the first case, then a robust inverse dynamic control for a robotic mechanism is evinced in the second case.

Disturbance rejection H-infinity control has been implemented recently due to its performance improvement in comparison with other controller that deal with disturbances. Disturbances in robotic system are common taking into consideration loads and many other kinds of perturbations found in the system. For this reason is important to mention the following research studies related to this present work. In [10] the H-infinity control of a MEMS gyroscope is shown. Meanwhile in [19] the H-infinity control of a multi DOF robotic manipulator is presented. Other important research studies found in the literature are [23,25] in which the H-infinity control for control affine systems and the robust control of pressurized water reactor are shown respectively. Then in [26] the robust H-infinity control of connected vehicles is shown.

To finalize this theoretical fundamental section, it is important to mention the following control strategies found in the literature for trajectory tracking of Delta parallel robots considering that they are crucial for this research study. It is crucial to cite the following references such as [1,2] in which in the first case a fractional order PID controller for this kind of parallel robot is presented and in the second case the compensation of a delta robot are evinced respectively.

Then in [7,17] are presented two control strategies for delta robots. In the first case, the model free collision detection and the control strategy for a direct drive delta robot are shown respectively. Finally in [12] the task space of a Delta robot is presented.

Based on the previous theoretical fundamentals, this research study consists first in the kinematic model demonstration because it is crucial for the dynamic modelling of the Delta parallel robot. Then an H-infinity disturbance rejection controller is designed by selecting an appropriate Lyapunov functional considering disturbance in the input force vector. This research study finalize with a numerical experimental section along with the respective discussion and conclusion sections.

2 Problem Formulation

In this section is evinced the kinematic and dynamic modelling of the Delta robot. It is important to mention that the main results of the kinematic model of the robot are shown in the following reference. In Fig. 1 the diagram of the Delta parallel robot is shown. This robot consists of active and passive joints in order to provide the adequate movement of the lower platform.

2.1 Delta Robot Forward Kinematics

The forward kinematics of this Delta parallel robot is given by the following position vector:

$$q = [r, t] \tag{1}$$

In which $r = [x_0, y_0, z_0]^T$ with the quaternion p. In which the length of each link is given by the following vector:

$$\begin{aligned} l(r,p,t) &= |\overrightarrow{OG}| + |\overrightarrow{GG'}| \\ &\quad + |\overrightarrow{G'D}| - |\overrightarrow{OA}| - |\overrightarrow{AH}| \\ l_0 &= |\overrightarrow{HD}| \end{aligned} \tag{2}$$

In which the vector $\overrightarrow{OG}$ is the vector in the position of home and $\overrightarrow{GG'}$ is the displacement vector of the lower platform. For each of the three kinematic chains the restriction function is given by:

$$F(r,p,t) = \begin{bmatrix} \phi_1(r,p,t) \\ \phi_2(r,p,t) \\ \phi_3(r,p,t) \end{bmatrix} = \begin{bmatrix} l_1(r,p,t) - l_{0,1} \\ l_2(r,p,t) - l_{0,2} \\ l_3(r,p,t) - l_{0,3} \end{bmatrix} \tag{3}$$

The derivative of the function of restrictions is given by:

$$\Delta q = F(r,p,t)F^{\dagger}(r,p,t) \tag{4}$$

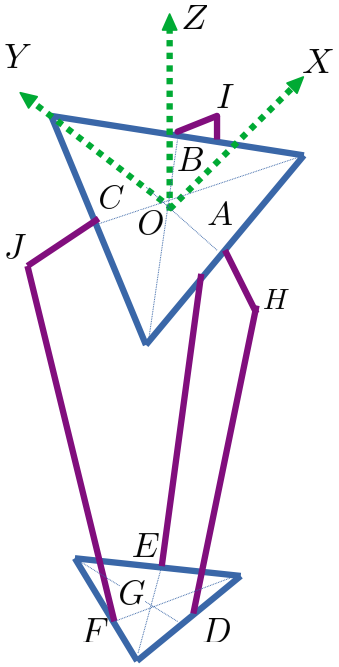

Fig. 1. Diagram of the Delta Parallel Robot

$F^{\dagger}$ is the Penrose-Moore pseudo-inverse. Meanwhile the solution of q is obtained numerically by [4]:

$$q_i = q_{i-1} + \Delta q \tag{5}$$

By the numerical solution of the position of the moving platform of the Delta parallel robot the dynamic model of the Delta robot is obtained as shown in the following subsection.

2.2 Delta Robot Dynamic Formulation

In order to obtain the formulation of the dynamic model of the Delta parallel robot consider the actuator joints angle $\Theta = [\theta_1, \theta_2, \theta_3]^T$ with the moving platform position vector $X = [x, y, z]^T$. Consider the following Lagrangian:

$$\mathcal{L} = K - P = \frac{1}{2}\dot{\Theta}^T J\dot{\Theta} + \frac{1}{2}\dot{X}^T M\dot{X} - mgX\epsilon \tag{6}$$

In which m is the link mass, g is the gravity vector and $\epsilon = [0, 0, 1]^T$. The Euler-Lagrange formulation for the angles and positions are given by:

$$\begin{aligned} \frac{d}{dt}\left[\frac{\partial \mathcal{L}}{\partial \dot{\Theta}}\right] - \frac{\partial \mathcal{L}}{\partial \Theta} &= \tau_\theta \\ \frac{d}{dt}\left[\frac{\partial \mathcal{L}}{\partial \dot{X}}\right] - \frac{\partial \mathcal{L}}{\partial X} &= \tau_X + \tau_d \end{aligned} \tag{7}$$

in which $\tau_\theta \in \mathbb{R}^3$ is the actuator torque vector, $\tau_X \in \mathbb{R}^3$ is the position force vector and $\tau_d \in \mathbb{R}^3$ is the force disturbance vector. The following property evince the actuator torque transformation to the force in the position of the delta robot:

Property 1. *Consider the following transformation $\mathcal{T} : \mathbb{R}^3 \to \mathbb{R}^3$ so the transformation of the force vector to the actuator torque vector is given by the following set:*

$$\mathcal{T}(\tau_X) = \left\{\tau_\theta = R\tau_X : R \in \mathbb{R}^{3\times 3}\right\} \tag{8}$$

with the matrix R given by:

$$R = \begin{bmatrix} 0 & z & -y \\ -z & 0 & x \\ y & -x & 0 \end{bmatrix} \tag{9}$$

3 H-Infinity Control Synthesis of the Delta Parallel Robot

Consider the following state space representation of the position dynamics with the state variables as shown below:

$$\begin{aligned} \eta_1 &= X \\ \eta_2 &= \dot{X} \\ \dot{\eta}_1 &= \dot{X} = \eta_2 \end{aligned} \tag{10}$$

with the following state-space model:

$$\begin{aligned} \dot{\eta}_1 &= \eta_2 \\ \dot{\eta}_2 &= M^{-1}\tau_X - M^{-1}mg\epsilon + M^{-1}\tau_d \end{aligned} \tag{11}$$

Now consider the following error variables:

$$\begin{aligned} e_1 &= \eta_{d1} - \eta_1 \\ e_2 &= \eta_{d2} - \eta_2 \end{aligned} \tag{12}$$

in which η_{d1} and η_{d2} are the desired position and linear velocities respectively.

Consider the following property in order to design a disturbance rejection controller for the Delta parallel robot.

Property 2. *Consider the following integral inequality in order to obtain a disturbance rejection control law in order to keep stable the closed loop system:*

$$\int_0^T |e_2^T(t_1)e_2(t_1)|dt_1 \leq \int_0^T |\tau_d^T(t_1)\tau_d(t_1)|dt_1 + \delta(X(0)) \tag{13}$$

In which e_2 is the velocity error and τ_d is the disturbance input force.

In order to obtain the disturbance rejection control law consider the following theorem:

Theorem 1. *In order to obtain the closed loop stability of the position dynamics of the Delta parallel robot consider the force input vector given by:*

$$\tau_X = M\dot{\eta}_{d2} + mg\epsilon - \tau_d + M^{-1}P\frac{1}{\|e_2\|^2}e_1^T Q\dot{e}_1 - M^{-1}P\frac{1}{\|e_2\|^2}\tau_d^T\tau_d + M^{-1}Pe_2 \tag{14}$$

In which $Q \in \mathbb{R}^{3\times3}$ and $P \in \mathbb{R}^{3\times3}$ are positive definite matrices.

Proof:
Consider the following Lyapunov functional:

$$V = \frac{1}{2}e_1^T Qe_1 + \frac{1}{2}e_2^T Pe_2 \tag{15}$$

obtaining the time derivative of the previous Lyapunov functional yields:

$$\begin{aligned}\dot{V} &= e_1^T Q\dot{e}_1 + e_2^T P\dot{e}_2 \\ \dot{V} &= e_1^T Q\dot{e}_1 + e_2^T P[\dot{\eta}_{d2} - \dot{\eta}_2]\end{aligned} \tag{16}$$

Now by substituting (14) in the previous Lyapunov functional derivative is obtained:

$$\begin{aligned}\dot{V} &= \tau_d^T\tau_d - e_2^T e_2 \\ \dot{V} &\leq |\tau_d^T\tau_d| - |e_2^T e_2|\end{aligned} \tag{17}$$

Integrating at both sides of the previous result yields:

$$\begin{aligned}\int_0^T \dot{V}(t_1)dt_1 &\leq \int_0^T |\tau_d^T(t_1)\tau_d(t1)|dt_1 - \int_0^T |e_2^T(t_1)e_2(t_1)|dt_1 \\ \int_0^T |e_2^T(t_1)e_2(t_1)|dt_1 &\leq \int_0^T |\tau_d^T(t_1)\tau_d(t1) + \delta(X(0))\end{aligned} \tag{18}$$

So Property 2 is met and the closed loop stability of the system is achieved.

4 Numerical Experiment

This numerical experiment consists of the simulation of the proposed control strategy for the Delta parallel robot. A force disturbance of 0.1 N is applied to the system. The following matrices are implemented in this numerical experiment:

$$J = \begin{bmatrix} I_x & 0 & 0 \\ 0 & I_y & 0 \\ 0 & 0 & I_z \end{bmatrix} M = \begin{bmatrix} m & 0 & 0 \\ 0 & m & 0 \\ 0 & 0 & m \end{bmatrix} \tag{19}$$

in which the inertia's are $I_x = I_y = I_z = 0.00001\ N.m^2$ and the masses are $m_1 = m_2 = m_3 = m = 0.1\ Kgs$. The gain matrices Q and P are given by:

$$Q = \begin{bmatrix} 2.8 & 0 & 0 \\ 0 & 2.8 & 0 \\ 0 & 0 & 2.8 \end{bmatrix} P = \begin{bmatrix} 0.06 & 0 & 0 \\ 0 & 0.06 & 0 \\ 0 & 0 & 0.06 \end{bmatrix} \tag{20}$$

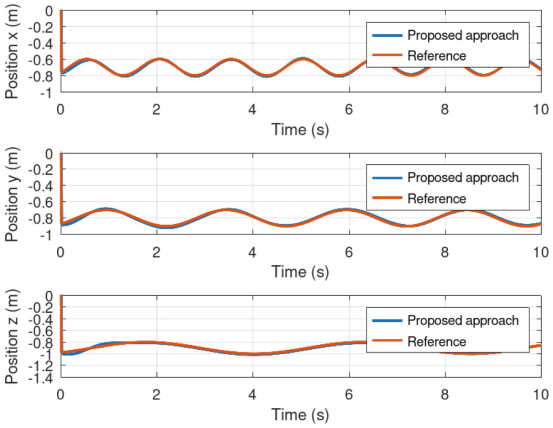

(a) Position of the moving platform of the Delta Parallel Robot

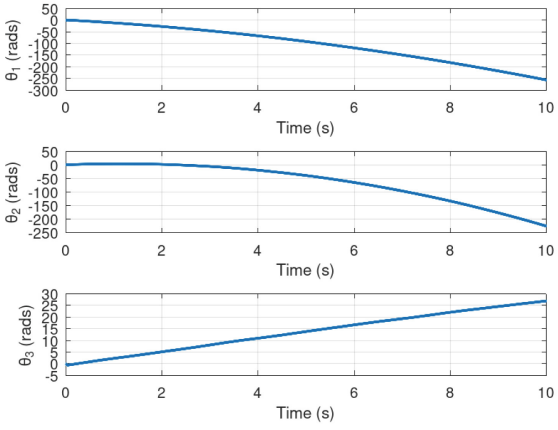

(b) Angles of the actuators of the Delta Parallel robot

Fig. 2. Position of the moving platform and actuator angles of the Delta parallel robot

In Fig. 2a it is shown the position of the moving platform of the Delta parallel robot in order to follow sinusoidal references trajectories. It can be seen that the references are tracked efficiently by the measured position of the Delta robot,

this is achieved by the action of the disturbance rejection controller despite there is a disturbance force at 5 s. Meanwhile, in Fig. 2b the angles of the actuator are presented showing how they evolve in time by the action of the disturbance rejection controller.

Meanwhile in Fig. 3a and Fig. 3b the linear and angular velocities of the moving platforms and the actuators are evinced showing their evolution in time. Then in Fig. 4a and Fig. 4b the force and the actuator angles of the Delta parallel robot are shown, evincing the control effort of each of the actuators and the platform forces.

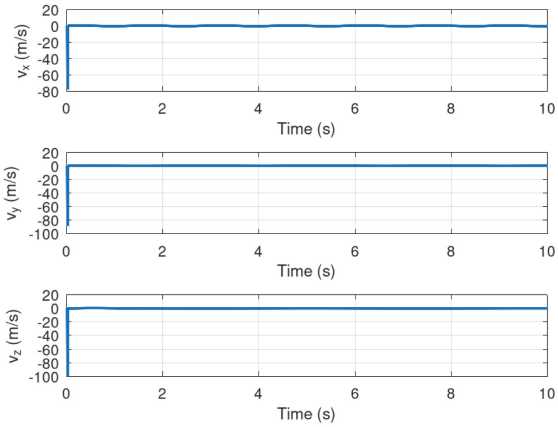

(a) Velocity of the moving platform of the Delta Parallel Robot

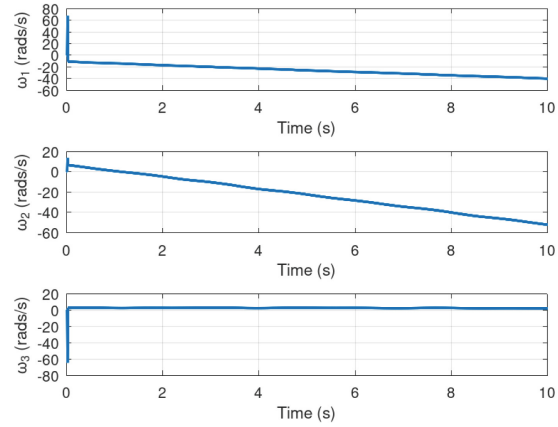

(b) Angular velocity of the actuators of the Delta Parallel robot

Fig. 3. Linear velocity of the moving platform and actuator angular velocities of the Delta parallel robot

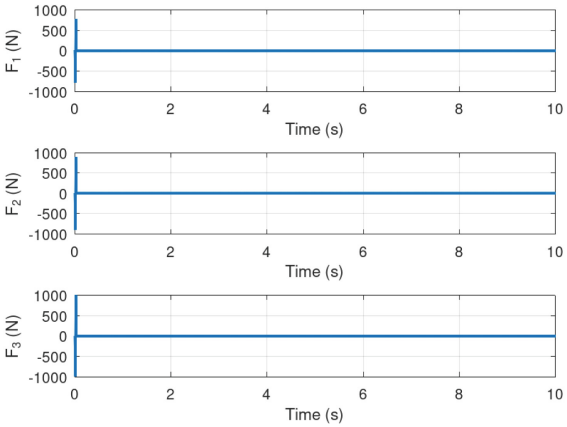

(a) Force of the moving platform of the Delta Parallel Robot

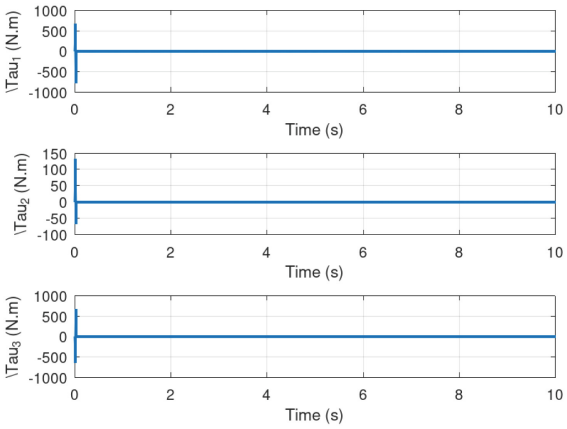

(b) Torque of the actuators of the Delta Parallel robot

Fig. 4. Force of the moving platform and actuator torques of the Delta parallel robot

Finally, in Fig. 5 the 3D plot of the trajectory of the moving platform of the delta parallel robot is shown in order to corroborate the results shown in Fig. 2a.

5 Discussion

In this research study is presented the theoretical and experimental results of the trajectory tracking of a Delta parallel robot with disturbance. It is verified first theoretically and then numerically that this parallel robot follow the pre-defined trajectory of the moving platform. It is verified that the trajectory of the Delta parallel robot is tracked accurately by the action of the disturbance rejection

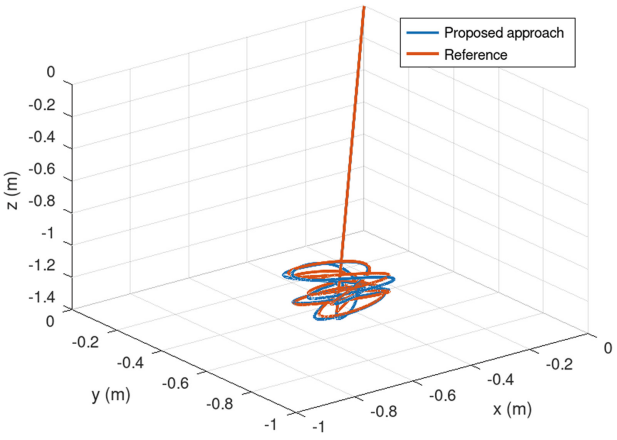

Fig. 5. 3D plot of the Delta parallel robot trajectory

H-infinity controller with a considerable low control effort. The velocities of the actuators act according to the torque applied on them. It is important to remark that the dynamic model posses the singularity restrictions considering the forward kinematic of the robot.

6 Conclusion

In this paper it is shown the results of this research study regarding to the H-infinity controller synthesis for a Delta parallel robot with disturbance. First by the use of the forward kinematic model a feasible dynamic model is obtained by Euler-Lagrange formulation in order to design the proposed control strategy. Then by the use of the disturbance rejection properties and the appropriate Lyapunov functional a control law is obtained. The experimental results validate the theoretical results obtained in this research study.

References

1. Alton Dsouza, D., Muhammad Rafikh, R., Jaiswal, A.: Position error estimation and compensation of 3-DOF delta robot under the effect of link tolerances. Mater. Today Proc. **62**, 1554–1559 (2022). International Conference on Recent Advances in Modelling and Simulations Techniques in Engineering and Science
2. Angel, L., Viola, J.: Fractional order PID for tracking control of a parallel robotic manipulator type delta. ISA Trans. **79**, 172–188 (2018)
3. Bedolla-Martinez, D., Kali, Y., Saad, M., Ochoa-Luna, C., Rahman, M.H.: Learning human inverse kinematics solutions for redundant robotic upper-limb rehabilitation. Eng. Appl. Artif. Intell. **126**, 106966 (2023)

4. Cardona, M.: A new approach for the forward kinematics of general Stewart-Gough platforms. In: 2015 IEEE Thirty Fifth Central American and Panama Convention (CONCAPAN XXXV), pp. 1–6 (2015). https://doi.org/10.1109/CONCAPAN.2015.7428478
5. Cardona, M.: Kinematics and Jacobian analysis of a 6UPS Stewart-Gough platform. In: 2016 IEEE 36th Central American and Panama Convention (CONCAPAN XXXVI), pp. 1–6 (2016). https://doi.org/10.1109/CONCAPAN.2016.7942377
6. Cardona Gutierrez, M.N.: Dimensional synthesis of 3RRR planar parallel robots for well-conditioned workspace. IEEE Lat. Am. Trans. **13**(2), 409–415 (2015). https://doi.org/10.1109/TLA.2015.7055557
7. Codourey, A., Clavel, R., Burckhardt, C.: Control algorithm and controller for the direct drive delta robot. IFAC Proc. Vol. **24**(9), 543–549 (1991). 3rd IFAC Symposium on Robot Control 1991 (SYROCO 1991), Vienna, Austria, 16–18 September 1991
8. Falezza, F., et al.: A novel inverse dynamic model for 3-DOF delta robots. Mechatronics **83**, 102752 (2022)
9. Fan, J., Vargas, L., Kamper, D.G., Hu, X.: Robust neural decoding for dexterous control of robotic hand kinematics. Comput. Biol. Med. **162**, 107139 (2023)
10. Fang, Y., Fei, J., Wang, S.: H-infinity control of mems gyroscope using t-s fuzzy model. IFAC-PapersOnLine **48**(14), 241–246 (2015). 8th IFAC Symposium on Robust Control Design ROCOND 2015
11. Feng, X., Tian, D., Wu, H., Qian, C., Zhu, D.: A matrix-solving hand-eye calibration method considering robot kinematic errors. J. Manuf. Process. **99**, 618–635 (2023)
12. Guglielmetti, P., Longchamp, R.: Task space control of the delta parallel robot. IFAC Proc. Vol. **25**(29, Part 1), 337–342 (1992). IFAC Workshop on Motion Control for Intelligent Automation, Perugia, Italy, 27–29 October 1992
13. Guglielmetti, P., Longchamp, R.: A closed form inverse dynamics model of the delta parallel robot. IFAC Proc. Vol. **27**(14), 51–56 (1994). Fourth IFAC Symposium on Robot Control, Capri, Italy, September 19–21, 1994
14. Liu, C., Cao, G., Qu, Y.: Safety analysis via forward kinematics of delta parallel robot using machine learning. Saf. Sci. **117**, 243–249 (2019)
15. Liu, Y., et al.: On a hierarchical adaptive and robust inverse dynamic control strategy with experiment for robot manipulators under uncertainties. Control. Eng. Pract. **138**, 105604 (2023)
16. Mai, T., Tran, H.: An adaptive robust backstepping improved control scheme for mobile manipulators robot. ISA Trans. **137**, 446–456 (2023)
17. Pham, P.C., Kuo, Y.L.: Model-based and model-free collision detection and identification for a parallel delta robot with uncertainties. Control. Eng. Pract. **139**, 105663 (2023)
18. Quinn, A.R., Saxby, D.J., Yang, F., de Sousa, A.C., Pizzolato, C.: A digital twin framework for robust control of robotic-biological systems. J. Biomech. **152**, 111557 (2023)
19. Rigatos, G., Siano, P., Raffo, G.: An h-infinity nonlinear control approach for multidof robotic manipulators. IFAC-PapersOnLine **49**(12), 1406–1411 (2016). 8th IFAC Conference on Manufacturing Modelling, Management and Control MIM 2016
20. Shehata, M., Elshami, M., Bai, Q., Zhao, X.: Parameter estimation for multibody system dynamic model of delta robot from experimental data. IFAC-PapersOnLine **54**(14), 72–77 (2021). 3rd IFAC Conference on Modelling, Identification and Control of Nonlinear Systems MICNON 2021

21. Shen, H., Meng, Q., Li, J., Deng, J., Wu, G.: Kinematic sensitivity, parameter identification and calibration of a non-fully symmetric parallel delta robot. Mech. Mach. Theory **161**, 104311 (2021)
22. Song, Y., Tian, W., Tian, Y., Liu, X.: An efficient calibration method for serial industrial robots based on kinematics decomposition and equivalent systems. Robotics Comput. Integrated Manuf. **84**, 102607 (2023)
23. Vladu, E., Rantzer, A.: Global solution to an h-infinity control problem for control-affine systems. IFAC-PapersOnLine **55**(30), 388–393 (2022). 25th International Symposium on Mathematical Theory of Networks and Systems MTNS 2022
24. Wang, X., Katupitiya, J.: Robust control of a dual-arm space robot to capture a non-cooperative target in 3D space. Aerosp. Sci. Technol. **141**, 108538 (2023)
25. Yan, X., Wang, P., Qing, J., Wu, S., Zhao, F.: Robust power control design for a small pressurized water reactor using an h infinity mixed sensitivity method. Nucl. Eng. Technol. **52**(7), 1443–1451 (2020)
26. Zhang, Y., Zhao, M., Sun, D., Liu, X., Huang, S., Chen, D.: Robust H-infinity control for connected vehicles in lattice hydrodynamic model at highway tunnel. Phys. A **603**, 127710 (2022)
27. Zhu, M., Briot, S., Chriette, A.: Sensor-based design of a delta parallel robot. Mechatronics **87**, 102893 (2022)

Development of a Digital Twin for a Laser Metal Deposition (LMD) Additive Manufacturing Cell

Brayan S. Figueroa(✉), Lucas Araújo, and Alberto Alvares

Brasília University, Brasília 70910-900, Brazil
brayan.s.figueroa47@gmail.com , alvares@alvarestech.com

Abstract. This work focuses on developing and implementing a Digital Twin for an additive metal manufacturing cell that utilizes the laser metal deposition (LMD) technique with a KUKA robot and MELTIO deposition head. The Digital Twin (DT) serves as a highly accurate virtual representation of the physical system, enabling operation simulations, real-time monitoring, and data collection for analysis. The DT architecture is designed following the ISO-23247 standard, providing a structured and standardized framework for Digital Twin implementation. To achieve this, various cutting-edge software tools are employed, including Grasshopper within Rhinoceros 7 for programming, modeling, and simulation, KUKA.sim for precise operation monitoring, Node-RED and AWS IoT Core for efficient data processing and communication, and an AWS DynamoDB database for secure and organized storage of all collected data. This comprehensive integration of advanced technologies allows for valuable insights into system performance and establishes a solid foundation for informed decision-making in the field of additive metal manufacturing.

1 Introduction

The current era is characterized by the continuous technological development, introducing new technologies and solutions into the market and industry daily. In this context of progress and innovation, Industry 4.0 emerges, marked by technologies such as the Internet of Things (IoT), artificial intelligence, Big Data, cloud computing, 5th generation mobile networks (5G), and additive manufacturing. Its objective is to achieve higher performance and efficiency at a lower cost by enabling the interaction between the physical and digital worlds [2]. In this scenario, the present work addresses the implementation of a Digital Twin for a metal additive manufacturing cell using laser metal deposition (LMD).

Laser metal deposition is a process that allows the creation of complex metal parts in various shapes and sizes, with precision, cost-effectiveness, and above all, flexibility [3,10]. When combined with industrial robotics, it enables the production of different parts within the same cell, with minimal setup time between each production, providing advantages for various industrial applications [9]. The aerospace sector is one area with prominent LMD applications [7,8]. The tools used in the cell simulated by the Digital Twin are the KUKA KR 70 R2100

M. N. Cardona et al. (Eds.): LACAR 2023, LNNS 940, pp. 68–76, 2024.
https://doi.org/10.1007/978-3-031-54763-8_7

robot and the KR C5 controller, both from KUKA, along with the MELTIO deposition head.

One of the most widely accepted definitions of a Digital Twin was introduced by NASA in 2012. They described it as "an integrated, multi-physics, multi-scale, and probabilistic simulation of a built vehicle or system that uses the best available physical models, sensor updates, historical data, etc., to mirror the life of its corresponding counterpart" [1]. In essence, a Digital Twin is a virtual representation that accurately mimics a physical element or process. This virtual model allows for various functionalities, such as operation simulations for testing, real-time monitoring, and data collection for analysis. By leveraging a Digital Twin, organizations can more effectively identify and prevent failures, as well as plan efficient strategies [5].

For this specific project, the Digital Twin adhered to the ISO 23247 standard developed by the Technical Committee ISO TC 184/SC 4. This standard defines the architecture of a Digital Twin manufacturing framework, offering the flexibility for context-dependent implementations, component composition, and structure reuse [4]. To implement the Digital Twin, the project utilized the KUKA.Sim software, which is designed to interpret instructions in the KUKA Robot Language (KRL), the communication language for KUKA technologies. While there are various software options available for generating KRL code, the project chose to work with the Grasshopper tool within the Rhinoceros 7 CAD software. Grasshopper enables algorithmic modeling using components, providing a user-friendly environment that can produce intricate designs from a simple and straightforward interface. It is employed in programming the geometry of the intended piece, as well as the deposition and robot movement strategy, which can be both planar and non-planar, ultimately leading to the conversion to KRL format.

With the operational simulation running, the data is collected and sent through a Python script to the Node-RED tool, where it is displayed on a dashboard for real-time visualization and analysis. Simultaneously, the data is stored in an AWS DynamoDB database, enabling remote access from anywhere and providing the ability to perform historical analysis to enhance the ongoing system. This comprehensive and efficient approach delivers valuable insights into performance and establishes a solid foundation for making informed decisions.

2 Digital Twin

The Digital Twin framework, developed in accordance with the ISO 23247 standard, can be seen in Fig. 1. It is structured into 4 layers or entities [6]: OME, DCDCE, DTE, and DTUE:

- OME (Observable Manufacturing Element): This is the physical layer where the observable elements (actuators) of the cell are located. In this case, it consists of the KUKA KR 70 R2100 robot and the MELTIO deposition head.

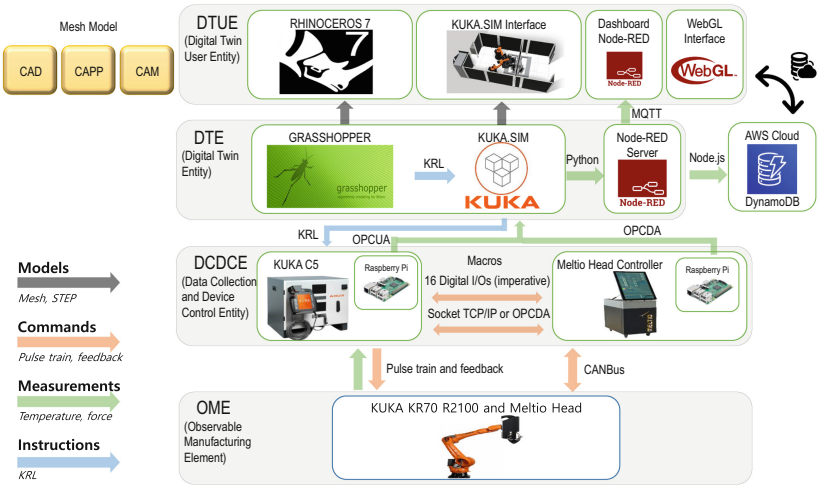

Fig. 1. Digital Twin Framework of the metal additive manufacturing cell using laser metal deposition, based on the ISO 23247 standard.

- DCDCE (Data Collection and Device Control Entity): This layer is responsible for data collection and control of the elements in the OME layer. The robot and head controllers, KR C5 and Meltio Head Controller respectively, are present here. Raspberry Pi devices are also used as PLCs to communicate with the KUKA.Sim controllers. The communication is achieved using TCP/IP sockets, utilizing the OPC-UA and OPC-DA protocols.
- DTE (Digital Twin Entity): This layer represents the actual Digital Twin, with the software used. In this case, Grasshopper is responsible for CAD/CAPP/CAM, KUKA.Sim for simulation, and Node-RED for data monitoring and storage in the database.
- DTUE (Digital Twin User Entity): This layer represents the user interface of the Digital Twin, with the software displaying the simulation and monitoring dashboards. Rhinoceros 7 generates the visualization of the modeling done in Grasshopper, and KUKA.Sim is responsible for the operation simulation. The visualization dashboards are accessed via a web interface using the HTTP and MQTT protocols, implemented by Node-RED.

3 User Requirements

The user requirements of the Digital Twin are divided into functional requirements (FU) and non-functional requirements (NFU), and they are listed below:

3.1 Functional Requirements (FU)

FU Requirement 1: The Digital Twin must be implemented in the KUKA.Sim software.

FU Requirement 2: Data visualization must be possible through the Web.
FU Requirement 3: Node-RED must be used in the Web implementation.
FU Requirement 4: The communication protocol between KUKA.Sim and Node-RED, as well as between Node-RED and AWS systems, must be MQTT protocol.
FU Requirement 5: Show the data in a 2D Node-RED dashboard.
FU Requirement 6: The database used must be AWS DynamoDB.
FU Requirement 7: The system will utilize the AWS IoT Core solution to mediate the communication between Node-RED and DynamoDB.
FU Requirement 8: It must be possible to monitor the movement of the robot's 6 joints during an operation.

3.2 Non-functional Requirements (NFU)

NFU Requirement 1: The data visualization must be compatible with the latest browsers (e.g., Chrome, Firefox, Edge).
NFU Requirement 2: Node-RED must function both in localhost and in the cloud.
NFU Requirement 3: The system must automatically start publishing data to the cloud upon server startup.

4 UML Modeling

An overview of the implementation can be seen in the UML subsystem diagram presented in Fig. 2. The modeling of the operation in this project was done using the Grasshopper software for Rhino 7, where the geometries to be produced and the extrusion path for each part are modeled. The Robots for Grasshopper plugin was used to handle the parts related to the robot. Parameters such as

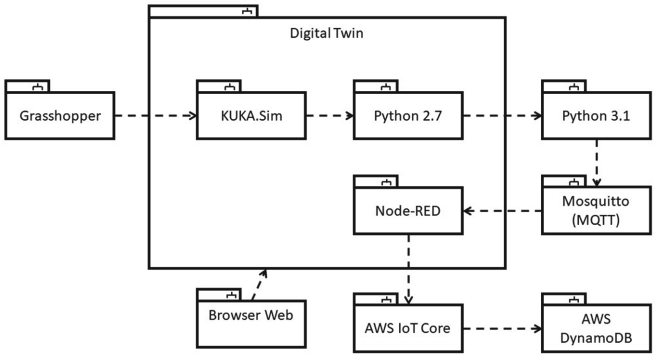

Fig. 2. UML diagram of the architecture of the Digital Twin for the manufacturing cell.

deposition speed and laser power are configured here to meet the requirements of each project, which vary according to the part to be produced. Grasshopper is a software for parametric modeling based on components, where complex geometries can be modeled quickly and efficiently. Its main advantage is its component-based structure, which allows the creation of parametric shapes that can be easily modified and updated in real-time, enabling designers to explore different variations and iterations of a design.

Grasshopper is responsible for the entire modeling and programming of the piece, and then it converts the program into KRL code, which is the language that allows communication with KUKA technologies. The KRL code is sent to the KUKA.Sim software, where the Digital Twin actually starts. In KUKA.Sim, simulations are performed, operations are monitored, and operation data is collected using Python code to be sent to Node-RED. Node-RED processes and organizes the data graphically for easy interpretation by the user. The communication between Python and Node-RED is done using the MQTT protocol through the Mosquitto broker. Node-RED also establishes a connection with AWS IoT Core, responsible for communicating with the AWS DynamoDB database. Data visualization and monitoring of dashboards are accessible via a web browser. Figure 3 shows the KUKA.Sim interface, with the KR 70 R2100 robot, KUKA C5 controller, MELTIO deposition head, and the support table for metal deposition.

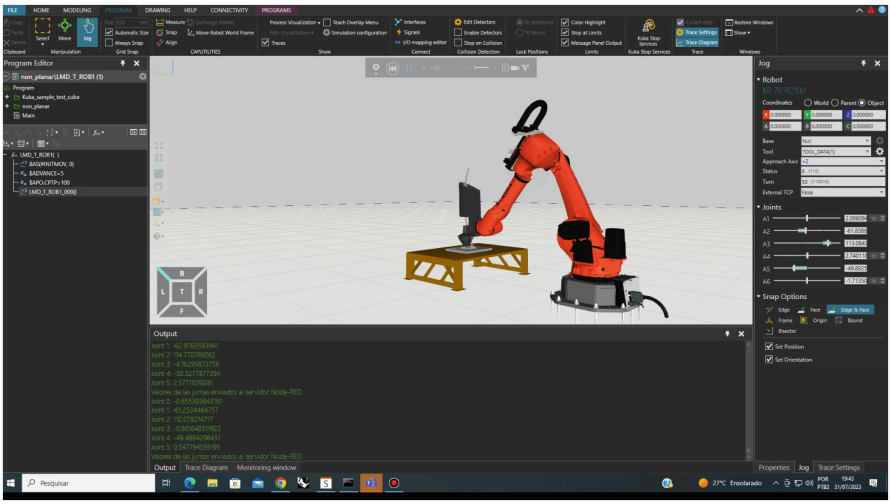

Fig. 3. KUKA.Sim simulation environment, with the KUKA robot and controller, the MELTIO deposition head, and the support table for deposition.

5 Use Cases

This document addresses a use case focused on monitoring the positions of a KUKA robot's joints during an operation. The robot has 6 degrees of freedom, represented by variables X, Y, Z, A, B, and C, corresponding to each of its 6 joints. To obtain the joint positions during the operation, a Python script within KUKA.Sim was utilized. However, KUKA.Sim comes with Python version 2.7, lacking functionalities related to the MQTT protocol, which are only available from version 3.1 onwards. As a result, the Python 2.7 script resorts to using UDP sockets to collect the values and sends them to an external Python program equipped with a compatible version of MQTT. In this setup, the second program establishes an MQTT connection with Node-RED using the Mosquitto broker (as depicted in the UML diagram in Fig. 2). To ensure proper communication, Mosquitto is specifically configured to use communication port 6000, as permitted by the University of Brasília to avoid issues with the university's firewall. Once the communication with Node-RED is established, the data is processed and presented in a dashboard with graphical representations (graphs).

The structure of the Node-RED nodes involved in data processing can be observed in Fig. 4. The MQTT Input node receives the data from the communication with Mosquitto and forwards it to the Process Data node, where it is organized into an object containing the timestamp of the data collection and the joint values. The function nodes from 1 to 6 are then responsible for separating the values of each joint and passing them to dashboard nodes. These dashboard nodes display the joint positions as graphs on a 2D dashboard. Additionally, there is a Debug node available for process debugging. The resulting graphical

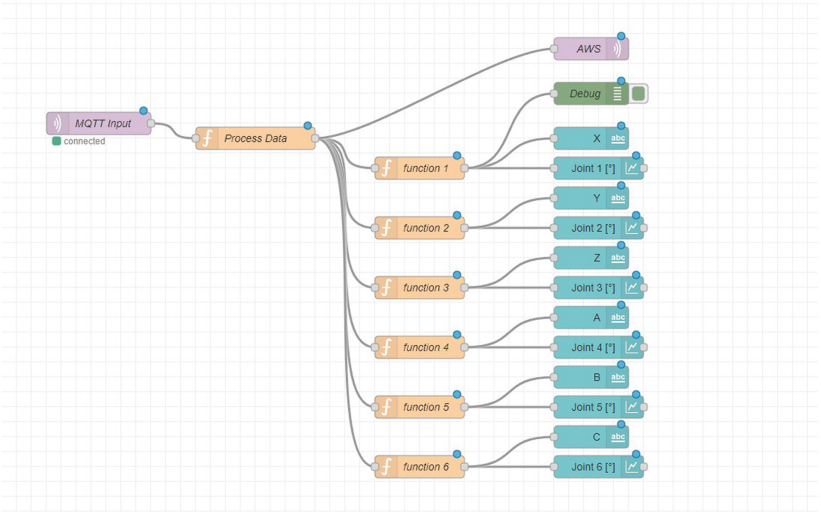

Fig. 4. Node-RED flow responsible for displaying the robot joint positions in graphs on the dashboard.

visualization obtained after processing the data in Node-RED is shown in Fig. 5. Each graph on the dashboard represents one joint of the robot, and the x-axis shows timestamps of each position collection, while the y-axis represents the corresponding joint values. With the data points separated by 1 s (the time between each joint position collection in KUKA.Sim), real-time monitoring of the joint values becomes feasible.

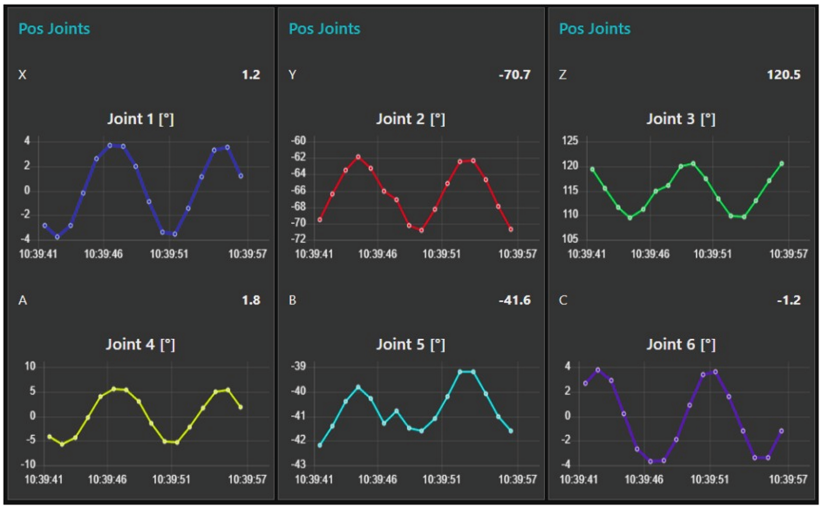

Fig. 5. Node-RED dashboard displaying the positions of the 6 robot joints during an operation.

The AWS node in Fig. 4 establishes MQTT communication with AWS IoT Core, which receives the values of the 6 robot joints and a timestamp to record the date and time related to those values. The AWS system then performs internal procedures to communicate IoT Core with the DynamoDB database. As both solutions belong to Amazon Web Services (AWS), it is easy to establish this communication, as there are documentations and tutorials from AWS that provide simple instructions on how to perform such procedures. As a result, the joint positions and timestamp are separated into columns and added to a table in the database, automatically registered every 1 s whenever new values are collected by the Digital Twin. An overview of the table is shown in Fig. 6. This allows real-time monitoring from any location, as DynamoDB operates in the cloud, facilitating the use of this data for predictive analysis, preventive and predictive maintenance, and all relevant inquiries and studies. It is worth noting that this particular use case is specific to monitoring the robot's joint positions, as can be visualized in the (https://youtu.be/80m1G-9dw7k)which displays the digital twin developed for monitoring the mentioned data [12].

Various other use cases can be considered, such as collecting and monitoring joint speed and acceleration values, position, speed, and acceleration of the tool

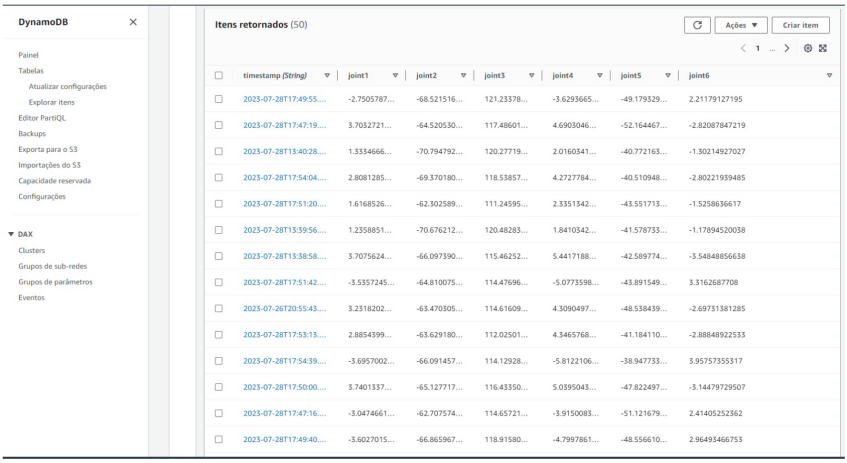

Fig. 6. DynamoDB Database Table, displaying multiple collections and their respective timestamp and joint position values.

tip (MELTIO head), deposition speed, laser power, creating a specific geometry, or triggering the cell's emergency button, which halts the operation. All these follow the same architectural logic presented here and can be implemented using the same technologies used in the discussed use case. Other use cases will be implemented in the future.

6 Conclusion

This work described the construction of a Digital Twin for a metal additive manufacturing cell using laser metal deposition (LMD) process. After a brief explanation of the terminologies, it covered the software used in the implementation of the proposed solution and the communication methods between them, aiming to detail the peculiarities of this increasingly used technology in today's industry and encourage new implementation proposals, serving as a reference for future research. Robotic additive manufacturing combined with laser metal deposition opens up a range of possibilities, always aiming for optimization, efficiency, and cost-effectiveness [11], and when combined with other Industry 4.0 technologies such as the internet of things, big data, and artificial intelligence, it becomes a valuable solution for modern challenges.

References

1. Glaessgen, E., Stargel, D.: The digital twin paradigm for future of NASA and U.S. air force vehicles. In: 53rd AIAA/ASME/ASCE/AHS/ASC Structures, Structural Dynamics and Materials Conference (2012). https://doi.org/10.2514/6.2012-1818

2. Jan, Z., Ahamed, F., Mayer, W., et al.: Artificial intelligence for industry 4.0: systematic review of applications, challenges, and opportunities. Expert Syst. Appl. **216**, 119456 (2023)
3. Bremer, J., Gasser, A., Schleifenbaum, J.H.: Measurement of robotic path deviations and its influence on additively manufactured components. In the composites and advanced materials expo (2019)
4. Shao, G., Helu, M.: Framework for a digital twin in manufacturing: scope and requirements. Manuf. Lett. **24**, 105–107 (2020)
5. Liu, C., Le Roux, L., Körner, C., et al.: Digital twin-enabled collaborative data management for metal additive manufacturing systems. J. Manuf. Syst. **62**, 857–874 (2022)
6. Cabral, J.V.A., Gasca, E.A.R., Alvares, A.J.: Digital twin implementation for machining center based on ISO 23247 standard. IEEE Lat. Am. Trans. **21**, 628–635 (2023)
7. Garmendia, I., Pujana, J., Lamikiz, A., et al.: Structured light-based height control for laser metal deposition. J. Manuf. Process. **42**, 20–27 (2019)
8. Gu, H., Li, L.: Computational fluid dynamic simulation of gravity and pressure effects in laser metal deposition for potential additive manufacturing in space. Int. J. Heat Mass Transf. **140**, 51–65 (2019)
9. Feng, A., Chen, C., Wu, C., et al.: Modeling of laser melting deposition equipment based on digital twin. Metals (2022). https://doi.org/10.3390/met12020169
10. Yan, L., Chen, Y., Liou, F.: Additive manufacturing of functionally graded metallic materials using laser metal deposition. Addit. Manuf. **31**, 100901 (2020)
11. Lettori, J., Raffaeli, R., Bilancia, P., et al.: A review of geometry representation and processing methods for cartesian and multiaxial robot-based additive manufacturing. Int. J. Adv. Manuf. Technol. **123**, 3767–3794 (2022)
12. Figueroa, B.S.: Digital Twin LMD Additive Manufacturing Cell (2023). https://youtu.be/80m1G-9dw7k

Synergistic Design of Optimal PI Controllers for Linear Time-Delayed Systems

Julián-Alejandro Hernández-Gallardo[1,2(✉)], Adrián-Josué Guel-Cortez[3], Emilio-J. González-Galván[1], Juan-Antonio Cárdenas-Galindo[1], Liliana Félix[1], and César-Fernando Méndez-Barrios[1]

[1] Facultad de Ingeniería, Universidad Autónoma de San Luis Potosí (UASLP), Dr. Manuel Nava No. 8, San Luis Potosí, S.L.P., Mexico
julian_@ieee.org, fernando.barrios@uaslp.mx

[2] Tecnológico Salesiano Carlos Gómez, J. Venegas No. 5, Virreyes, C.P. 78240, San Luis Potosí, S.L.P., Mexico

[3] Brill Power Limited, 3-5 Hythe Bridge Street, Oxford OX1 2EW, UK

Abstract. This article explores an innovative approach for fine-tuning Proportional-Integral (PI) controllers to achieve rapid and energy-efficient responses in linear time-delayed dynamical systems. The method synergistically combines a classical meta-heuristic algorithm with an analytical-geometric stability analysis procedure to minimise a cost function based on quadratic regulator principles. In particular, we employ the $\mathcal{D}-$composition method to characterise the stability map of the closed-loop system, narrowing down the optimisation search space for a genetic algorithm. This holistic strategy not only effectively tackles the complexities introduced by time delays within the optimisation procedure, but also permits us to improve PI controls performance across diverse real-world applications. Furthermore, we include a comprehensive comparative analysis between our results and a PI control that is analytically engineered to elicit maximal exponential decay. The article culminates by showcasing both numerical simulations and experimental control applications, underscoring the practical efficacy of the proposed methodology.

1 Introduction

It is well known that any plant or process is subject to time delays due to physical inertia, state variable measurements, computational costs, or communication procedures (latency) (see, for instance, [2,5]). Hence, when designing controls for time-delayed systems, understanding and modeling time delays is critical to prevent stability problems and to improve overall system performance [5].

From all the existing control techniques, low-order controllers such as the Proportional Integral (PI) controllers are of great interest due to their simplicity in implementation and structure. In addition, PIs are essential in the design of servo systems due to their ability to balance stability, speed of response, and

M. N. Cardona et al. (Eds.): LACAR 2023, LNNS 940, pp. 77–88, 2024.
https://doi.org/10.1007/978-3-031-54763-8_8

accuracy. The response of a PI controller involves the sum of the responses due to a proportional control (P), which will be instantaneous to the detection of the error signal, and with an inevitable delay will come into action the integral control (I), which will be responsible for cancelling the entire error signal [6].

The literature presents different PI control tuning methods. For instance, [13] shows explicit design formulas of P and PI controllers for unstable first-order plus delay processes derived using the Nyquist stability criterion. In [9], throughout a geometric approach, presents the study of PI controllers stability and fragility in Linear-Time-Invariant (LTI) Single-Input-Single-Output (SISO) systems subject to delays in the input or output. In [12], the authors focus on the characterization of the maximum exponential decay rate for closed-loop time-delayed first-order systems with PI controllers, providing a fully analytical tuning rule to achieve an optimal response in terms of the speed of the output response. Finally, in [11], authors present a new concept for PI control design named weighted geometric center of the stabilizing controller parameters.

While closed-loop stability is an obligatory requirement in all control systems, practicioners also commonly need, at the same time, to satisfy multiple objectives such as the settling time, overshoot, control effort, energy consumption or heat production. In this context, population based multi-objective optimization algorithms such as the Genetic Algorithm (GA) [10], Differential Evolution (DE) [3], Ant Colony Optimization (ACO) [1], and Particle Swarm Optimization (PSO) [8] are the most popular methods in several controller tuning approaches.

Nontheless, population-based optimisation algorithms (PBOAs) do not guarantee that you will always obtain a global minimum, must be given a search region, have a long computation time, etc. In this regard, this work proposes including analytic results in PBOAs to alleviate their drawbacks. Specifically, we use the $\mathcal{D}$-Decomposition theory [4] to generate the closed-loop system stability region in the space of the PI control parameters. Next, we apply this region to compact the search space of a classic GA seeking PI controls with rapid and energy-efficient responses. The synergy increases the probability of getting a global minima and reduces computational costs. We use our method in a numerical and experimental scenario. Furthermore, using one of these scenarios, we compare our results with the PI control analytically designed to have the maximal exponential decay.

2 Preliminary Results and Problem Formulation

Let us consider a LTI-SISO system with constant time delay $h > 0$ given by the following transfer function

$$G(s) = \frac{N(s)}{D(s)} e^{-hs}, \quad h \in \mathbb{R}_+, \tag{1}$$

subject to a classical PI controller defined by

$$C(s) = k_p + \frac{k_i}{s}, \quad k_p, k_i \in \mathbb{R}. \tag{2}$$

To perform a closed-loop stability study for (1) subject to (2), it is necessary to make the following definitions and notes.

Definition 1. The closed-loop system of the plant (1) with the controller (2) is defined as follows

$$T(s;k_p,k_i) := \frac{(k_p s + k_i)N(s)e^{-hs}}{sD(s) + (k_p s + k_i)N(s)e^{-hs}}. \tag{3}$$

Definition 2. The characteristic quasi-polynomial of the closed-loop system (3) is given by

$$\Delta(s;k_p,k_i) := sD(s) + (k_p s + k_i)N(s)e^{-hs}. \tag{4}$$

Definition 3 ([9]). The frequency crossing set $\Omega \subset \mathbb{R}$ is the set of all $\omega \in \mathbb{R}$ such that, there exists at least a duplet $(k_p, k_i) \in \mathbb{R}^2$ for which:

$$\Delta(\boldsymbol{i}\omega;k_p,k_i) = 0. \tag{5}$$

Remark 1. Definition 3 considers only positive frequencies. The reason for such a consideration follows from the observation:

$$\Delta(-\boldsymbol{i}\omega;k_p,k_i) = \overline{\Delta(\boldsymbol{i}\omega;k_p,k_i)}. \tag{6}$$

Definition 4 ([9]). The *stability crossing curves* (also called stability boundaries in this work) $\mathcal{T}$ is the set of all parameters $(k_p, k_i) \in \mathbb{R}^2$ for which there exists at least one $\omega \in \Omega$, such that, $\Delta(\boldsymbol{i}\omega;k_p,k_i) = 0$. Moreover, any point $\boldsymbol{k} \in \mathcal{T}$ is known as a *crossing point*.

Now, note that when the quasipolynomial (4) is stable, we have all its roots in the left-hand side of the complex plane. Furthermore, these roots can only cross the unstable side (or become unstable) in three possibilities: through the origin of the complex plane (Real Root Boundary), through infinity (Infinite Root Boundary) and at a finite number of singular frequencies (Complex root Boundary), forming what we call the closed-loop stability map $\mathcal{S}$ (see Fig. 1). The objective of generating such stability maps is to reduce the search space of the optimization algorithm by providing the search set $\mathcal{G} \supset \mathcal{S}$ defined as

$$\mathcal{G} := \left\{ (k_p,k_i) \,\middle|\, k_p^l \le k_p \le k_p^u \wedge k_i^l \le k_i \le k_i^u \right\} \tag{7}$$

This benefits the algorithm by only considering control gains that result in stable responses, ignoring (k_p, k_i) duplets of no interest. The *synergistic design* for control systems comes with combining these two tuning techniques.

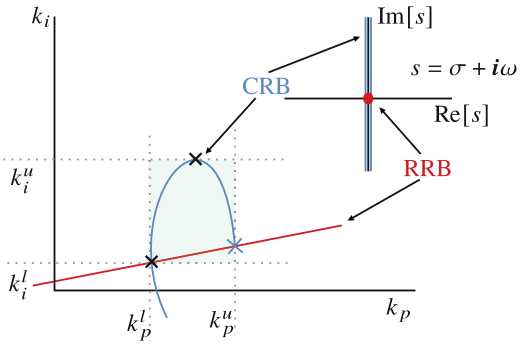

Fig. 1. Mapping of the stability crossing curves from the complex plane to the parameters plane.

As a byproduct, this work compares the control with the fastest response according to the maximum exponential decay (MED) method and the optimal control produced by our synergistic algorithm. The MED of a control system is said to occur when a root has a multiplicity of two or greater. The MED is the maximum value on the real axis of the complex plane to which the spectral abscissa can be shifted, that is, the maximum to which the dominant roots of a system can move. The design of a controller that guarantees the MED depends on several factors, the degrees of freedom of the controller (gains to be tuned), how the $\mathcal{T}$ curve behaves, to know if it occurs in a double real root, double complex root, triple real root, etc. We discuss more about MED in Sect. 3.

Based on the above, in this work, we solve the following two problems:

Problem 1. Obtain analytical conditions on the parameters (k_p, k_i) such that the controller PI asymptotically stabilizes the closed-loop plant described by the transfer function in (3).

Problem 2. Given

$$\begin{aligned} &\text{minimize} \quad J \\ &\text{subject to} \quad \boldsymbol{k}^* \in \mathcal{G}, \end{aligned} \tag{8}$$

obtain the vector of optimal control gains $\boldsymbol{k}^*$, where $\boldsymbol{k}^* = [k_p^*, k_i^*]^T$, $\mathcal{G}$ is the controls search region (see Sect. 3) and J is a cost function seeking to adjust: Settling time (t_s) + Absolute Control Effort Square (ACES) + Absolute Control Variation Square (ACVS) defined as

$$J = t_s + \int_0^{t_s} \left(\beta|u(\tau)|^2 + \gamma|\dot{u}(\tau)|^2\right) \mathrm{d}\tau\,, \quad \beta, \gamma \in \mathbb{R}_+, \tag{9}$$

where $t_s := \inf\{\tau \in \mathbb{R}_+ : |y(t) - r(t)| \leq \alpha, \quad \forall t \geq \tau, \quad 0 < \alpha < 1\}$.

3 Main Results

As mentioned in the previous section, this paper proposes a synergistic design between two tuning methods of different natures. Here, we separately discuss them through subsections *analytical approach* and *metaheuristic approach*.

3.1 Analytical Approach

To study the stability, we use the $\mathcal{D}$-composition method, a technique that maps the stability boundary of the complex plane to the controller's parameter space generating a "stability map". This mapping from the complex plane to the parametric plane is derived employing the following analytic results.

Proposition 1 (Complex Root Boundary (CRB)). *The stability crossing boundaries associated with (5) are described*

$$k_p(\omega) = -\frac{1}{\omega} \operatorname{Im}\left[\boldsymbol{i}\omega\, G(\boldsymbol{i}\omega)^{-1}\right] \tag{10}$$

$$k_i(\omega) = -\operatorname{Re}\left[\boldsymbol{i}\omega\, G(\boldsymbol{i}\omega)^{-1}\right] \tag{11}$$

Proposition 2 (Real Root Boundary (RRB)). *Then, the line* $\boldsymbol{k}_0 = [k_{p_0} \;\; k_{i_0}]^T \in \mathbb{R}^2$ *defined by*

$$\boldsymbol{k}_0 := \left\{ \begin{bmatrix} k_p \\ 0 \end{bmatrix} \middle| \, k_p \in \mathbb{R} \right\}, \tag{12}$$

defines a stability crossing curve. Furthermore, this line characterizes a crossing through the origin of the complex plane.

As mentioned previously, we also want to make a comparison between results from the synergestic approach against a design via looking at the maximal exponential decay MED in the $\mathcal{D}$-composition method. In this regard, let us consider the change of variable $s \to s - \sigma$ in Δ (4) to obtain:

Proposition 3 (σ-Stability Regions).

$$\begin{aligned} k_p(\omega, \sigma) &= \frac{1}{\omega} \operatorname{Im}\left[(\sigma - \boldsymbol{i}\omega)\; G(\boldsymbol{i}\omega - \sigma)^{-1}\right] \\ k_i(\omega, \sigma) &= \operatorname{Re}\left[(\sigma - \boldsymbol{i}\omega)\; G(\boldsymbol{i}\omega - \sigma)^{-1}\right] + \sigma k_p \end{aligned} \tag{13}$$

From (13), we can obtain the MED as follows: First, we use the σ-stability tuning method which consists of shifting the imaginary axis with the origin, sigma units to the left, to obtain relative stability to that mapping. As the σ parameter increases, in the parameter space (k_p, k_i) they gradually decrease and end up collapsing to a single point; visually these collapse points, correspond to the MED [7]. Note that, in order to know the multiplicity of the roots, it is necessary to know the movement of the roots with respect to the parameters. For example, in the P control there is a double real root, and in the PI control a triple real root. Second, once we know the multiplicity of the roots, we find the MED defined as σ^* by deriving (13) $n-1$ times, where n is the multiplicity of the roots, to obtain a system of equations that depend on σ^*.

3.2 Metaheuristic Approach

Since solving Problem 2 is analytically not straightforward, we proposed applying a GA as shown in Algorithm 1. The algorithm shows a pseudocode summarising the relevant parts in the algorithm. This includes selecting the gene's space $\mathcal{G} \supset \mathcal{S}$.

Algorithm 1: Synergestic Optimal Control.

Data: The system to be controlled $G(s)$; the maximum frequency ω_f; the frequency step ω_s; the simulation time t_f; the number of generations N; the weights β and γ.
Result: The optimal control $\boldsymbol{k}^* = [k_p^*, k_i^*]^T$.

```
/* D-composition method */
```
Function `D_method`$(G(s), \omega)$**:**
- $\mathcal{T} := [k_p(\omega), k_i(\omega)]^\top = [-\frac{1}{\omega} \operatorname{Im}\left[\boldsymbol{i}\omega\, G(\boldsymbol{i}\omega)^{-1}\right], -\operatorname{Re}\left[\boldsymbol{i}\omega\, G(\boldsymbol{i}\omega)^{-1}\right]]^\top$
- $\mathcal{T}_0 := \begin{bmatrix} k_p \\ 0 \end{bmatrix} | k_p \in \mathbb{R}$
- **return** $\mathcal{T}, \mathcal{T}_0$

```
/* Cost function */
```
Function $J(G(s), \alpha, \beta, \gamma, t_f)$**:**
- $\text{cost} = t_s(\alpha) + \int_0^{t_s} \left(\beta |u(\tau)|^2 + \gamma |\dot{u}(\tau)|^2\right) \mathrm{d}\tau$
- **return** cost

```
/* Main procedure */
```
Function `Main(`$\boldsymbol{k}$`)`**:**
- $\omega = 0^+ : \omega_s : \omega_f$ `// Initialise the frequency set` ω
- $[\mathcal{T}, \mathcal{T}_0]$=`D_method(`$G(s), \omega$`)`
- `/* Define` $\mathcal{G}$ `*/`
- $[k_p^l, k_d^l]^\top = \min_\omega(\mathcal{T}, \mathcal{T}_0)$
- $[k_p^u, k_d^u]^\top = \max_\omega(\mathcal{T}, \mathcal{T}_0)$
- `/* MATLAB ga optimization method */`
- sol=`ga(@(`$\boldsymbol{k}$`)` $J(G(s), \alpha, \beta, \gamma, t_f)$`,2,[],[],[],[],[`$k_p^l, k_d^l$`],[`$k_p^u, k_d^u$`])`
- **return** sol

4 Applications

This section presents numerical and experimental case studies where the results shown in Sect. 3 are applied.

4.1 Numerical Case: Haptic Device

A haptic interface is a technology that enables communication and feedback between a digital system and a user through the sense of touch. The goal of a

haptic interface is to provide a more immersive and realistic experience to the user, either through vibrations, textures, movements, or other forms of tactile feedback, in various fields, such as electronic devices, virtual reality (VR), augmented reality (AR), simulators, video games, medical devices, among others. The dynamics of the device can be described as a set of decoupled time-invariant linear models formed by three mechanical admittances given by the following equation for each joint of the haptic unit (Fig. 2):

Fig. 2. Haptic unit: Touch 3D Stylus.

$$G(s) = \frac{1}{s(ms+b)} e^{-hs}, \tag{14}$$

where $m = 0.0131$, $b = 0.0941$ and $h = 0.1$. In this case, the cost function J will be optimized for different cases.

- $\boldsymbol{t_S}$ **vs MED**: The optimization procedure was executed under the influence of a step-type input. The graphical representation in Fig. 3 elucidates the time response achieved using a PI controller modified by a genetic algorithm (PI_{GA}). This achieved response is compared against the time response of a PI (PI_{MED}) controller and a P (P_{MED}) controller, both fine-tuned using the MED methodology. Note that, the PI_{GA} controller displays a distinct swiftness in converging within the 1% threshold of the reference signal. This rapid response is accompanied by a nearly negligible overshoot, underscoring the controller's adeptness at maintaining stability. Furthermore, this PI_{GA} controller demonstrates an exceptional capability in eradicating steady-state errors, thus contributing to precise and robust control performance.

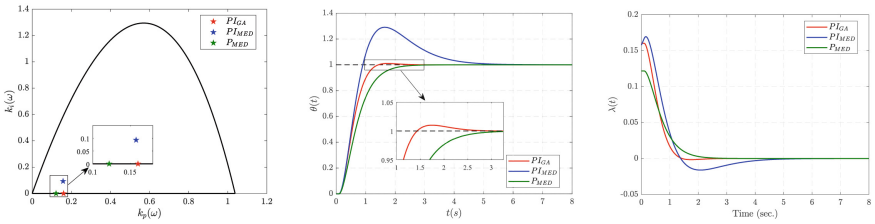

(a) Stability region and controllers. (b) Time responses. (c) Control efforts.

Fig. 3. Total time response with step-type entry case No. 1.

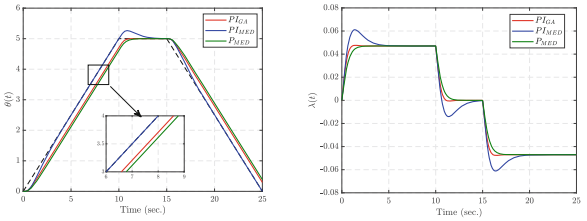

(a) Time responses. (b) Control efforts.

Fig. 4. Total time response with ramp-type entry case No. 1.

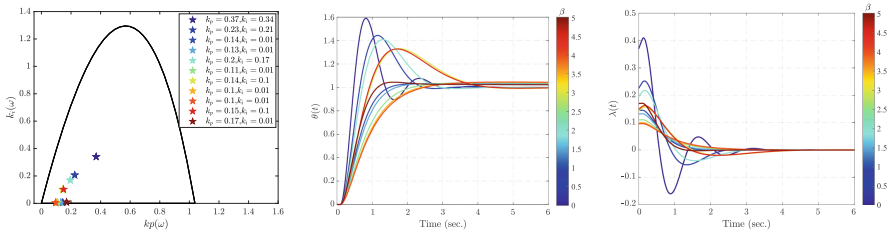

(a) Stability region and controllers. (b) Time responses. (c) Control signals.

Fig. 5. Total time response with step-type entry case No. 2.

When regulating the system's output in response to a ramp-type reference input under the same controls, a discernible shift in performance characteristics becomes evident (refer to Fig. 4). Specifically, the PI_{MED} controller exhibits a notably enhanced response compared to its counterpart synthesized via the optimization algorithm. Note that PI_{GA} is only a proportional controller, i.e., k_i is almost zero, which is not good enough to have zero steady-state error when the input is a ramp. Recall that the synergetic design assumes a unit step as a reference. Thus, while the results of the synergistic approach depend on the design assumptions, the MED design results do not.

- $\boldsymbol{t_s}$**+ACES**: The next scenario introduces the application of a cost function encompassing set-up time and control effort, as determined through the ACES criterion. In this regard, we solve (9) using $\beta \in [0, 5]$ and $\gamma = 0$. The results are illustrated in Fig. 5. As expected, the control effort u time response is smoother and quicklier as β increases its value.
- $\boldsymbol{t_s}$**+ACES+ACVS**: Concluding this application, we introduce the ACVS criterion into cost function (9) by using $\gamma > 0$. Specifically, we set $\beta = 1$ and $\gamma \in [0, 5]$. As illustrated in Fig. 6, the ACVS criterion produces output y and force u time responses with less oscilations and overshoot as γ increases its value.

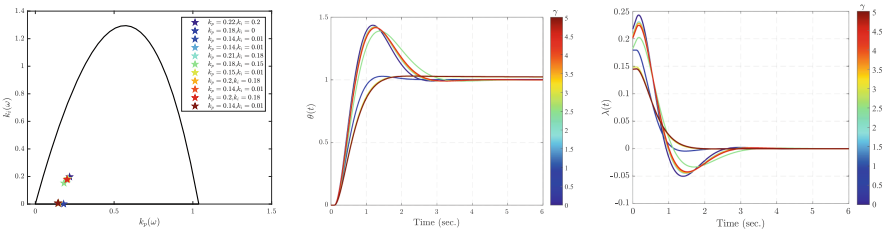

(a) Stability region and controllers.

(b) Time responses.

(c) Control signals.

Fig. 6. Total time response with step-type entry case No. 3.

4.2 Experimental Case: Servo System

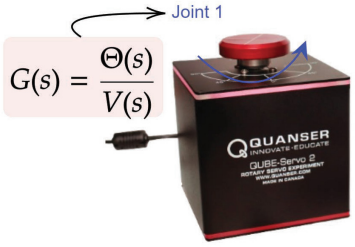

Fig. 7. QUBE-Servo 2.

A servo system (also known as a servo) is a control device or system that uses a feedback mechanism to maintain a variable (usually position, velocity, or acceleration) at a desired value. These systems are widely used in the automation and control of machinery, robotics, military industry, tracking systems, power electronics, and various industrial and commercial applications. Here, we apply our fine-tuning method to an experimental servo system testbench called Qube-Servo 2 from QUANSER® (see Fig. 7). This testbench consists of a direct current motor connected to an inertia disk and a sensor to provide feedback on its position. The voltage-to-position transfer function is:

$$G(s) = \frac{K}{s(Ts+1)}e^{-hs}, \tag{15}$$

where $K = 23.651$, $T = 0.13144$ and $h = 0.005174$.

In the design, we explore diverse combinations of $\beta \in [0, 3]$ and $\gamma \in [0, 5]$ weights within the cost function (9). This tuning process was conducted as part of the optimization procedure utilizing the transfer function (15). After tunning all the gains, a series of 24 experiments were conducted. For each of these experiments, we evaluate the control performance through eight different parameters (see Table 1) whose values are shown in Fig. 8.

Once we compute the value of the metrics in Table 1, we can use the L_2 norm of the eight designated parameters to select the best and worst PI controllers from the 24 conducted experiments. This L_2 norm is defined as

$$\mathcal{C} = \sqrt{t_s^2 + \mathcal{I}_{ACES}^2 + \mathcal{I}_{ACVS}^2 + \mathcal{I}_{M_p}^2 + \mathcal{I}_{IAE}^2 + \mathcal{I}_{ISE}^2 + \mathcal{I}_{ITAE}^2 + \mathcal{I}_{ITSE}^2}. \tag{16}$$

Table 1. Time response performance indexes.

Parameter index	Description	Expression
t_s	Settling time	$\lvert r(t) - y(t)\rvert \leq \alpha,\ \forall t \geq t_s$
$\mathcal{I}_{ACES}$	Absolute Control Effort Square	$\int_0^{t_s} \lvert u(\tau)\rvert^2 \, \mathrm{d}\tau$
$\mathcal{I}_{ACVS}$	Absolute Control Variation Square	$\int_0^{t_s} \lvert \dot{u}(\tau)\rvert^2 \, \mathrm{d}\tau$
$\mathcal{I}_{M_p}$	Overshoot	$\frac{y(t_p)-y(\infty)}{y(\infty)} \cdot 100\%$
$\mathcal{I}_{IAE}$	Integral Absolute Error Criterion	$\int_0^{t_s} \lvert e(\tau)\rvert \, \mathrm{d}\tau$
$\mathcal{I}_{ISE}$	Integral Square-Error criterion	$\int_0^{t_s} e(\tau)^2 \, \mathrm{d}\tau$
$\mathcal{I}_{ITAE}$	Integral of Time multiplied Absolute Error Criterion	$\int_0^{t_s} \tau \lvert e(\tau)\rvert \, \mathrm{d}\tau$
$\mathcal{I}_{ITSE}$	Integral of Time multiplied Squared Error Criterion	$\int_0^{t_s} \tau e(\tau)^2 \, \mathrm{d}\tau$

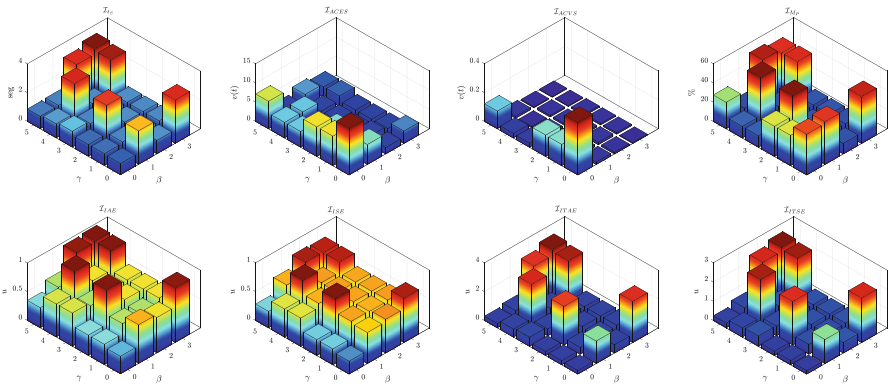

Fig. 8. Performance indexes.

Therefore, from the array of evaluated controllers, the best PI control corresponds to the minimum value of (16) or $\mathcal{C}_{best} = 10.7429$. This value is obtained when $(\beta, \gamma) = (1, 5)$, which corresponds to the finely tuned configuration $(k_p, k_i) = (0.1134, 0.001)$. On the contrary, the worst PI control corresponds to the maximum of (16) or $\mathcal{C}_{worst} = 52.7277$, which is associated to $(\beta, \gamma) = (1, 2)$ and the tuning configuration $(k_p, k_i) = (0.1835,\ 0.2716)$. Figure 9 shows the time response when using the best and worst PI controls in the experiments. The experimental results can be observed in the following site:

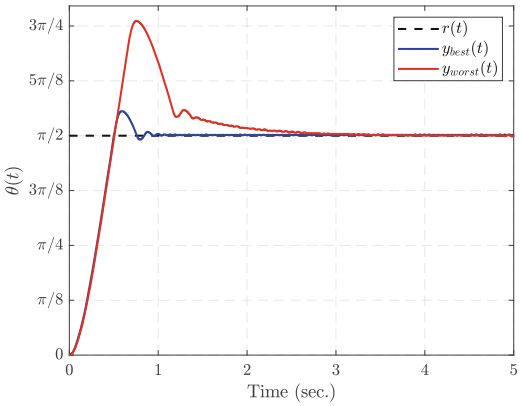

Fig. 9. Time responses.

https://sites.google.com/view/jhernandezg/principal/doctorado/publicaciones/synergestic

5 Conclusions and Future Work

The numerical and experimental results allow us to conclude that the synergy between the GA and the analytical-derived results permits guaranteeing the choice of gains of a PI controller that minimizes a multi-objective cost function. Consequently, the synergetic approach allows one to choose a pair (k_p, k_i) that guarantees the fastest response with a minimum energy cost.

By means of analytical analysis, future work will include determining an accurate stability region, which will allow us to improve the optimization method, which in addition will ensure finding the global minimum.

Appendix: Practical Implementation

The implementation has been performed in Simulink® by means of the QUARC® real-time control test bench. The block diagram used in the implementation is depicted in Fig. 10.

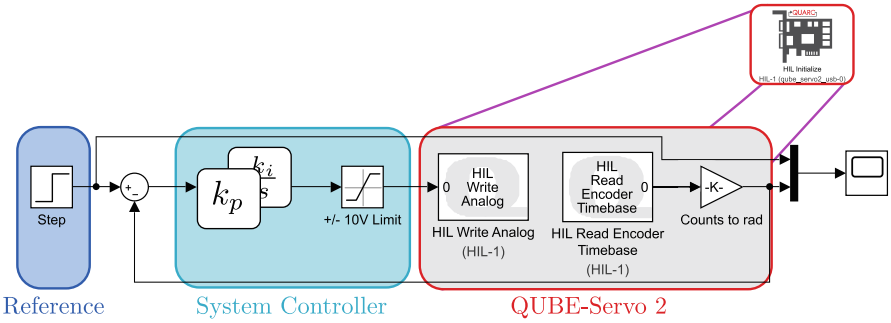

Fig. 10. Block diagram for implementation of the controllers.

The implementation comprises three primary components: (i) the generation of a signal reference; (ii) the code programming of the PI controller within the control system, along with the saturation of the control signal at $\pm 10V$; and finally, (iii) the writing of the voltage blocks and the reading of the encoder counts for conversion to radians, culminating in the closure of the control loop.

References

1. Dorigo, M., Birattari, M., Stutzle, T.: Ant colony optimization. IEEE Comput. Intell. Mag. **1**(4), 28–39 (2006)
2. El'sgots', L., Norkin, S.: Introduction to Theory and Applications of Differential Equations with Deviating Arguments. Academic Press, New York, NY (1973)

3. Feoktistov, V.: Differential Evolution. Springer, Heidelberg (2006). https://doi.org/10.1007/3-540-31306-0
4. Gryazina, E.N., Polyak, B.T., Tremba, A.A.: D-Decomposition technique state-of-the-art. Autom. Remote. Control. **69**(12), 1991–2026 (2008)
5. Gu, K., Chen, J., Kharitonov, V.L.: Stability of Time-Delay Systems. Springer, Heidelberg (2003). https://doi.org/10.1007/978-1-4612-0039-0
6. Hagglund, T., Astrom, K.J.: PID Controllers: Theory, Design, and Tuning. ISA-The Instrumentation, Systems, and Automation Society (1995)
7. Hernández-Gallardo, J.-A., Guel-Cortez, A.-J., Gonzalez-Galvan, E.J., Méndez-Barrios, C.-F.: Designing proportional delayed integral control for fast regulation in second-order systems: a geometric approach. In: 2023 9th International Conference on Control, Decision and Information Technologies (CoDIT), pp. 01–06 (2023)
8. Kennedy, J., Eberhart, R.: Particle swarm optimization. In: Proceedings of ICNN'95-International Conference on Neural Networks, vol. 4, pp. 1942–1948. IEEE (1995)
9. Méndez-Barrios, C.-F., Niculescu, S.-I., Morarescu, C.-I., Gu, K.: On the fragility of PI controllers for time-delay SISO systems. : 2008 16th Mediterranean Conference on Control and Automation, pp. 529–534. IEEE (2008)
10. Mishra, D.P., Raut, U., Gaur, A.P., Swain, S., Chauhan, S.: Particle swarm optimization and genetic algorithms for PID controller tuning. In: 2023 5th International Conference on Smart Systems and Inventive Technology (ICSSIT), pp. 189–194. IEEE (2023)
11. Onat, C.: A new concept on PI design for time delay systems: weighted geometrical center. Int. J. Innov. Comput. Inf. Control **9**(4), 1539–1556 (2013)
12. Torres-García, D., Méndez-Barrios, F., Ramírez, A.: Maximum exponential decay rate for first-order time-delay systems with PI controllers. In: Moreno, H.A., Carrera, I.G., Ramírez-Mendoza, R.A., Baca, J., Banfield, I.A. (eds.) LACAR 2021. LNNS, vol. 347, pp. 34–42. Springer, Cham (2022). https://doi.org/10.1007/978-3-030-90033-5_5
13. Venkatashankar, V., Chidambaram, M.: Design of P and PI controllers for unstable first-order plus time delay systems. Int. J. Control **60**(1), 137–144 (1994)

Rehabilitation Upper Limb Exoskeleton: Human-Robot Simulation Framework

Deira Sosa Méndez[1(✉)], Cecilia E. García Cena[1], and Roque Saltarén Pazmiño[2]

[1] Centro de Automática y Robótica, Escuela Técnica Superior de Ingeniería y Diseño Industrial, Universidad Politécnica de Madrid, C/ Ronda de Valencia, no3, 28012 Madrid, Spain
sosam.deira@gmail.com, deira.sosa.mendez@alumnos.upm.es, cecilia.garcia@upm.es

[2] Centro de Automática y Robótica, Escuela Técnica Superior de Ingenieros Industriales, Universidad Politécnica de Madrid, C/ José Gutiérrez Abascal, no2, 28006 Madrid, Spain
roquejacinto.saltaren@upm.es

Abstract. In this article we present a simulation framework for the mechatronics development and validation of robotics exoskeletons. The framework is focus on a serial-link upper-limb rehabilitation robots where specific therapies for shoulder, elbow and/or wrist rehabilitation can be simulated and tested prior to be applied on the patient extremity. Such a simulation framework incorporates human-robot interaction through its coupling with the patient, and is evaluated by implementing different trajectories, which can be customized according to the range and speed of movement (conditions dependent on each treatment and patient). Kinematic model of the exoskeleton is presented and validated through its equivalent in the MATLAB® software. In addition, the equivalent of the device in the MSC ADAMS View^{TM} software is used for the evaluation of physical rehabilitation trajectories, in which the coupling between the robot and the user is considered through their physical characteristics. Therefore, this virtual environment helps the designer to improve the safety and accuracy of the robotic device.

1 Introduction

It is estimated that one in every three people in the world need rehabilitation at some point of their injuries or illnesses (disability or decrease in physical, mental and social functioning). This number of people is increasing, therefore interventions such as rehabilitation are necessary for anyone who has mobility, vision or cognition problems. So globally 2.41 million of this type of people would benefit from rehabilitation services [1].

Early intervention by rehabilitation services has been shown to improve the functioning and quality of life of the population, which makes it necessary to integrate them as an essential strategy in short- and long-term care. At the

M. N. Cardona et al. (Eds.): LACAR 2023, LNNS 940, pp. 89–96, 2024.
https://doi.org/10.1007/978-3-031-54763-8_9

primary level, the main challenges presented by these services are: the need for training of health personnel and the inclusion of rehabilitation specialists (physiotherapists, occupational therapists, etc.) [1]. Due to this, more and more technological and digital solutions are being applied, such as: end-effector devices and exoskeletons.

Exoskeletons are robotic systems designed to attach externally to the human body (match form and function), so they are part of the group called wearable robots. Its main applications are: power amplification, motor function replacement, teleoperated systems, haptic devices and rehabilitation or assistance devices [2–4]. In recent years, rehabilitation exoskeletons have gained importance, as they have proven their efficiency in improving the functionalities of the limbs in activities of daily living [5–8].

According to Gull in [4], the development of exoskeletons presents challenges such as: kinematic compatibility (anthropomorphic parameters), limited workspace, mechanical system singularity problem, discomfort and misalignment, among others. Thus, the authors suggested that exoskeletons meet the following characteristics: ergonomic and standardized design, biomechanical modeling, compatible articulation and actuation, performance evaluation (duration, speed, ergonomics, planning uncertainty, among others) and adaptive control.

In upper limb rehabilitation treatments: generally the joints are the centers of movement, the muscles the power parts and the bones the objects of execution [9]. Therefore, in order for the rehabilitation robot to be safe, it must move the patient's upper extremity within the joint anatomical ranges to avoid risks during use [10] and it must provide assistance as much as possible to meet the user's requirements. Therefore, it is essential to calculate the trajectories and power demand necessary during its use [11].

The use of digital twins in simulations allows combining the different needs of each patient making it possible for treatments to be personalized, precise and flexible [5,9,12]. In addition, the simulations complement the validation of the prototypes, which leads to greater efficiency in the human-robot iterations, and also allow predicting aspects such as: trajectory planning (position, speed and acceleration), torque of the actuators, gains of admissible controllers, safety measures for users, among others [9,13]. Developing safe prototypes that involve experiments with humans is time-consuming and expensive, and the use of simulations helps reduce these aspects.

Although in most human-robot systems one-dimensional linear simulations are sufficient, in the case of exoskeletons a more precise representation is necessary because they are physically coupled human-robot systems, which must be contemplated in the simulation [13]. Some examples of upper limb exoskeleton are:

- Hou et al. in [9] show the results of simulation of trajectories of a robotic arm (3DOF) for different poses of the arm and forearm. They conclude that to implement precise and flexible personalized treatments, it is necessary to use a simulation analysis that combines the different needs of each patient, and also allows the adjustment of movement parameters.

- Toth et al. in [10] use a set of flexible software tools to assess the risks of the RACA rehabilitation robot (adaptable to any type of rehabilitation robot). The test system is based on fictitious limbs (it allows to test all the relevant operations of the robot and eliminates the biggest disadvantage of systems based on motion capture), and for each movement determines: the type of movement, its speed and whether it is within a safe zone.
- Dalla et al. en [12] show the modular rehabilitation platform AGREE (4 degrees of freedom (DOF)), which has: modular and reconfigurable software architecture, allows path generation routines for custom exercises (uses Simulink and ROS to calculate custom accessible 3D workspace, and it uses 5th order minimum-jerk trajectory to generate smooth movements).
- Blanco et al. in [14] performed simulations of a 3DOF exoskeleton in MSC ADAMS View^{TM} in co-simulation with Matlab-Simulink®, which considered: the anthropometric dimensions of the user in the exoskeleton and the weight of each limb segment of an average patient of 80 kg. In the same study, smooth trajectories were tracked, knowing the start, end and time points between them (Bézier polynomials), these passive movements do not reach the joint ends to avoid excessive loads of muscle or joint stretching.
- Nguyen et al. in [15] show a graphical simulator of a 5 DOF exoskeleton, which combines SoliWorks® and Matlab® software to solve the kinematic and dynamic problems of the robot. Its main drawback was the planning of trajectories for the endpoint, because the trajectories with which it was evaluated were obtained from a human motion capture system. To improve the software it is suggested to focus on the development of trajectories of the robot endpoint.

2 Human-Robot Simulation Framework

In this work, a human-robot simulation framework of an upper limb exoskeleton for rehabilitation was developed, which helps to validate the device (design and hardware) and implement different personalized therapeutic routines for each patient. Simulations satisfy two objectives: 1) forward kinematics and workspace in Matlab®, and 2) device motion evaluation using smooth trajectories in MSC ADAMS^{TM} software.

2.1 Kinematics Modeling

The exoskeleton was designed in Solidworks® and considers the following: anthropometric aspects (allows the variation of the lengths of the arm (0.24–0.40 m) and forearm (0.24–0.39 m)) and physiological aspects of the human body (maximum weight 120 kg), it also has a modular design made in 3D printing (see figure in Table 1. It allows the movements: shoulder, elbow and wrist, it is assumed that the robot is aligned with the patient during the execution of the movements (the starting position of all movement is when the patient is seated with the upper limb hanging from the side of the body with the palm of the hand facing inwards).

For the exoskeleton analysis, the Denavit-Hartenberg (D-H) representation is used. Table 1 shows the forward kinematic model of the exoskeleton, which has 5 DOF and its D-H parameters are those shown in Table 2.

Table 1. Upper limb exoskeleton

Exoskeleton in SolidWorks®	D-H notation for upper limb exoskeleton.
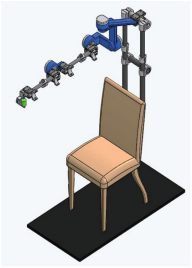	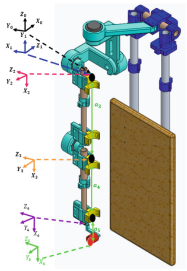

Table 2. D-H parameters of the upper limb exoskeleton

Joint	Motion (θ_i)	θ_i	d_i	a_i	α_i
Shoulder	Internal-external rotation θ_1 (-30° to 70°)	$\theta_1 + 90°$	0	0	+90°
Shoulder	Abduction-adduction θ_2 (0° to 90°)	$\theta_2 - 90°$	0	0	−90°
Shoulder	Flexion-extension θ_3 (-50° to 160°)	θ_3	0	a_3	0
Elbow	Flexion-extension θ_4 (0° to 140°)	θ_4	0	a_4	0
Wrist	Abduction-adduction θ_5 (-15° to 45°)	θ_5	0	a_5	0

2.2 Exoskeleton Workspace

In order to analyze the exoskeleton workspace (the volume of space that can be reached by the end effector of the robot). It is necessary to evaluate the range of motion of each joint separately and as a whole. Table 3 shows the workspace for which the exoskeleton was designed (indicated in the second column of Table 2 and based on [16]), the last cell of Table 3 shows the complete workspace of the exoskeleton considering the maximum arm and forearm lengths, as well as the complete ranges of motion of each joint (red and blue colors). However, in this work is considered as an achievable workspace only the positions that are in front of the patient (blue color).

Table 3. Exoskeleton workspace in Matlab®

Shoulder: Internal-external rotation	Shoulder: Abduction-adduction	Shoulder: Flexion-extension
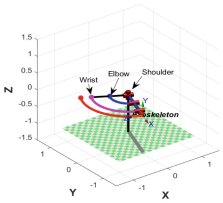	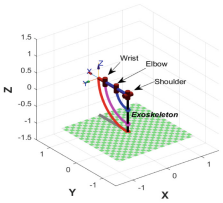	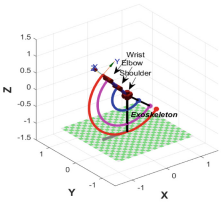
Elbow: Flexion-extension	Wrist: Abduction-adduction	Full and achievable workspace
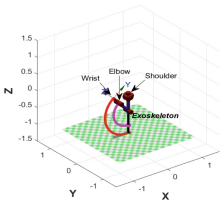	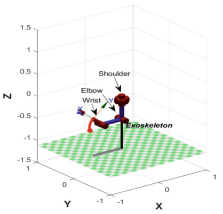	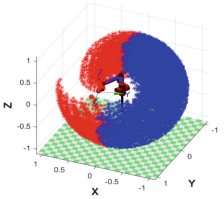

2.3 Movement Evaluation

This section shows the functional performance of the exoskeleton through its equivalent model in MSC ADAMS View^{TM}. This model has the following characteristics: 5 rotational joints in which it is possible to modify the modes of action (torque or movement), the mechanical properties of the parts can be adjusted (material density), sensing (position, speed, acceleration, torque of the actuator), among others. Therefore, the movement of the joints can be independent or jointly: receiving as input parameters the positions or equations of movement, and the necessary torques for each movement are obtained as output parameters, and finally they are evaluated by means of graphical simulations.

In order to obtain more accurate results, the virtual simulations considered the mechanical properties of the exoskeleton (weight) and the weight corresponding to the upper limb of a patient of 120 kg, which includes in a simple way the physical characteristics of the patient during the simulation. The revolutes lack friction, the Table 4 shows the equations that were implemented independently for each joint in [deg] (the q'n that do not appear are equal to zero), the selection of each equation is within the working range of each joint and also show smooth trajectories such as those performed in rehabilitation. The same Table shows the maximum output torques measured during the execution of each motion. Their motion and torque graphs as well as its virtual representation are shown in Table 5, and the movements are described below:

Table 4. Joint equations of independent motions at input and output joint torques

Motion	Joint equations [deg]	T_1 [Nm]	T_2 [Nm]	T_3 [Nm]	T_4 [Nm]	T_5 [Nm]
S Int-ext Rot	$q_1 = 30\sin(2.5t)$, $q_3 = 90$	6.93	3.88	36.05	8.06	0.02
S Abd-add	$q_{2_{0-3}} = 10t^2$	0.02	36.90	0.07	0.07	0.02
S Flex-ext	$q_{3_{0-4}} = 8.75t^2$	0.13	3.85	36.63	8.23	0.03
E Flex-ext	$q_{4_{0-5}} = 3.6t^2$	0.00	3.79	7.94	8.08	0.03
W Abd-add	$q_5 = 30\sin(2.5t)$	0.00	3.79	0.07	0.07	0.03

Table 5. Exoskeleton motion evaluation in MSC ADAMS View^{TM}

Shoulder: Internal-external rotation

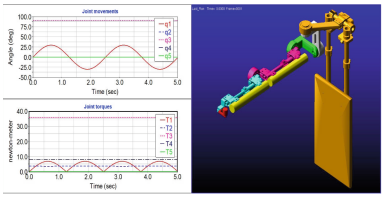

Shoulder: Abduction-adduction

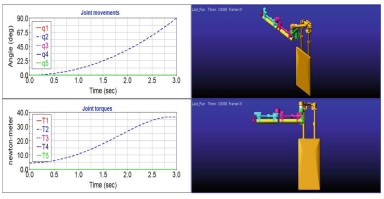

Shoulder: Flexion-extension

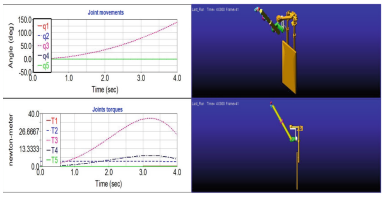

Elbow: Flexion-extension

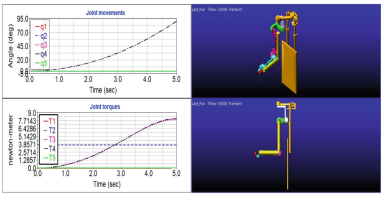

Wrist: Abduction-adduction

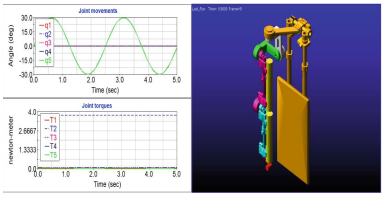

1. **Shoulder internal-external rotation (S Int-ext Rot):** A sinusoidal equation was implemented for q_1 whose maximum amplitude is 30° and constant for $q_3 = 90°$.
2. **Shoulder Abduction-adduction (S Abd-add):** A quadratic function was implemented for q_2, where the start point is zero and the end is 90°, the latter is reached in 3 s.
3. **Shoulder flexion-extension (S Flex-ext):** A quadratic function was implemented for q_3, where the start point is zero and the end is 140°, the latter is reached in 4 s.

4. **Elbow flexion-extension (E Flex-ext):** A quadratic function was implemented for q_4, where the start point is zero and the end is 90°, the latter is reached in 5 s.
5. **Wrist abduction-adduction (W Abd-add):** The equation implemented was a sinusoidal signal for q_5 whose maximum amplitude is 30°.

The results show the behavior of smooth equations (sinusoidal and quadratic), where the maximum joint torques measured during the movements were: $T_1 = 6.93\,\text{Nm}$, $T_2 = 36.90\,\text{Nm}$, $T_3 = 36.63\,\text{Nm}$, $T_4 = 8.23\,\text{Nm}$ and $T_5 = 0.03\,\text{Nm}$. However, the motion equations can change according to the patient features and the therapies executed in physical rehabilitation, which will generate their corresponding changes in the output parameters (joint torques).

3 Conclusions and Future Work

The main objective of designing and evaluating a robotic exoskeleton through a human-robot simulation framework (physically coupled systems), was to evaluate the kinematic model of the exoskeleton and test its functionality through the generation of smooth trajectories (sinusoidal and quadratic) applicable in physical rehabilitation.

This analysis has a significant value in research since during its evaluation it can be improved: the design of the robot, the planning of precise and flexible personalized rehabilitation treatments (the simulations present parameters closer to reality), in addition the times and costs to perform physical experiments are reduced. The safety evaluation of the exoskeleton allowed to estimate the online risks that the robot could cause and also allowed its graphic visualization. Although this work only shows the results of position and joint torques, it also provides the possibility of analyzing joint speeds to avoid risks in them.

It is suggested to consider the simulations mainly for: the design of personalized treatments (behavior and performance of the system) and to validate the hardware and software decisions used for the development of the device. It is proposed as future work to implement the human-robot simulation framework in a graphical interface, through which different trajectories, more complete mathematical models of the patient and dynamic control strategies are implemented, to later implement them in the physical exoskeleton.

Acknowledgements. The first author thanks the National Council of Science and Technology (CONACYT) of Mexico for the scholarship for doctoral studies awarded under CVU No. 642069.

References

1. Cieza, A., Causey, K., Kamenov, K., Hanson, S.W., Chatterji, S., Vos, T.: Global estimates of the need for rehabilitation based on the Global Burden of Disease study 2019: a systematic analysis for the Global Burden of Disease Study 2019. Lancet **396**(10267), 2006–2017 (2020)
2. Rocon, E., Pons, J.L.: Exoskeletons in Rehabilitation Robotics: Tremor Suppression, vol. 69. Springer, Heidelberg (2011). https://doi.org/10.1007/978-3-642-17659-3
3. Pons, J.L.: Wearable Robots: Biomechatronic Exoskeletons. Wiley, New York (2008)
4. Gull, M.A., Bai, S., Bak, T.: A review on design of upper limb exoskeletons. Robotics **9**(1), 16 (2020). https://doi.org/10.3390/robotics9010016
5. Zhao, Y., Wu, H., Zhang, M., Mao, J., Todoh, M.: Design methodology of portable upper limb exoskeletons for people with strokes. Front. Neurosci. **17**, 1128332 (2023)
6. Moulaei, K., Bahaadinbeigy, K., Haghdoostd, A.A., Nezhad, M.S., Sheikhtaheri, A.: Overview of the role of robots in upper limb disabilities rehabilitation: a scoping review. Arch. Publ. Health **81**(1), 84 (2023)
7. Clark, W.E., Sivan, M., O'Connor, R.J.: Evaluating the use of robotic and virtual reality rehabilitation technologies to improve function in stroke survivors: a narrative review. J. Rehabil. Assist. Technol. Eng. **6**, 2055668319863557 (2019)
8. Postol, N., Grissell, J., McHugh, C., Bivard, A., Spratt, N.J., Marquez, J.: Effects of therapy with a free-standing robotic exoskeleton on motor function and other health indicators in people with severe mobility impairment due to chronic stroke: a quasi-controlled study. J. Rehabil. Assist. Technol. Eng. **8**, 20556683211045836 (2021)
9. Hou, H., Jiang, Z.: Design and simulation of an upper limb rehabilitation exoskeleton robot. In: Proceedings of the 2022 2nd International Conference on Control and Intelligent Robotics, pp. 91–101, June 2022
10. Tóth, A., Pilissy, T., Bauer, M.O., Al-Absi, G., Dávid, S., Fazekas, G.: Testing the limit range of motion safety function of upper limb rehabilitation robots with an anthropometrically adjustable and sensorized dummy limb. In: 2022 International Conference on Rehabilitation Robotics (ICORR), pp. 1–6. IEEE, July 2022
11. Yin, P., Yang, L., Liu, B.: Design and optimization of a wearable upper limb exoskeleton based on Adams. IOP Conf. Ser. Mater. Sci. Eng. **717**(1), 012004 (2020). IOP Publishing
12. Dalla Gasperina, S., et al.: AGREE: an upper-limb robotic platform for personalized rehabilitation, concept and clinical study design. In: 2022 International Conference on Rehabilitation Robotics (ICORR), pp. 1–6. IEEE, July 2022
13. Zimmermann, Y., et al.:: Digital Guinea Pig: Merits and Methods of Human-in-the-Loop Simulation for Upper-Limb Exoskeletons. In: International Conference on Rehabilitation Robotics (ICORR) 2022, pp. 1–6 (2022). https://doi.org/10.1109/ICORR55369.2022.9896520
14. Blanco-Ortega, A., et al.: A Robust controller for upper limb rehabilitation exoskeleton. Appl. Sci. **12**(3), 1178 (2022)
15. Nguyen, T.T., Nguyen, T., Pham, H., Bui, T.: Proposing a graphic simulator for an upper limb exoskeleton robot. Appl. Bionics Biomech. (2023)
16. Kapandji, I.A., Lacomba, M.T.: Fisiologia Articular. Tomo 1: Miembro Superior. Hombro, codo, pronosupinación, muñeca, mano. (2006). Editorial Medica Panamericana SA de CV

Prototype of a Waste Classification System Based on Deep Learning

José Pascasio(✉) and Robinson Mela

Universidad Tecnológica de Panamá, Panama City, Panama
{jose.pascasio,robinson.mela}@utp.ac.pa

Abstract. This article presents the implementation of hardware tools such as Raspberry Pi, cameras, sensors, motors, and controllers, along with software components like convolutional neural networks and a mobile application for waste classification. In the future, the proposed waste collector and classifier implementation will contribute to environmental care and environmental education. The project's innovation lies in the automation of waste classification using neural networks, automatic notifications generated by the prototype when a container is full and transmitted to the mobile application via a web server, and the flexibility of the prototype for various environments, including educational, office, and industrial settings. The advancements in the project include the creation of a mobile application to monitor container levels, the construction of the prototype, training results of selected neural networks, and the evaluation of the final network with test images.

Keywords: Convolutional neural networks · Raspberry Pi · mobile application · waste sorting

1 Introduction

Waste sorting and recycling activities should be of interest to everyone, as they are ways to contribute to the care of the planet. In the case of Panama, approximately 4,800 tons of waste are generated daily, of which less than 5% is recycled, according to estimates presented by the Municipality of Panama in 2019. About 50% of the generated garbage consists of materials that can be recycled, such as plastic, cardboard, metals, and other materials. The remaining half is composed of organic waste.

There are few companies or facilities dedicated to the final disposal or treatment of waste, and the public infrastructure needs to be strengthened with training initiatives, as well as the provision of the necessary financial and technical resources for proper management. Generative companies do not have their own treatment systems, and in most cases, they simply bury the waste without any environmental controls, as indicated in the 2003 Study on the Solid Waste Management Plan for the Municipality of Panama.

M. N. Cardona et al. (Eds.): LACAR 2023, LNNS 940, pp. 97–103, 2024.
https://doi.org/10.1007/978-3-031-54763-8_10

1.1 Problem Description

Among the most evident environmental problems caused by humanity for many years, with a significant impact on pollution of natural resources, ecosystems, health, and environmental quality, are: population growth, consumerism, ignorance, lack of knowledge, and poor environmental education.

Furthermore, this environmental issue is known as the generation of Solid Waste, which is critical due to its effects on environmental degradation, health, and the quality of life of future generations. Poor management of urban and industrial waste constitutes today the greatest environmental, economic, and social problem on a global scale, mainly because the volume of waste is increasing at a faster rate than the world's population. This is the problem that will receive primary attention through the intelligent waste sorting bin.

1.2 Proposal

Among the most evident environmental problems caused by humanity for many years, with a significant impact on pollution of natural resources, ecosystems, health, and environmental quality, are population growth, consumerism, ignorance, lack of knowledge, and poor environmental education.

Furthermore, this environmental issue is known as the generation of Solid Waste, which is critical due to its effects on environmental degradation, health, and the quality of life of future generations. Poor management of urban and industrial waste constitutes today the greatest environmental, economic, and social problem on a global scale, mainly because the volume of waste is increasing at a faster rate than the world's population. This is the problem that will receive primary attention through the intelligent waste sorting bin.

1.3 Justification

To address the inappropriate handling of waste, viable alternatives that harness the potential of technology are required to provide solutions or reduce the consequences of poor waste disposal. Without innovative proposals in this regard, the problem will continue to escalate, and the negative effects on life and the environment will also increase. This project presents an alternative solution to the issue of solid waste management, which is very evident not only in the Santiago district, Veraguas province but also throughout the Republic of Panama.

1.4 Background - Research Studies

The literature review revealed that there are already projects related to solid waste treatment in progress. All of these projects mentioned use traditional techniques, such as waste collection and separation in different bins. Some of the works that can be mentioned in this context are (Guzmán, 2019; Farfán, 2014; Domínguez, 2015).

Furthermore, waste collection and sorting techniques have evolved, incorporating technologies that can facilitate the classification and collection of solid waste, making it easier for people. An example of this is (Diaz and Caldas, 2018), which involves a series of sensors designed to capture and classify each of the waste items.

1.5 Implementation of Convolutional Neural Networks in Similar Projects

These networks are capable of learning input-output relationships from many images used for training. They are derived from the works presented in (Poole, 2018; LeCun et al., 1989; LeCun et al., 1990; Haußecker, 2000). Recognizing the impact and the convenience they offer to specialists from different fields, these networks have been incorporated into projects that require greater precision and effectiveness, as demonstrated in (Martínez Llamas, 2015; Uribe, 2017; Acosta Casatillo, 2017; Quintero, 2008).

Deep neural networks have been successfully applied to waste detection, segmentation, and recognition, as seen in (Bai et al., 2018; Chen and Wang, 2019; Sreelakshmi et al., 2019). Therefore, it is proposed to use a CNN (Convolutional Neural Network) for waste classification based on images.

2 Design and Methodology

2.1 Neural Network Training

Initially, a dataset (Bircanoğlu et al., 2018) with a total of 2,527 images was downloaded, and an additional 380 images were added to balance the quantity of each class. This helps the model to learn equally from all types of waste. Furthermore, when loading the images, they are rotated to change their orientation, effectively doubling the number of images.

The dataset was divided into six classes (paper, cardboard, plastic, metal, glass, and others) to enhance the model's capacity, as shown in Table 1.

Table 1. Division of Dataset (source own elaboration)

Division of Dataset				
Type of waste	Number of images	Training (70%)	Validation (20%)	Tests (10%)
Paper	594	416	119	59
Cardboard	462	323	92	46
Plastic	608	426	122	61
Metal	507	355	101	51
Glass	501	351	100	50
Others	475	333	95	48
Total	3147	2203	629	315

For training, a computer with the following specifications was used: Intel(R) Core (TM) i7-8750H CPU @ 2.2 GHz processor, 16 GB of RAM, and a GeForce GTX 1050 graphics card. Various tests were conducted using the following neural networks (VGG16, ResNet50, Inceptionv2).

2.2 Design of the Smart Waste Bin Prototype

The processing begins when the magnetic sensor detects the deposition of waste. This sensor is connected to the Raspberry Pi board, which triggers the LED lights and powers the motors. Subsequently, a photo of the waste is taken using a camera. This photo is then classified by a neural network, resulting in the assignment of the container in which it should be deposited.

This information is sent to the Arduino Mega board, which controls the mechanical axis system, directing the waste to one of the four containers for storage. The containers are divided as follows: Cardboard (where paper and cardboard are combined), Plastic (for plastic waste only), Metal (for metal waste only), Others (for glass and other waste that doesn't fit into the previous categories) (Fig. 1).

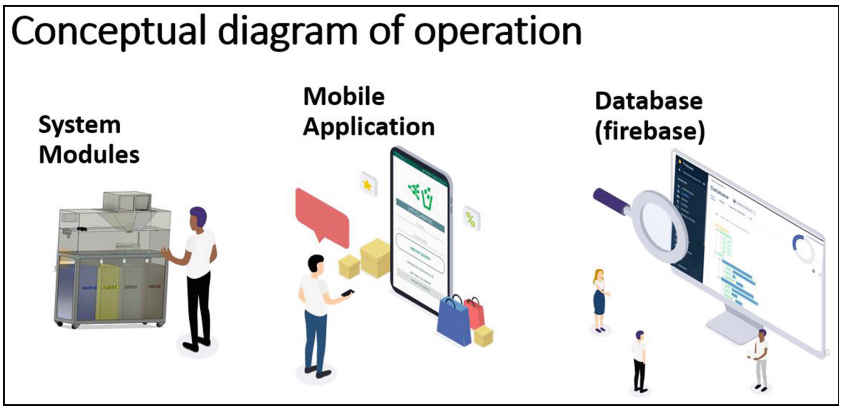

Fig. 1. Conceptual diagram of the operation in the smart trash can prototype.

2.3 Technologies and Methods

Type of Research: Applied, as it proposes a technological product as a solution to a problem. Research Area: Innovative Technology. The technologies and methods that will be implemented in the waste collection and sorting prototype are described as follows, the following technologies are implemented: Raspberry Pi 4 B+: Used as the hardware platform, Android Studio: As the development environment, Firebase Realtime Database: As the web server, enabling data storage and synchronization in real-time, allowing data accessibility from any device, whether web or mobile, and facilitating collaborative work, TensorFlow: An open-source library for machine learning, used in conjunction with the Keras development library. These libraries were used to train the convolutional neural networks, Four neural network architectures: MobileNet, VGG16, ResNet50, and InceptionResNetV2. These were used to evaluate which one performs best during training with waste images (Fig. 2).

Fig. 2. Assembling the various components of the smart trash can prototype.

3 Results

3.1 Construction and Validation of the Prototype

A physical prototype was constructed using a combination of hardware tools such as Raspberry Pi, cameras, sensors, motors, controllers, and software components, including neural networks, a database, and a mobile application. This is depicted in Fig. 3A.

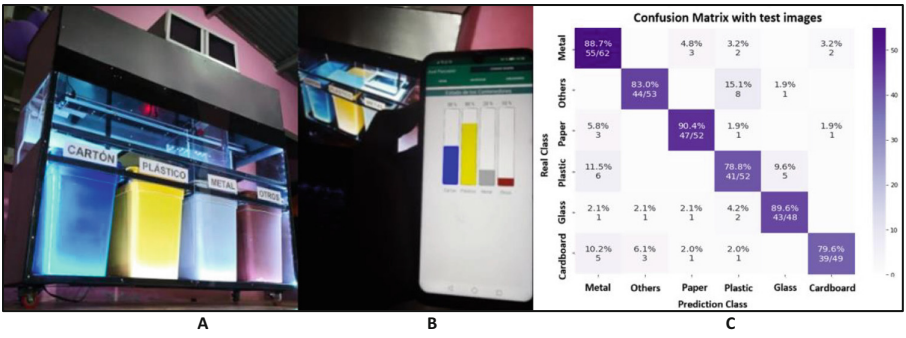

Fig. 3. (A) Physical prototype built, (B) Mobile application, and (C) Confusion matrix.

An innovative mobile application was developed, enabling real-time monitoring of the fill levels in each waste container. Additionally, the application receives automatic notifications generated by the prototype through the web server when a container is nearly full. This is illustrated in Fig. 3B. The selected neural networks were trained using the dataset, as depicted in Table 2.

After analyzing the training results, considering the accuracy level and the loss function, ResNet50 was selected for implementation in the prototype as it achieved the

Table 2. Results of the learning curve training (source own elaboration)

Training Results					
Neuronal Model	Parameters	Optimizer	Epochs	Batch Size	Precision
Mobile Net	7,168,198	Adam	100	32	64%
VGG16	23,704,646	Adam	100	32	88%
ResNet50	23,600,006	Adam	100	34	91%
InceptioResNetV2	54,345,958	Adam	100	24	80%

highest accuracy. This network was evaluated with test images that were not used during training and are unknown to it. The confusion matrix was generated, as seen in Fig. 3C, which compares the actual class with the classification made by the ResNet50 network. This indicates that the system can automatically distinguish between different types of waste.

3.2 Prototype Development Opportunities

The market study conducted when proposing this solution for waste treatment and recycling indicates that it is an innovative product. Therefore, potential markets extend beyond just businesses to various types of institutions. One of the key drivers of innovation is the implementation of artificial intelligence techniques, which are revolutionizing the market when combined with other disciplines like electronics and mechanics to create an innovative, educational, and user-friendly product.

The cost of implementing this smart waste bin prototype amounts to the modest sum of $1,268.75 per unit for a business-sized container with a total capacity to store 320 lbs of waste. The individual storage capacity for each container would be 80 lbs of waste.

4 Discussion

The completion of this research led to the following achievements:

- Implementation of neural network algorithms for waste classification in a smart bin, including MobileNet, VGG16, ResNet50, and InceptionResNetv2. Among these, the ResNet50 algorithm was chosen due to its 91% accuracy.
- Development of a mobile application that provides real-time visibility of the fill level of each container and automatic notifications when one or more are full. This communication is facilitated through a real-time database that connects the Raspberry Pi board with the mobile application.
- Presentation of a flexible prototype that offers an alternative to educate people about proper waste classification. It is designed for implementation in various environments, including educational institutions, offices, industries, and more.
- Successful achievement of the proposed objectives, demonstrating the prototype's ability to classify waste types accurately.

References

Acosta Casatillo, F.: Automatic Detection of Mitotic Cells in Histological Images Using Deep Convolutional Neural Networks, 1st edn, pp. 1–6. Universidad Pontifica Católica de Valparaíso (2017)

Bai, J., Lian, S., Liu, Z., Wang, K., Liu, D.: Deep learning based robot for automatically picking up garbage on the grass. IEEE Trans. Consum. Electron. (c), 1 (2018). https://doi.org/10.1109/TCE.2018.2859629

Bircanoğlu, C., Atay, M.S., Beser, F., Genc, O., Kizrak, M.A.: RecycleNet: intelligent waste sorting using deep neural networks (2018). https://doi.org/10.1109/INISTA.2018.8466276

Quintero, C.F.M.: Use of Convolutional Neural Networks for Automatic Recognition of Macroinvertebrate Images for Participatory Biomonitoring, 1st edn, pp. 1–6. Universidad Tecnológica Panamá (2008)

Chen, G., Wang, H.: Application of image recognition technology in garbage classification education platform. In: 2019 5th International Conference on Control, Automation and Robotics (ICCAR), pp. 290–294 (2019)

Diaz C.C., Caldas V.J.: Automatic Control System for the Recognition and Classification of Recyclable Waste, 1st edn, pp. 19–30. Universidad Católica de Colombia (2018)

Domínguez, F.: Garbage Separation and Collection Project in Mexico, 1st edn, pp. 1–6 (2015)

Farfán, J.: Innovation Project with an Environmental Focus, 1st edn, pp. 1–6 (2014)

Guzmán, A.: Recycling Project: Changing Habits, Transforming Lives, 1st edn, pp. 1–6 (2019)

Haußecker, B.J.H.: Computer Vision and Applications, A Guide for Students and Practitioners. Academic Press, London (2000)

Martínez Llamas, J.: Image Recognition Using Convolutional Neural Networks, 1st edn, pp. 1–50. Universidad Politécnica de Madrid: ETSI Sistemas Informáticos (2015)

Poole, D.: Computational Intelligence: A Logical Approach (2018)

Sreelakshmi, K., Akarsh, S., Vinayakumar, R., Soman, K.P.: Capsule neural networks and visualization for segregation of plastic and non-plastic wastes. In: 2019 5th International Conference on Advanced Computing and Communication Systems (ICACCS), pp. 631–636 (2019)

Uribe, S.: Implementation of Neural Networks and Performance Analysis for Embedded Systems. Universidad Autónoma de Barcelona (UAB), pp. 1–10 (2017)

LeCun, Y., Boser, B., Denker, J.S., Henderson, D., Howard, R.E., Hubbard, W.L.D.J.: Backpropagation applied to handwritten zip code recognition (4), 541–551 (1989)

LeCun, Y., B., Boser, J. S. Denker, D. Henderson, R. E. Howard, W. Hubbard, and L. D. J. (1990). Handwritten digit recognition with a back-propagation network. Touretzky, D. S., 396–404

FPSoC Integration in ROS-Enabled Mobile Robots for Enhanced Functionality

Jairo Cuero[1], Pedro-F Cardenas[2(✉)], and Rony Trespalacios[1]

[1] Universidad de los Llanos, Villavicencio, Colombia
{jairo_cuero,rony.trespalacios}@unillanos.edu.co
[2] Universidad Nacional de Colombia, Bogotá, Colombia
pfcardenas@unal.edu.co

Abstract. In this study, we present a preliminary approach to the integration of Field-Programmable System on a Chip (FPSoC) technology into a Robot Operating System (ROS)-enabled mobile robot, specifically a TurtleBot3 platform. Our goal was to replace the original Raspberry Pi board with an FPSoC board, thereby providing the robot with access to a Field-Programmable Gate Array (FPGA) block for accelerating functions through codesign. Through a carefully executed integration process, we successfully transformed the TurtleBot3 into a functional prototype that retained its core operational features while harnessing the enhanced capabilities offered by hardware function acceleration. Despite the successful transformation of the robot, this study represents a preliminary stage of development but it paves the way for applications that demand real-time responsiveness and efficient processing of sensor data. The robot operates at a level consistent as the original setup with the Raspberry Pi board, providing a foundation for further exploration. Our next phase of research will focus on designing, implementing, and testing specific hardware functions through codesign to realize the full potential of the FPSoC integration. Our findings and ongoing efforts contribute to the growing body of research aimed at advancing robotics capabilities for various applications, including autonomous navigation, object recognition, and sensor data processing.

1 Introduction

Mobile robots have witnessed remarkable advancements in recent years, revolutionizing industries ranging from logistics and manufacturing to healthcare and agriculture [1]. The ubiquitous TurtleBot, an iconic member of the robotics community, exemplifies this revolution [2]. This compact yet versatile platform, equipped with various sensors, navigation capabilities, and a Raspberry Pi at its core, represents the initial strides in creating more intelligent and adaptable robotic systems. However, as the complexity of tasks assigned to mobile robots grows, a need arises for more potent development boards than the Raspberry Pi [3,4].

M. N. Cardona et al. (Eds.): LACAR 2023, LNNS 940, pp. 104–112, 2024.
https://doi.org/10.1007/978-3-031-54763-8_11

The execution of intricate tasks, such as autonomous navigation, simultaneous localization and mapping (SLAM), and human-robot interaction, demands increased computational power and enhanced real-time processing capabilities [5,6]. With their reconfigurable hardware, FPGAs offer a significant performance advantage over conventional microcontrollers [7] and even single-board computers like the Raspberry Pi [8]. They excel in parallel processing tasks, such as sensor data fusion, image processing, and control algorithms, making them well-suited for real-time applications in mobile robotics [6]. While field-programmable gate arrays (FPGAs) hold the potential to meet these requirements, their integration into mobile robots has been limited by the inherent complexities associated with the challenging learning curve of FPGA programming and the specific software framework commonly used in the field, the Robot Operating System (ROS) [9].

In one of the initial efforts to achieve ROS integration with FPGA in robotics, the work by [10] showcases the development of the "Hero" hardware-software (HW/SW) platform designed for accelerating the tasks of autonomous systems. The Hero platform boasts a state-of-the-art Intel Core i5 processor intricately paired with an Intel Arria 10 FPGA, seamlessly integrated with the OpenCL framework. Subsequently, [11] introduced an open-source ROS robot stack based on the Parallax Arlo robot, integrated with the Zybo z7-10 FPSoC platform. Similarly, [12] devised an autonomous vehicle based on ROS, with the Zybo z7-20 as the primary board.

In unrelated research, two studies by Nitta in 2018 and 2019 [13,14] demonstrated the capabilities of ZytleBot, a robot that utilized the Ultra96 rev1 FPSoC and ran ROS on Ubuntu 18.04. ZytleBot was able to work in conjunction with a TurtleBot3 chassis and employed FPGA technology for camera and motor interfacing. Furthermore, Wu's 2020 work introduced the HydraMini robot [15], which was equipped with the Xilinx PYNQ-Z2 board and was responsible for managing mechanical control, AI inference, and computer vision analysis, all with the benefit of hardware acceleration.

Based on the previous ideas, we propose the integration of ROS with an SoC-FPGA board in a robotic platform to enhance the robot's capabilities. We chose the TurtleBot3 (TB3), a differential traction mobile robot with two Dynamixel motors, a ball caster-type freewheel, a Raspberry Pi 3B+, and a LiDAR sensor, and an OPENCR 1.0 board for navigation and odometry. The TB3 can perform several typical mobile robot tasks, such as autonomous navigation, map construction, and obstacle detection. However, by having ROS, the restrictions are more present in the hardware system than in the software. As the number of robot tasks increases, processor power consumption, and computational demand increase. Therefore, we propose replacing the Raspberry Pi card with a system on chip (SoC) that integrates both the processor and the programmable logic parts so that tasks can be partitioned and assigned to the processor or the FPGA.

2 HW/SW Architecture

A robot is made up of three systems: an electronic system, a mechanical system (hardware), and an information processing system (software). In order to develop a mobile robot that can navigate and interact with its environment autonomously, these three systems must be integrated. This integration is known as the robot's hardware-software (HW/SW) architecture [16,17].

The software design typically consists of several layers, such as application, controllers, and communication, among others. It is executed in one or more of the processors that the system has. On the other hand, the hardware design is mapped and depends on the device's available resources.

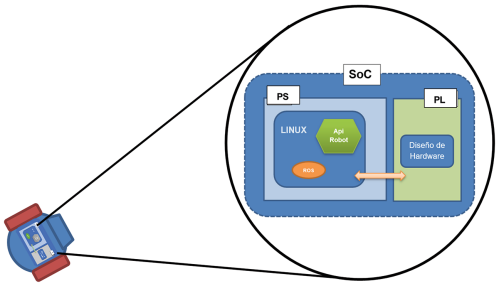

Fig. 1. Hardware-Software HW/SW Architecture proposed

In order to accelerate navigation tasks in mobile robots, a HW/SW architecture has been proposed. This architecture consists of a robotic structure governed by a SoC with an ARM processor and a programmable logic block (FPGA). This allows for the application of co-design techniques with the implementation of functions in hardware, so that tasks can be partitioned and assigned for execution in the software block or in the hardware block according to the complexity and need of the design. Figure 1 Illustrates this HW/SW architecture.

2.1 Hardware Adjustments

The TurtleBot3 Burger comes wholly disassembled from the factory, so in the assembly process, we established that the 11.1 V and 1800 mAh LiPo battery in the lower plate offers little autonomy to the robot. Therefore, we chose a 3-cell LiPo battery in a 3S1P configuration with 3000 mAh and 12.6 V with a full charge. This offer greater capacity, and the dimensions allow it to continue occupying the same space as the original. We also remove the Raspberry Pi from the third plate of the robot to house the SoC-FPGA, the Ultra96V2.

Upon initial testing, the temperature of the Ultra96V2 reached over 53 °C in a few minutes of operation. Therefore, we adapted a fan to the SoC heatsink case to reduce the overheating of the development board. This solution kept the temperature below 45 °C, as shown in Fig. 2.

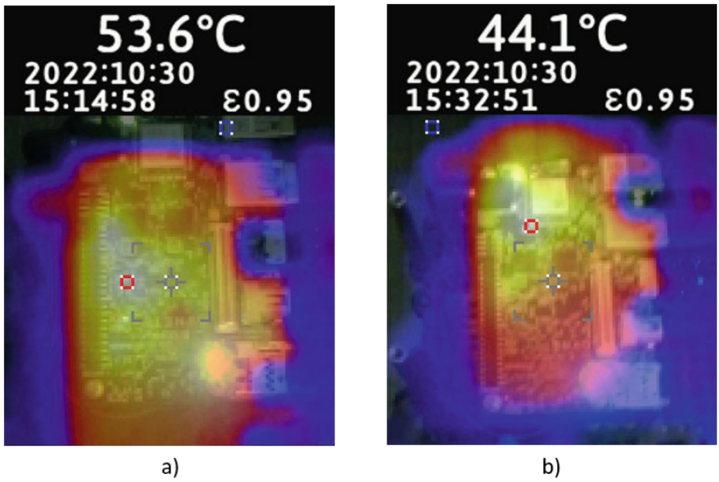

Fig. 2. Thermographic image on the SoC. a) without a fan. b) with a fan.

For the fan connection, we analyzed two possibilities: connecting it to the Ultra96v2 through the dedicated pins on the board or supplying power from the OpenCR. The first option offers better temperature and power control of the fan as the FPSoC has a dedicated PWM pin. However, it also requires more electrical intervention from the board because it does not have the pins as a connector, so we would have to solder them directly. In contrast, supplying power from the OpenCR uses the same connector that initially supplies voltage to the Raspberry, so there is no need to intervene in the board physically.

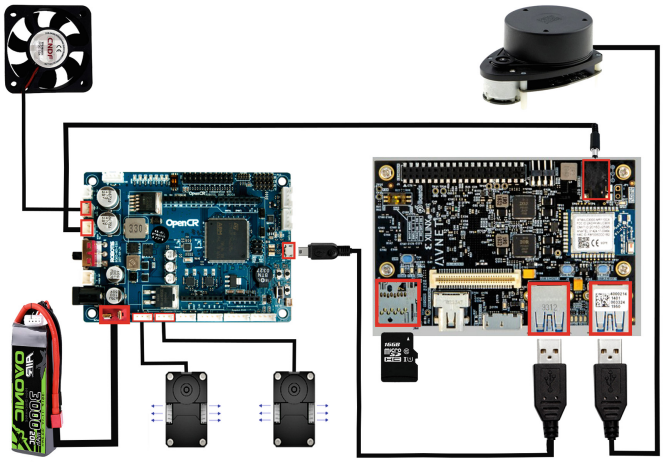

Fig. 3. Diagram of the connections between the components that make up the robot.

Figure 3 presents the electrical and communication interconnection of the elements that compose the robot. As can be seen, the USB communication between the OpenCR and the Ultra96V2 remains unchanged from the original connection. Likewise, through the USB2LDS controller, the LiDAR connects the Ultra96v2 board.

2.2 Operating System

We selected the PYNQ framework V2.6, based on the UBUNTU Bionic Beaver distribution, as the primary OS for the Ultra96V2. PYNQ environment uses Jupyter, a web-based interactive computing platform, to create Notebooks, write Python programs, manage storage, and manage folders and files. It also has a fully functional terminal that allows the installation of packages via apt-get. Through this terminal, we installed ROS Melodic by overriding the automatic detection of the operating system with the environment variable `ROS_OS_OVERRIDE` to force the installation from the list of packages for UBUNTU Bionic. This previous step is mandatory because the PYNQ's UBUNTU distribution codename is not Bionic but WHF as it is shown in Fig. 4, so the installer does not find the packages for that distribution in the official ROS repository.

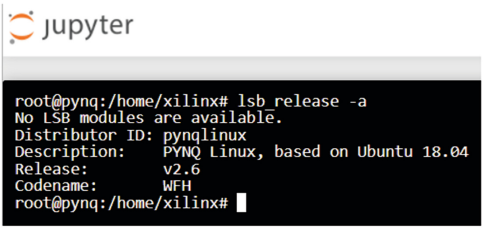

Fig. 4. Jupyter Terminal displaying the OS version.

2.3 Network Configuration

The next stage in the integration consists in setting up the work environment for the communication between the robot and the remote PC. Typically, the ROS Master goes in the remote PC. Still, this configuration doesn't allow operating the robot from a remote computer without ROS installed, as the nodes must register with the Master. Then, we decided to set the Ros Master in the robot because the access to the robot is not by SSH as usual without PYNQ Framework. We can access the robot by the Jupyter notebook from any web browser, including a mobile phone.

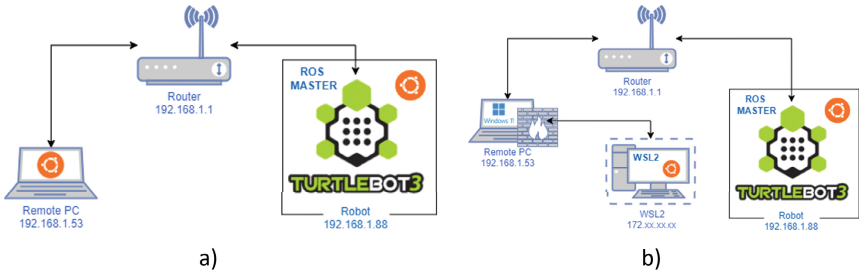

Fig. 5. Network diagram. a) In Linux. b) In Windows 11 using WSL2

We also decided to explore two operating system options to deal with the various compatibility problems that might arise in the project and to optimize the development time. Thus, we configured the remote PC in Dual Boot with Ubuntu 18.04 and Windows 11 with Ubuntu Bionic in the Windows Subsystem for Linux (WSL2). Figure 5 shows the two network configuration options we tested. The first configuration is the usual one but with the ROS Master located in the robot. In the second one we used WSL2 with Ubuntu Bionic because ROS1 doesn't run in windows. Here we dealt with some issues by establishing port forwarding and creating some rules in the firewall. On the other hand, to solve the absence of a graphical interface in WSL2, we used an x server to display in windows 11 some GUI applications such as RViz and `Rqt_Graph`.

3 Conclusions

The integration of the different hardware and software elements in the turtlebot3 is presented in Fig. 6.

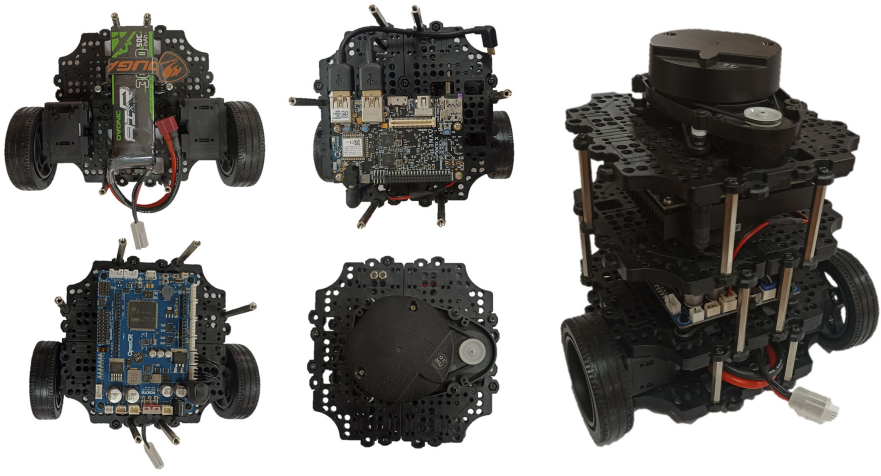

Fig. 6. Robot modification with the battery adaptation, motor and OpenCR connection, Ultra96V2 integration, LiDAR installation and the final structure.

We executed the original tutorial with the modified robot to validate the prototype. Our goal was to verify that the robot functioned seamlessly from the Raspberry and Ultra96v2 processors. We created a node to capture the LiDAR data and executed nodes for robot teleoperation, basic trajectory tracking in structured environments, and the construction of the environment map.

We used Rviz and Jupyter notebooks provided by the PYNQ ecosystem to develop the environment map. Figure 7 shows the result of the map generation, and Fig. 8 shows the graph of the running nodes and topics. In all cases, substituting the CPU with an FPSoC card was transparent, meaning the robot worked equally well with either of the two development cards.

The HW/SW architecture design presented in this project can tackle complex tasks such as autonomous navigation, obstacle avoidance, pattern recognition, object classification, and human-robot interaction. These tasks are computationally intensive and require a high-performance development card for mobile robots. Besides, since increased computational capabilities are often associated with high energy consumption, utilizing powerful yet low-power devices like FPGAs becomes crucial for a robot's autonomy, particularly if it operates on batteries.

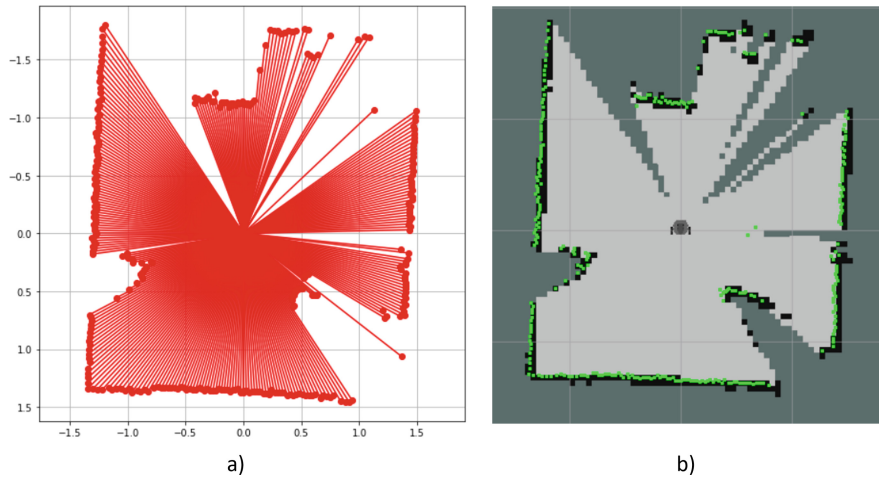

Fig. 7. Map from the LiDAR data. a) Plotted in a jupyter Notebook. b) displayed in Rviz.

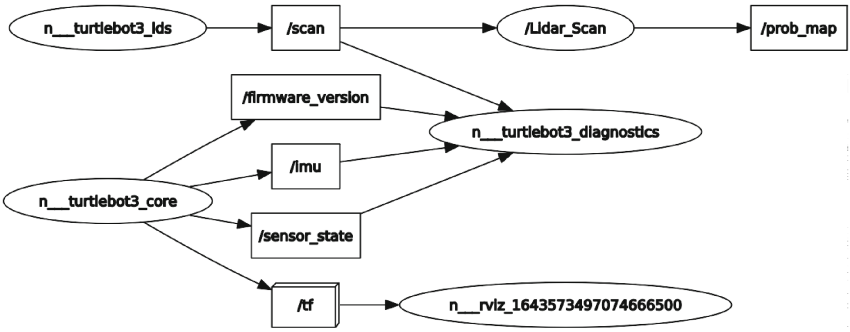

Fig. 8. Running ROS nodes and topics in FPSoC

Acknowledgment. This work was supported and funded by the Directorate General Research at Universidad de Los Llanos, Colombia, and under the research project N° C09-F02-018 2022.

References

1. Simoens, P., Dragone, M., Saffiotti, A.: The internet of robotic things: a review of concept, added value and applications. Int. J. Adv. Rob. Syst. **15**, 1–11 (2018)
2. Amsters, R., Slaets, P.: Turtlebot 3 as a robotics education platform. In: Merdan, M., Lepuschitz, W., Koppensteiner, G., Balogh, R., Obdržálek, D. (eds.) RiE 2019. AISC, vol. 1023, pp. 170–181. Springer, Cham (2020). https://doi.org/10.1007/978-3-030-26945-6_16
3. Mathe, S.E., Pamarthy, A.C., Kondaveeti, H.K., Vappangi, S.: A review on raspberry Pi and its robotic applications. In: 2022 2nd International Conference on Artificial Intelligence and Signal Processing (AISP), pp. 1–6 (2022)
4. Karthikeyan, S., Aakash, R., Cruz, M.V., Chen, L., Ajay, V.J.L., Rohith, V.S.: A systematic analysis on raspberry Pi prototyping: uses, challenges, benefits, and drawbacks. IEEE Internet Things J. **10**(16), 14397–14417 (2023)
5. Bouhoun, S., Sadoun, R., Adnane, M.: OpenCL implementation of a SLAM system on an SoC-FPGA. J. Syst. Archit. **111**, 101825 (2020)
6. Liu, R., Yang, J., Chen, Y., Zhao, W.: eSLAM: an energy-efficient accelerator for real-time ORB-SLAM on FPGA platform, pp. 1–6 (2019)
7. Rappl, V.: Comparison between microcontroller and FPGA: Advantages and suitable fields of application. FMS-BERICHTE (2022)
8. Mounir, T.A., et al.: Performance evaluation of basic image processing algorithms in CPU GPU raspberry Pi and FPGA. Int. J. Comput. Sci. Eng. (IJCSE) **9**(4), 312–325 (2020)
9. Podlubne, A., Gohringer, D.: FPGA-ROS: Methodology to augment the robot operating system with FPGA designs (2019)
10. Shi, X., et al.: HERO: accelerating autonomous robotic tasks with FPGA. In: IEEE International Conference on Intelligent Robots and Systems, pp. 7766–7772 (2018)
11. Joseph, T., Whitaker, L.: Towards a prototype platform for ROS integrations on a ground robot (2019)

12. Hasegawa, K., Takasaki, K., Nishizawa, M., Ishikawa, R., Kawamura, K., Togawa, N.: Implementation of a ROS-based autonomous vehicle on an FPGA board. vol. 2019, pp. 457–460 (2019)
13. Nitta, Y., Tamura, S., Takase, H.: A study on introducing FPGA to ROS based autonomous driving system, pp. 424–427. IEEE (2018)
14. Nitta, Y., Tamura, S., Takase, H.: ZytleBot : FPGA integrated development platform for ROS based autonomous mobile robot. pp. 422–423. IEEE (2019)
15. Wu, T., Wang, Y., Shi, W., Lu, J.: HydraMini: An FPGA-based affordable research and education platform for autonomous driving. pp. 45–52 (2020)
16. Flores, I.A.C.: Navegación autónoma de un robot móvil usando técnicas probabilísticas de localización y mapeo basadas en métodos monte carlo secuenciales (2014)
17. Ohkawa, T., Yamashina, K., Kimura, H., Ootsu, K., Yokota, T.: FPGA components for integrating FPGAs into robot systems. IEICE Trans. Inf. Syst. **E101D**, 363–375 (2018)

Eye Tracking and Machine Learning Non-invasive Biomarker for Alzheimer's Disease and Frontotemporal Dementia Diagnosis

Alberto Calvo Córdoba[1(✉)], Cecilia E. García Cena[2], Carmen Lage[3], and Pascual Sánchez Juan[4]

[1] Universidad Politécnica de Madrid. Centro de Automática y Robótica. ETSII. C/ de José Gutiérrez Abascal, 2, 28006 Madrid, Spain
alberto.calvo.cordoba@alumnos.upm.es

[2] Universidad Politécnica de Madrid. Centro de Automática y Robótica. ETSIDI. C/ Ronda de Valencia, 3, 28012 Madrid, Spain
cecilia.garcia@upm.es

[3] Instituto de Investigación Marqués de Valdecilla (IDIVAL), Universidad de Cantabria y departamento de neurología, hospital universitario Marqués de Valdecilla, Santander, Spain

[4] Fundación Cien. C/ Valderrebollo, 5. Centro Alzheimer Fundación Reina Sofía, 28031 Madrid, Spain

Abstract. In this publication, it is presented the first diagnostic biomarker for Alzheimer's disease (AD) and the behavioural variant of frontotemporal dementia (BvFTD) based on machine learning techniques applied to eye movement analysis. Nowadays, the diagnostic of these dementias is clinic, so it is based on the specialist doctor by their own expertise knowledge and the results of complementary medical tests. This study includes 39 control participants, 38 participants with moderate AD diagnosis and 24 participants with a diagnosis of BvFTD. Ocular movements were recorded with video-oculography (saccadic, fixation and smooth pursuit paradigms). Results: applied methodology to data mining and feature extraction shows clear evidence of the differences between each type of participants. Accuracies and AUC overcome 95%. Conclusion: Video-oculography is a non-invasive, low expensive, objective and fast technique for cognitive evaluation that could help to the clinical diagnosis.

1 Introduction

The study of the behaviour of eye movement have provided sensible biomarkers for the detection of different neurodegenerative diseases. Progressively, it is adopted as a medical tool for the clinical diagnosis [1–3].

Ocular movements and brain activity has a deep relation which makes unavoidable its study to understand the different changes that the neuropathologies could provoke on these processes. Different brain region are involved in the

M. N. Cardona et al. (Eds.): LACAR 2023, LNNS 940, pp. 113–122, 2024.
https://doi.org/10.1007/978-3-031-54763-8_12

generation of each ocular movement (saccadic, fixation, smooth pursuit, etc. movements) according to the wilfulness and propose of them. Different changes could be observed based on the neuropathology and the brain regions affected within the ocular movements [3,4]. Moreover, there are several papers that report the different changes according to AD and BvFTD. For a more detailed information, readers are referred to [5–10].

There are several techniques to record ocular movements. Coil systems have been considered as the gold standard thanks to their great temporal and spatial resolution [11]. However, it is a completely invasive system that requires very specialised staff to record the experiment. Another alternative is referred to electrode systems [12,13]. The electro-oculography is based on the correct position of electrodes to measure extraocular muscles activity and, therefore, ocular activity. Nevertheless, this kind of systems records a lot of noise and different artefacts that affects to the quality and the processing of the signal.

Finally, video-oculography systems have extended their utility with the advance and disruption of computer vision and machine learning techniques. Usually, this kind of system are based on cameras and infrared illumination to search for the contrast of the pupil and the iris as well as the reflexes over the cornea [14–16].

The main contributions of this work is to present a optimised methodology of the analysis of ocular movement experiments to help to the diagnosis of different neurodegenerative diseases (AD and BvFTD) based on the exploratory analysis of ocular movement and cognitive evaluation features and machine learning techniques. The biomedical protocol of these experiments have been tested in different studies [17–21]. The reader is referred to these papers for a more detailed and description of the ocular movement features.

2 Participants

Every participant involved in this study were recorded by specialist medical staff of the cognitive disorder unit of the Maqués de Valdecilla hospital of Santander. They are all in the same range age, between 60 and 80 years old, and all of them have signed a consent form. It is included in the study 39 control participants, 38 participants with AD diagnosis and 24 with BvFTD diagnosis. These participants were recruited under the same conditions considering general cognitive scales like Mini-mental test [22] and Global deterioration scale [23]. Patient diagnosis were made by agreed criteria for probable AD [24] and BvFTD [4]. These diagnoses were validated by at least one type of biomarker and the absolute agreement of a dedicated multidisciplinary team to minimise missclassification errors and heterogeneity due to the possibility of co-pathology. This study has been approved by local ethics committees.

3 Methods

The methodology described in this work is shown in Fig. 1 where different stages could be identified:

- Experiment recording: it is based on the realization of the biomedial protocol of ocular movements. This protocol is similar to the one described in [17–21]. At first, participant diagnosis is made by the hospital specialised unit. Then, ocular tests are performed (saccadic, fixation and smooth pursuit paradigms) horizontally and vertically.
- Data mining: after the recording of the ocular tests it is needed to extract the gaze from the medical images in order to analyse ocular activity. When the device ends to perform this task, ocular movement features could be extracted from each test. A statistical summary is provided from each test.
- Feature selection: Each participant is defined by statistical summaries which define them performance in the different ocular tests. Due to the limited number of samples, it is necessary to study the relevance of each ocular feature for the corresponding discrimination task. First, the type of distribution of each variable within the dataset is assessed by means of the Lilliefors (LF) [25]. Next, if it is parametric, the ANOVA test is performed [26]. Otherwise, the Kruskal-Wallis test [27]. And, finally, the significance of each feature is assessed through the P-value obtained previously. To complete this stage, with the characteristics that have exceeded this significance threshold, a dimensionality reduction is applied using partial least squares (PLS) [28] on which the Fisher discriminant ratio (FDR) is evaluated [29] to choose only the most significant features.
- Machine learning classification: At this stage, classical machine learning models such as k nearest neighbours, support vector machines, etc., are built for each of the discrimination tasks. In order to avoid biases or other problems derived from the small sample size, we proceed to perform a 5 folds cross-validation and orchestrated repetition of the experiment a thousand times on different training, testing and validation subsets. The correlation of the features selected in the previous stage were computed before training begins.
- Validation of the results: Once the machine learning experiment has been completed, the results of the experiment are discussed. In this case, different metrics such as accuracy, false or true positive/negative ratios, area under the ROC curve [30], posterior probabilities [31], etc., are evaluated.

4 Results

The first result that is important to mention is the relationship between the expected significance and the number of variables obtained in each discrimination task. As can be seen in Table 1 in the case of AD versus healthy participants, 21 features were considered as representative (P-value < 0.01), for BvFTD versus healthy participants, 17, and in the differential case, the threshold had to be increased as the number of significant variables was not so high. Finally, 17 were included, setting a significance threshold of 0.05. The main reason lies in the need for a large subset so that the PLS step can be properly applied.

Secondly, Table 2 shows the results obtained from classification task with different types of supported vector machine (SVM) classifier. This type of classifier

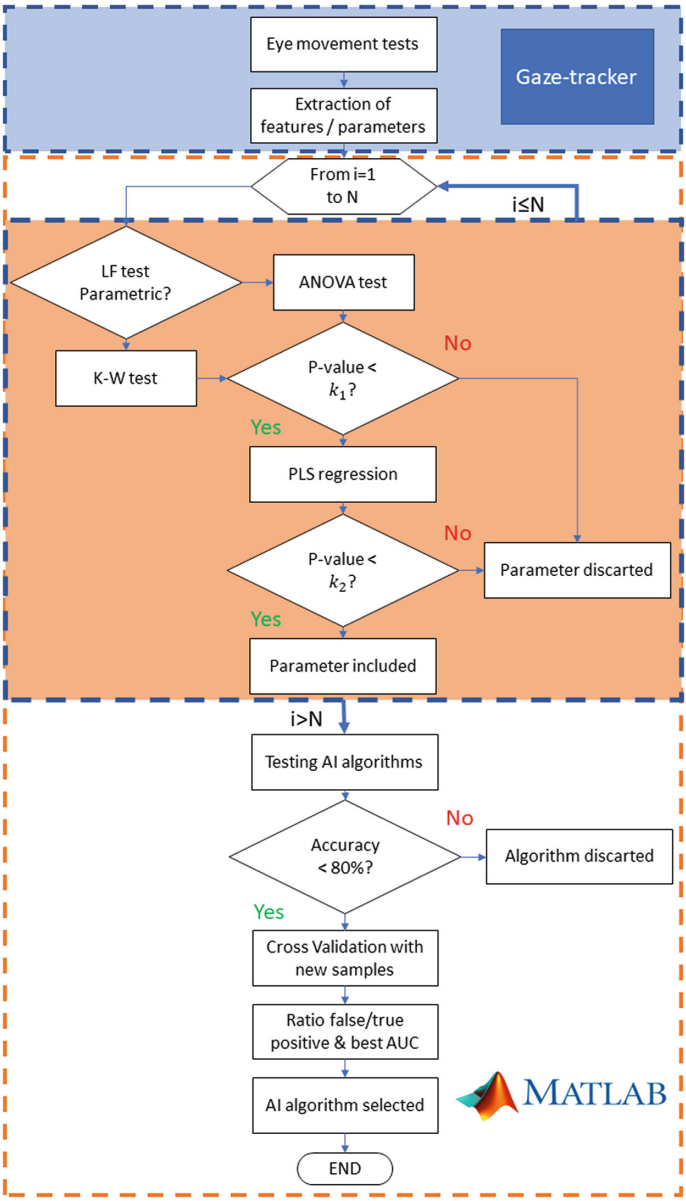

Fig. 1. Methodology flowchart.

has offer better results than the other alternatives studied in this work. As it could be observed, the results are highly promising in the cases of the study versus control participants. In the case of AD, the best results are obtained from quadratic kernel, while for BvFTD is the cubic one.

Table 1. Significant analysis. Number of ocular significant features included in the study of each ocular movement test. Significant features have gotten over the indicated P-value threshold.

Discriminatory analysis	Control vs AD			Control vs BvFTD			AD vs BvFTD		
P - value threshold	<0.001	<0.01	>0.01	<0.001	<0.01	>0.01	<0.01	<0.05	>0.05
Prosaccades	–	4	14	–	2	16	–	3	15
Memory saccades	4	–	2	4	–	2	1	1	4
Antisaccades	4	10	10	4	6	14	–	4	20
Fixation	–	–	12	–	–	12	–	–	12
Smooth pursuit	–	3	17	–	1	19	1	7	12

Table 2. Clasification results

SVM Classifier	Discriminatory analysis	Mean accuracy before PLS	Best PLS: n var	N var after of FDR	Accuracy			AUC
					Medio	Max	Min	
Lineal	Control vs AD	0.9047	10	7	0.9265	0.9778	0.8889	0.9963
	Control vs BvFTD	0.9719	10	2	0.971	0.9762	0.9524	1
	AD vs BvFTD	0.754	9	5	0.8057	0.8974	0.6667	0.8682
Quadratic	Control vs AD	0.9213	9	7	0.966	0.9778	0.9111	0.9925
	Control vs BvFTD	0.9716	12	3	0.9831	1	0.9524	0.9999
	AD vs BvFTD	0.7799	14	5	0.694	0.8205	0.4872	0.7038
Cubic	Control vs AD	0.9304	14	7	0.958	0.9778	0.8889	0.988
	Control vs BvFTD	0.97	14	3	0.9897	1	0.9286	0.9997
	AD vs BvFTD	0.7253	–	–	–	–	–	–
Gaussian Fine	Control vs AD	–	7	6	0.8611	0.9111	0.7556	0.9231
	Control vs BvFTD	–	12	3	0.9828	1	0.881	0.9984
	AD vs BvFTD	–	15	5	0.7786	0.8718	0.641	0.7989
Medium	Control vs AD	0.8906	9	7	0.9314	0.9778	0.8889	0.9746
	Control vs BvFTD	0.9347	12	6	0.9524	0.9524	0.9524	0.9997
	AD vs BvFTD	0.7898	12	5	0.8279	0.8974	0.6923	0.8751

In the case of the differential classifier between both dementias, such good results have not been obtained. However, it shows a first promising approximation to achieve the help to the differential diagnosis between these two pathologies.

Finally, posterior probabilities are gathered with the best results of each classifier. This metric is a really valuable indicator of the reliability and confidence with which the classifier algorithm makes a decision for each sample. Table 3 summarises, from left to right, when the participants have been classified properly with a high level of confidence (posterior probability near to their true class) or low one. Next, it shows which of them have been clearly misclassified or when the classifier is not sure about its decision but makes an error in the classification as well.

Table 3. Posterior probabilities.

Discriminant analysis	Classes	Posterior probabilities (P)			
		Properly classified		Misclassified	
		High confidence score	Low confidence score	Low confidence score	High confidence score
Control vs AD	C	23	1	0	0
	AD	18	2	1	0
Control vs BvFTD	C	24	0	0	0
	BvFTD	17	1	0	0
AD vs BvFTD	AD	10	4	5	2
	BvFTD	15	2	0	1

5 Discussion

The alteration in the ocular movements and cognitive capacities of AD and BvFTD patients could contribute and help to the diagnosis of this pathologies when they are compared to control pattern according to the results of this study.

On the one hand, in the case of AD, results show up a sensitivity of 95.2% with a specificity of 100%. According to other tests that have established the diagnosis criteria for the diagnosis of this disease, this approach shows similar sensitivities (73% – 100%) and specificities (62% – 92.4%). Some examples of those tests are cerebrospinal fluid-tau protein [32], positron emission tomography approach [33], the Bamberg Dementia Screening Test [34] or magnetic resonance imaging test of the brain [35].

On the other hand, in the case of BvFTD, the experiment proposed have provided a sensitivity and specificity of 100%. These results are far superior of the ones that the medical literature gather for the clinical diagnosis of BvFTD. Full neuropsychological tests, structural magnetic resonance imaging of the brain, positron emission tomography or single photon emission computed tomography [36], are tests included in the clinical diagnosis of this pathology and show sensitivities between 75% to 95% and specificities between 68% to 95%. In the case of the help to the differential diagnosis between AD and BVFTD, our best classifier provides a sensitivity of 66.7% and a specificity of 94.4% considering AD samples as the positive class. In comparison to reference literature, our results are not as good as them mostly in the correct classification of the AD samples. The reader is referred to [37,38] for a more detailed information.

Table 1 reveals the main significant ocular movement tests for each classification task. The success and relevance of the tests linked to the saccadic paradigm, namely those linked to memory and anti-saccade, also the most cognitively complex, disassociates the slow tracking and fixation tests from the analysis versus control participants. The two diseases are closely related in these tests so that their response is very similar. However, in the differential case, the smooth pursuit test is used for better accuracy of the results.

The results of the classification tasks presented in Table 2 show that for the cases of the detection of the possibility of suffering from a dementia disease, are superb, whereas for the differentiation between pathologies, they need to be further investigated and improved as this is a much more complex case.

Finally, the posterior probabilities indicated in Table 3 validate the hypothesis that this methodology has justified and reliable tools for detecting the different diseases, although doubts and, therefore, failures arise in the differential task. These probabilities show that there are not only differences between the diseases but also similarities that should be studied in depth in order to avoid mistakes in the differential diagnosis. Having in mind that the golden rules in the diagnosis of these diseases include long-term neuropsychological tests, as well as another set of tests to verify clinical indicators, it is vital to provide the team of specialists with objective, non-invasive, simple and short tests with which to assess the cognitive capacity of the patient.

In the case of eye movement tests, we have worked on their optimisation, focusing on the most significant variables to reduce the time of the experiment while ensuring the best possible results. Its usefulness and usability on the detection of ocular alterations in dementia patients has been demonstrated, improving the results of the best techniques and practices of the current state of the art [36,38].

However, the main limitation of this work is the amount of data samples. Large-scale and massive trials should be conducted for full verification and improved differential diagnostic help. The associated cost of these samples together with the amount of resources to follow the evolution of these patients are the main concerns and there is a need to understand how both pathologies evolve from the very beginning of the ocular and cognitive impairments.

6 Conclusions

Summarising, in this study it is presented a methodology to analyse different cognitive processes through the study of ocular movements for the evaluation of neurodegenerative diseases such as the Alzheimer's disease and the behavioural variant of the frontotemporal dementia. The fixation test is excluded because it does not provide any significant ocular feature to these discrimination tasks. Smooth pursuit test is limited to those cases where there is a doubt according with the type of dementia. Saccadic movements tests (visually guided prosaccades, antisaccades and memory saccades) are enough to offer the needed help to the clinical diagnosis of the patient. This methodology provides a reliable, objective and optimised metric in less than 10 min.

This method could end up in the improvement of the help to the clinical diagnosis of the Alzheimer's disease or the behavioural variant of the frontotemporal variant. However, this methodology does not have to be seeing as an unique step in this process, it could provide initial inputs for the clinical diagnosis of the patient that have to be complemented with a more extensive process that should include neuropsychological tests, neuroimaging tests, specific biomarkers, etc., as well as any other step included in the clinical diagnosis of each disease.

Ocular movement tests suppose a non-expensive screening tool for these pathologies or a fast and quantitative examination tool for the evaluation of

the cognitive condition of the patient. Nevertheless, large-scale and massive trials should be conducted for full verification and improved differential diagnostic help.

References

1. Anderson, T.J., MacAskill, M.R.: Eye movements in patients with neurodegenerative disorders. In: Nature Reviews Neurology (2013)
2. Antoniades, C.A., Kennard, C.: Ocular motor abnormalities in neurodegenerative disorders. In: Eye, Elsevier(2015)
3. Klarendic, M., Kaski, D.: Deep brain stimulation and eye movements. In: European Journal of Neuroscience, Wiley Online Library (2021)
4. Rascovsky, K., et al.: Sensitivity of revised diagnostic criteria for the behavioural variant of frontotemporal dementia. In: Brain, Oxford University Press (2011)
5. Meyniel, C., Rivaud-Péchoux, S., Damier, P., Gaymard, B.: Saccade impairments in patients with fronto-temporal dementia. In: Journal of Neurology, Neurosurgery & Psychiatry, BMJ (2005)
6. Burrell, J.R., Hornberger, M., Carpenter, R.H.S., Kiernan, M.C., Hodges, J.R.: Saccadic abnormalities in frontotemporal dementia. In: Neurology, AAN Enterprises (2012)
7. Molitor, R.J., Ko, P.C., Ally, B.A.: Eye movements in Alzheimer's disease. In: Journal of Alzheimer's disease, IOS Press (2015)
8. Fernández, G., Schumacher, M., Castro, L., Orozco, D., Agamennoni, O.: Patients with mild Alzheimer's disease produced shorter outgoing saccades when reading sentences. In: Psychiatry research, Elsevier (2015)
9. Douglass, A., Walterfang, M., Velakoulis, D., Abel, L.: Behavioral variant frontotemporal dementia performance on a range of saccadic tasks. In: Journal of Alzheimer's Disease, IOS Press (2018)
10. Przybyszewski, A.W., Śledzianowski, A., Chudzik, A., Szlufik, S., Koziorowski, D.: Machine Learning and Eye Movements Give Insights into Neurodegenerative Disease Mechanisms. In: Sensors, MDPI (2023)
11. Robinson, D.A.: A method of measuring eye movemnent using a scieral search coil in a magnetic field. In: IEEE Transactions on Bio-Medical Electronics (1963)
12. Aungsakun, S., Phinyomark, A., Phukpattaranont, P., Limsakul, C.: Robust eye movement recognition using EOG signal for human-computer interface. In: Zain, J.M., Wan Mohd, W.M., El-Qawasmeh, E. (eds.) ICSECS 2011. CCIS, vol. 180, pp. 714–723. Springer, Heidelberg (2011). https://doi.org/10.1007/978-3-642-22191-0_63
13. Atmaji, C., Putra, A.E., Hanif, A.: Sliding window method for eye movement detection based on electrooculogram signal. In: 2018 International Conference on Information and Communications Technology (ICOIACT), IEEE (2018)
14. Larrazabal, A.J., Cena, C.E.G., Martínez, C.E.: Eye corners tracking for head movement estimation. In: 2019 IEEE International Work Conference on Bioinspired Intelligence (IWOBI), IEEE (2019)
15. Hernández, E., Hernández, S., Molina, D., Acebrón, R., García Cena, C.E.: OSCANN: technical characterization of a novel gaze tracking analyzer. In: Sensors, MDPI (2018)
16. Lukander, K.: A system for tracking gaze on handheld devices. Behav. Res. Methods **38**, 660–666 (2006). https://doi.org/10.3758/BF03193899

17. Cena, C.E.G., Andrés, D.G., Valdeolivas, I.P.: Measurement and analysis of eye movements performance to predict healthy brain aging. In: IEEE Access (2020)
18. Lage, C., et al.: Distinctive oculomotor behaviors in Alzheimer's disease and frontotemporal dementia. In: Frontiers in aging neuroscience (2021)
19. Casanova-Ferrer, F., et al.: Minimal hepatic encephalopathy is associated to alterations in eye movements. In: Scientific Reports, Nature (2022)
20. García Cena, C., Costa, M.C., Saltarén Pazmiño, R., Santos, C.P., Gómez-Andrés, D., Benito-León, J.: Eye movement alterations in post-COVID-19 condition: a proof-of-concept study. In: Sensors, MDPI (2022)
21. García Cena, C.E., et al.: Toward an automatic assessment of cognitive dysfunction in relapsing–remitting multiple sclerosis patients using eye movement analysis. In: Sensors, MDPI (2022)
22. Folstein, M.F., Folstein, S.E., McHugh, P.R.: "Mini-mental state": a practical method for grading the cognitive state of patients for the clinician. In: Journal of psychiatric research, Pergamon (1975)
23. Reisberg, B., Ferris, S.H., de Leon, M.J., Crook, T.: The global deterioration scale for assessment of primary degenerative dementia. In: The American journal of psychiatry, American Psychiatric Assn (1982)
24. McKhann, G.M., et al.: The diagnosis of dementia due to Alzheimer's disease: recommendations from the National Institute on Aging-Alzheimer's association workgroups on diagnostic guidelines for Alzheimer's disease. In: Alzheimer's & dementia, Elsevier (2011)
25. Lilliefors, H.W.: On the Kolmogorov-Smirnov test for normality with mean and variance unknown. In: Journal of the American statistical Association, Taylor & Francis (1967)
26. Ramírez, J., et al.: Ensemble of random forests One vs. Rest classifiers for MCI and AD prediction using ANOVA cortical and subcortical feature selection and partial least squares. In: Journal of neuroscience methods, Elsevier (2018)
27. Leandri, M., et al.: Balance features in Alzheimer's disease and amnestic mild cognitive impairment. In: Journal of Alzheimer's Disease, IOS Press (2009)
28. Jimenez-Mesa, C., et al.: Optimized one vs one approach in multiclass classification for early Alzheimer's disease and mild cognitive impairment diagnosis. In: IEEE Access (2020)
29. López, M., et al.: Principal component analysis-based techniques and supervised classification schemes for the early detection of Alzheimer's disease. In: Neurocomputing, Elsevier (2011)
30. Bradley, A.P.: The use of the area under the ROC curve in the evaluation of machine learning algorithms. In: Pattern Recognition, Elsevier (1997)
31. Platt, J., et al.: Probabilistic outputs for support vector machines and comparisons to regularized likelihood methods. In: Advances in Large Margin Classifiers, Cambridge (1999)
32. Gaugler, J.E., Kane, R.L., Johnston, J.A., Sarsour, K.: Sensitivity and specificity of diagnostic accuracy in Alzheimer's disease: a synthesis of existing evidence. In: American Journal of Alzheimer's Disease & Other Dementias, Sage Publications (2013)
33. Khoury, R., Ghossoub, E.: Diagnostic biomarkers of Alzheimer's disease: a state-of-the-art review. In: Biomarkers in Neuropsychiatry, Elsevier (2019)
34. Trapp, W., Röder, S., Heid, A., Billman, P., Daiber, S., Hajak, G.: Sensitivity and specificity of the Bamberg Dementia Screening Test's (BDST) full and short versions: brief screening instruments for geriatric patients that are suitable for infectious environments. In: BMC Medicine, BioMed Central (2021)

35. Jack Jr, C.R., et al.: NIA-AA research framework: toward a biological definition of Alzheimer's disease. In: Alzheimer's & Dementia, Elsevier (2018)
36. Gossye, H., Van Broeckhoven, C., Engelborghs, S.: The use of biomarkers and genetic screening to diagnose frontotemporal dementia: evidence and clinical implications. In: Frontiers in neuroscience (2019)
37. Harris, J.M.: Sensitivity and specificity of FTDC criteria for behavioral variant frontotemporal dementia. In: Neurology, AAN Enterprises(2013)
38. Ferrando, R., Damian, A.: Brain SPECT as a biomarker of neurodegeneration in dementia in the era of molecular imaging: still a valid option?. In: Frontiers in Neurology (2021)

Exploring Delay-Based Controllers. A Comparative Study for Stabilizing Angular Positioning

Diego Torres-García[1,2(✉)], Julián-Alejandro Hernández-Gallardo[1,3], César-Fernando Méndez-Barrios[1], and Silviu-Iulian Niculescu[2]

[1] Universidad Autónoma de San Luis Potosí (UASLP), Facultad de Ingeniería, Dr. Manuel Nava No. 8, San Luis Potosí, SLP, Mexico
{diego.torres,fernando.barrios}@uaslp.mx, julian_@ieee.org
[2] Université Paris-Saclay, CNRS, CentraleSupélec, Inria, Laboratoire des Signaux et Systèmes (L2S, UMR CNRS 8506), 91192 Gif-sur-Yvette, France
{diego.torres-garcia,silviu.niculescu}@l2s.centralesupelec.fr
[3] Tecnológico Salesiano Carlos Gómez, J. Venegas No. 5, Virreyes, C.P. 78240 San Luis Potosí, SLP, Mexico

Abstract. This study aims to perform a comparison of different control schemes, which are characterized by their *delay-based* nature, where the time delay is considered as a parameter of the control law. To facilitate this research, we look at a second-order linear time-invariant (LTI) single-input single-output (SISO) system as our test bench. Moreover, we propose a simple but efficient methodology to compute the *delay margin* for these control schemes, which exploits the continuity of the characteristic roots with respect to the parameters of the characteristic function of the closed-loop system. Furthermore, we evaluate the performance and robustness of the closed-loop system by numerical simulations and physical experiments. By conducting this in-depth analysis, we gain valuable insight into the strengths and limitations of each control scheme, providing a clearer understanding of their real-world applicability.

1 Introduction

Proportional-Integral-Derivative (PID) controllers have long been recognized as one of the most widely used controller structures in various industries [1,2]. Over several decades, they have consistently demonstrated their effectiveness in dealing with common industrial problems [3]. In parallel, Delay-Based (DB) controllers, such as the Proportional Minus Delay (PMD) [4,5], the Proportional-Integral-Retard (PIR) [6], more recently the so-called proportional-delayed controller (P-δ) [7], to name a few, where a delay h is used as a control parameter, gained in popularity in recent years. All these controllers are of low complexity because they have a reduced number of parameters. However, delay-based controllers are infinite-dimensional and, as noted in the references mentioned above, in some cases, they have certain advantages over finite dimensional controllers

M. N. Cardona et al. (Eds.): LACAR 2023, LNNS 940, pp. 123–136, 2024.
https://doi.org/10.1007/978-3-031-54763-8_13

but also certain disadvantages in other cases. We refer to [8] for an overview of time-delay systems and their applications to control theory.

Interestingly, a common feature shared by these two control approaches is that a *derivative-like* action can be implemented using a delay-difference operator. Although this approach is commonly employed to incorporate derivative actions, the selection of the delay parameter is often overlooked in the tuning process. Typically, a value is chosen as "sufficiently small" to approximate the derivative accurately. However, it is important to note that the behavior of a closed-loop system strongly depends on the location of the solutions of its characteristic function. Moreover, these roots are continuous functions of the system parameters (see, for instance, [9] in the finite-dimensional case and [10] in the delay case), which implies that the choice of parameters, including, in this case, the delay parameter, can have a significant impact on the roots location and, therefore, on the overall behavior of the system.

With the above discussion in mind, it is natural to consider a control design that incorporates the derivative action using a delay-difference operator, with the delay parameter h being a control parameter. In this note, we explore four different control schemes based on the well-known finite-difference method. The first case aims to approximate the derivative in the simplest manner, given by:

$$\frac{dy(t)}{dt} \approx \frac{y(t) - y(t-h)}{h}.$$

The second structure employs the three-points backward difference [11] and is defined as follows:

$$\frac{dy(t)}{dt} \approx \frac{3y(t) - 4y(t-h) + y(t-2h)}{2h}.$$

Inspired by these schemes and the P-δ control, we also propose a control scheme of the following form:

$$u(t) = \sum_{j=0}^{n} k_j y(t - jh),$$

with $n \in \{1, 2\}$. Unlike backward difference methods, which aim to approximate the derivative, such structures can bear an *average* derivative action but also provide more *freedom* in their design. It is worth mentioning that, although including a time-delay in the closed-loop system makes it infinite-dimensional, the controller remains of *low-complexity* type since we are considering commensurate delays and therefore adding only one (delay) parameter. The objective of this note is to investigate whether one of the structures introduced above offers advantages, in terms of closed-loop system performance and robustness with respect to the system parameters (including the delay). In particular, to measure the robustness of the proposed controllers with respect to the delay parameter, we propose methodologies to compute the *delay margin* [10,12,13], that is the maximum value of the delay h such that the stability of the closed-loop system can be preserved under the assumption that such a property holds

for the system free of delays. In other words, we are explicitly computing the first delay interval guaranteeing stability without analyzing if this interval is the only one guaranteeing the stability in closed-loop.

It is worth mentioning that recent research studies have addressed the issue of "improperly-posedness" associated with these types of approximations. Improperly-posedness refers to the potential instability that may arise in a closed-loop system for "small delays" when replacing the derivative action with its delay-difference counterpart. In order to avoid such problems, we specifically focus our comparative study on systems that are properly-posed (for further details, refer to [14,15]).

2 Preliminaries

In the following, we focus on LTI-SISO systems, which can be represented by a transfer function of the form:

$$H(s) := \frac{k}{s(Ts+1)}, \tag{1}$$

where s represents the Laplace variable, $k \in \mathbb{R}_+$ is the open-loop gain of the plant, and $T \in \mathbb{R}_+$ is the system time-constant. This particular type of plant is of general industrial interest since it captures the dynamics of several industrial processes such as car suspension systems and pendulum oscillation [16], electric motors [17], reactor batch [18], thermal systems, and heating systems or an air conditioning (HVAC) system [17] (see also [19] and the references therein). We also examine the closed-loop system when a Proportional-Derivative (PD) controller is employed, which has a frequency domain representation given by:

$$C_0(s) = k_p + k_d s, \tag{2}$$

where k_p and k_d represent the proportional and derivative gains, respectively. Such a control scheme is well-suited for the dynamics of the plants under consideration. Firstly, these plants are *integral* in nature, which means they naturally achieve a steady-state error of zero without requiring an integral action in the control scheme. Secondly, incorporating a *derivative action* in a control process is commonly necessary to enhance the speed of such processes, which is a common requirement for this type of plant. In this study, we propose replacing the controller $C_0(s)$ with the DB controllers in Table 2, where $h > 0$ (i.e., $h \in \mathbb{R}_+$) is a time delay, and it is considered as a control parameter. The controllers C_1 and C_2 correspond to the aforementioned approximation of the derivative action, while C_3 and C_4 are inspired by the P-δ controller and aims to simplify the stability analysis while retaining the main properties of a derivative action (Table 1).

Table 1. DB Control schemes under consideration

Delay-difference derivative	P-δ-alike controller
$C_1(s) = k_p + \frac{k_d}{h}(1 - e^{-hs})$	$C_3(s) = k_0 + k_1 e^{-hs}$
$C_2(s) = k_p + \frac{k_d}{h}\left(\frac{3}{2} - 2e^{-hs} + \frac{1}{2}e^{-2hs}\right)$	$C_4(s) = k_0 + k_1 e^{-hs} + k_2 e^{-2hs}$

When considering a classical unity feedback loop, the characteristic function of the closed-loop system can be represented as $\Delta_{hi} : \mathbb{C} \to \mathbb{C}$:

$$\Delta_{hi}(s; h) = s(Ts + 1) + kC_i(s), \quad i \in \{1, 2, 3, 4\}, \tag{3}$$

where $C_i(s)$ represents the controller, depending on the subscript i. The characteristic function is a quasi-polynomial and exhibits an infinite number of characteristic roots. In this regard, the closed-loop system is considered exponentially stable if and only if all the roots of $\Delta_{hi}(s; h)$ are located in the open left-half plane of the complex plane ($\mathbb{C}_-$). It is also worth mentioning that these solutions are continuous functions of the delay parameter h.

With the above discussion in mind, consider the following definitions:

Definition 1 (Spectrum). Consider the dynamical system represented by the transfer function (1) with closed-loop characteristic function (3). The *spectrum* of Δ_{hi} is the set $\sigma(\Delta_{hi}) \subset \mathbb{C}$ defined by

$$\sigma\left(\Delta_{hi}\right) := \{s^* \in \mathbb{C} : \Delta_{hi}(s^*; h) = 0\}.$$

Definition 2 (Delay margin). Consider the closed-loop characteristic function (3) and its spectrum $\sigma(\Delta_{hi})$. Under the assumption that the closed-loop system free of delay is exponentially stable, the *delay margin* $h_{\max}$ is the bound defined by

$$h_{max} := \sup\{\beta \in \mathbb{R}_+ : \sigma\left(\Delta_{\beta i}\right) \subset \mathbb{C}_-\}.$$

Bearing in mind all these definitions, the following section introduces our main results.

3 Main Results

In the following, we aim to compute the delay margin of the closed-loop system for the different controllers under consideration. Since any digital implementation of a PD controller requires a discretization process, the delay margin is of crucial importance.

3.1 Delay-Margin Computation

We have the following propositions:

Proposition 1 ***(Delay margin of the system in closed-loop with*** C_1***):*** *Consider the system* (1) *in closed-loop with the controller* C_1 *and assume that* $k_p \leq \frac{1}{4kT}$*. Then, if* C_0 *is a stabilizing controller, the delay margin* h_{max} *of the closed-loop system is given by:*

$$h_{max} = \frac{2\left(kk_dT\omega^2 - k^2k_dk_p\right)}{k^2k_p^2 - 2kk_pT\omega^2 + T^2\omega^4 + \omega^2}, \tag{4}$$

where $\omega \in \mathbb{R}_+$ *is the smallest value satisfying:*

$$\frac{\pi}{2}(1 - sign(k_d)) = arg\{h_{max}\boldsymbol{i}\omega(T\boldsymbol{i}\omega + 1) + kk_ph_{max} + kk_d\} + h_{max}\omega. \tag{5}$$

Proof. Let $\tilde{\Delta}(s;h) := h\Delta_{h1}(s;h)$, which share the same solutions for $h > 0$. Taking $s = \boldsymbol{i}\omega$ and considering $\tilde{\Delta}(\boldsymbol{i}\omega;h) = 0$, it is easy to obtain the following system of equations:

$$k(hk_p + k_d) - kk_d\cos(h\omega) - hT\omega^2 = 0, \tag{6}$$

$$kk_d\sin(h\omega) + h\omega = 0. \tag{7}$$

Note that, as was expected, $h = 0$ is a solution, however, it is not of interest. Hence, by solving for $h \neq 0$ yields to (4). Next, since $s = \boldsymbol{i}\omega$ is a solution when $h = h_{\max}$ we must have:

$$h_{\max}\boldsymbol{i}\omega(T\boldsymbol{i}\omega + 1) + kk_ph_{\max} + kk_d = kk_de^{-h_{\max}\boldsymbol{i}\omega}. \tag{8}$$

Finally, (5) results straightforwardly by considering the argument on both sides of (8). □

Proposition 2 ***(Delay margin of the system in closed-loop with*** C_3***):*** *Consider the system* (1) *in closed-loop with the controller* $C_3(s)$*. If the system is stable for* $h = 0$*, then the delay margin* h_{max} *of the system is given by the smallest value of* $h \neq 0$ *such that:*

$$\cos(h\omega) = \frac{T\omega^2 - kk_0}{kk_1} \wedge \sin(h\omega) = \frac{\omega}{kk_1}, \tag{9}$$

where $\omega \neq 0$ *is given by:*

$$\omega^2 = \frac{2Tkk_0 - 1 \pm \sqrt{1 + 4kT(-k_0 + kk_1^2T)}}{2T^2}. \tag{10}$$

Proof. The closed-loop characteristic equation reads as:

$$\Delta_{h3}(s;h) = s(Ts + 1) + k(k_0 + k_1e^{-hs}).$$

Define $f_1(s) := s(Ts + 1 + kk_0)$ and $f_2(s;h) := kk_1e^{-hs}$. Thus, $\Delta_{h3}(s;h) = f_1(s) + f_2(s;h)$. By continuity, we know that if $\Delta_{h3}(s;0)$ is stable, it will remain stable for a sufficiently small h. Furthermore, if any root crosses from stability to instability, the crossing must occur by the $\boldsymbol{i}\mathbb{R}$ axis. Suppose now that $s = \boldsymbol{i}\omega$ is a solution of $\Delta_{h3}(s;h)$ for some $h \in \mathbb{R}^+$, thus $s = -\boldsymbol{i}\omega$ is also a solution and we can consider the equation $f_1(\boldsymbol{i}\omega)f_1(-\boldsymbol{i}\omega) - f_2(\boldsymbol{i}\omega;h)f_2(-\boldsymbol{i}\omega;h)$, which bears:

$$k^2k_0^2 - k^2k_1^2 + \omega^2(1 - 2kk_0T) + T^2\omega^4 = 0. \tag{11}$$

Direct computations yield to (10). Next, since $\Delta_{h3}(\boldsymbol{i}\omega;h) = 0$, both the real and the imaginary parts have to be zero. From this observation, it is easy to obtain (9). □

Proposition 3 ***(Delay margin of the system in closed-loop with C_4):*** *Consider the system (1) in closed-loop with the controller $C_4(s)$. If the system is stable for $h = 0$, then the delay margin h_{max} of the system is given by the smallest value of $h \neq 0$ such that:*

$$\cos(h\omega) = \Re\left\{-\frac{k^2(k_0 - k_2)(k_0 + k_2) - 2kk_0T\omega^2 + T^2\omega^4 + \omega^2}{kk_1(k(k_0 - k_2) - \omega(T\omega + \boldsymbol{i}))}\right\}, \tag{12}$$

and:

$$\sin(h\omega) = \Im\left\{\frac{k^2(k_0 - k_2)(k_0 + k_2) - 2kk_0T\omega^2 + T^2\omega^4 + \omega^2}{kk_1(k(k_0 - k_2) - \omega(T\omega + \boldsymbol{i}))}\right\}, \tag{13}$$

hold, where $\omega \neq 0$ is given by:

$$\omega^2 = \sqrt{x}, \tag{14}$$

with $x \neq 0$ being the smallest real solution of:

$$ax^4 + bx^3 + cx^2 + dx + e = 0,$$

where:

$$\begin{aligned}
a &= T^4,\\
b &= 2T^2 - 4kk_0T^3,\\
c &= 6k^2k_0^2T^2 - k^2k_1^2T^2 - 2k^2k_2^2T^2 - 4kk_0T + 1,\\
d &= -4k^3k_0^3T + 2k^3k_0k_1^2T + 4k^3k_0k_2^2T - 2k^3k_1^2k_2T + 2k^2k_0^2 - k^2k_1^2 - 2k^2k_2^2,\\
e &= k^4k_0^4 - k^4k_0^2k_1^2 - 2k^4k_0^2k_2^2 + 2k^4k_0k_1^2k_2 - k^4k_1^2k_2^2 + k^4k_2^4 + x^2.
\end{aligned}$$

Proof. The closed-loop characteristic equation reads:

$$\Delta_{h4}(s;h) = s(sT + 1) + kk_0 + kk_1e^{-hs} + kk_2e^{-2hs}.$$

Next, define $f_1(s) = s(sT+1)+kk_0$ and $f_2(s;h) = kk_2$. If $s = \boldsymbol{i}\omega$ is a solution of $\Delta_{h4}(s;h)$, then $s = -\boldsymbol{i}\omega$ is also a solution and we can write the following system of equations:

$$F_1(\boldsymbol{i}\omega;h) = f_1(-\boldsymbol{i}\omega)\Delta_{h4}(\boldsymbol{i}\omega;h) - f_1(\boldsymbol{i}\omega)\Delta_{h4}(-\boldsymbol{i}\omega;h)e^{-h\boldsymbol{i}\omega},$$
$$F_2(\boldsymbol{i}\omega;h) = f_1(\boldsymbol{i}\omega)\Delta_{h4}(-\boldsymbol{i}\omega;h) - f_1(-\boldsymbol{i}\omega)\Delta_{h4}(\boldsymbol{i}\omega;h)e^{h\boldsymbol{i}\omega}.$$

While this system of equations shares solutions with the characteristic equations, it only presents one exponential term, allowing to repeat the procedure followed for the case of $C_3(s)$. □

Finally, if we consider the system in closed-loop with the controller $C_2(s)$, the following algorithm allows to compute its corresponding delay margin:

Data: $\Delta_{h2}(s;h)$, h_0, δh
Result: $h_{\max}$
Initialize: flag $\leftarrow 1$, $h_{\text{aux}} \leftarrow h_0$;
do
  QPmR($\Delta_{h2}(s;h_{aux})$);
  if $\Delta_{h2}(s;h_{aux})$ *is stable* **then**
    $h_{\text{aux}} \leftarrow h_{\text{aux}} + \delta h$;
  else
    $h_{\max} \leftarrow h_{\text{aux}}$;
    flag $\leftarrow 0$;
  end
while *flag* $= 1$;

Algorithm 1: Delay margin explicit computation.

Note that in order to verify whether $\Delta_{hi}(s;h_{aux})$ is stable or not, we make use of the QPmR algorithm (see [20] for further details). An implementation of the algorithm in Python 3.8 can be found in Appendix 1.

Remark 1. Algorithm 1 facilitates the computation of the delay margin independently of the selected controllers. However, whenever feasible, opting for analytical computation is generally advisable for achieving optimal results.

4 Numerical Results

Through this section we first introduce the system under consideration and then we present some numerical results in the form of the output of the system in closed-loop with the different control schemes that are being presented.

Fig. 1. QUBE-Servo 2 rotary servo experiment.

4.1 System: QUBE-Servo 2

The system under consideration is the QUBE-Servo 2 (see Fig. 1), a servo motor for which we aim to control its angular position. The transfer function that models the relationship between the output $\Theta(s)[rad]$ and the input $V(s)[V]$ reads:

$$\frac{\Theta(s)}{V(s)} = \frac{k}{s(Ts+1)}, \tag{15}$$

which correspond to the class of system considered in this study.

4.2 Numerical Simulations

Throughout this section, we present some numerical simulations of the system in closed-loop with the different controllers under study (Appendix 2). The plant parameters were obtained via an identification process, $k = 23.65$ and $T = 0.345$, while the controller gains correspond to those indicated in Table 2. Using Algorithm 1 and the methodologies previously mentioned, we obtain the delay margins and the crossing frequency that are shown in Table 2.

Note that the smallest tolerance with respect to the delay h corresponds to $h_{max} \approx 0.03$, thus, we can easily consider $h = 0.005$ to avoid losing stability.

From the numerical simulation, it can be observed that the controllers performing an "*approximate*" derivative action achieve a faster response with less overshoot when regulating with an input reference of $\theta = \pi/4$. However, it is worth mentioning that the performance of the PD controller with the derivative approximated via a delay-difference operator can be also achieved by $C_3(s)$ and $C_4(s)$ by simple choosing $k_0 = k_p + k_d/h$ and $k_1 = -k_d/h$ in $C_3(s)$, and $k_0 = k_p + 3k_d/(2h)$, $k_1 = -2k_d/h$ and $k_2 = k_d/(2h)$ in $C_4(s)$ (Fig. 2).

Table 2. Delay margin for the different controllers. The different controller gains were chosen such that the delay-free systems have the same right-most root.

Controller	h_{max}	Crossing frequency ω	Control Gains
$C_1(s)$	0.07473...	43.8984...	$(k_p, k_d) = (700/473, 1)$
$C_2(s)$	0.03658...	87.1097...	$(k_p, k_d) = (700/473, 1)$
$C_3(s)$	0.04410...	11.3446...	$(k_0, k_1) = (1, 1)$
$C_4(s)$	0.03372...	11.2988...	$(k_0, k_1, k_2) = (1, 0.5, 0.5)$

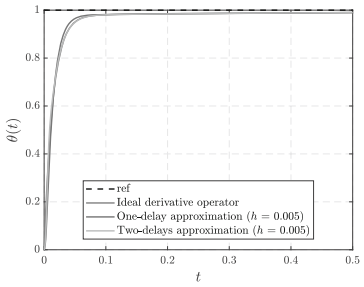

(a) System output when in closed-loop with the PD-controller and its two different approximations.

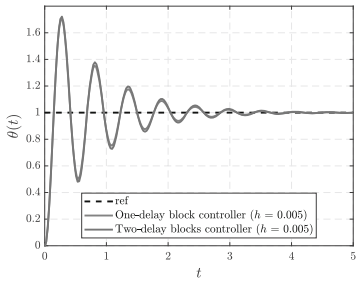

(b) System output when subjected to controllers C_3 and C_4.

Fig. 2. System output when simulating the closed-loop considering the different proposed controllers.

It is important to note that the simulations do not account for any mechanical constraints inherent to the physical system, such as the maximum rotation velocity it can achieve. As a result, the observed speeds in the case of the controllers $C_1(s)$ and $C_2(s)$ may not be achievable in the actual system. To address this issue, the subsequent section presents experiments conducted on the physical plant.

5 Experimental Results

The same experiments that were performed numerically were also done in the real plant. In the case of the physical experiment, not only the system output but also the control output was measured. The implementation does not allow control outputs outside of the interval $[-10, 10]$, and therefore one have to ensure that the control signal is not outside of such a range to assure the expected performance (Fig. 3).

Remark 2. Note that a pure derivative action cannot be implemented in a real plant, it was implemented with the scheme: $k_d N/(1 + N/s)$ where $N = 100$. The larger value of N is the better approximation of the derivative action. This,

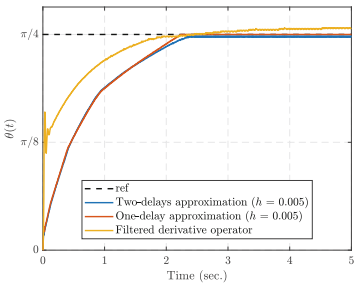

(a) Plant output when in closed-loop with the controllers C_0 implemented with a filter, C_1 and C_2.

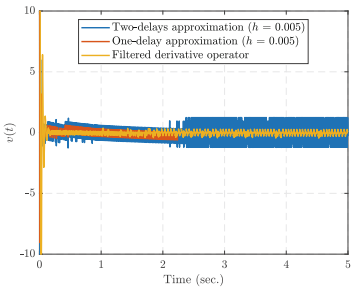

(b) Control output of the filtered PD controller and both approximations.

Fig. 3. System output considering the different proposed controllers.

together with the one-delay approximation, is the most common way to implement a derivative action (Fig. 4).

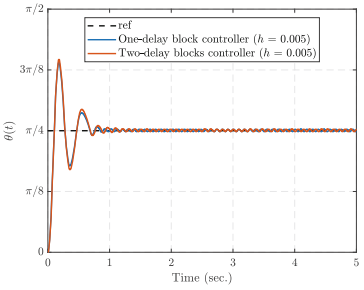

(a) Plant output when in closed-loop with the controllers C_3 and C_4.

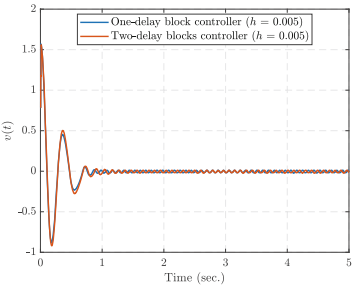

(b) Control output of the controllers C_3 and C_4.

Fig. 4. Real plant output considering the different proposed controllers.

As expected from the numerical simulations, the chosen values of the controller gains as well as the delay value achieve regulation in the real plant. The experimental results can be observed in the following site: https://sites.google.com/view/jhernandezg/principal/doctorado/publicaciones/delay-difference.

5.1 Verification of the Delay Margin

The accuracy of the delay margin computations can be readily verified by progressively increasing the value of h within the closed-loop system. As illustrated in Figs. 5, a gradual increment in the delay h leads to the emergence of oscillations. These oscillations correspond to the pair of complex conjugate solutions that approach the imaginary axis.

Furthermore, it is evident that the frequency of the oscillations, as depicted in Table 2, is consistent with expectations. Specifically, when considering controllers $C_1(s)$ and $C_2(s)$, the oscillation frequency is higher compared to when using $C_3(s)$ and $C_4(s)$. These results align with the corresponding values of ω obtained from the previous analysis.

The significance of these observed phenomena lies in the understanding that the selection of the delay value for controller implementation cannot be arbitrary. Rather, it is crucial to account for both margins and crossing frequencies during the design process to mitigate undesirable system behaviors. Depending on the application's requirements, one may prioritize mitigating high-frequency oscillations, minimizing overshoot values, or optimizing the time taken to reach a steady state.

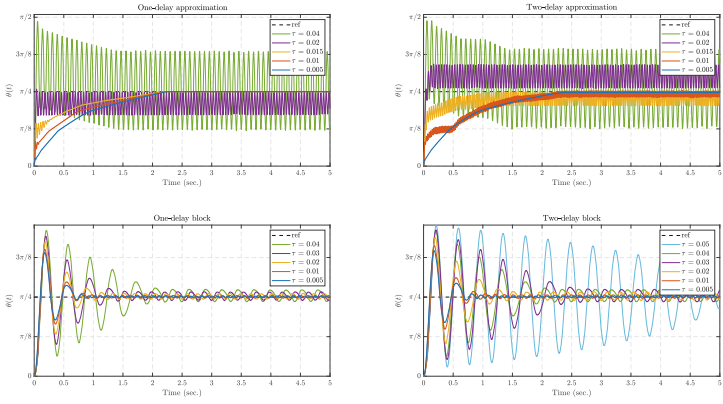

Fig. 5. Experimental proofs of the delay margin.

6 Concluding Remarks

The efficacy of various delay-based controllers has been demonstrated through numerical simulations and real-world experimentation. We also emphasized how the delay-margin may change when changing the control scheme. Moreover, we accentuate the role played by the selection of the delay parameter, and its impact on system stability and performance.

Appendix 1: Algorithm Implementation

The following code is a Python implementation of Algorithm 1. For the Python implementation of the QPmR algorithm, please refer to the repository available at the following link: https://github.com/DSevenT/QPmR

```
sol = []
i = -1
h = np.linspace(0.000001, 1, 3500)
for tau in h:
    qp = T*s**2+s+k*(kp+kd*(3-4*exp(-tau*s)+exp(-2*tau*s))/(2*tau))
    r = QPmR(qp, R, 0.1*np.pi/2.5,0.0000001)
    sol.append(r)
    i = i+1
    if all(j < 0 for j in sol[i].real):
        continue
    else:
        print('Critical value of h:' + str(tau))
        break
figure_1 = plt.figure("Figure 1")
b = 1
r = 0
for n in range(len(sol)):
    plt.plot(sol[n].real, sol[n].imag, 'o', color=[r, 0, b], markersize=1.5)
    if b>0:
        b = b-1/len(sol)
    else:
        b = b+1/len(sol)
    if r <1:
        r = r+1/len(sol)
    else:
        r = r-1/len(sol)
plt.axvline(x = 0, color = 'k', ls = '--')
plt.axhline(y = 0, color = 'k', ls = '--')
plt.show()
```

This implementation generates Figure 6, which illustrates the stability crossing of the system roots as the value of the delay parameter h increases.

Appendix 2: Practical Implementation

The physical implementation of the controller can be done using the QUARC Real-Time Control Software in Simulink (for more information we refer to their website: https://quanser.com/products/quarc-real-time-control-software/), using the scheme depicted on Figure 7.

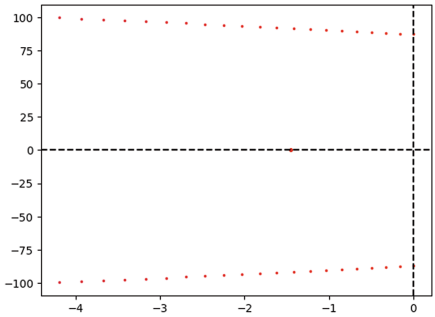

Fig. 6. Delay margin detection through Algorithm 1.

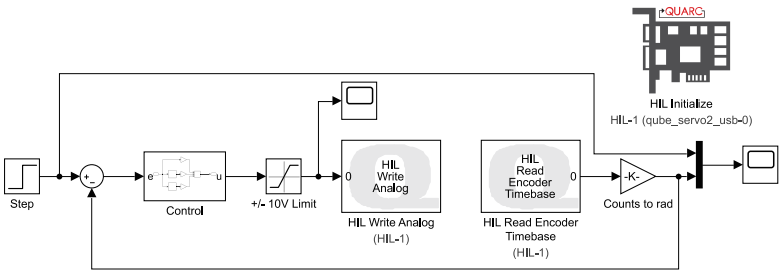

Fig. 7. Implementation of the controller using Simulink.

References

1. Åström, K.J., Hagglund, T.: PID Controllers: Theory, Design, and Tuning, 2nd edn. Instrument society of America, Research Triangle Park (1995)
2. O'Dwyer, A.: Handbook of PI and PID Controller Tuning Rules, 3rd edn. Imperial College Press (ICP), London (2009)
3. Silva, G.J., Datta, A., Bhattachaiyya, S.P.: PID stabilization of first-order systems with time delay. In: PID Controllers for Time-Delay Systems, pp. 161–190. Birkhäuser, Boston (2005)
4. Suh, H., Bien, Z.: Proportional minus delay controller. IEEE Trans. Autom. Control **24**(2), 370–372 (1979)
5. Suh, H., Bien, Z.: Use of time-delay actions in the controller design. IEEE Trans. Autom. Control **25**(3), 600–603 (1980)
6. Ramírez, A., Mondié, S., Garrido, R., Sipahi, R.: Design of proportional-integral-retarded (PIR) controllers for second-order LTI systems. IEEE Trans. Autom. Control **61**(6), 1688–1693 (2015)
7. Hernández-Díez, J.-E., Méndez-Barrios, C.-F., Niculescu, S.-I.: Proportional-delayed controllers design for LTI-systems: a geometric approach. Int. J. Control **91**(4), 907–925 (2018)
8. Sipahi, R., Niculescu, S.-I., Abdallah, C., Michiels, W., Gu, K.: Stability and stabilization of systems with time delay. IEEE Control Syst. Mag. **31**(1), 38–65 (2011)
9. Marden, M.: Geometry of Polynomials, no. 3. American Mathematical Society (1949)

10. Michiels, W., Niculescu, S.-I.: Stability, Control, and Computation for Time-Delay Systems. An Eigenvalue-Based Approach. Advances in Design and Control, 2nd edn. SIAM, Philadelphia (2014)
11. LeVeque, R.J.: Finite Difference Methods for Ordinary and Partial Differential Equations: Steady-State and Time-Dependent Problems. SIAM (2007)
12. Gu, K., Kharitonov, V.L., Chen, J.: Stability of Time-Delay Systems. Control Engineering, Birkhäuser, Boston (2003)
13. Ma, D., Chen, J.: Delay margin of low-order systems achievable by PID controllers. IEEE Trans. Autom. Control **64**(5), 1958–1973 (2018)
14. Méndez-Barrios, C.-F., Niculescu, S.-I., Martínez-González, A., Ramírez, A.: Characterizing some improperly posed problems in proportional-derivative control. Int. J. Robust Nonlinear Control **32**(18), 9452–9474 (2022)
15. Torres-García, D., Méndez-Barrios, C.-F., Niculescu, S.-I., Martínez-González, A.: Delay-difference approximation of PD-controllers. Insights into improperly-posed closed-loop systems. IFAC-PapersOnLine **55**(40), 79–84 (2022)
16. Nise, N.S.: Control Systems Engineering. Wiley, New York (2020)
17. Salivahanan, S., Rengaraj, R., Venkatakrishnan, G.R.: Control Systems Engineering. Pearson, London (2014)
18. Seborg, D.E., Edgar, T.F., Mellichamp, D.A., Doyle, F.J., III.: Process Dynamics and Control. Wiley, New York (2016)
19. Hernández-Gallardo, J.-A., Guel-Cortez, A.-J., Gonzalez-Galvan, E.J., Méndez-Barrios, C.-F.: Designing proportional delayed integral control for fast regulation in second-order systems: a geometric approach. In: 2023 9th International Conference on Control, Decision and Information Technologies (CoDIT), pp. 01–06 (2023)
20. Vyhlidal, T., Zítek, P.: Mapping based algorithm for large-scale computation of quasi-polynomial zeros. IEEE Trans. Autom. Control **54**(1), 171–177 (2009)

Occupant Behavior Revealed from Sensor-Fusion-Based Clustering Analysis: Case of a University Building Office

Ana Rivera[1], Erick Reyes[1], Ignacio Chang[2], and Miguel Chen Austin[1,2(✉)]

[1] Research Group Energy and Comfort in Bioclimatic Buildings (ECEB), Faculty of Mechanical Engineering, Universidad Tecnológica de Panamá, Ciudad de Panamá, Panama
miguel.chen@utp.ac.pa

[2] Research Group Intelligent Control Systems and Industrial Computing (SCIII), Faculty of Electrical Engineering, Universidad Tecnológica de Panamá, Ciudad de Panamá, Panama

Abstract. Occupant behavior is among the main drivers in building energy consumption. However, due to its stochastic nature, it isn't easy to model and is often oversimplified in building simulations. Moreover, obtaining explicit occupancy data for modeling purposes is a tedious endeavor. This has led to the implementation of indirect occupancy sensing systems, and when coupled with machine learning algorithms, have proven effective for occupancy estimation. This work applies k-means clustering to experimental data recorded for 25 days to reveal occupancy profiles in a university office. Four clusters were obtained from electric current, light luminosity, and motion sensor data. These clusters are interpreted as occupancy profiles, with varying degrees of occupancy level and arrival and departure times. While electric current and motion sensor data clusters could bring forth relevant occupancy information, light luminosity was not as informative in our case study. This approach to occupancy profiling has the advantage of not requiring ground truth occupancy data, thus facilitating the modeling process. The information obtained from clustering analysis is useful for building systems' control strategy design, supervised learning algorithm tuning, and building energy simulation.

1 Introduction

The building sector accounts for around one-third of global energy consumption and emissions, making it one of the main targets for implementing strategies to improve energy efficiency [1]. Building energy consumption is driven by several key factors, such as the surrounding thermal environment, building design and construction, and occupant behavior, among others [2]. Unlike the other factors mentioned, occupant behavior is more complicated to model due to its stochastic

M. N. Cardona et al. (Eds.): LACAR 2023, LNNS 940, pp. 137–144, 2024.
https://doi.org/10.1007/978-3-031-54763-8_14

nature, and it is thus oversimplified in building simulation [2,3]. An appropriate understanding of occupant behavior is key to achieving the desired performance levels in building energy-saving strategies.

Obtaining informative occupancy data is the main bottleneck for occupant behavior modeling [4,5]. Occupancy sensors include passive infrared (PIR), indoor air quality (AIQ), luminous intensity (LI), and vision-based sensors. When employed in a standalone manner to correlate the received signals into occupancy information, these sensors (especially PIR, AIQ, and LI) may be highly uncertain. While most accurate, vision-based sensors are memory intensive and have privacy concerns[6]. However, multiple sensor data can be aggregated (sensor fusion) to improve occupancy information and overcome the shortcomings of a single sensor. Then, a mathematical model is used to transform sensor data into occupancy behavior patterns, occupant count/presence, and other useful occupancy information for control strategy design or building simulation [6,7].

Machine learning algorithms, both supervised and unsupervised, have been successfully employed to estimate occupancy and obtain occupancy patterns [8]. Supervised learning algorithms are used to learn either occupancy count or presence, while unsupervised learning algorithms are used to find occupancy patterns [9]. Some common supervised algorithms for occupancy estimation include artificial neural networks (ANN), k-nearest neighbors (kNN), and decision trees (DT) [8]. Clustering or data mining algorithms are common unsupervised learning algorithms used for occupancy pattern learning [4].

A single algorithm is rarely used for occupancy estimation in the reviewed works. Clustering algorithms are used in pre-processing or post-processing for data analysis or dimensionality reduction [10]. The insights from this stage are then used to tune a supervised learning algorithm for occupancy prediction. In [3], they propose a data mining framework for occupancy schedule learning in 16 offices in Germany. They created a DT model to predict office binary occupancy from the available features (season, day of the week, time of day, window change). From the results of the DT, they derive pruned sets of decision rules. Finally, k-means clustering is used to obtain typical working schedules and occupancy rates for the 16 offices. Similarly, in [5], they combine k-means cluster analysis and DT to recognize occupancy patterns in an office building in Philadelphia. They obtain four different patterns of occupancy presence, with varying levels of occupancy rates, working times, arrival/departure times, and noon break times. From the insights gathered with clustering, they learn schedule rules with a DT and finally predict occupancy schedules. In [9], they designed a machine-learning-based cooling control strategy. They apply k-means clustering to describe four main occupancy patterns, which only differ in occupants' arrival/departure time. Then, they predict occupancy through a kNN algorithm. The occupancy information learned through these algorithms is used to infer the real-time setpoints of a commercial building's cooling system, demonstrating energy savings of around 21% compared to conventional control and providing more robust control actions against occupant behavior. In [11], they use hierarchical clustering to evaluate

CO2 and electric power sensors' capability to reproduce occupancy patterns. From the resulting dendrograms, they identify three occupancy levels. They also propose occupancy models based on logical flowcharts that take as inputs several types of sensor data. Models that take as inputs three variables had errors of less than 9%, demonstrating the advantage of sensor fusion for occupancy prediction. In [12], they studied the relationship between building electricity consumption and WiFi connection count (as an occupant presence variable) across four university campus buildings in Singapore. They compared multiple clustering techniques and concluded that applying DBSCAN with PCA pre-processed data had the best results based on the Calinski Harabasz score. In [13], they analyzed the performance of two Convolutional ANNs on an edge device to identify occupancy in real time. They studied the correlation between the environmental variables recorded and occupancy ground truth, showing that the occupancy is best correlated with the light level data. They implemented 1D-CNN and 2D-CNN models to the edge device, obtaining 99.72% and 99.76% real-time accuracy, respectively.

While supervised algorithms have proven effective for occupancy estimation, the need for occupancy ground truth (GT) complicates model training. In the reviewed studies, GT has been collected through tedious processes, such as the review of recordings, surveys, or manual tabulation, that require high participant engagement. On the other hand, unsupervised learning algorithms do not require GT for tuning. However, some form of explicit GT data is used when clustering algorithms have been used in the reviewed works to obtain occupancy profiles [3,5] . Moreover, clustering algorithms have yet to be explored in the literature as a standalone technique to obtain occupancy information from indirectly related variables, such as energy consumption or environmental variables. This work aims to bridge this gap, providing a detailed description of a k-means clustering algorithm to obtain occupancy profiles in a university office/laboratory. This work explores the capabilities of the clustering algorithm as a standalone technique, aiming to obtain occupancy schedules from environmental, motion sensors, and power consumption data without the need for explicit occupancy for model tuning. These occupancy profiles have application in building control and automation, and they could potentially be used to guide the dynamic adjustment of HVAC and lighting systems based on occupancy.

2 Materials and Methods

2.1 Description of the Case Study

Figure 1 shows a schematic of the case study and the experimental setup. The 60 m^2 university office at the Technological University of Panama is occupied by research assistants, professors, and students. The study involved the use of five monitoring modules for data acquisition. The modules were placed at various points in the office. Each module consisted of a NodeMCU ESP-12E board that receives signals from multiple sensors depending on the monitoring module. Data is then uploaded every five seconds to a ThingSpeak server. The experimental setup also included a camera that recorded the door to have GT available.

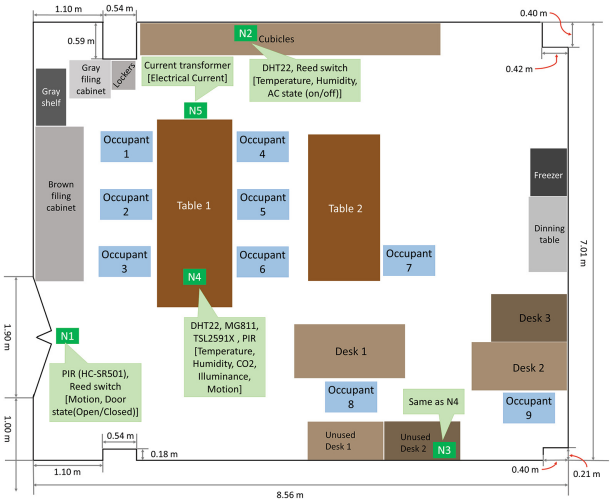

Fig. 1. Case study schematic and monitoring module layout.

The dataset was collected from June 16th, 2023, to July 11th, 2023. Data is preprocessed differently depending on the variable type (binary or continuous). Binary variables are resampled at five-minute intervals. For continuous variables, the five-minute average is computed. During this stage, missing and outlier values are also handled to improve dataset quality.

As part of the preliminary analysis, the Pearson correlation coefficient (PCC) is computed to find the monitored variables with the strongest linear relationship to occupancy count and occupancy state (a binary variable), as obtained from the available GT. The day selected for this analysis is July 4th, 2023. The correlation analysis revealed that the variables most correlated to occupancy count and state are electric current (EC) and illuminance (IL) from the N3 and N4 modules (`IL_N3` and `IL_N4`, respectively). The PCC between these variables and the occupancy count is, in the same order as they were mentioned, 0.85, 0.71, and 0.7; for occupancy state, 0.60, 0.83, and 0.82.

Figure 2 plots EC and `IL_N3` over ground truth data. These plots again leave evidence of the strong correlation between EC and occupancy count, while IL seems most indicative of the arrival/departure times of the occupants in the office, as it has non-zero values only between the first arrival and last departure.

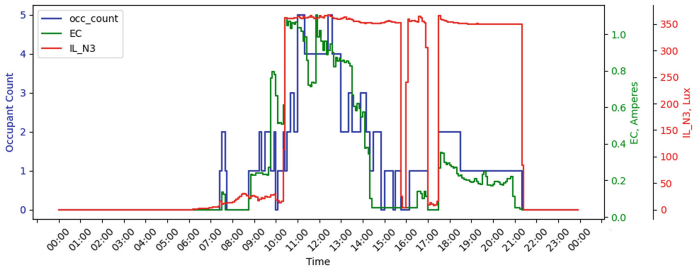

Fig. 2. Ground truth with Electric current (EC) and Illuminance from N3 (`IL_N3`).

PIR sensor raw data was not strongly correlated to occupancy, which could be attributed to the type of activity in the case study, mostly office work. One of the main shortcomings of the PIR sensor is that, unless a motion is detected, the PIR sensor retains a low value. However, it is possible to transform this raw data into a dataset with more useful characteristics. Inspired by [9], PIR data from N1 is transformed into a two-dimensional dataset containing the hour of first arrival (first HIGH output of the PIR sensor) and last departure (last HIGH output of the PIR sensor) for each day of the original dataset. This same transformation is applied to `IL_N3`.

From this preliminary data analysis, clustering will only be applied to the following variables: as raw data, EC and `IL_N3`; as transformed arrival/departure data, PIR sensor from N1, and `IL_N3`.

2.2 K-Means Clustering

Clustering algorithms group unlabeled data points into different clusters so that the data points that belong to the same cluster are similar based on a distance metric (Euclidean distance in this work) [10]. In this work, we evaluate the performance of k-means clustering to obtain occupancy patterns in a university office/laboratory. Each day of the available dataset will be assigned to a different cluster. The k-means clustering algorithm groups the examples in a dataset into k clusters. Readers are referred to [10] for a full description of the k-means clustering algorithm. In this work, by studying the inertia and the silhouette scores as a function of k and incorporating previous knowledge into the occupancy profiles in the case study, the number of clusters is set to k = 4.

3 Results and Discussion

For EC data, the resulting occupancy profiles observed from the clustering analysis can be described as follows: in EC Cluster 1 (not presented), activity starts at 8:00 a.m. and ends at 11:00 p.m., encompassing all lecture shifts. This cluster includes most days and all workdays and describes an overall high energy

consumption. EC Cluster 2, shown in Fig. 3a, describes days with low to no occupancy, typically weekends and some abnormal weekdays with little activity. EC Cluster 3, shown in Fig. 3b, particularly describes activity on Mondays, in which activity starts at 10:00 a.m., with peaks between 10:00 a.m. and 12:00 p.m. and 3.00 p.m. and 5:00 p.m., and then decreases to zero at 11:00 p.m. Peak EC stays below one ampere in this cluster. Finally, EC Cluster 4 (not presented) has the same activity start and end times as Cluster 3 (including another Monday) but with overall higher energy consumption.

The results from illuminance (IL) clusters were less informative than EC clusters. This can be observed in Fig. 3c, which shows the days assigned to IL Cluster 1. The algorithm clustered these days because the illuminance stays high between the morning and afternoon/evening hours. However, the clusters do not provide relevant information on arrival/departure times or occupant count. The clustering results for transformed `IL_N3` data reflected the same behavior. Another technique may be more suitable for extracting unambiguous information from such data.

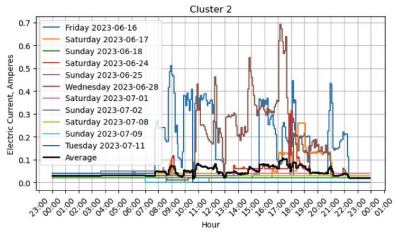

(a) Electric current cluster No.2

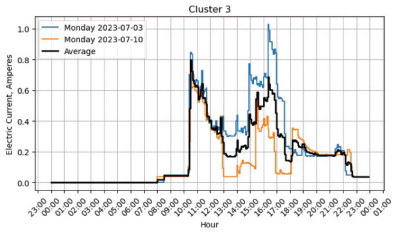

(b) Electric current cluster No.3

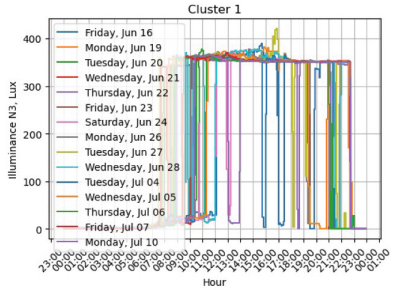

(c) Illuminance cluster No.1

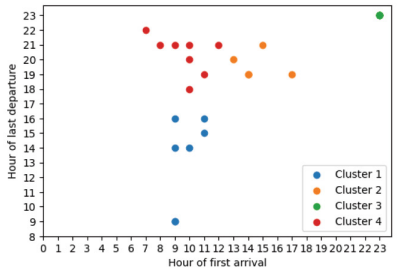

(d) Transformed PIR sensor data clusters

Fig. 3. Results from the k-means clustering analysis.

Figure 3d presents the clustering results of transformed PIR sensor data. Because of the location of this sensor (above the only door), this sensor is the most informative about arrival and departure times. The clusters are interpreted as follows: Cluster 1 represents morning arrival (between 8:00 a.m. and 12:00 p.m.) and afternoon departure (between 2:00 p.m. and 5:00 p.m.); Cluster 2

represents afternoon arrival (between 12:00 p.m. and 6:00 p.m.), and nightly departure (between 7:00 p.m. and 10:00 p.m.); Cluster 3 represents weekends (no arrival or departure); finally, Cluster 4 represents morning arrival (between 7:00 a.m. and 12:00 p.m.) and nightly departure (between 6:00 p.m. and 11:00 p.m.).

The EC clustering results show potential for estimating both occupancy state and count, also encountered by [11,12]. However, EC clusters are unreliable for determining the arrival/departure times of occupants at the office since it is possible that an occupant arrives but does not immediately connect equipment to the main power strip. On the other hand, the clustering results from the N1 PIR sensor data brought forth information about occupants' arrival/departure times.

Other works [13] found light-level data most correlated with occupancy. However, this was not our case; we obtained weaker correlations, and the clustering results were not informative of occupant behavior. This could be explained by the occupants' habit of leaving the lights on even when leaving the office.

Finally, the clustering results have demonstrated the capabilities of sensor fusion to obtain more complete occupancy information. The ultimate goal of obtaining occupancy information is to incorporate it into HVAC control actions for energy-saving strategies. While the clustering results are promising for getting the information required to bring optimal actions in HVAC control, it is important to note that the office in question occupant profiles change every semester as the class schedules for the occupants change. This means that new occupancy schedules would need to be derived periodically, which is a limitation of the proposed method.

4 Conclusion

This work applied a k-means clustering algorithm to electric current, illuminance, and transformed PIR sensor data to obtain insights into occupancy schedules in a university office. While the experimental setup recorded multiple variables such as motion sensor data, temperature, humidity, CO2, door state, indoor AC unit state, electric current, and light intensity, correlation analysis revealed that only the last two were most correlated with occupancy count and state. The available observations, each corresponding to a different day, were grouped into four clusters, which resulted in four occupancy profiles. Electric current data revealed activity start/end times and occupancy levels throughout the day. Illuminance data clusters were not as informative and could not bring relevant information into occupants' arrival/departure times. However, the PIR sensor output clusters revealed four typical office arrival and departure schedules. The results obtained in this work are contextual, but the proposed method has the advantage of not using ground-truth data. Clustering analysis has only applied to the available dataset, which consists of 25 days. Further work includes applying clustering analysis to a larger dataset, preferably several months of data. Moreover, it would be interesting to apply other clustering techniques, such as DBSCAN, which are more equipped to deal with noisy data.

Acknowledgements. The authors extend their gratitude to the Research Group Energética y Confort en Edificaciones Bioclimáticas of the Faculty of Mechanical Engineering within the Universidad Tecnológica de Panamá. This publication is part of the project FID22-086 and FIED22-09, which has received funding from Secretaría Nacional de Ciencia, Tecnología e Innovación (SENACYT), together with the Sistema de Nacional de Investigación (SNI).

References

1. Buildings - Energy System. IEA. https://www.iea.org/energy-system/buildings
2. Yan, D., et al.: IEA EBC Annex 66: definition and simulation of occupant behavior in buildings. **156**, 258–270. https://linkinghub.elsevier.com/retrieve/pii/S0378778817318820
3. D'Oca, S., Hong, T.: Occupancy schedules learning process through a data mining framework. **88**, 395–408. https://linkinghub.elsevier.com/retrieve/pii/S0378778814010329
4. Saha, H., Florita, A.R., Henze, G.P., Sarkar, S.: Occupancy sensing in buildings: A review of data analytics approaches. **188–189**, 278–285. https://linkinghub.elsevier.com/retrieve/pii/S0378778818333176
5. Liang, X., Hong, T., Shen, G.Q.: Occupancy data analytics and prediction: a case study. **102**, 179–192. https://linkinghub.elsevier.com/retrieve/pii/S036013231630110X
6. Sharma, H., Bhattacharya, S. Kundu, S., Adetola, V.A.: On the impacts of occupancy sensing on advanced model predictive controls in commercial buildings. **222**, 109372. https://linkinghub.elsevier.com/retrieve/pii/S0360132322006059
7. Dong, B., Prakash, V., Feng, F., O'Neill, Z.:A review of smart building sensing system for better indoor environment control. **199**, 29–46. https://linkinghub.elsevier.com/retrieve/pii/S0378778819309302
8. Dai, X., Liu, J., Zhang, X.: A review of studies applying machine learning models to predict occupancy and window-opening behaviours in smart buildings. **223**, 110159. https://linkinghub.elsevier.com/retrieve/pii/S0378778820303017
9. Peng, Y., Rysanek, A., Nagy, Z., Schlüter, A.: Using machine learning techniques for occupancy-prediction-based cooling control in office buildings. **211**, 1343–1358. https://linkinghub.elsevier.com/retrieve/pii/S0306261917317129
10. Géron, A.: Hands-On Machine Learning with Scikit-Learn, Keras, and TensorFlow
11. Mora, D., Fajilla, G., Austin, M.C., M. De Simone, M.: Occupancy patterns obtained by heuristic approaches: cluster analysis and logical flowcharts. A case study in a university office. **186**, 147–168. https://linkinghub.elsevier.com/retrieve/pii/S0378778818317250
12. Zhan, S., Chong, A.: Building occupancy and energy consumption: case studies across building types. **2**(2), 167–174. https://linkinghub.elsevier.com/retrieve/pii/S2666123320300829
13. Sayed, A.N., Bensaali, F., Himeur, Y., Houchati, M.: Edge-based real-time occupancy detection system through a non-intrusive sensing system. **16**(5), 2388. https://www.mdpi.com/1996-1073/16/5/2388

A Wireless Tree Climbing Robot: REDA-Design and Implementation

Rafaela Villalpando-Hernandez(✉), Cesar Vargas-Rosales, Rene Diaz-M., J. Jorge Nuñez Gonzalez, Francisco Ruvalcaba Galindo, and Isai Fritshe Barajas

Tecnologico de Monterrey, Monterrey, Mexico
{rafaela.villalpando,cvargas,renejdm}@tec.mx, {A01231630, A07124237}@itesm.mx

Abstract. In this paper, we propose a low cost, low power consumption tree climbing robot for multipurpose applications, such as surveillance or inspection tasks. This type of collaborative robot is able to support or assist in order to avoid risks and dangers. The robot has been constructed with minimal resources and is equipped with two pair of tree grippers that facilitate the robot to adhere and climb regular shaped trees without any branches. REDA has only with five actuators that were used in the mechanism. In consequence, it maintains a compact size and lightweight. REDA weighs only 800 g, it has payload capability of 1 kg. In this paper, we present the design, analysis and implementation of a low cost tree climbing robot.

1 Introduction

In recent years, climbing robots have been the focus of attention of researchers and students for monitoring, service missions and rescue applications. Nowadays, we can find robots capable of climbing almost any surface or structure, using different materials as fastening mechanisms, [1]. Typically, research in this area focuses on climbing man-made structures, such as vertical walls and glass windows on buildings [1, 2]. In order, to scale flat surfaces, most robots use suction cups, adhesive materials, magnetic forces (electromagnets), different types of spines, either elastomeric plastics or metal guides [3–6]. However, tree surfaces present different characteristics, as they are un-even, un-predictive and hazardous. Therefore, there is a necessity to carry out a deep research, on robot designs to climb structures of natural origin such as trees.

Throughout history, there have been many human accidents or deaths due to accidents at high altitudes scenarios in rescue, monitoring, exploratory and military applications. As an example for the operators, to reach the upper parts of a pole tree represents a high risk. Also, in telecommunications, electrical networks and other occupations, people must climb structures or tree poles to complete their jobs. Most pole trees in urban areas require regular maintenance. Thus, the development of a tree-climbing robot could assist or replace operators in their work.

Several robots have been designed to climb pole trees. RiSE V3 [7], is a robot designed to climb straight trees at high speed. However, most trees present a curved

M. N. Cardona et al. (Eds.): LACAR 2023, LNNS 940, pp. 145–153, 2024.
https://doi.org/10.1007/978-3-031-54763-8_15

structure and have irregular branches, which strongly restricts the application of this robot. Treebot [8], is another robot designed to climb trees. This type of robot has high maneuverability and a pair of omni-directional tree grippers. It enables the robot to attach on large trunks and small branches. Other authors have proposed different tree climbing robot designs [9], with different characteristics and capabilities, however, new low cost and low complexity design proposals are needed to full fill new and existing applications.

In this paper, the complete design of the REDA is shown in Fig. 1. The structure consists in four double legs and a linear actuator. The linear actuator is attached to one of the structural legs and ends in the other structural legs. The legs adhere to the tree with sharpened nails, letting the robot to have always a pair of structural legs in the tree while the linear actuator moves up or down the other structural legs.

In Sect. 2, the proposed REDA mechanical design is discussed. Section 3 introduces locomotion system. In Sect. 4, the kinematic analysis is presented. Finally, conclusions and future work are discussed in Sect. 5.

2 Mechanical Design

In this section the design and implementation of the proposed tree climbing robot is presented (Fig. 1).

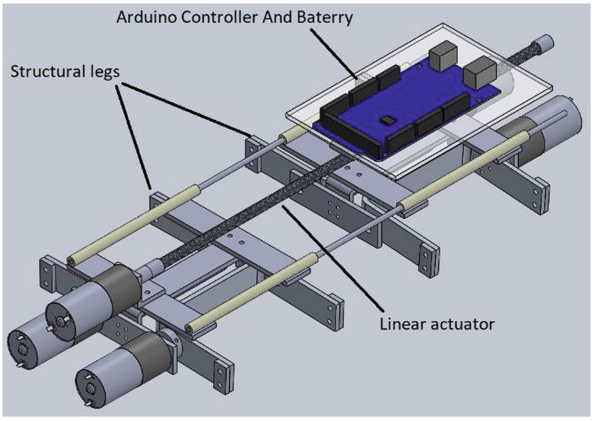

Fig. 1. Mechanical design of REDA

2.1 Structural Legs

In the proposed design, we consider four direct current (DC) motors that move a double leg each, see specifications in Table 1. This provides sufficient grip to each leg letting the robot stay in one structural leg at the time to move upward the tree. The legs are made from an aluminum sheet in "U" shape attached to the motor see Fig. 2, providing

a circular movement. At the end of the legs, a sharpened nail allows the leg to insert in the tree. The movement made by the legs is shown in Fig. 2. Each structure has two pairs of legs, the robot's bottom one has another DC motor (Table 1) that moves the worm to produce the linear movement. In the upper part of the robot the microcontroller (Arduino), the motor drivers and the batteries are installed.

Table 1. Drivers and devices specifications

	Voltage (V)	Current (A)	RPM
Linear actuator	6–12	0.4–0.6	100
DC motor	6–12	0.6–0.8	220
Arduino	3.5	20	–
Bluetooth HC-05	3.3	35	–

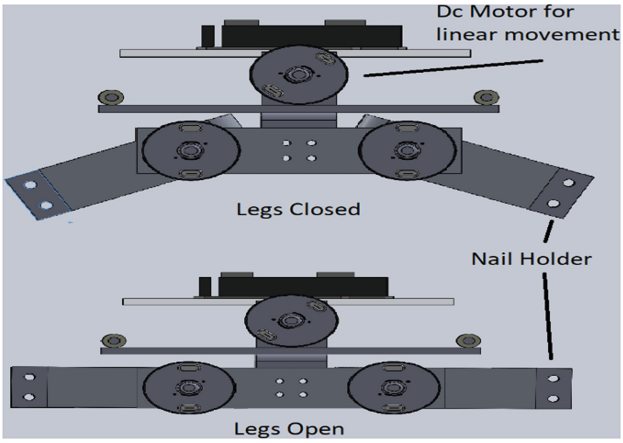

Fig. 2. Motion system

2.2 Linear Actuator

The linear movement is provided by a DC linear actuator (Table 1), placed at the bottom structural leg this DC motor is faster than the other four motors allowing a faster linear movement. The DC motor has a coupler that attaches to a 15-inch worm. In the other structural leg, a nut is placed in the upper part letting the worm to pass through it. As the motor moves the worm to any of the two sides, the nut moves the other structural leg upward or downward. The two structural legs, are connected by an aluminum rod, that moves through a motion guide that provides stability to the robot motion is shown in Fig. 3.

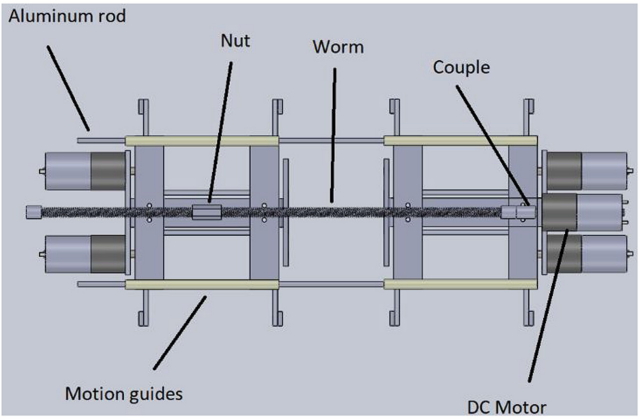

Fig. 3. Linear movement structure.

3 Robot Locomotion

The movement of REDA is inspired in the worm movement. Figure 4, shows a simple illustration of a complete climbing gait of the locomotion. It is composed of six climbing steps. The solid square presents the closed gripper that attached on the substrate while the empty square represents the opened gripper. The order of motion in the figure represents the translation for the forward movement. The locomotion of moving backward is just in reverse order.

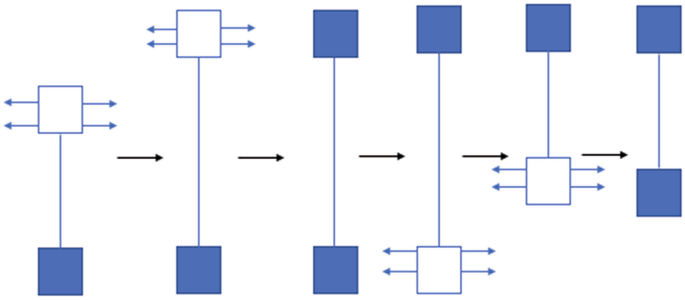

Fig. 4. A complete climbing translation of REDA.

4 Robot Kinematics

For the mathematical characterization of the proposed tree-climbing robot, three analysis were implemented as follows, forward kinematics, inverse kinematics and jacobians, [10].

4.1 Forward Kinematics

Forward kinematics analysis provides information about location of the end frame, when variables of the robot changes. Five frames are needed to perform this analysis. Figure 5, shows the frames, and with the Denavith Hartenberg [10] parameters in Table 2 were obtained. This table basically shows the geometric parameters of the robot.

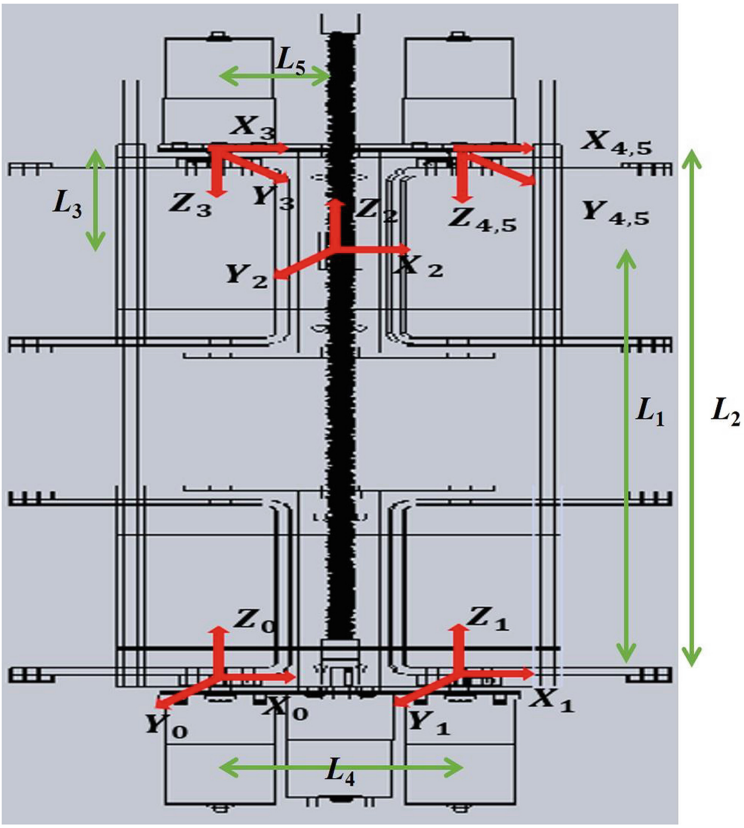

Fig. 5. *Y* frames of the robot.

Where, frame lengths L_1, L_2, L_3, L_4, L_5 are associated with the robot geometry and can be seen in the Fig. 5. With the parameters of Table 2 the final rotation matrix is given by the following equation. Please note that the rotation transformation matrix is respect to the z axis.

$$R_5^0 = \begin{bmatrix} A_1 & A_2 & 0 & A_3 \\ A_4 & A_4 & 0 & A_5 \\ 0 & 0 & -1 & L_3 + L_1 \\ 0 & 0 & 0 & 1 \end{bmatrix}, \tag{1}$$

Table 2. Denavith Hatenberg parameters

Joint	Θ	d	A	α
1	θ_1	0	L_4	0
2	θ_2	L_1	L_5	0
3	0	L_3	L_5	$\pi/2$
4	θ_3	0	L_4	0
5	0	0	0	0

where

$$
\begin{aligned}
A_1 &= \cos\theta_3(\cos\theta_1\cos\theta_2 - \sin\theta_1\sin\theta_2) + \sin\theta_3(\cos\theta_1\sin\theta_2 + \sin\theta_1\cos\theta_2),\\
A_2 &= \sin\theta_3(\sin\theta_1\sin\theta_2 - \cos\theta_1\cos\theta_2) + \cos\theta_2(\cos\theta_1\sin\theta_2 + \sin\theta_1\cos\theta_2),\\
A_3 &= (L_4\cos\theta_3 + 2L_5)(\cos\theta_1\cos\theta_2 - \sin\theta_1\sin\theta_2)\\
&\quad + L_4\sin\theta_3(\cos\theta_1\sin\theta_2 + \sin\theta_1\cos\theta_2) + L_4\cos\theta_1\ ,\\
A_4 &= \cos\theta_3(\sin\theta_1\cos\theta_2 + \cos\theta_1\sin\theta_2) + \sin\theta_3(\sin\theta_1\sin\theta_2 + \cos\theta_1\cos\theta_2),\\
A_5 &= (L_4\cos\theta_3 + 2L_5)(\sin\theta_1\cos\theta_2 + \cos\theta_1\sin\theta_2)\\
&\quad + L_4\sin\theta_3(\sin\theta_1\sin\theta_2 - \cos\theta_1\cos\theta_2) + L_4\sin\theta_1\ .
\end{aligned}
$$

Please recall that in the Denavit Hartenberg method the homogenous transformation matrix A represent the translation.

4.2 Inverse Kinematics

In this sub-section inverse kinematics of the proposed climbing robot is presented. In Fig. 6 we illustrate the lateral view of the robot's legs structure, where some parameters associated with the inverse kinematic analysis are shown.

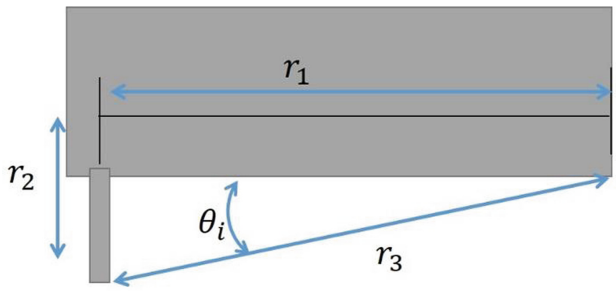

Fig. 6. Diagram of leg structure. Lateral view.

The inverse kinematics is given by the next equation:

$$\theta_i = tan^{-1}\left(\frac{r_2}{r_1}\right), \tag{2}$$

where θ_i is the angle in all the legs of the robot and r_1, r_2 can be seen in Fig. 6.

4.3 Jacobian Analysis

With the parameters presented above in Table 2, the translation matrices were obtained in order to find the Jacobian matrix. Recall that the Jacobian analysis allows to calculate the linear and the angular. These parameters can be used for further control velocity.

$$\begin{bmatrix} J_v \\ J_w \end{bmatrix} = \begin{bmatrix} -A_5 & -B_1 & 0 & B_2 & 0 \\ A_3 & B_3 & 0 & -B_4 & 0 \\ 0 & 0 & 1 & 0 & 0 \\ 0 & 0 & 0 & 0 & 0 \\ 0 & 0 & 0 & 0 & 0 \\ 1 & 1 & 0 & -1 & -1 \end{bmatrix}, \tag{3}$$

where,

$$\begin{aligned} B_1 =& (L_4 \cos\theta_3 + 2L_5)(\sin\theta_1 \cos\theta_2 + \cos\theta_1 \sin\theta_2) \\ &+ L_4 \sin\theta_3(\sin\theta_1 \sin\theta_2 - \cos\theta_1 \cos\theta_2), \\ B_2 =& L_4 \cos\theta_3(\sin\theta_1 \cos\theta_2 + \cos\theta_1 \sin\theta_2) + L_4 \sin\theta_3(\sin\theta_1 \sin\theta_2 + \cos\theta_1 \cos\theta_2), \\ B_3 =& (L_4 \cos\theta_3 + 2L_5)(\cos\theta_1 \cos\theta_2 + \sin\theta_1 \sin\theta_2) \\ &+ L_4 \sin\theta_3(\cos\theta_1 \sin\theta_2 + \sin\theta_1 \cos\theta_2), \\ B_4 =& L_4 \cos\theta_3(\cos\theta_1 \cos\theta_2 - \sin\theta_1 \sin\theta_2) + L_4 \sin\theta_3(\cos\theta_1 \sin\theta_2 + \sin\theta_1 \cos\theta_2). \end{aligned}$$

Finally in Fig. 7 and Fig. 8, we can observe the final implementation and operation respectively of the proposed tree climbing robot.

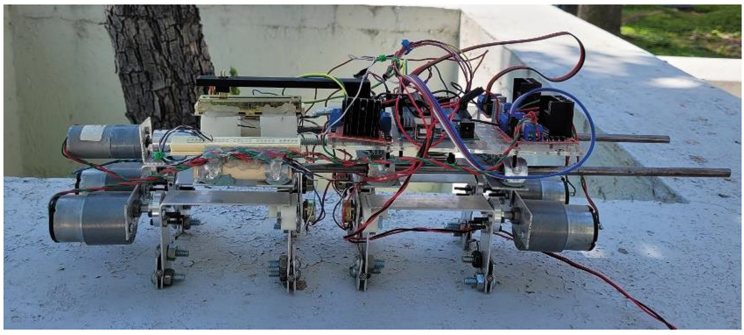

Fig. 7. Tree climbing robot final prototype.

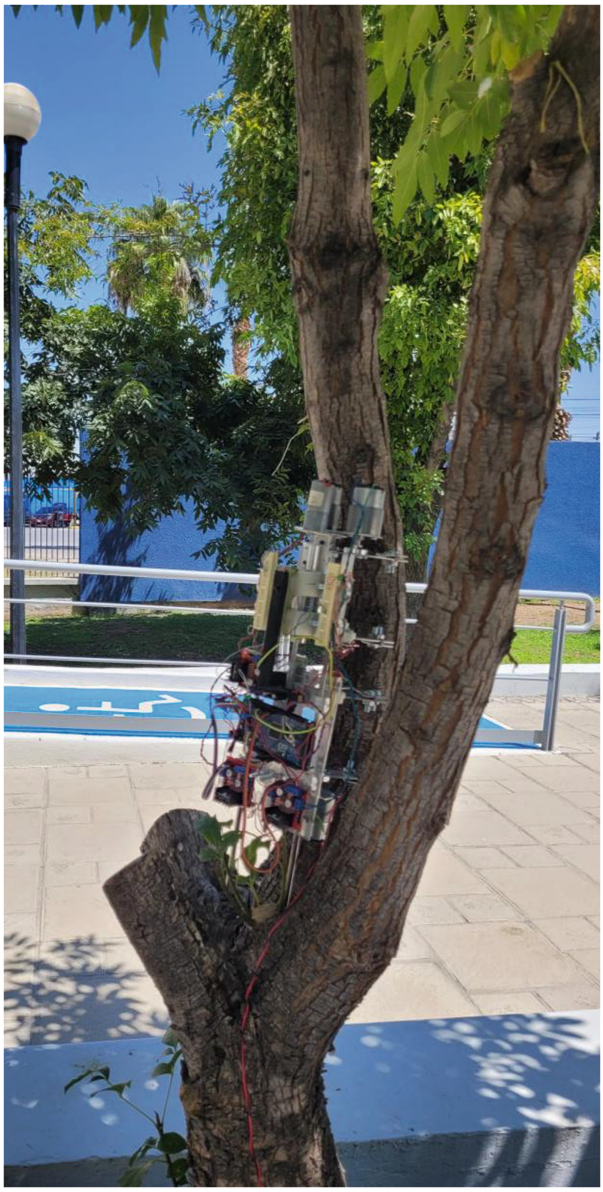

Fig. 8. Tree climbing robot operation.

5 Conclusions

As a conclusion, in this paper we present the mechanical design and mathematical analysis of a tree climbing robot. The REDA represents a low cost and low complexity design for climb trees with a diameter smaller than the total length of its legs. This

design provides fast movements in order to complete the task. As a future work, some improvements can be made for better performance.

- Better claws that provide more grip when climbing.
- An adjustable length of the legs to climb trees with different diameters.
- More torque in the leg motors to have more force to press the claws to the tree.
- An extra DOF to help climb trees with irregular form, not only straight trees.

References

1. Nansai, S., Mohan, R.E.: A survey of wall climbing robots: recent advances and challenges. Robotics **5**(3), 14 (2016)
2. Zhang, H., Zhang, J., Zong, G., Wang, W., Liu, R.: Sky cleaner 3: a real pneumatic climbing robot for glass-wall cleaning. Robot. Autom. Mag. IEEE **13**, 32–41 (2006)
3. Zhang, H., Zhang, J., Zong, G.: Effective nonlinear control algorithms for a series of pneumatic climbing robots. In: Proceedings of the 2006 IEEE International Conference on Robotics and Biomimetics, ROBIO 2006, Pisa, Italy, 20–22 February 2006, pp. 994–999 (2006)
4. Zhang, H., Zhang, J., Liu, R., Zong, G.: A novel approach to pneumatic position servo control of a glass wall cleaning robot. In: Proceedings of the 2004 IEEE/RSJ International Conference on Intelligent Robots and Systems (IROS 2004), Sendai, Japan, 28 September–2 October 2004, vol. 1, pp. 467–472 (2004)
5. Tokhi, O., Zhang, H., Zhang, J., Wang, W., Liu, R., Zong, G.: A series of pneumatic glass-wall cleaning robots for high-rise buildings. Ind. Robot Int. J. **34**, 150–160 (2007)
6. Wang, W., Wang, K., Zong, G.H., Li, D.Z.: Principle and experiment of vibrating suction method for wall-climbing robot. Vacuum **85**, 107–112 (2010)
7. Haynes, G.: Rapid pole climbing with a quadrupedal robot. In: IEEE International Conference on Robotics and Automation, Kobe, Japan, 12–17 May 2009
8. Tin, L.L., Yangsheng, X.: A flexible tree climbing robot: treebot design and implementation. In: IEEE International Conference on Robotics and Automation, 9–13 May 2011, Shanghai, China (2011)
9. Fang, G., Cheng, J.: Advances in climbing robots for vertical structures in the past decade: a review. Biometrics MDPI J. **8**(1), 47 (2023)
10. Craig, J.: Robotics, 3rd edn. Pearson, London (2006)

A Multi-object Detection for Classification System Using Machine Learning and Robotic Manipulator

F. Pilco-Villa Jonathan[1], P. Romero-Riera Paul[1,2], L. Hernández-Ambato Jorge[1], and F. Isa-Jara Ramiro[1,3(✉)]

[1] Escuela Superior Politécnica de Chimborazo - ESPOCH, Riobamba, Ecuador
{francisco.pilco,p_romero,jhernandez,ramiro.isa}@espoch.edu.ec
[2] University of Calabria - UNICAL, Rende, Italy
[3] CONICET - UTN National Technological University, Buenos Aires, Argentina

Abstract. In recent years, industrial automation has made it possible to improve the quality of control systems of mobile robotics to reduce time and increase accuracy in applications such as object detection for product classification. In this work, a multi-object detection for classification and packing system has been developed using image processing, machine learning, and a robotic arm model KUKA KR10. Objects are detected using an adaptive threshold binarization and morphological operations to smooth and fill regions. Machine learning algorithms have been trained and evaluated using Neural Networks and Random Forest using color in RGB space as a feature to classify objects. Finally, objects are moved from the current to the assigned position through the robotic arm. The robot movements are executed by RoboDK and Python with a controller using a local area network and the trajectories are calculated using inverse kinematics. For tests, a controlled environment with 9 objects with cube shapes of different colors has been used to detect colors and classify those of blue and red only. The results show the vision system has an accuracy of 94.50% in color detection. The time that the robotic arm takes to classify all the objects is on average 116.65 sec. at 10% of its maximum speed. Future work focuses on object detection in industrial environments using a conveyor belt and other object features to classify such as shape or size.

1 Introduction

Currently, the industrial sector is made up of technologies such as industrial robotics and artificial vision systems that allow the efficient development of its production lines. The importance of artificial vision systems lies in the recognition of a scene to process it and make decisions. Therefore, it is possible to provide a certain degree of intelligence to the technological devices for the automation processes. Much of modern industry contains several stages, including handling, inspection, sorting, welding, and assembly of parts and materials

M. N. Cardona et al. (Eds.): LACAR 2023, LNNS 940, pp. 154–164, 2024.
https://doi.org/10.1007/978-3-031-54763-8_16

where several of them are repetitive and carried out manually, which require time and effort [24]. Robotics and artificial vision systems are promising technologies due to their application in the industry would allow an increase in quality, production, and the ability to customize on a large scale. Moreover, these integrated technology systems open the way to new tasks such as quality control and the construction of safer scenarios [26].

In [1], a multi-stage process of the development of a vision-based object-sorting robot manipulator is presented. The main aim of this research was to integrate the vision system with the existing Scorbot with MatLab and Visual Basics to widen the capability of the integrated camera-robot system in industrial applications. In [9], a vision-based system for the advanced recognition of dangerous situations for safety control is presented. The main aim of this research is the stereo vision from two cameras located above the robot to detect a new object appearing in a dangerous zone, near the robot arm. In [8], a novel algorithm combining object detection and potential field algorithm for the autonomous operation of the SCARA arm is presented. The main aim of this research is the obstacles, and goal states that are located and detected through the RetinaNet Model for planning a suitable path.

In [3], a methodology to improve the application of industrial robots within food manufacturing is presented. The main aim of this research is to use the Food Industrial Robot Methodology (FIRM) to define, classify, and identify their foodstuff and automation solution. In [23], an approach for packing activity by a mobile robot to pick up items from shelves and then pack items in boxes is presented. The main aim of this research is to use efficient bin packing optimization algorithms (2D, 3D) of Optim Suite of KLS OPTIM.

The main contribution of this work is to design a computer vision system using a Gabor filter and morphological operations for multi-object detection and a Supervised Machine Learning model using a neural network to classify objects by color feature and compare them with results from the Random Forest algorithm. The database used to train ML algorithms contains 5052 data with RBG values referred to 11 different colors (classes) [5]. The model obtained is applied to frames from a webcam in real-time to predict the color object and classify it using the KUKA robotic arm.

This paper is organized as follows: Section 2 shows a brief description of image processing, machine learning algorithms and the KUKA robotic arm. Section 3 shows the proposed methodology. In the first part, the image processing techniques are applied to segment objects from an individual frame. In the second part, the machine learning algorithms are described with the neural network design and random forest classifiers to predict the color of objects. Section 4 shows the experimental results and finally, Sect. 5 shows the discussion about results, conclusions, and future work.

2 Referential Framework

2.1 Computer Vision System

Computer vision allows a computer to process and interpret images or videos by extracting features associated with objects [2]. Image processing is summarized in the following steps: ***1) Image acquisition:*** This consists of capturing the scene using a camera. Due to their low cost and easy installation, webcams are generally used in computer vision projects [2]. However, lighting is a relevant factor to capture a correct scene. According to [15], there are several lighting models for vision applications; ***2) Preprocessing:*** This applies various techniques to improve the details of the objects in the images using the conversion to different color spaces such as HSV or RGB and the filtering to smoothing interest regions [16]. Among the most used filters are median, Gaussian and Gabor [19,27]; ***3) Segmentation:*** Allows to identify regions of interest in an image. Segmentation for a captured image can be based on transitions, by growing regions, and by establishing thresholds in which comparisons of the pixels of interest are made with a reference known as the threshold [10]; ***4) Feature extraction:*** Allows to detect features of an object of interest such as lines, circles, edges, colors, or patterns. Edge detection is the most common task in artificial vision systems because through them, the position, color, and other characteristics of a given object can be determined [25]. They are control systems to use in the integration of computer vision systems with industrial manipulators.

2.2 Machine Learning (ML)

Machine learning is a subset of artificial intelligence that develops dynamic algorithms capable of data-driven decisions. For image classification, ML has a robust benchmark of algorithms focused on three paradigms Supervised, Unsupervised, and Reinforcement Learning. Several classical supervised ML algorithms along with deep learning methods and transfer learning have significantly improved their performance to generate innovative applications in different areas [12]. Supervised Learning includes regression and classification processes. For classification, Artificial Neuronal Networks and Convolutional Networks [13,17], Support Vector Machines, and Random Forests [4] are methods applied to data and images with high performance and accuracy.

2.3 Visual Control

These control systems are used in the integration of artificial vision systems with industrial manipulators. Visual control uses an image as a feedback parameter in the development of a process [21]. The feedback information is expressed by coordinates in a two-dimensional image [22]. A visual control system works from two models of camera placement. These models are Eye in-hand and Eye to hand [7].

2.4 Industrial Robotic Arm KUKA KR10 R900 Sixx

It is a multipurpose industrial manipulator robot with 6 degrees of freedom capable of handling net loads of up to 10 Kg. It is a very versatile robot used for applications such as assembly, palletizing, painting, welding, and sorting of parts and objects [14]. The robotic arm is programmed based on 3 types of paths point-to-point, linear, and circular. To do this, users can use the Smart PAD or a computer through languages such as Python or C++, as well as its proprietary language KUKA Robot Language (KRL) [6].

3 Proposed Methodology

3.1 Methodology Design

In this work, a computer vision system is proposed to classify objects using color features. Objects have different colors and a measure of 0.05×0.05 m with a cube shape. The camera is placed according to the eye-to-hand model. The ML paradigm is based on Supervised Learning. This has been trained and tested with the database that contains 5052 data described in 4 columns: R, G, B, and Label [5]. The label describes the colors related to RGB values for 11 different colors: black, blue, brown, green, gray, orange, pink, purple, red, white, and yellow. The obtained ML model has been evaluated in the real-time process using new frames to detect multi-objects with their respective colors and to move those with blue and red colors to a specific place assigned previously using a KUKA robotic arm.

3.2 Workspace Design

A controlled space has been designed with a template based on a 3×3 matrix with the spaces corresponding to the positions where the objects will be located. It also contains two sections on the left and right, where objects are placed according to their color. In Fig. 1, the workspace is presented where the measures are described in meters.

Moreover, the work environment in the RoboDK software has been designed to have a monitoring environment for all the tasks and movements carried out by the manipulator to obtain a system with greater security. Figure 2 shows the workspace programmed using the software.

3.3 Conexion with the Manipulator

The connection between the vision system and the physical manipulator is done using the RoboDK. This software allows the online or offline programming of several robot models. The Kukavarproxy toolset enables the connection. This controller is an interface to works with the TCP/IP protocol in the communication port 7000 as a server and in a point-to-point ethernet connection between the robot and the computer as a client.

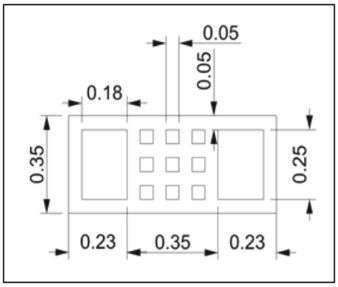

Fig. 1. The workspace template for objects with specific positions.

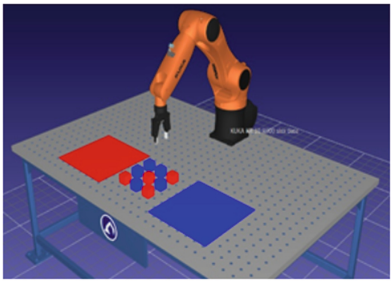

Fig. 2. RoboDK is used to program a virtual workspace.

3.4 Computer Vision Algorithm

The image is taken using a webcam of Coolshark with a resolution of 1080p and 30 frames per second. The workspace is displayed with objects of different colors located randomly on the template for the classification process. The general process is presented in Fig. 3.

To reduce the changes in contrast, the CLAHE [18] preprocessing process is used. A Gaussian-type filter is also applied to minimize the noise in the original image. Following to [11], the Gabor filter is used to enhance the borders of regions of interest in images. Then, the adaptive thresholding technique is applied to binarize the image where the morphological operations such as diltate and erosion are applied to homogenize regions of the object detected. The extraction of color features is performed by each object to obtain the mean of each channel in RGB space. Finally, the color features are evaluated by an ML model previously trained to predict the object color.

3.5 Machine Learning Algorithms

The neuronal network architecture is presented in Fig. 4 which is obtained using the Playground_Tensorflow toolbox. The input layer has 3 neurons for each RGB value. Moreover, 5 hidden layers have been defined to give more effectiveness to the process. The output layer has 11 neurons to classify in 11 different colors or

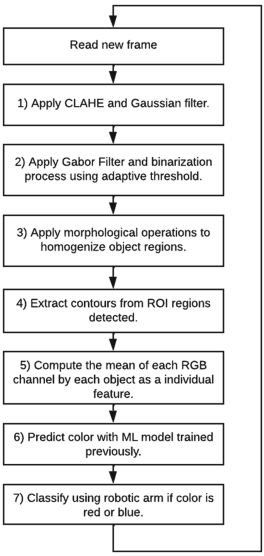

Fig. 3. Flowchart of the proposed algorithm to detect and classify objects.

classes according to the database. The activation function is RELU, the optimizer is RMSPROP, and the metrics are CATHEGORICAL_CROSSENTROPY and ACCURACY to evaluate the performance of the model. The train set contains 80% and the test set 10% of the dataset. The number of epochs is 2000 and the batch size is 1024. The Random Forest algorithm has been defined with 250 predictors and to train and test sets have the same dimensions defined previously. To evaluate the accuracy of classification in the two cases, the metrics used are Confusion matrix, PRECISION, RECALL, and F1-SCORE.

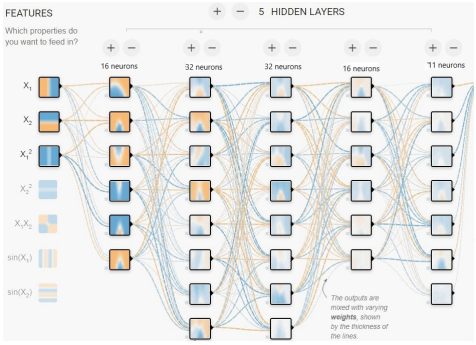

Fig. 4. Neuronal Network architecture with 3 inputs and 11 outputs for categorical classification.

3.6 Robot Movement Programming

The webcam is the input and the robot manipulator is the actuator for the control system which is designed in a closed loop where the feedback is performed by the artificial vision process. In Fig. 5, the description of the system is presented.

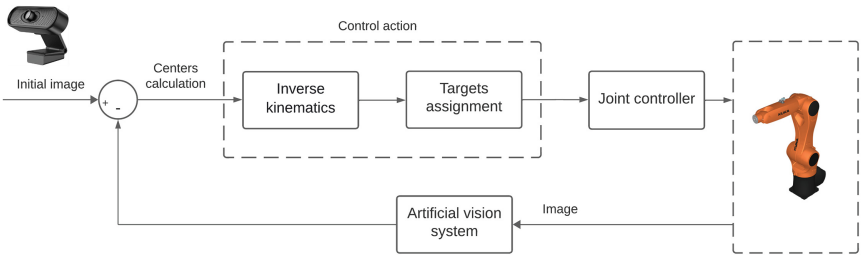

Fig. 5. The control system used to detect and classify objects.

The robot has been programmed using the position of the detected objects to perform the trajectories. Therefore, RoboDK allows the creation of targets at desired positions in a virtual scenario built into the software. The targets are created to carry out the process of classifying the objects placed in the workspace. These targets are defined in Table 1.

Table 1. Motion Targets definition

Targets	Description
Pick	Targets in the array positions when the gripper attaches the object
Approx	Targets in the array positions before attaching the object
Red	Aim at the target position for red objects
Blue	Aim at the target position for blue objects
Home	Waiting position before approaching to each position in the array

4 Results

Implementation of the methodology and program developed including results are available in [20]. The mean scores achieved by algorithms using the dataset to train and test models to classify colors using RGB values are presented in Table 2.

Table 2. Mean scores of ML algorithms

Algorithm	Set and samples	Precision	Recall	F1-score
Neuronal Network (ANN)	Train: 4547	89%	86%	87%
Neuronal Network (ANN)	Train: 505	87%	83%	84%
Random Forest (RF)	Train: 4547	100%	100%	100%
Random Forest (RF)	Train: 505	80%	73%	73%

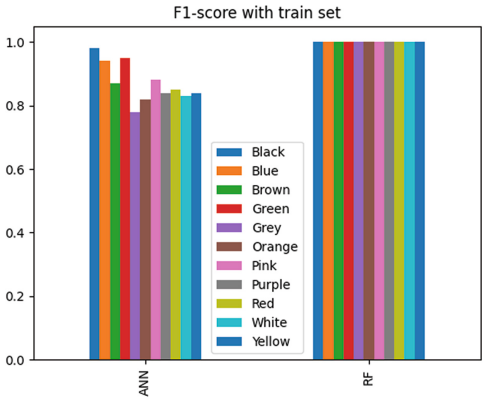

Fig. 6. F1-score during to training by each color of the database.

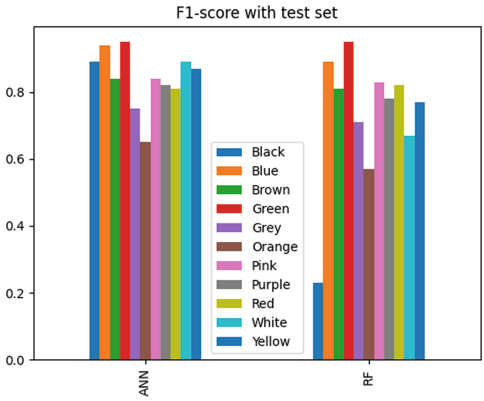

Fig. 7. F1-score during for testing by each color of the database.

4.1 Color Detection

In order to compare the performance of ANN in front of RF, Fig. 6 and Fig. 7 present the F1-score metric during to training and testing of the model.

To evaluate the performance of the detection system focused on blue and red colors using ANN to move with the robotic arm, 81 samples divided into 9 frames have been taken. Each frame has been taken every 30 s with changes in the scenery related to the objects on the template. This is detailed in Table 3.

Table 3. Color detection for classification with robotic arm

Color	Samples	Success	Failures	Precision	F1-score
Red	37	37	0	100%	100%
Blue	32	32	0	100%	100%
Others	21	19	2	90%	89%

Once the object and its color are detected, the center of its position is computed and the trajectory is automatically carried out using inverse kinematics. In order to evaluate the time to pick up the objects, the speed in the robot's automatic operation has been set at 10% of the maximum value to avoid unnecessary risk or damage. Therefore, two tests have been carried out, the first in a scenario with 5 red and 4 blue objects, while the second in a scenario with 5 blue and 4 red objects to evaluate the time used in seconds with different levels of velocity of the robotic arm. These results are shown in Table 4.

Table 4. Time used by robotic manipulator to move objects

Test	Velocity	Time Red Objects	Time Blue Objects	Total Time (sec)
1	5%	122.83	94.98	217.81
	10%	62.51	54.38	116.89
	30%	26.63	20.75	47.38
	50%	18.90	15.11	34.01
2	5%	98.20	120.48	218.68
	10%	53.75	60.65	114.4
	30%	21.61	24.70	46.32
	50%	14.24	18.66	32.90

5 Discusion and Conclusions

An object classification system has been implemented using Computer Vision, Machine Learning and a robotic manipulator. RoboDK allows the establishment

of a connection between the software system, for color feature detection, and the hardware system, for controlling the movement of the robotic arm using a standard ethernet connection through port 7000 under the TCP/IP protocol. The database contains 5052 data with 11 different colors related to RGB values. Although the RGB space is commonly used in image processing, the HSV space could also be used to obtain greater robustness in color definition. Two algorithms of ML have been used to compare the performance to classify objects based on color features presented in Fig. 5 and Fig. 6. The Artificial Neuronal Network during the training for classifying 11 colors achieves a mean F1-score of 87.10% in front of Random Forest with a 100%. During the testing algorithms, the artificial neuronal network achieves a mean F1-score of 84.10% in front of Random Forest with 73%. Therefore, ANN presents better performance than RF in 13.10% with unknown data. During the analysis in real-time with samples for red and blue colors, there is a recognition of 100% of the objects. However, when the system has to discriminate between objects with other colors in the template, the recognition percentage is 89%. This can be due to changes in ambient lighting. Therefore, establishing an average of the color detection percentages, a recognition of 94.50% is obtained for the computer vision system. Considering that the speed of the robot in automatic mode is defined at 10% of its capacity, the spent time depends on the position in the matrix, since, for particular objects, the trajectory carried out by the robot turns out to be longer than for others. From the analysis carried out, the average time is 115.65 s for the classification of all the objects in the workspace with a 10% of robotic arm velocity which according to tests is the safest for classifying objects. Future work is focused on object detection in industrial environments using a conveyor belt and other object features such as shape or size to classify. Furthermore, the proposed system also could be used in quality control systems.

References

1. Ali, M.H., Aizat, K., Yerkhan, K., Zhandos, T., Anuar, O.: Vision-based robot manipulator for industrial applications. Procedia Comput. Sci. **133**, 205–212 (2018)
2. Alvear-Puertas, V., Rosero-Montalvo, P., Peluffo-Ordóñez, D., Pijal-Rojas, J.: Internet de las Cosas y Visión Artificial, Funcionamiento y Aplicaciones: Revisión de Literatura. Enfoque UTE **1**, 244–256 (2017)
3. Bader, F., Rahimifard, S.: A methodology for the selection of industrial robots in food handling. Innovative Food Sci. Emerg. Technol. **64**, 102379 (2020)
4. Bharadwaj, A., Minz, S.: Hybrid approach for classification using support vector machine and decision tree. In: Proceedings of the International Conference on Advances in Electronics, Electrical and Computer Science Engineering - EEC, pp. 337–341 (2012)
5. Chavan, A.: Building RGB color classifier: Part 1 (2020)
6. Colorado, R.M.: Cinemática Y Dinámica De Robots Manipuladores. Alfaomega (2016)
7. García, A.: Diseño de algoritmos de control visual basado en imagen y basado en posición para sistemas robotizados y validación mediante simulación y experimentación real. PhD thesis, Universidad Politécnica de Valencia (2017)

8. Gautam, Y., Prajapati, B., Dhakal, S., Pandeya, B., Prajapati, B.: Vision-based intelligent path planning for SCARA arm. Cogn. Robot. **1**, 168–181 (2021)
9. Grabowski, A., Kosiński, R., Dźwiarek, M.: Vision based safety system for human and robot arm detection. IFAC Proc. Volumes **42**, 68–72 (2009)
10. Huérfano, Y., et al.: Métodos de segmentación de imágenes cardiacas: Fundamentos y alcance. Revista Latinoamericana de Hipertensión, 10 (2015)
11. Isa-Jara, R., et al.: GEMA-an automatic segmentation method for real-time analysis of mammalian cell growth in microfluidic devices. J. Imaging **8**(10), 281 (2022)
12. Koulali, R., Zaidani, H., Zaim, M.: Image classification approach using machine learning and an industrial Hadoop based data pipeline. Big Data Res. **24**, 100184 (2021)
13. Krizhevsky, A., Krizhevsky, A., Sutskever, I., Hinton, G.E.: ImageNet classification with deep convolutional neural networks. In: Advances in Neural Information Processing Systems, vol. 25 (2012)
14. KUKA. KUKA.Sim: software de simulación — KUKA AG
15. Kumar, V., Sudheesh Kumar, C.P.: Investigation of the influence of coloured illumination on surface texture features: a machine vision approach. Measurement **152**, 107297 (2020)
16. La Madrid Távara, E.: Implementación de un algoritmo de control de calidad para la selección de productos agrícolas utilizando visión artificial. PhD thesis, UNIVERSIDAD NACIONAL PEDRO RUIZ GALLO (2019)
17. López-Monroy, A.P., García-Salinas, J.S.: Neural networks and deep learning. Biosignal Processing and Classification Using Computational Learning and Intelligence: Principles, Algorithms, and Applications, pp. 177–196 (2022)
18. Maheshwari, S., Agarwal, A., Yadav, G.: Contrast limited adaptive histogram equalization based enhancement for real time video system. In: International Conference on Advances in Computing, Communications and Informatics, pp. 2392–2397 (2014)
19. Marcos, A.G., et al.: Técnica y Algoritmos Básicos de Visión Artificial. Number 23 (2006)
20. Pilco-Villa, J., Isa-Jara, R.: Multiobject detection - color classification (20230
21. Baeza, J.P.: Control visual 2D indirecto para el seguimiento intemporal de trayectorias y su aplicación a estrategias de control visual-fuerza en manipuladores. PhD thesis, Universidad de Alicante (2004)
22. Mariscal, I.P.: Control por realimentación visual de un brazo robot para tareas de agarre. PhD thesis, Universidad Politécnica de Valencia (2019)
23. Rhiat, A., Aggoun, A., Lachere, R.: Combining mobile robotics and packing for optimal deliveries. Procedia Manufact. **44**, 536–542 (2020)
24. Rosas-Arias, L., de Vallejo-Meraz, J.J., PÉrez-BailÓn, W., Rojas-Cid, J.D.: Robot clasificador de objetos de color utilizando técnicas de filtrado RGB. Revista de Prototipos Tecnológicos **3**(10), 50–59 (2017)
25. Serrano, J.F.V., Díaz, A.B.M., Calle, Á.S., Sánchez-Marín, J.L.E.: Visión por computador. Universidad Rey Juan Carlos, 2nd edition (2008)
26. Vélez, C., Orosco, F., Álvarez, M.A.: Control de los movimientos de un brazo robótico desde un computador utilizando software libre de control y comunicación inalámbrica con módulos X-BEE. ACI Avances en Ciencias e Ingenierías, **6**(2), C1–C8 (2014)
27. Wang, F.-P., Zhang, W.-C., Zhou, Z.-F., Zhu, L.: Corner detection using Gabor filter. IET Image Process. **8**, 639–646 (2014)

Trusting Delivery Drones Through Academic Experimentation

Pablo Rangel(✉) and José Baca

Texas A&M University - Corpus Christi, 6300 Ocean Drive, Unit 5797, Corpus Christi, TX 78414, USA
{pablo.rangel,jose.baca}@tamucc.edu

Abstract. Unmanned Aircraft Systems (UAS) have rapidly emerged as essential tools for various applications, including delivery services across all scales. However, their integration into our daily lives raises pressing safety concerns due to their potential to cause injury or property damage. Ensuring the safety of these cyber-physical systems is paramount, necessitating a robust evaluation of their capabilities through effective Test and Evaluation (T&E) processes. Existing T&E methodologies, developed for deterministic systems, fall short in addressing the inherent non-determinism of UAS operations. This study addresses the imperative of establishing new, rigorous yet adaptable T&E processes capable of effectively evaluating the safety aspects of UAS, even after their deployment in the market. This paper states initial hypothesis and present preliminary results towards a more comprehensive T&E implementation. More in-lab experiments and work has to be done. However, initial functional principles are introduced for the reader evaluation. By identifying safety-related failures in real-world scenarios, valuable lessons can be gleaned to inform the advancement of future UAS technology. Our research introduces a post-design T&E framework focused on uncovering safety-critical failures, thereby enhancing the level of autonomous drone safety. To build trust in the safety of UAS, we draw upon the Fundamentals of Software Testing and propose a hypothetical integration of Safety Integrity Levels (SILs), akin to the ISO 26262 automotive standard, into the UAS domain. This approach leverages a proven autonomy model to establish comprehensive safety guidelines tailored to delivery drones. Furthermore, we extend our investigation to include practical T&E methods in an academic laboratory setting, particularly for small drones. This exploration not only contributes to the broader research goals but also provides a tangible platform for testing and refining UAS safety strategies. In sum, our work strives to fortify the foundation of UAS safety assessment, fostering confidence in their secure integration into modern airspace.

1 Introduction

Drone-based delivery systems are poised to revolutionize various industries, offering efficiency gains, environmental benefits, and improved accessibility. However,

M. N. Cardona et al. (Eds.): LACAR 2023, LNNS 940, pp. 165–191, 2024.
https://doi.org/10.1007/978-3-031-54763-8_17

the acceptance and safe integration of these technologies into society remain complex challenges that require comprehensive evaluation and innovative solutions. In a recent study by Knutsson et al. [1], the case of Wing's drone delivery service demonstrates the potential of such systems, as evidenced by over 300,000 successful deliveries, including essential items during the COVID-19 pandemic. Despite these advancements, safety concerns, particularly regarding privacy, persist. Addressing these concerns, Wing's approach employs dedicated delivery drones devoid of recording capabilities.

Recognizing the transformative potential of drone delivery, regulatory bodies like the Federal Aviation Administration (FAA) are gradually authorizing beyond-line-of-sight operations for heavier unmanned aerial vehicles (UAVs) [2]. Leading companies, including Phoenix Air Unmanned, Wing, Zipline, UPS Flight Forward, and uAvionix, have demonstrated the viability of drone delivery services while upholding safety and privacy standards [1,2]. However, despite these advancements, academia plays a crucial role in unlocking the full potential of drone applications, particularly in ensuring safe autonomous operations.

In this context, the principle articulated by Koopman and Wagner [3] emphasizes the need to empirically demonstrate the safety of computer-based systems. This principle resonates profoundly in the realm of autonomous systems, where theoretical assurances must be substantiated through real-world testing. As drones transition from controlled environments to real-world scenarios, the challenge lies in assessing their capacity for safe autonomous decision-making without human intervention.

Our research aims to address this challenge by proposing a post-design Test & Evaluation (T&E) framework that centers on off-the-shelf systems. Preliminary work is been introduced to expose the reader into new principles of T&E. Leveraging an academic laboratory environment and the widely used Parrot Mambo mini drone, the study seek to extract actionable insights that can enhance the safety and reliability of future drone designs. The initial system under test (SUT) was the Parrot Mambo drone which has been slowly replaced by the Ryze Tello. The reason involves the phase out of the Mambo system by Parrot [4]. However, if a SUT stopped been manufactured the T&E principles should remain for new technologies. While autonomous systems pose complexities beyond the scope of traditional T&E methods [5–7], we focus on safety-related and safety-critical failures, recognizing the need for a targeted approach that aligns with the critical aspects of autonomous drone operations.

This paper is structured as follows: Sect. 2 defines the problem at hand, highlighting the need for improved testing methodologies. Section 3 underscores the original significance of the Parrot Mambo mini drone as our chosen System Under Test. In Sect. 4, we outline our proposed testing process tailored to small autonomous drones within academic settings. Section 5 demonstrates the implementation of our testing methodology through representative use cases. Section 6 presents the results of our hands-on laboratory testing with the two SUTs and their subsequent analysis. Finally, Sect. 7 concludes the paper by summarizing our findings and suggesting future directions for this research.

2 Problem Statement

The rapid proliferation of Unmanned Aircraft Systems (UAS) for commercial and recreational purposes has spurred innovation, yet the successful integration of autonomous drones into vital sectors like delivery remains a challenge. To propel drone technology into the mainstream, it is essential to establish reliable and standardized approaches for testing and evaluating UAS capabilities, particularly in terms of safe autonomy for drone delivery applications.

Presently, there is a conspicuous gap in effective testing methodologies that address the complexities of drone systems. While isolated instances of drone delivery operations have received approval from regulatory bodies like the Federal Aviation Administration (FAA), comprehensive solutions to restrict UAS from sensitive areas, along with rigorous methods to ensure the safety of autonomous operations, remain elusive. The need for practical testing and validation methods is evident, as current research perspectives on autonomous drone testing often overlook the larger industry and operational context. For instance, studies that focus solely on Sense and Avoid algorithms or elaborate frameworks may lack practicality or industry-wide applicability.

To bridge this gap, there is a compelling opportunity to draw inspiration from established industries, such as the automotive sector, which has made significant strides in ensuring safe autonomy through quantifiable measures. Automotive Safety Integrity Levels (ASIL) provide a structured framework to evaluate and categorize critical components in vehicles, which could be adapted to quantify safe autonomy in UAS. Additionally, the principles of software testing, as standardized by the International Software Testing Qualifications Board (ISTQB), offer a practical approach to assessing autonomous systems' reliability and functionality.

This research seeks to leverage the insights from ASIL parameters and software testing principles to develop a comprehensive framework for testing safe autonomy in UAS, with a specific focus on drone delivery operations. Building upon the existing body of work, this study aims to formulate testing methods that are both practical and relevant to real-world drone applications. By adapting ASIL parameters and software testing concepts, it is hypothesized that a standardized testing process can be developed, enabling the assessment of UAS safety and integrity.

Ultimately, this research addresses a critical gap in the field of autonomous drone testing and evaluation. By advancing practical methodologies, it aspires to empower drone delivery companies and industry stakeholders to adopt safe and reliable autonomous operations seamlessly, paving the way for a more integrated and secure airspace.

The common resources encountered in the literature when seeking methods to T&E or (V&V) autonomous drones involve the study of Sense and Avoid algorithms (SAA) as seen in [8]. While been of interest, such perspective have been narrow and very specific. It does not contemplate the bigger picture that such evaluation have to be done by more simplified methods that can include technicians that operate the drones in their industry or workplace. Or the other

perspective focuses on identifying frameworks that might show promise but at the end are far from becoming an industry standard as seen in [9]. And this kind of framework is usually tested under simulated conditions that are far from been practical in an actual hardware implementation. All of this work is meaningful and assist with the discovery process and development of new ideas, but are far from becoming reliable industry applications.

It is critical to enhance academic exercises to progress into applications that meet commercial purposes. Academic research through many years of ideas can be simplified to develop practical applications and implementations that meet the rapid demands of industry. As an example, it can be possible to use as a reference with drones already proven efficient T&E methods from the automotive and software development industries. That way it is possible to start evolving beyond the academic exercise or case study. When trying to T&E autonomous systems any researcher in the field can turn back to the work done in the development of autonomous cars. The car industry has been working in the development of a truly autonomous vehicle for a long time. In that process, the Society of Automotive Engineers (SAE) International has developed the J3016 standard to measure Vehicle Automation Modes [10]. The levels are defined from 0 to 5. Level 0 indicating no autonomy to Level 5 been fully autonomous. Before continuing the discussion it is important to properly define **"autonomy"** and identify its contrast with **"automation"**. There exists a wide variety of definitions and arguments of how these two terms differentiate from each other. For the purpose to simplify their differences in definition, one can look back to one of the leading companies in vehicle development such as Caterpillar (CAT). At the end it is common that the industry leaders do set the standards and create the most proper definitions for the development of technology. CAT defines three terms to simplify and develop consistency among terms [11]:

- *Automation: a noun - refers to a set of related functions performed automatically by equipment. Automation assumes that the operator performs any requirements before or after the automated sequence in order to complete the task. Multiple automation sequences are required to enable equipment to work semi-autonomously or autonomously.*
- *Semi-autonomous: an adjective - describes multiple automated sequences a machine can perform without human input that result in a task being completed. Semi-autonomous machine operation assumes that the operator performs some tasks.*
- *Autonomy: a noun - refers to a state of equipment in which it can perform the programmed operations under defined conditions without human input or guidance. When we talk about this type of equipment, we use the adjective, autonomous. For example, some mines run autonomous trucks.*

In perspective, the claim to have a fully autonomous system involves developing a computer-based system that does not need human interaction to complete its task or mission. It also needs to ensure that no intentional or decrease accidental damage to the user, property and itself. And from not been human operated it comes the main interest for the process been identified for this research work:

testing safe autonomy. And if safe autonomy can be tested then a level of integrity shall be provided from it. For the benefit of the drone delivery industry, the automotive industry has develop a quantifiable way to address safe autonomy in automobiles [12]. They developed the Automotive Safety Integrity Levels (ASIL) contained withing the ISO 26262 industry standard [13,14]. And the ISO 26262 is an evolution or adoption from the IEC 61508 Safety Integrity Levels (SIL) [15]. The ASIL utilizes three probability defined variables in order to perform hazard analysis and risk assessment: severity, exposure and controllability [14]. Severity defines the kind of injuries that passengers and drivers can received; exposure defines the how much can a vehicle been exposed to a hazard; and controllability defines how much a driver or operator can do to avoid been injured. The addition of these three variables specify a numeric ASIL value defined from the letter A to D. An ASIL is assigned to each critical component of the vehicle such as the Antilock Braking systems. Different assignment of ASIL can be observe in Fig. 1.

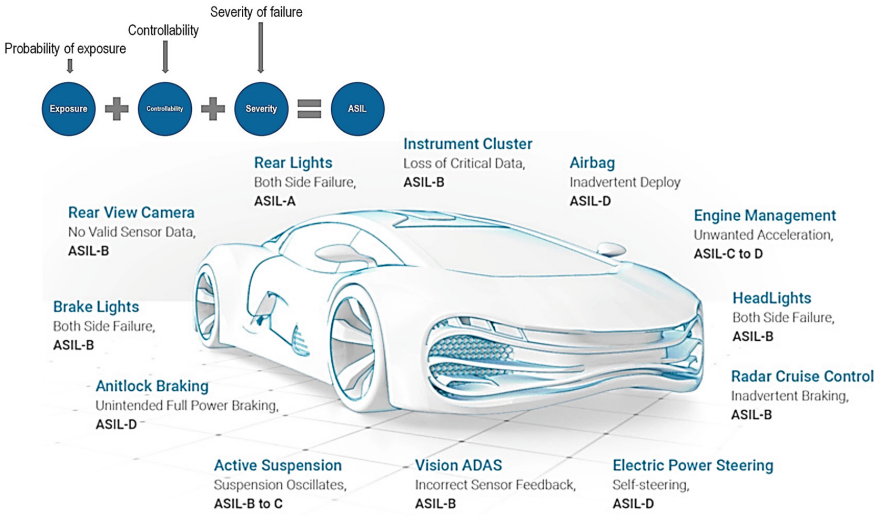

Fig. 1. Automotive Safety Index Level (ASIL) Allocation & Calculation [12,14].

The involvement or attention needed to ensure safety increases with the letter. An ASIL-D shows a component or subsystem requiring "the most safety critical processes and strictest testing regulations" [12]. The work done by Koopman and Wagner in [3] focuses on mapping the V-model with a monitor/actuator with redundancy test architecture. Such connection can be also done to for drone delivery systems that have to be tested for safe autonomy for the following subsystems: 1) electro-mechanical, 2) control, 3) software, 4) Artificial Intelligence (AI)/machine learning, and 5)sensing. And it can be hypothesized that those critical realms can be defined by ASIL-like parameters emulating existing T&E methods. It is of interest that tools of software testing can be implemented to

allocate test parameters that can be use to develop safe integrity levels for drones. The preparation for the professional software testers have been developed by the International Software Testing Qualifications Board (ISTQB). The ISTQB Certification website [16] and the information provided by Black, Veenendaal and Graham [17] provide the main concepts to match software testing process with autonomous systems. The process of how testing is done for software can then be implemented into autonomous systems. The idea is to take advantage of its practicality and its already proven efficiency.

At the intersection of software testing expertise and the realm of autonomous systems, a pressing need arises to develop robust evaluation methodologies tailored to complex entities such as drones. This paper is rooted in the authors' extensive experience in industry-based software testing, a journey that has led to a crucial realization: the Foundations of Software Testing Tools, revered in the software domain, could offer valuable insights and methodologies to enhance the Test and Evaluation (T&E) processes for autonomous systems like drones.

The realm of software testing, recognized as an industry standard, encompasses a methodical approach to assess system functionality and identify defects, ensuring the production of high-quality products that meet predefined specifications. This process of testing is a distinct phase, separate from debugging, and crucial for ensuring the reliability and integrity of software applications.

However, extending the principles of software testing to autonomous systems presents unique challenges. The authors identify a pivotal distinction between dynamic and static testing techniques (Fig. 2). The former involves executing the system to evaluate its behavior and performance, while the latter focuses on assessing system requirements and design products without actual execution. This divide further branches into black-box testing, which examines input-output responses, and white-box testing, which delves into internal system functionality.

In the case of autonomous systems like drones, the intricacies multiply as hardware-software interactions come into play. Translating software testing principles to the evaluation of drone systems requires a comprehensive understanding of both dynamic and static aspects, acknowledging the unique challenges of testing real-world operations alongside software behavior.

The forthcoming sections delve into the adaptation of software testing methodologies to the realm of autonomous systems, with a specific focus on drones. By harnessing the insights from the Foundations of Software Testing Tools, this research aims to bridge the gap between proven software testing practices and the intricate demands of testing complex autonomous systems.

At the core of both software development and autonomous system deployment lies the necessity to grasp the intricate interplay between errors, faults, and failures. These interrelated terms form the foundation of comprehensive software testing techniques, and their significance extends to the evaluation of autonomous systems' reliability and safety.

Errors, as depicted in Fig. 3, originate at the source code level, introduced by programmers during software development [18]. Under specific conditions, errors evolve into faults, which might not necessarily disrupt the full functionality of

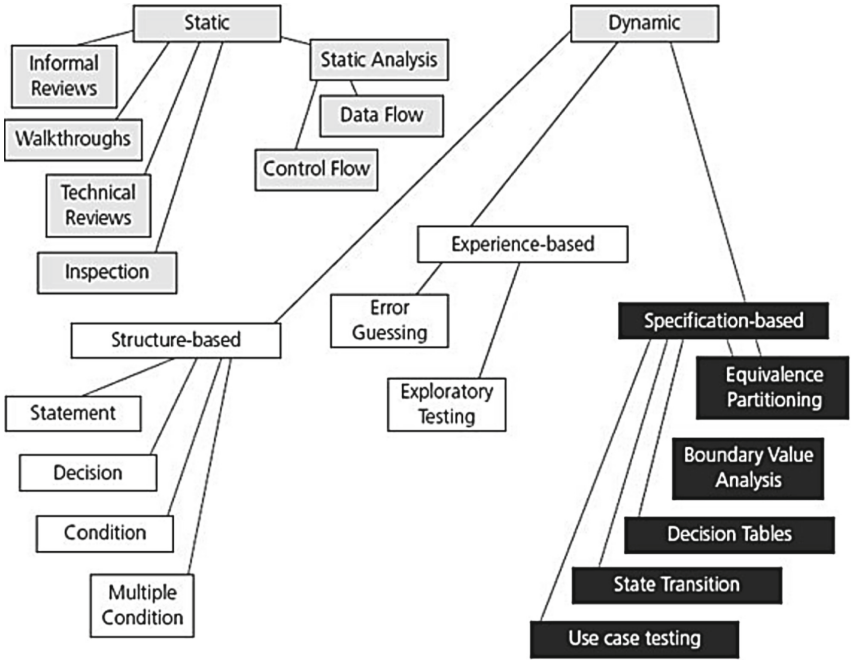

Fig. 2. Principal Testing Techniques Branches in Software Testing [17].

the software. Effective testing processes play a vital role in identifying potential failures and their underlying defects, enabling developers to initiate the debugging process. This iterative, organized testing approach is a cornerstone of the software industry.

As we draw parallels between software and autonomous systems, a critical distinction emerges. Failures within autonomous systems can yield consequences that extend beyond the realm of software. The interaction of hardware components with the physical environment and users introduces an additional layer of complexity. Consequently, failures in autonomous systems can have more profound implications, necessitating a meticulous evaluation process that extends beyond traditional software testing.

Breaking down autonomous systems into safety integrity levels becomes essential. These levels facilitate the allocation of testing techniques that address the specific vulnerabilities and complexities inherent in each system. By strategically adapting and applying software testing principles, we can create a structured approach to evaluate autonomous systems, enhancing their reliability and ensuring that potential failures are mitigated effectively.

In the following sections, this paper delves deeper into the application of software testing methodologies to the realm of autonomous systems. By leveraging the knowledge from the software domain, we aim to formulate systematic testing

approaches that tackle the unique challenges posed by the intricate interactions of hardware and software in autonomous systems.

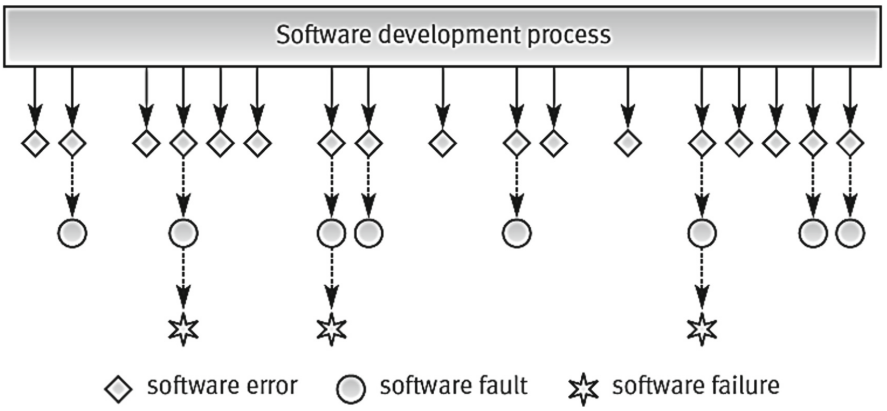

Fig. 3. Software Errors, Faults and Failures Connections/Sequence [18].

At the heart of software development lies a critical phase: testing. This phase serves as a pivotal gateway to identifying defects and errors that may have emerged during the development process. However, the scope of this work extends beyond the mere development of a testing process. It seeks to empower and educate the human tester, transforming them into agents of Quality Assurance.

The objective of this work is twofold: to streamline the testing process for autonomous systems and to equip testers with the tools and knowledge needed to ensure Quality Assurance. This entails simplifying the intricate process of testing, aligning it with the already established and effective methodologies from software testing. By forging a connection between these methodologies and the domain of autonomous systems, we aim to foster an ecosystem of reliable and robust autonomous technologies.

To illustrate this convergence, consider the case of a small drone. Within this context, our testing exercise focuses on minimizing the complexities inherent in testing autonomous systems. The small drone serves as a foundational unit to illustrate the principles and methods that can be applied to more intricate systems. By grounding our exploration in this tangible example, we aspire to not only create a testing methodology but also offer a path for testers to become champions of Quality Assurance.

As we embark on this journey, the small drone serves as a microcosm of the broader challenges and opportunities presented by autonomous systems. Through the lens of this exercise, we seek to develop a holistic approach that streamlines the testing process while elevating the role of testers in ensuring the integrity and reliability of autonomous technologies.

3 Characteristics of the System Under Test

When searching on Google Scholar using the keywords **parrot mambo drone**, multiple peer reviewed publications entries can be found. The utilization of this small device can be seen documented in Master's Thesis, journals, and conference proceedings among other important scientific and technical documentation. This just demonstrates that such a simple small drone have been an essential tool in the study of autonomous systems for a while. In this study, the Parrot Mambo drone is selected as an example of a small easy to fly racing drone designed for beginners. Figure 4 shows the technical specifications of the system. It also supports many coding platforms, blocks coding and text coding to program the drone to change its working functionalities. It can be program using the MATLAB command line, through blocks in Simulink, and with C-language via ROS (Robotic Operating System). Sadly, the Mambo drone is not longer in production or supported by Parrot. However, due to its legacy it is still a relevant drone to be tested due to the many years and time invested on researching autonomous systems capabilities.

The drone contains and Inertial Measurement Unit (IMU) with 6-degrees of freedom, and ultrasound sensor and a camera. The weight of the device is about 63 g with a 550 mAh LiPo battery that can allowed about 9 min of flight time. And its dimensions are about 18 by 18 cm. All this details can be encountered online or on specific research documents such as [19] that documents the Mambo drone application to study adaptive control. It is a basic drone which performs a control with good stability and could be found at a good price before 2020. It has a vertical camera integrated which captures when it flies from top angle.

The other SUT (Ryze Tello) was the natural upgrade to the Mambo [20]. It is a small drone with similar capabilities but with an Software Development Kit (SDK) that can be manipulated with Python. Future work will replicate the results obtained with the Mambo.

The Safety Integrity Levels (SILs) are similar to the ones proposed by ISO 26262 and they can be derived with respect to UAS. Recalling Fig. 1, an exercise can be done through experimentation and historical data on the Mambo drone (Fig. 4) to gather SIL parameters. They can be then defined among different realms of autonomous devices or cyber-physical systems once the knowledge exits and can be utilized to simplify the testing of safe autonomy.

Developing or formalizing SILs for drones is out of the scope of this document but critical principles on ASIL allocation can be encountered in the following documents for future references: [3,21–25].

However, It is important to start the discussion of what post-design T&E methodology is needed.

The tests being performed in this work will assist in identifying SILs probabilistic parameters focused on Severity, Exposure and Controllability in small drones. The testing can be initialized by detecting any physical damage and imperfection. Such a test can involved verifying that all electrical wires are plugged or all propellers are not damage. And then verify the drone basic functions such as hovering for 9 min or being able to make flips in all four directions.

To simplify the T&E process, two process frameworks have been generated and further explored in the next section: Hardware Testing and Combination Testing.

There are few different types of testing which are performed on a system to make them safe and a valid product for use. Substantial testing needs to be done to verify whether there are any problems exists in the drone's system or not. There are few things that needs to be considered as a prerequisite to begin the test. They are:

- Before beginning the tests, the information about the system needs to be noted to identify the drones being tested (static testing). The information is noted into two types. One "Detailed Information" and the other is "Relevant Information". The detailed information contains all the information about the technician name, test serial number, test date, drone name, drone's model, serial number of drone if available etc. and the relevant information contains the details of the product specification, environment that's being tested, product manuals, etc.
- Check for any visual damage on all the visible components and make sure all the components, parts are in good condition (dynamic testing). Any damaged component changes the drone to work improperly. Check for any damages on chassis, propellers, batteries, sensors, cameras, screws, remote controller, wires, LED lights etc. If there are any problems identified with the hardware of the drone, kindly replace its parts before the test.
- Kindly check the batteries of the drone are charged at least 75% to complete the test. Since these quadcopters have less battery stands of 10 min fly time, we at least need few minutes to observe the functional behavior that we test. So, the minimum recommended battery charge is set as 75%.
- Most important thing is to understand the complete functionalities of the drone. Understand the main objective that the drone is built for. Why the drone is used? What tasks the drone can perform? Identify the different modules it has? etc.

Then, it is important to list understandable functionalities of Parrot Mambo drone:

- Can hover for about 9 min with its 100% battery charged, without performing any special tasks like flips, video recording.
- Can fly in all direction based on the instructions from the user.
- Can be able to make flips in all four directions.
- Can be able to capture photos.
- Additional add-on's can be attached on top of the drone,

4 The Testing Process

Through experience and following the Fundamentals of Software Testing, two testing processes have been identified to assist with the T&E of small drones. The methodology and the content of each of its blocks are described on the following sections.

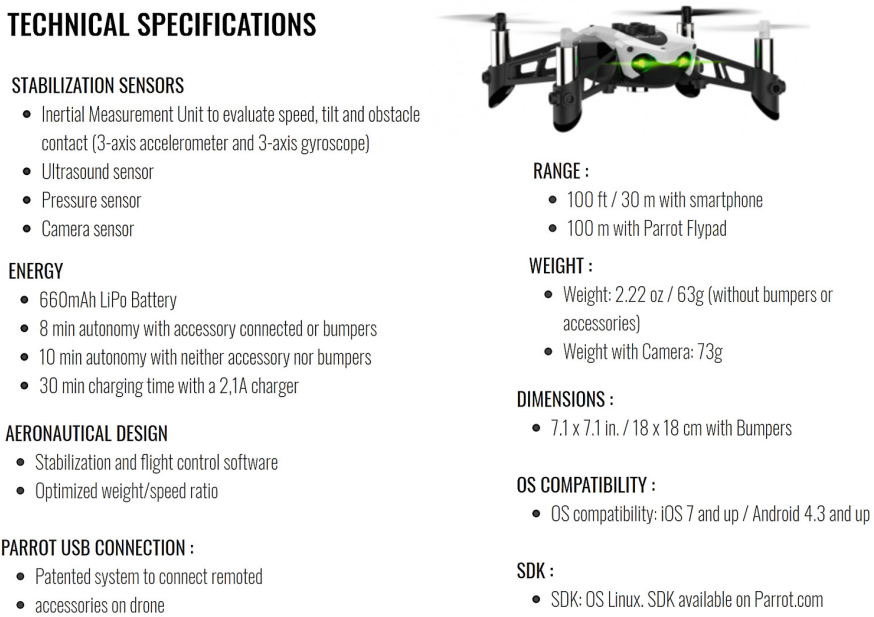

Fig. 4. Parrot Mambo Technical Specifications. Source: https://www.ftw-robotics.com/diy-parrot-mambo

4.1 Hardware Testing

Testing the hardware of a system is very essential when it is used in a process that can have any effect on the safety, efficiency, quality of a product. Figure 5 breaks down the proposed T&E process. The Unit Testing is mainly the testing the individual components of a system. In case of drone testing, the tester is going to visually check and verify all its hardware components are good or not. The Integration Testing is done to test the modules/components when integrated to verify that they work as its expected functionalities i.e. to test the modules which are working fine individually does not have issues when integrated. The Load Testing is the process that tests the application under specific load. Under hardware testing we can do load testing in such a way by installing add-on modules like camera, or any other sensor, then hover the drone. The System Testing (Combination) validates/tests the end to end complete integrated product. Its main objective is to evaluate the end to end specification of the system.

Components like chassis, propellers, body parts, sensors, etc. are checked here. Testing the individual units or components of a software is called unit testing too. In part of testing the drone's software, all the individual components present in the application are tested. Testing the buttons, any second windows, etc. present in the application are tested.

It can be manage to do integration testing with the drone when all the hardware components mentioned above are installed on drone and then check if the drone turns on and fly or not.

Secondly by adding two additional modules and fly the drone. Thirdly by hovering a free drone without add-on's and observe the co-relation between all three scenarios. Is there any latency observed when hovering the drone? Is there any drift of position from its original position due to additional weight? These things need to be tested here. It is testing process that tests the application under specific load. When it comes to software load testing, we can test the drone under one working functionality coded using Simulink, note the results of hovered time, etc. And then add multiple functionalities, then test the same and compare both the outcomes. As an expected output, if not very stressful task is performed on the drone, the speeds of the drone should not vary.

This testing is performed before acceptance testing, in here we test the complete system. In here we perform each operation which can be performed by the drone, that is from taking-off to take few flips and land.

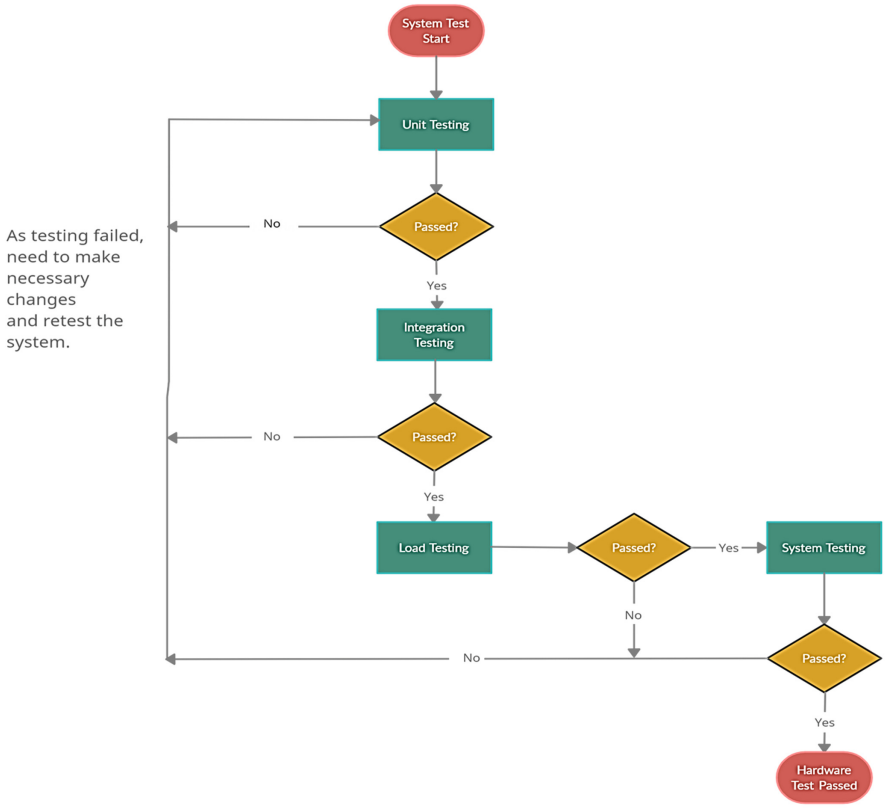

Fig. 5. Proposed Hardware Testing Framework.

4.2 Combination Testing (Software and Hardware)

The combination of hardware and software is a system. Testing the system with respect to both hardware and software perspective combined is called Combination Testing (Fig. 6). The Software Testing is a method of assessing the functionality of a software application to evaluate whether the developed software meets the stated specifications and to identify defects, and to ensure that the product is free from defects. The Smoke testing (combination) is one of the preliminary testing and an important testing that needs to be performed that helps us to decide whether the system is stable enough to proceed with further testing. Usability Testing: This technique is being used to evaluate the user-friendliness features of the system to ensure no issues to the end-users while using and handling the system.

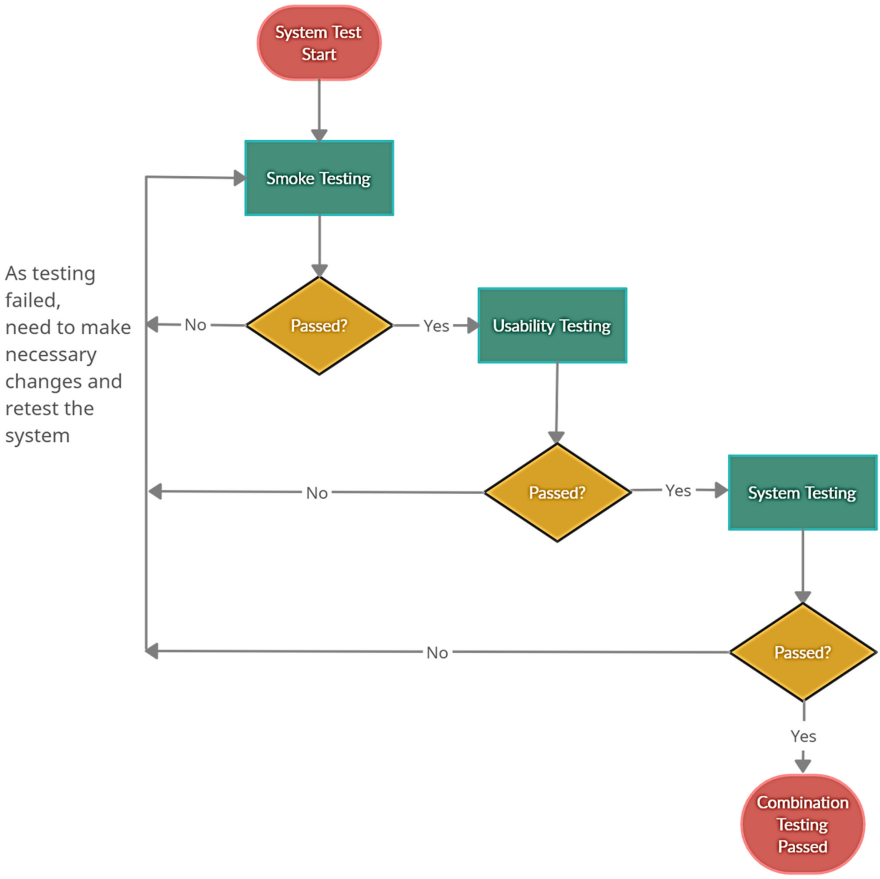

Fig. 6. Proposed Combination Testing (Software and Hardware) Framework

4.3 Optional or Additional Testing

Other tests can be done in addition to the previous proposed methods. These tests can further enhance the process to detect critical failures in the system.

Volume Testing (software): This testing is done by subjecting the system to huge volume of data. Volume testing is done to analyze the system performance by increasing the volume of data in the database.

Compatibility Testing (Software): This testing is necessary to evaluate the compatibility of a software product with its expected working environment including multiple platforms, OS, devices, software and hardware to execute its intended functionalities properly without any issues. This testing can be performed by installing the Parrot mini app on both Android and IOS devices and then try to operate the drone and test it.

Performance Testing: This testing is very similar to load testing. It tests the system's speed, responsiveness, and stability under heavy load. We can test the drone using performance testing using few test scenarios. Few of them are:

- Flying the drone under heavy winds, record its speed and test it inside a lab with zero wind. Compare the results.
- Add weight on the system by adding add-on is and test its performance under heavy wind and zero wind.

Regression Testing (software): It is a type of testing that is done to validate whether any code change/add functionalities do not affect the existing functionalities of the system. These mambos can work on the Simulink built codes. So, when we code it using Simulink, each function modules are developed individually and then combine them. So, at that time, Regression testing is preferable to be done.

5 Testing Implementation and Use Cases

The previous methods have been implemented on manual testing for the Mambo drone. About 15 tests have been done and examples of 5 of them are presented in the Parrot Mambo Fly Tests Cases. However, before the tests were done it was important to add an statement on the basic functionality of the System Under Test (SUT).

5.1 Understanding the Workings of Parrot Mambo

Parrot Mambo has few pre-developed capabilities that needs to be understood. It is designed in such a way to be safer to use. It is piloted in Bluetooth mode via an app FreeFlightMini or with a Parrot Fly pad. There are two jogs present to control. One jog to turn in all directions and the other jog to move. It has a predefined ability to flip in forward, backward, left and in right directions. It can take a photo, record a video, and cast a live video.

5.2 Parrot Mambo Fly Test Cases

Test Cases: To perform and observe the behavior of the drone during this test, It might require to re-test the same test case many times to get accurate results. Hence it is suggested to charge the battery of the drone at-least 80% so that multiple time the task can be performed on the same drone. The figure below summarizes T&E processes that can be implemented on small drones (Fig. 7).

Test Case	Assumption	Test Steps	Expected Results	Actual Results
A. Testing the take-off	Drone's battery is charged at least 75% and is connected to smartphone via FreeFlightApp.	• Connect the drone to a smartphone via Bluetooth. • Place it on a flat surface. • Make sure that the pre-adjusted height for the drone to fly is set at 1m . It is pre-adjusted to 1m because it is the minimum recommended height to hover, fly and do flip operations. • Click on take-off button to fly the drone.	Drone takes off and flies at 1m height .	Test passed. The mambo took off well. There is no very much difference in position before and after landing. 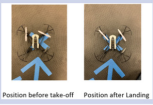 Position before take-off Position after Landing
B. Testing the cameras	Drone's battery is charged at least 75% and is connected to smartphone via FreeFlightApp.	• Place drone on stable surface • Power on drone. • Clean the camera lens. • Fly the drone. • Click on camera button to capture a photo. • Check the position of the drone after taking a picture. • Assess image quality of the image. • Test the camara during night to check night vision.	Captures a good quality image standing at a constant position.	Test failed. Unable to locate the captured images on app's gallery. There is a lot deviation its position after an image was captured. 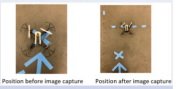 Position before image capture Position after image capture
C. Testing the drone speed	Drone's battery is charged at least 75% and is connected to smartphone via FreeFlightApp.	• Connect the drone to a smartphone via Bluetooth. • Place it on a flat surface. • Click on take-off button to fly the drone. • Then move the drone using the jogs.	Initially when the drone is hovered, the speed of the drone should be 0.0MPH. When the drone starts moving, speed bar should show the accurate speed of the movement of the drone.	Test passed. Initially the drone speed was 0.0Mph. After flying the MPH has shown the actual speed of the moving drone. 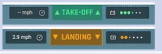
D. Testing the Flip forward ability	Drone's battery is charged at least 75% and is connected to smartphone via FreeFlightApp.	• Connect the drone to a smartphone via Bluetooth. • Place it on a flat surface. • Click on take-off button to fly the drone. • Then click on flip forward button.	Drone should take a forward flip and comes back to its original position.	Test failed. The drone landed with much deviation compared to the take-off position as shown in the below images 1 & 2. 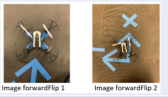 Image forwardFlip 1 Image forwardFlip 2
E. Testing the Bluetooth connection	Drone's battery is charged at least 75%.	• Connect the drone to a smartphone-1 via Bluetooth. • Once the connection is successful, open free flight mini app on another smartphone and try to connect to the same Mambo drone.	Drone should connect to the first smartphone and should not appear for free connection on the second device.	Test passed. The images proves the connection was successful to phone via Bluetooth. 

Fig. 7. Small Drones Test Cases

From those cases its was learn the basic features and controllability of the drone. There is however as semi-autonomous function involving the flip command in which the user does give full control to the SUT to do what is commanded. Other than that, the control of the drone is dependent on the user feedback and the maintenance of control and communications from the controller to the drone.

5.3 Selecting the Automated Control and the Especial Case: Lost of Control

There exists two options to control or program for autonomous routines the Mambo drone in MATLAB. The first one involves sending scripted commands

through the MATLAB control panel or scripts while communicating with the drone through the WiFi with the camera add-on. The other way is developing a Simulink program and communicate to the drone through Bluetooth. The first option allows for immediate control through simple commands while the second option through Bluetooth allows for more sophisticated control theory based experimentation or testing. The Bluetooth through Simulink option takes further steps and is a more involved process to control the drone. The main perspective is to keep a simple T&E process that does not require the implementation of sophisticated control algorithms or dependency of rigorous sensor feedback. The WiFi communication and control through the add-on camera was selected. The discovery process on how to implement scripted commands to the drone brought interesting results. When a MATLAB script was run in full the drone would do the task with not issues. However, when the command was sent line by line a risk of lost of control was encountered. The observation is that the data packet containing the command might not be received by the drone causing total failure in the command and control mechanism of the drone. On that situation, the drone was always allocated inside a meshed testing area in the laboratory. And to stop or recover the Parrot drone has an emergency off mechanism when manually flip 180° on its Z-axis. In order to do that, the operator had to enter the safety net wearing gloves and safety glasses, then approach safely the drone with two padded or foam plates to grab the top and bottom of the drone and flip it to shut it down.

Through this process it was learn a critical flaw of the Parrot Mambo when the communication is lost. In such circumstance, it can be said that the controllability risk reach a maximum point. And the WiFi based communication subsystem or module could receive a SIL level of extreme critically. The accidental discovery and undocumented flaw will then be evaluated through the T&E process as failing. This then leave further room to enhance future design of small drones with better safety critical mechanisms that does not involve the operator putting themselves at risk or fully loosing the device to a collision that can damage property. Such situations are what is needed to be encountered through the T&E process. For the next section, the WiFi enabled control method through MATLAB was utilized to test and compared the drone while been operated by a human versus and scripted or automated routine.

Other testing that is in consideration but need further analysis and exploration performance in an obstacle environment, test their performance at high speeds, and some focus on performance under high loads. As a researcher once a SUT has expire its shelf life, the next updated technology has to be approached. The Tello drone is then utilize to continue the research assuming that the previous procedures and T&E principles will hold true. An example on the high load or weight performance involves the use of 10-gram weights attached to the bottom of the drone itself. From this point the weight can be increased by 10-grams until the drone is unable to lift itself from the ground thus concluding the test. The test results allow to determine the final weight our additional tools such as lifting mechanisms or extra sensing devices. Figures 8 and 9 show a test

done on a Ryze Tello drone to identify its capabilities to lift extra payload. Further details are out of the scope to this document, but this serve as an example of further testing procedures that can complement the developed on this work. Developing test standards are very involves and take time to be fully developed. Such work requires to be applied in many types of tested objectives rather than a single device. However, there is an attempt to start with a simple method with the capabilities to open the capabilities to enhance the T&E of autonomous systems.

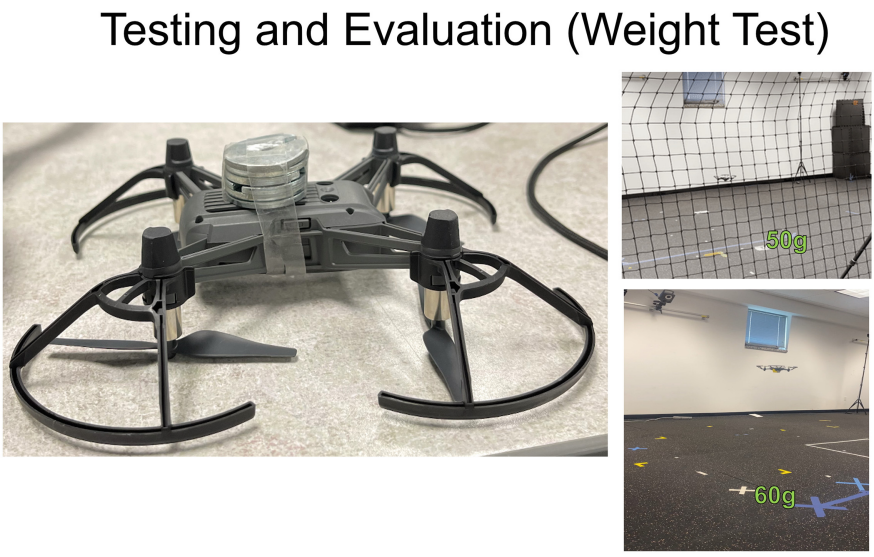

Fig. 8. Weight Test done in Ryze Tello drone

6 Testing Results and Analysis

To allocate parameters to evaluate the capabilities of the SUT several test were done following the method listed on the previous section. The drone was flight through manual and automated or scripted control. The manual control was done using the Parrot mini Android application through Bluetooth communication. And the automated consisted on programming a scripted routine to the drone using MATLAB and the WiFi communication of the add-on camera.

It is essential to further the observations that can assist comparing how the SUT will operate in manual control versus a computerized one. On that perspective, there was experimentation done in the TAMU-CC Collaborative Robots and Agents Lab (CORAL) motion caption system enable by twelve Vicon cameras.

The experimental setup can be observed in Fig. 10 and all the preliminary testing is summarize in Table 1. Markers are allocated on the SUT and the Vicon cameras aided by the Tracker software. The data reported by tracker consists on the overall translation XYZ motion (in millimeters), the individual X, Y and Z translation per frame (in frames vs. millimeters), and the individual X, Y and Z rotation per frame (in frames vs. radians). Nine data points are collected and processed through MATLAB to develop the visualization. By using that system the plan was to discern system critical functions in which the SUT would need a greater emphasis into identifying safety goals differences between manual and automated operation.

For each one of the tests a simple MATLAB scripted code was done in order to have the drone operate without immediate human control. The scripts consisted into testing the drone take-off, landing, flip in four directions (left, right, forward and back), camera capture, fly forward a timed distance and navigate the room in an square routine.

Drone Weight Bearing Test						
	UAV Only	UAV + Payload 1	UAV + Payload 2	UAV + Payload 3	UAV + Payload 4	UAV + Payload 5
Payload Mass (g)	0	20	30	40	50	60
Total Mass (g)	80	100	110	120	130	140
Ability to take off	3	3	3	3	3	2
Ability to maneuver	3	3	3	2	2	2
Ability to stop	3	2	2	2	2	1

3 - No Difficulty | 2 - Fair | 1 - Poor | 0 - Failure

Feasible payload weight constraint = 20g - 30g

Fig. 9. Results on Weight Test done in Ryze Tello drone

The implemented scripts involved simple to complex tasks that could enable a wide spectrum to observe and capture the drone dynamic behavior.

In order to realize each test routine the following prerequisites had to be met:

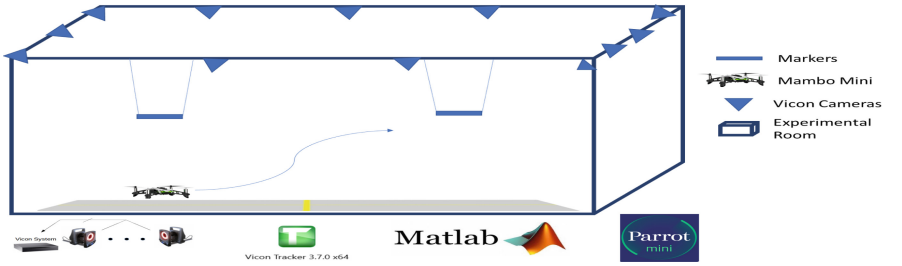

Fig. 10. CORAL Small UAS Testing Environment.

Table 1. Preliminary Manual and Automated Test Runs

Test name	Manual test runs	Automated test runs
Move forward	2	2
Take-off	2	2
Landing	2	2
Left-Flip	2	2
Right-Flip	2	2
Forward-Flip	2	2
Back-Flip	2	2
Battery Drain Test	Need to be addressed	Need to be addressed
Camera Test	Need to be addressed	Need to be addressed

1. Mambo battery fully or charged at least 80
2. Attach camera module to the MAMBO.
3. Connect the target Mambo to the computer in which you run this script.

Through this experimental exercise it was necessary to explore or study controllability by a human operator vs controllability by a built in or scripted automated process. It has to be explained that to have autonomy it is necessary for the SUT to make its own decisions without human interaction. However, the scripted routine is assumed to be an important step or building block into further identify how safety critical process affect autonomy.

And the following are the fundamental steps that have to be taken in consideration for the testing process:

- Quadcopter Testing and Validation
  - Study the behavior of the quadcopter.
  - Identify test cases and test scenarios.
  - Run the documented testing on different drones.

– Validate them to check whether they are safe to use.

The testing process and iterative discovery is still in progress. Many data points were generated and not everything can be reported in this publication. However, the testing that was identify as critical into the test to verify drone capability to lift-off and navigate in an straight line towards a destination to land for certain time. This was done manually and scripted. Figures 11, 12, and 13 break down the visualization of the test results of the manual test.

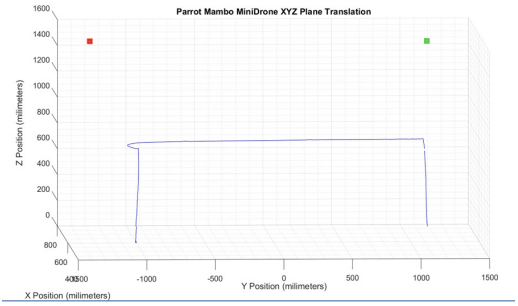

Fig. 11. Parrot Mambo Forward Travel Manual Test XYZ Plane Translation.

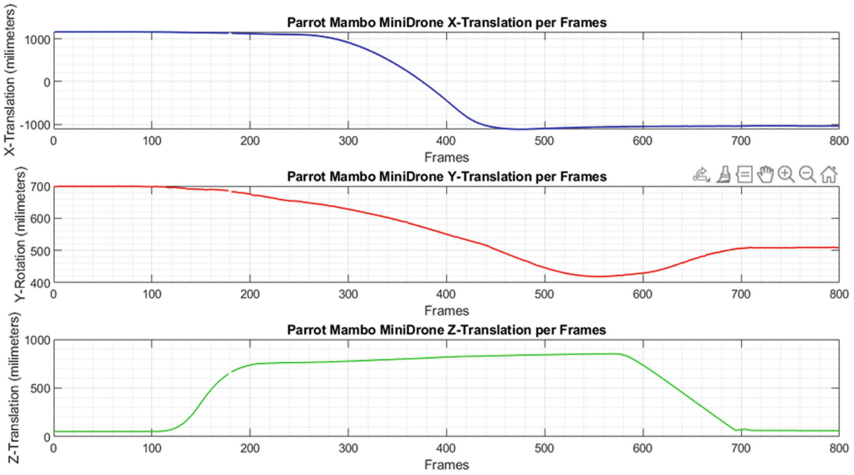

Fig. 12. Parrot Mambo Forward Travel Manual Test Separated Translations.

And Figs. 14, 15, and 16 depicted the experimental results from the automated or scripted process.

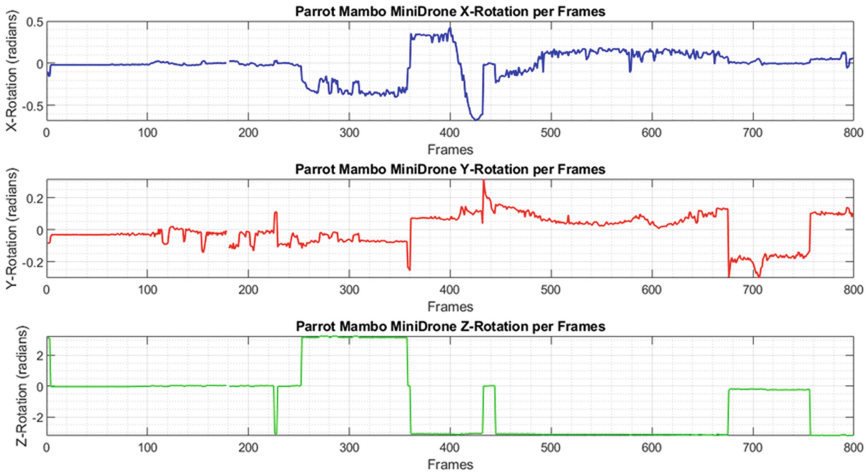

Fig. 13. Parrot Mambo Forward Travel Manual Test Separated Rotations.

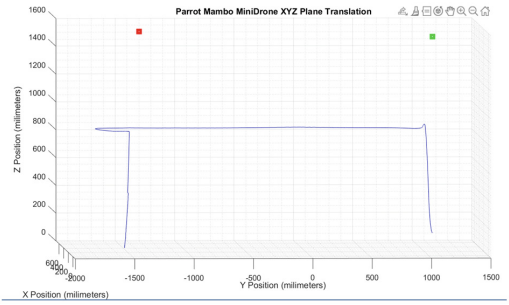

Fig. 14. Parrot Mambo Forward Travel Automated Test XYZ Plane Translation.

When comparing manual versus automated, it is more notorious the discrepancies in the rotation planes. It is understandable that the human operation does lack the precision of a machine and depends on the vision capability to move the drone through the room. Therefore, the process involves just a forward motion but the human-in-the-loop has to correct the SUT for not rotation and keep consistency in the straight line path. The automated process seems to be more precise and accurate through the test. It was then important to develop a more complex test in which rotation should be involved as a critical feature. The other test to be reported is the test involved with the drone capability to navigate and rotate through the room through an squared path. The experimental results are reported in Figs. 17 and 18 for the manual test; and Figs. 19 and 20 for the automated testing.

It is clear that the Inertial Measurement Unit lacks precision and control through the automated process. And through the literature and expert devel-

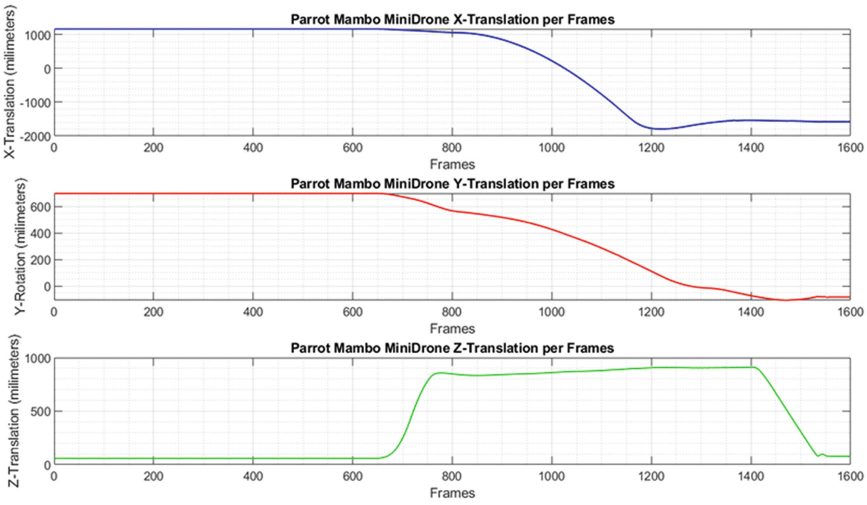

Fig. 15. Parrot Mambo Forward Travel Automated Test Separated Translations.

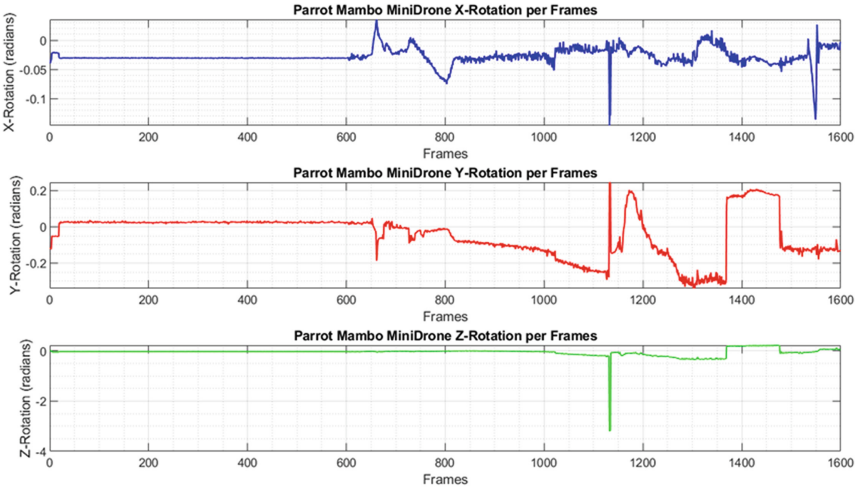

Fig. 16. Parrot Mambo Forward Travel Automated Test Separated Rotations.

oped work it is known that autonomous multi-copter control is essential in the feedback loop while enabling the Yaw, Roll and Pitch dynamics. Rotation or the devices that measure such dynamic while controlling a drone shall have a high Safety Integrity Level. Simple forward or background motion can be hypothesized as not as critical under ideal conditions (no wind or other nature based phenomena). From these perspective UAS SIL weighted values should be developed understanding the complex dynamics of a device that can translate itself

Fig. 17. Parrot Mambo Squared Navigation Manual Test XYZ Plane Translation.

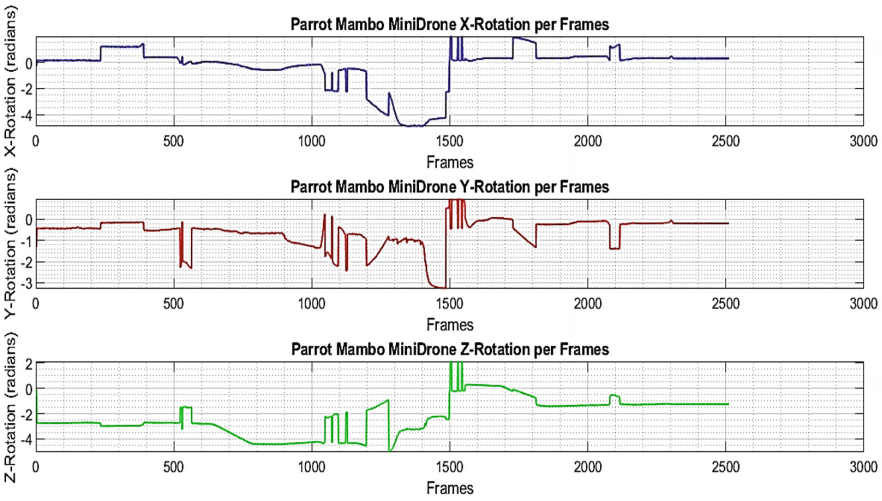

Fig. 18. Parrot Mambo Squared Navigation Manual Test Separated Rotations.

in six degrees of freedom opposite to automobiles or fix-winged devices that lack such dynamic freedom. Through this simple heuristic process, it can be identified that even if multi-copter drone enable more degrees of motion to operate, more complexities exist opposite to already studied ASILs. This paper then calls for further work into developing methods to allocate UAS SILs.

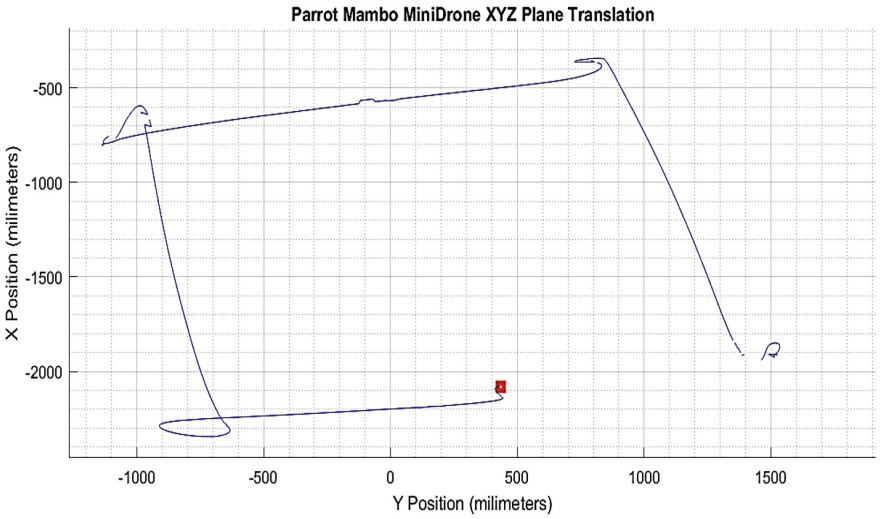

Fig. 19. Parrot Mambo Squared Navigation Automated Test XYZ Plane Translation.

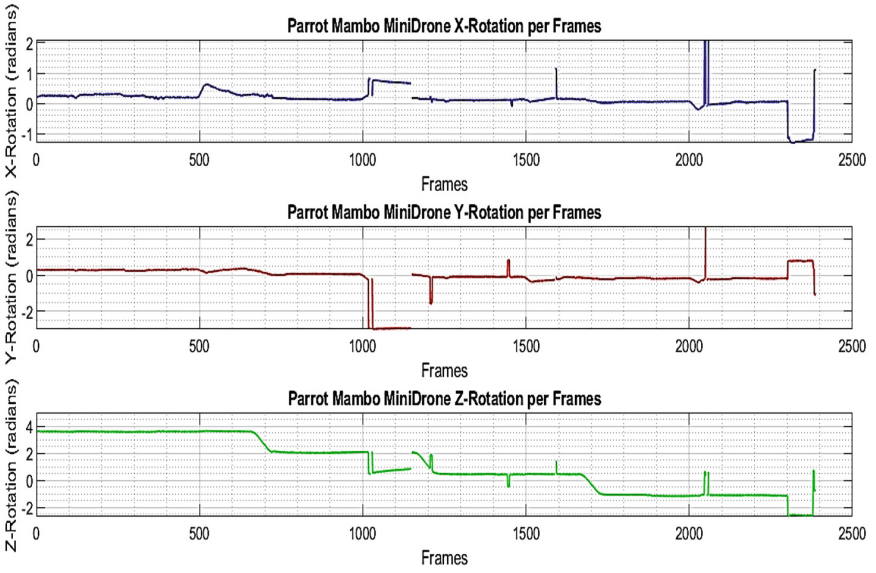

Fig. 20. Parrot Mambo Squared Navigation Automated Test Separated Rotations.

7 Conclusions

An important question should arise when defining UAS SILs: *can the principles that define safety autonomy are beyond severity, exposure and controllability?*

Sensing and Autonomy should be a factor into developing Safety Integrity Levels for cyber-physical or robotic systems. It is critical to utilized what has been learnt through the development of ASILs to be allocated and then formalize into small drones. That way uncertainties behind safety of UAS can become standardized through trusted weighted values.

The work done by professional software testers is critical and new products based on non-deterministic behaviors are becoming part of society. Through this paper a comprehensive exploration in T&E methods was done to assist with the validation and verification of safe drone autonomy. Such autonomy will enable trust that drones can efficiently and safely deliver a parcel to its destination. The SUT was defined to be an small drone that has been part of the control and autonomy research community for a while. Test cases of how to verify the functionality of the device were introduced. And there was a preliminary experimentation into identifying critical components that can bring critical failure consequences to the SUT. The provided document is in service to start the discussion and identify what else need to be tested to better enable UAS technologies first to assist the delivery industry that has been proven to become a reality in our society. Safety-critical requirements are essential and they must go beyond the design process. It has to become a continues and iterative process. From the further exploration of UAS SILs better benchmarks could be developed. Such benchmarks would be enabled by replicating the software development T&E method with newer devices replacing the Mambo Parrot mini-drone. With enhanced or added SIL weighted values, the development of autonomous systems will just become more resilient and safe for the user.

Future work involved plans to explore Fuzzy Logic strategies similar to the one in [25], and implement more rigorous mathematical modeling such as in [26]. The plan is to continue formalizing and identifying what is needed to for the next level of a methodology to Test & Evaluate the safe autonomy of small drones.

Acknowledgements. This work is been supported by the National Science Foundation CNS Division of Computer and Network Systems, NSF AWARD #2131263 titled: CISE-MSI: DP: SaTC: Dynamically Enforcing User-Oriented Geospatial Restrictions for Drone Fly-Overs."

References

1. Knutsson, K.: They're in their 80s and addicted to drone deliveries, 11 August 2023. Fox News, https://www.foxnews.com/tech/couple-80s-addicted-drone-deliveries. Accessed 31 Aug 2023
2. Singh, I.: 191-pound drone gets nationwide exemption from FAA to fly BVLOS, 28 August 2023. DroneDJ, https://dronedj.com/2023/08/28/phoenix-air-bvlos-drone-exemption/. Accessed 31 Aug 2023
3. Koopman, P., Wagner, M.: Challenges in autonomous vehicle testing and validation. SAE Int. J. Transp. Saf. **4**(1), 15–24 (2016). https://doi.org/10.4271/2016-01-0128
4. Murison, M.: Parrot to Step Away From Toy Drone Market, DRONELIFE (2019). https://dronelife.com/2019/07/22/parrot-to-step-away-from-toy-drone-market

5. Macias, F.: The test and evaluation of unmanned and autonomous systems. ITEA J. **29**, 388–395 (2008)
6. Ferreira, S., Hess, J.: Unmanned and autonomous systems of systems test and evaluation: challenges and opportunities. In: IEEE Systems Conference (2010)
7. Helle, P., Schamai, W., Strobel, C.: Testing of autonomous systems - challenges and current state-of-the-art. INCOSE Int. Symp. **26**(1), 571–584 (2016). https://doi.org/10.1002/j.2334-5837.2016.00179.x
8. Zou, X., Alexander, R., McDermid, J.: Safety validation of sense and avoid algorithms using simulation and evolutionary search. In: Bondavalli, A., Di Giandomenico, F. (eds.) SAFECOMP 2014. LNCS, vol. 8666, pp. 33–48. Springer, Cham (2014). https://doi.org/10.1007/978-3-319-10506-2_3
9. Yildirim, A.S., Berker, E., Kayakesen, M.E.: System level test automation in UAV development. In: Proceedings of the AUTOTESTCON, vol. September 2018, pp. 1–6 (2018). https://doi.org/10.1109/AUTEST.2018.8532551
10. SAE clarifies autonomous driving level definitions. https://www.therobotreport.com/sae-clarifies-autonomous-driving-level-definitions/. Accessed 14 June 2021
11. Automation & Autonomy: What's the Difference? Caterpillar. https://www.cat.com/en_US/articles/ci-articles/automation-autonomy-whats-the-difference.html. Accessed 14 June 2021
12. What is the ISO 26262 Functional Safety Standard? - NI. https://www.ni.com/en-us/innovations/white-papers/11/what-is-the-iso-26262-functional-safety-standard-.html#toc2. Accessed 14 June 2021
13. ISO - ISO 26262–1:2018 - Road vehicles—Functional safety—Part 1: Vocabulary. https://www.iso.org/standard/68383.html. Accessed 14 June 2021
14. What is ASIL (Automotive Safety Integrity Level)? - Overview – Synopsys Automotive. https://www.synopsys.com/automotive/what-is-asil.html. Accessed 14 June 2021
15. Safety and functional safety—IEC. https://www.iec.ch/safety. Accessed 14 June 2021
16. Why ISTQB® Certification? - ISTQB® International Software Testing Qualifications Board. https://www.istqb.org/certification-path-root/why-istqb-certification.html. Accessed 14 June 2021
17. Black, R., van Veenendaal, E., Graham, D.: Foundations of Software Testing, 3rd edn. CENGAGE Learning (2012)
18. Galin, D.: Software Quality Assurance: From Theory to Implementation. Pearson, London (2004)
19. Virdi, J.: Flight evaluation of deep model reference adaptive control. Thesis. Master of Science in Mechanical Engineering. University of Illinois at Urbana-Champaign (2020)
20. Tello. https://www.ryzerobotics.com/tello/specs. Accessed 31 Oct 2023
21. Sorokos, I., Azevedo, L.P., Papadopoulos, Y., Walker, M., Parker, D.J.: Comparing automatic allocation of safety integrity levels in the aerospace and automotive domains. IFAC-PapersOnLine **49**(3), 184–190 (2016). https://doi.org/10.1016/j.ifacol.2016.07.031
22. Gheraibia, Y., Kabir, S., Djafri, K., Krimou, H.: An overview of the approaches for automotive safety integrity levels allocation. J. Fail. Anal. Prev. **18**(3), 707–720 (2018). https://doi.org/10.1007/s11668-018-0466-9
23. George, J.: C2000 MCU SafeTI control solutions: an introduction to ASIL decomposition and SIL synthesis (2019). http://www.ti.com/lit/wp/sway028/sway028.pdf

24. Ward, D.D., Crozier, S.E.: The uses and abuses of ASIL decomposition in ISO 26262. In: IET Conference Publisher, vol. 2012, no. 607 CP, pp. 1–6 (2012). https://doi.org/10.1049/cp.2012.1523
25. Min Kim, S.: Quantitative ASIL estimation using fuzzy set theory. Int. J. (2012). https://doi.org/10.1007/s12239
26. Mitra, S.: Verifying Cyber-Physical Systems. MIT Press, Cambridge (2021)

Advances in Automatic Feature Inspection with a Robot UR5e Programmed Using Force or Impact Commands

Cesar Augusto Peña Cortes, Cristhian Ivan Riaño Jaimes(✉), and Diego Armando Mejia Bugallo

University of Pamplona, Km 1 vía Bucaramanga, Pamplona, Colombia
{cesarapc,cristhian.riano,diego.mejia}@unipamplona.edu.co

Abstract. A complete integration between advanced manufacturing systems and automated robotic systems is one of the pillars that supports the future of intelligent manufacturing. For this reason, this article proposes using a UR5e collaborative robot as part of the feature inspection system in manufactured parts. The objective is to enable, as a measurement tool using the force and position sensors incorporated in the robotic system, to capture the dimensional data of a piece in a studio case. The precision, the control system, and the robotic system's speed are evaluated in manufacturing features' measurement tasks, enabling a digital measurement with which a closed-loop inspection can be applied. This article presents the results and experimental advances obtained in estimating the dimensional values of a piece manufactured through additive manufacturing.

1 Introduction

Additive manufacturing processes are consolidated as a pillar in productive development due to their different advantages concerning conventional manufacturing processes[1]. Concepts such as mass production and custom production operating together in a manufacturing environment are possible thanks to the importance that additive manufacturing acquires day after day [2]. In a product's life cycle, design ensures any project's success. Additive manufacturing allows the creation of prototypes, making decision-making more efficient. Custom production requires a high cost and is more difficult to achieve with conventional manufacturing systems, but supported by 3D printing; it can meet very particular requirements and specifications [3]. All these findings show that solutions that contribute to improving the quality of products and increasing the productivity of flexible manufacturing systems based on additive manufacturing require contributions and technologies compatible with current requirements [4].

The automatic inspection of features is an issue that faces various technological barriers, preventing its complete consolidation within manufacturing environments [5]. Measurement is one of the processes that mainly involves human

M. N. Cardona et al. (Eds.): LACAR 2023, LNNS 940, pp. 192–200, 2024.
https://doi.org/10.1007/978-3-031-54763-8_18

intervention and currently presents lags within the demands placed within the Industry 4.0 context. Automating quality control enables new possibilities if the data is fed back to all the processes involved in the development life cycle of a product [6]. The Closed-loop Manufacturing strategy is based on the feedback of measurement results. The possibilities of optimizing processes and making production systems more sustainable and efficient depend on the correct collection of data on the manufacturing process [7]. The automatic dimensional and geometric inspection of features through the data sheds traces on the manufacturing process; if the machine tool presents errors in its assembly, those errors will be evident in the manufactured parts [8]. Collecting, monitoring, analyzing, and feedback results guarantee continuous optimization and efficient management of resources [9].

Collaborative robots have specific differential operational characteristics ideal for working in different environments. Precision, repeatability, and accuracy are desired characteristics that define the ability to perform measurement tasks within automatic part inspection [10]. Computer-Aided Inspection Planning (CAIP) defines an approach to plan and optimize a part's dimensional and geometric inspection process [11]. The result of this approach is an efficient inspection procedure that ensures correct verification of projected specifications for a manufactured part. Although there are computer tools that help create an inspection plan, it usually requires toolpath programming to perform an automatic feature inspection. The UR5e robot presents several possibilities in the definition of trajectory and movements that facilitate the programming of the robot to execute an automatic inspection plane [12]. Due to the multiple sensors incorporated, the capture of robot operation data yields diverse data, generating possibilities within a digital environment. The records and reports enable an integration not only at the physical level but also at the logical level for treating new concepts. These characteristics of the collaborative robotic arm create a variety of possibilities for use within manufacturing environments [13].

Different studies on this line of automatic measurement of features are currently led [14]. The motivation for this research lies in enabling the adoption of collaborative robots such as the UR5e within a closed-loop inspection strategy [15]. This document presents the automatic inspection of features to guarantee the quality of the analyzed parts, having an experimental validation approach based on the calculation of the error of the part concerning the defined requirements. The system involves using force sensors incorporated into the robot to detect collisions, inspection programming with the creation of routines, real-time data capture, and statistical analysis of the results for decision-making. The project envisions new application possibilities and the incorporation of new lines of research, which contribute to eliminating integration and interoperability barriers of measurement systems within flexible manufacturing environments based on additive manufacturing.

2 Materials and Method

The robotic system is evaluated as a measurement system, for which a prismatic piece is designed for manufacturing through additive manufacturing, which allows, through measurements, to provide both dimensional and geometric data. Figure 1 shows the projected parts' respective tolerances within the precision ranges defined in the robot specifications.

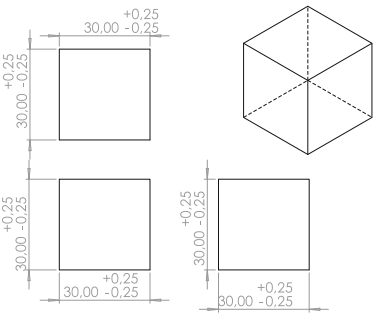

Fig. 1. Prismatic part for dimensional inspection.

The UR5e robot from the Universal Robot Company was used to conduct the experiments. This collaborative industrial robot has a reach of 850 mm, a load capacity of 5 Kg, and a weight of only 20.6 Kg. One of the most relevant characteristics of the proposed application is its excellent repeatability. It has a variation of less than ±30 µm.

The dimensional and geometric inspection begins by positioning the end effector at a safe distance above the piece to be examined. Following a programmed trajectory, the end effector descends with a linear movement until it comes into contact with the part's surface. The procedure is carried out at speeds less than 100 mm/s to avoid collisions. The robot force control is in charge of establishing the limit to apply a 0.1 mm retraction later, and the measurement is recorded by extracting the position of the robot's end effector. This procedure is repeated similarly to establish a reference point that defines the measurement of the feature concerning that reference point.

Figure 2 presents the UR5e Robot from Universal Robots equipped with a Gripper RG2 from OnRobot. The system used for measurement. The experiment with this case study aims to evaluate the ability of the Robot UR5e and a Gripper RG2 in dimensional inspection tasks. The flexibility of the robot and its programming represent advantages over other methods in automatic measurement applications. Repeatability and reproducibility are characteristics that define the performance and capability of the robot in inspection tasks.

The experimental tests accumulated 244 automatic executions of the trajectory defined for measurement. By measuring both the reference surface and the

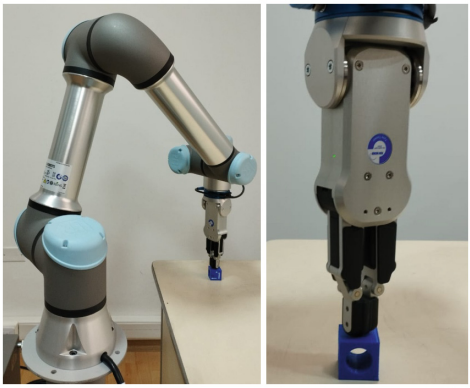

Fig. 2. Measuring system. a) UR5e Robot from Universal Robots. b) Gripper RG2 from OnRobot.

feature of the part, 488 values are reached that contain the measurement results. Therefore, each one of the experimental groups consisted of a repetition of 122 executions. All experimental tests were performed using the robot control software provided by the manufacturer. This was done considering that the general idea is not to use external or additional elements to the automation system, avoiding increasing costs and evaluating the robot as a technological solution in quality control and feature inspection tasks.

Figure 3 presents the code implemented in URScript Programming Language for e-Series. In the case of measurement with a gripper, the effector is first closed in order to increase the rigidity. Subsequently, the robot is brought to the initial position (`Point_Home`) following the industrial recommendations for repeatability analysis. Additionally, utilizing a joint movement (`MoveJ`), the robot is positioned at a point in the work zone (`Point_Departure`), and later it is positioned on a nearby point and above the Manufactured part (`Point_Near`).

The program code enables the execution of commands incorporated in the control of forces of the robot. In the first instance, a linear movement (`MoveL`) is imposed in the opposite direction to the Z axis of the base (descent on the vertical) until the system detects the contact force between the end effector and the part's surface. In this last movement, a speed of 5 mm/s is configured, an acceleration of the tool of 1200 mms^2, and a deceleration of 3000 m/s^2. This movement profile is made so that contact with the feature to be measured is made smoothly and safely.

Once the system detects the contact with the part on the feature to be measured, the robot retracts the position of the tool 0.1 mm, records, displays, and stores the position in the h1 variable. Subsequently, through linear movements raised on the Z and X axes of the robot base, the tool is taken to a safety position above the reference surface. Immediately afterward, the linear and vertical movement occurs until the robot descends and comes into contact with the reference surface. Once again, a 0.1 mm retraction of the tool is carried out; the

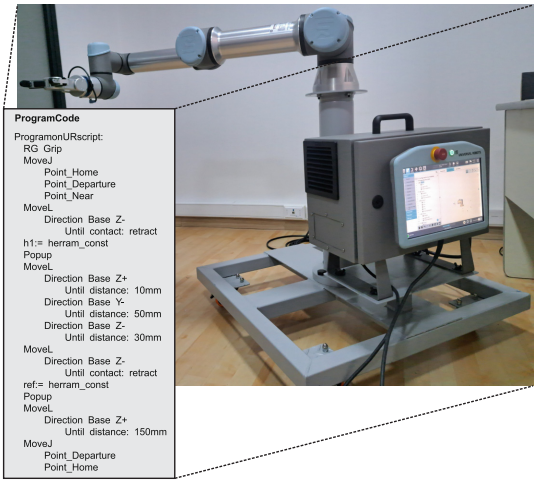

Fig. 3. Program on URscript to UR5e Robot.

position is recorded and displayed in the variable ref. Finally, the measurement cycle is restarted by applying three safe movements to bring the robot to the initial position to finish and restart the execution cycle.

3 Results

After configuring the experiment, programming the execution of routines, and preparing the acquisition environment, once the experiment has been carried out, there is a set of data that, when correctly analyzed, can define the difference between the projected part and the manufactured part in terms of error. However, the contributions of that calculated error can come from, among others, two primary sources: one part of the error is that which adheres to the part through the manufacturing process, and another is due to measurement errors. Next, present a capability analysis for the manufacturing process and a repeatability analysis of the measurement system.

The analysis consists of using the dimensional measurements that define the manufacturing feature and comparing it with the projected feature to obtain the error. In this case, the error is defined as the difference between the measured and desired values projected in the study case (See Fig. 1). Table 1 presents only some of the one hundred and twenty-two (122) samples for the selected measurement characteristic.

The repeatability given in the specifications for the UR5e robot is ±0.03 mm, indicating that the robot can repeat a position with a maximum deviation of 0.03 mm. By linking the force sensor as a measurement system, it may happen that this specification has a variation, which is the objective of evaluating the robot as a measurement instrument. Initially, for the analysis, a dimensional

Table 1. Part inspection report.

ITEM	Target	USL	LSL	Sample	Measurement				
1	30	30,05	29,95	A	30,089	30,181	30,058	30,105	30,194
2	30	30,05	29,95	B	30,182	30,121	30,138	30,177	30,114
3	30	30,05	29,95	C	30,128	30,137	30,119	30,109	30,109
4	30	30,05	29,95	D	30,086	30,140	30,170	30,148	30,092
5	30	30,05	29,95	E	30,113	30,156	30,081	30,221	30,115
6	30	30,05	29,95	F	30,113	30,171	30,164	30,185	30,126

tolerance of ±0.05 mm was defined in the design specification, with which the manufacturing system's capability is calculated. It is necessary to calculate the process capability index; this value indicates the ability of the system to manufacture parts within projected specifications. The C_{pk} capability index value is calculated based on tolerances and process variability (See Eq. (1)).

$$C_{pk} = mim\left(\frac{USL - \frac{\sum_{i=1}^{n} x_i}{n}}{3\sigma}, \frac{\frac{\sum_{i=1}^{n} x_i}{n} - LSL}{3\sigma}\right) \tag{1}$$

where,

- USL: Upper Specification Limit.
- LSL: Lower Specification Limit.
- x_i: Measurement results.
- $\bar{X}$: The mean of the measurements.
- σ: Sigma is the standard deviation of the measurements.

In the analysis applied to the measurement system, a mean ($\bar{X}$) value of 30.1354 mm is obtained. This result presents a slight deviation concerning the nominal value; however, a systematic trend is not necessarily distinguished. The mean value of 30.1354 mm is close to the nominal specification, so the measurement result is centered around the projected dimensional magnitude for the manufacturing feature. The sum of the squares of the differences is obtained; as a result, a magnitude of 0.1731 represents the total amount of squared variability in the acquired measurement data, and a relatively stable measurement can be assumed.

The average variance (s^2) reflects the dispersion of the data, and the calculation yielded a value of 0.0014, which indicates how much each value differs concerning the data set from its average. The standard variation (σ) of 0.0378 shows low variability, and individual data values tend to be 0.0378 mm away from the data set's mean. It can relate this result to precision in measurement. The value of 1.0103 obtained for the measurement system capability index (C_{pk}) demonstrates that the inspection process can yield consistent measurements within the limits of the specifications in a stable, reliable, and precise manner.

Table 2. Process capability index

$\bar{X}$	$\sum_{i=1}^{n} {d_i}^2$	s^2	σ	C_{pk}	Repeatability	Measuring range
30,1354	0,1731	0,0014	0,0378	1,0103	0.2225	0,1700

The difference in the measured value concerning the value of the projected feature is not due to measurement errors but to the manufacturing process. The measurement system provides measurements close to reality, and the probability of uncertainty in the measurement due to values outside the limits of the specifications is low. The repeatability value of 0.225 also reinforces the conclusion that there is low variability between measurements and close to reality. The excellent precision of the system is also related to the low-value repeatability, yielding reliable measurements. Table 2 summarizes the results presented in this section, carried out to evaluate the performance of the robotic system as a feature measurement instrument.

Figure 4a) presents a normal distribution of the acquired measurement data sample. The normality test yields a value of $p : 0.341$, indicating clear evidence to affirm that the data follow a normal distribution. Graphically, a symmetric bell-shaped distribution is observed, which, together with the value of the normality test, suggests that the data acquired come from a normal distribution. Figure 4b) compares the quantiles of the observed data with the quantiles of the theoretical or normal distribution. It is observed that the measurement results fit a theoretical distribution.

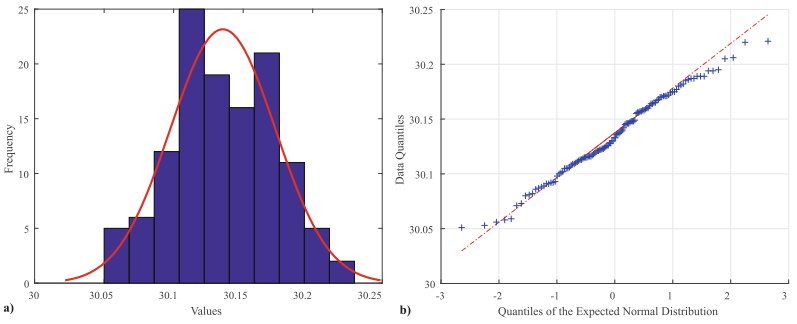

Fig. 4. Verification of data distribution and normality analysis, a) Measurement Data Histogram, b) Q-Q Graph and Anderson-Darling Test.

4 Conclusions

According to the experimental results, it can be concluded that the UR5e robot is suitable for performing quality control operations. This is due to its good precision and the excellent repeatability rate. In the same way, the force control

system proved to be an easy and intuitive way to detect contacts or impacts, with which tool positions can be estimated accurately. This feature allows the development of inspection applications without the need to use additional accessories that increase costs.

Obtaining the capacity indices of the robot using the RG2 gripper was very encouraging. Despite the pads of the fingers and the mechanism of the clamp, outstanding results were obtained, for which it is proposed that it is not necessary to exchange tools for the inspections of the manufactured parts as long as the desired precision margins are not less than 0.17 mm.

References

1. Wang, C., Tan, X., Tor, S.B., Lim, C.: Machine learning in additive manufacturing: state-of-the-art and perspectives. Addit. Manuf. **36**, 101538 (2020)
2. Sathish, K., et al.: A comparative study on subtractive manufacturing and additive manufacturing. Adv. Mater. Sci. Eng. **1–8**, 2022 (2022)
3. Gibson, I., et al.: Additive Manufacturing Technologies, vol. 17. Springer, New York (2021)
4. Tavares, T.M., Ganga, G.M.D., Godinho Filho, M., Rodrigues, V.P.: The benefits and barriers of additive manufacturing for circular economy: a framework proposal. Sustain. Prod. Consum. (2023)
5. Hedberg, T.D., Jr., et al.: Defining requirements for integrating information between design, manufacturing, and inspection. Int. J. Prod. Res. **60**(11), 3339–59 (2022)
6. Azamfirei, V., Psarommatis, F., Lagrosen, Y.: Application of automation for in-line quality inspection, a zero-defect manufacturing approach. J. Manuf. Syst. **67**, 1–22 (2023)
7. Sundaram, S., Zeid, A.: Artificial intelligence-based smart quality inspection for manufacturing. Micromachines **14**(3), 570 (2023)
8. Jaimes, C.I.R., Alvares, A.J.: Integrated inspection system step-compliant for the exchange of dimensional metrology data. Procedia Manuf. **38**, 1205–12 (2019)
9. Andersen, A.L., et al.: Changeable closed-loop manufacturing systems: challenges in product take-back and evaluation of reconfigurable solutions. Int. J. Prod. Res. **61**(3), 839–58 (2023)
10. Rettig, O., Müller, S., Strand, M.: A marker based optical measurement procedure to analyse robot arm movements and its application to improve accuracy of industrial robots. In: Ang Jr, M.H., Asama, H., Lin, W., Foong, S. (eds.) IAS 2021. LNNS, vol. 412, pp. 551–562. Springer, Cham (2022). https://doi.org/10.1007/978-3-030-95892-3_42
11. Zhao, F., Xu, X., Xie, S.Q.: Computer-aided inspection planning-the state of the art. Comput. Ind. **60**(7), 453–66 (2009)
12. Hurtado, C.V., Flores, A.R., Elizondo, V., Palacios, P., Zamora, G.: Work-in-progress: virtual reality system for training on the operation and programing of a Collaborative Robot. In: 2021 IEEE Global Engineering Education Conference (EDUCON), p. 1650-3. IEEE (2021)
13. Marvel, J.A., Bagchi, S., Zimmerman, M., Antonishek, B.: Towards effective interface designs for collaborative HRI in manufacturing: metrics and measures. ACM Trans. Hum. Robot Interact. (THRI) **9**(4), 1–55 (2020)

14. Aminzadeh, M., Kurfess, T.R.: Online quality inspection using Bayesian classification in powder-bed additive manufacturing from high-resolution visual camera images. J. Intell. Manuf. **30**, 2505–23 (2019)
15. Saif, Y., Yusof, Y., Latif, K., Kadir, A.Z.A., Lliyas, A.M.: Systematic review of STEP-NC-based inspection. Int. J. Adv. Manuf. Technol. **108**, 3619–44 (2020)

Author Index

M. N. Cardona et al. (Eds.): LACAR 2023, LNNS 940, pp. 201–202, 2024.
https://doi.org/10.1007/978-3-031-54763-8